Heterogeneity and clinical potential of boundary cap cells and their derivatives

Gaspard Gerschenfeld

SORBONNE UNIVERSITÉ
CRÉATEURS DE FUTURS
DEPUIS 1257

IBENS
Institut de Biologie de l'Ecole Normale Supérieure

Thèse de Doctorat de Sorbonne Université

Spécialité Biologie Cellulaire et Développement

École Doctorale Complexité du Vivant (ED 515)

Présentée par

Gaspard Gerschenfeld

Pour obtenir le grade de Docteur de Sorbonne Université

Hétérogénéité et potentiel clinique des cellules capsules frontières et leurs dérivés.

Heterogeneity and clinical potential of boundary cap cells and their derivatives.

Présentée et soutenue publiquement le 4 juin 2019

Devant un jury composé de :

Dr	Alain Chédotal	Président
Pr	Carmen Ruiz de Almodóvar	Rapporteur
Dr	Igor Adameyko	Rapporteur
Dr	Isabelle Brunet	Examinateur
Pr	Nathalie Kubis	Examinateur
Dr	Piotr Topilko	Directeur de thèse
Pr	Patrick Charnay	Membre invité

Résumé

Hétérogénéité et potentiel clinique des cellules capsules frontières et leurs dérivés

Au cours du développement embryonnaire, la crête neurale donne naissance aux cellules gliales et neuronales du système nerveux périphérique, mais aussi aux cellules capsules frontières (CF) qui forment transitoirement des amas aux points d'entrée/sortie des nerfs crâniens et spinaux. Notre équipe a réalisé l'étude du devenir des CF grâce à des souris transgéniques combinant l'expression de la Cre sous le contrôle des marqueurs des CF *Prss56* ou *Krox20*, et un rapporteur dont l'expression est induite par la Cre. Nous avons montré que les CF qui expriment *Prss56* donnent naissance à des dérivés qui migrent le long des racines des nerfs où ils sont à l'origine de la majorité des cellules de Schwann (CS), puis dans le ganglion rachidien (GR) où ils forment des neurones sensoriels, avant d'atteindre la peau, ou ils donnent naissance aux CS, à la glie terminale et une population de cellules potentiellement souches (SKP). Récemment, le traçage des dérivés des CF (dCF) au moyen d'un autre marqueur, *Krox20*, nous a conduit à réaliser une découverte inattendue. Alors que l'identité des dérivés issus des CF qui expriment *Krox20* sont les mêmes dans les racines et les GR, une fois arrivés dans la peau ils se détachent des nerfs pour intégrer le plexus vasculaire et se différencier en cellules murales.

Dans la première partie de ma thèse, j'ai étudié les mécanismes qui gouvernent le détachement des dCF des nerfs puis leur différenciation en cellules murales. Ainsi, j'ai montré que : (i) le détachement des dCF des nerfs est transitoire, a lieu entre E12,5 et E15.5, et est accompagné par l'extinction de marqueurs gliaux et l'activation des marqueurs muraux ; (ii) chez l'adulte, environ un tiers des cellules murales de la vascularisation cutanée proviennent des CF ; (iii) le changement d'identité (glial versus mural) a lieu dans les cellules attachées aux nerfs, bien avant leur décollement ; (iv) en plus des cellules murales, les dCF sont à l'origine de fibroblastes péri-vasculaires, une population cellulaire récemment décrite comme à l'origine de la fibrose dans le système nerveux central. Ces résultats m'ont conduit à proposer un nouveau modèle pour le développement de la vascularisation de la peau, dans lequel les CS agissent d'abord comme une source de cellules murales avant de sécréter des signaux pour remodeler le plexus vasculaire en vaisseaux sanguins matures et fonctionnels. Dans la deuxième partie de ma thèse, j'ai étudié le potentiel des SKP à participer à la régénération du cerveau après un infarctus cérébral. Malgré l'utilisation de nombreuses approches *in vitro* et *in vivo*, dont l'exploration de plusieurs types de biomatériaux pour la culture et la greffe des SKP, j'ai montré que les SKP ne possèdent pas le potentiel de générer des neurones fonctionnels. Toutefois, en collaboration avec une autre équipe, j'ai mis au point un biomatériau à base de polysaccharides adapté à la culture et la manipulation de neurones embryonnaires. Enfin, j'ai montré que les explants ou suspensions cellulaires de cortex sensoriel embryonnaire s'intègrent efficacement lorsqu'ils sont greffés après un infarctus cérébral, soutenant la faisabilité d'une telle approche.

Abstract

Heterogeneity and clinical potential of boundary cap cells and their derivatives.

In addition to peripheral glia and neurons, the neural crest gives rise to boundary cap cells (BC) that form transient clusters at the entry/exit points of all cranial and spinal nerves. Fate-mapping experiments using mice in which Cre expression is under control of BC marker *Prss56*, in combination with a Cre-inducible reporter, have revealed that BC derivatives migrate along nerve roots into the dorsal root ganglia (DRG) and then peripheral nerves to reach the skin. Whereas BC cells are at the origin of most, if not all, nerve root Schwann cells (SC) and a subpopulation of DRG sensory neurons, in the skin they give rise to SC, terminal glia on lanceolate and free nerve endings and a population of stem-like skin progenitor cells (SKP). More recent experiments using another BC marker, *Krox20*, have led us to an unexpected observation. Indeed, while Krox20-traced BC derivatives in the nerve roots and DRG correspond respectively to SC and sensory neurons, those reaching the skin detach from nerves and undergo a "glial to vascular" switch to provide mural cells to the developing vasculature.

In the first part of my PhD, I have focused my efforts on understanding the mechanisms of this "glial to vascular" switch. I have shown that: (i) Krox20-traced BC derivatives detachment from nerves occurs between E12.5 and E15.5, concomitantly with the extinction of glial and the activation of mural markers; (ii) about a third of adult skin mural cells originate from BC cells; (iii) the expression of several mural markers is detectable at E12.5 in cells closely attached to axons suggesting that their switch of identity occurs well before their detachment (iv) in addition to mural cells, they also give rise to perivascular fibroblast-like cells, a cell population recently described in central nervous system (CNS) fibrosis. These findings suggest a new skin vasculature development model, in which peripheral glia first acts as a source of mural cells before providing molecular signals to shape the vascular plexus into mature and functional blood vessels. In the second part of my PhD, I explored the SKP regenerative potential in the brain after a stroke. Despite numerous *in vitro* and *in vivo* attempts, including the use of several types of biomaterials for cell culture and grafting, I came to the conclusions that SKP do not have the potential to generate functional CNS-like neurons. However, in collaboration with another team, I have developed a polysaccharide-based scaffold that can be used to culture and manipulate embryonic neurons *in vitro*. Finally, I have shown that explants or cell suspension of embryonic sensory cortex, when grafted after a stroke, efficiently integrate and form numerous projections in the host parenchyma, supporting the feasibility of such an approach.

Acknowledgements

Before switching to French, I would like to express my gratitude to the members of the jury: Pr Carmen Ruiz de Almodóvar and Dr Igor Adameyko for accepting to read and comment on my manuscript; Dr Isabelle Brunet, Pr Nathalie Kubis and Dr Alain Chédotal for accepting to evaluate my work.

Un mémoire de thèse représente l'étape finale du travail réalisé au cours du doctorat. Néanmoins, ce mémoire représente surtout pour moi la fin d'une aventure qui s'est étalée sur dix années au sein de l'équipe Charnay. En effet, j'ai découvert l'univers des cellules capsules frontières en 2009 (M1), puis j'ai continué en 2010 (M2) avant d'y retourner en 2013 (stage d'été post-ECN) et enfin en 2015 pour ma thèse. Au cours de ces passages successifs, j'ai eu la chance de rencontrer de nombreuses personnes sans lesquelles ce travail n'aurait pas été possible, et la vie au labo aurait été bien moins sympathique. Je voudrais donc profiter de ces lignes pour les remercier.

Je commencerais donc par t'exprimer ma reconnaissance, Patrick, pour m'avoir accueilli à quatre reprises dans ton laboratoire. Passé mon intimidation initiale, j'ai pu découvrir et apprécier ton sens de l'humour, nos discussions politiques et en apprendre plus sur tes passions comme le golf ou, parait-il, le compost. Je te suis aussi très reconnaissant pour tes conseils et ta franchise lors de mes atermoiements scientifiques.

Et bien sûr, je te remercie Piotr d'avoir accepté de m'encadrer pour chacun de mes passages, jusqu'à la thèse. Lors de notre première rencontre, tu m'as convaincu grâce à ton enthousiasme contagieux. Par la suite, j'ai grandement apprécié ta créativité, ton optimisme inébranlable, ton intuition scientifique et ta disponibilité. J'ai toujours trouvé nos discussions scientifiques stimulantes et motivantes. Enfin, je te remercie d'avoir été un patient régulier au cours de ma thèse afin de me faire des rappels de médecine.

Je te remercie chaleureusement, Fanny, pour tout ce que tu m'as appris au cours de ces années, et pour le plaisir que j'ai eu à travailler plus directement avec toi sur le « switch ». J'ai été impressionné par ton talent t'expérimentatrice et la grande diversité de tes connaissances, le tout en étant toujours de bonne humeur. Nos arrachages de cheveux devant des clusters de cellules incompréhensibles ou dans notre quête de Robo3 me manqueront (presque), mais à la place on pourra plutôt faire une partie de Splendor ou 7wonders !

I also want to thank you, Kasia, for putting up with me to share our office during the last four years. You have been my primary source of sarcasms, and you know that I need them as much as I need coffee during my day. You have taught me a lot, especially on goats and how cute they are or on Australian music with Tash Sultana.

Je continue en te remerciant, Pernelle, pour avoir été une super stagiaire à encadrer. Derrière ta timidité se cache un sens de l'humour aiguisé, et aussi Aliona parce qu'elle est toujours là où on ne l'attend pas. Travailler avec toi a été un plaisir, et je suis certain que la thèse que tu t'apprêtes à débuter dans le laboratoire sera un succès. J'espère qu'un jour tu me diras quelle était cette musique que tu écoutais et tenais absolument à garder secrète.

Je souhaiterais aussi remercier les anciens membres du laboratoire. Renata, avec qui j'ai cherché des neurones et parfois trouvé des cardiomyocytes, et qui a essayé de modérer mon caractère obsessionnel avec plus ou moins de succès. Pascale, toujours disponible pour un conseil de PCR ou

d'hygiène et sécurité, ou bien discuter lors des pauses café. Elodie, qui m'a convaincu d'arrêter le sucre dans mon café en début de thèse (excellente idée !). Aurélie, qui a été à l'origine du projet « switch ». Carole, qui m'a montré comment utiliser un agitateur pour simuler un tremblement de terre. Aliona, parce que décidemment elle est partout. Graziella, pour son aide dans la gestion des souris. Yassine, pour m'avoir supporté dans son box il y a longtemps. Et bien sûr, last but not least, petit Patrick ! Merci pour ces discussions sur la politique américaine où nous avons souvent fait fuir tout le monde, mais aussi et surtout pour ton influence positive qui m'a amenée à être convoqué par Pierre Vincens suite à un premier avril mémorable. Je ne me serais pas autant amusé au labo sans toi.

Je voudrais aussi remercier Rachida et Didier avec qui j'ai collaboré sur les biomatériaux. J'ai beaucoup apprécié travailler avec vous, toujours de bonne humeur et enthousiastes, et je vous suis extrêmement reconnaissant pour l'aide que vous m'avez fourni au cours de cette thèse. Je tiens à remercier d'autres membres de l'IBENS qui m'ont été d'une aide précieuse : Amandine, Déborah, Dolores, Éléonore, Abder et Christophe à l'animalerie ; Astou, Simon et Benjamin pour l'imagerie ; Aurélie à la laverie du 1er ; Béatrice, Virginie, Abdoul, Pierre-Emmanuel et Rouben pour leur aide administrative ; et plus récemment Claudia à l'IMRB.

Je m'éloigne (un peu mais pas tant) du laboratoire pour remercier ma famille, qui m'a transmis la curiosité essentielle qui m'a amené à faire cette thèse. Je vous suis très reconnaissant pour votre soutien et aussi votre aide statistique (maman), humoristique (papa) ou sarcastique (Antoine). Serge, pour m'avoir appris à bricoler et à avoir la patience nécessaire à la recherche expérimentale. Hersch (Coco) et Dora (Cuca), dont le parcours a été une source d'inspiration, et dont j'ai ressenti la trace persistante à l'IBENS entre les courriers adressés au Pr Gerschenfeld que j'ai reçu ou les vieux passeports retrouvés au 9e. J'en profite aussi pour remercier Philipe et Jacsue, pour ces repas du 1er janvier mémorables de commérages scientifiques, et Philipe aussi pour ton rôle dans la création de l'école de l'INSERM et ta participation à mon comité de thèse. Je finirai par remercier les super baby-sitters, maman et l'Eco-team (Isabelle, Camille et Patrick), qui m'ont permis de finir ma thèse à temps.

Enfin, je voudrais saluer mes amis, qui m'ont soutenu malgré mon humeur fluctuante au cours de mes péripéties : les Koreboul, avec Stéphanie la rhumatologue-réanimatrice d'astreinte, Maxime l'orthopédiste omniprésent et Clemi et Lili, qui ont réussi à (presque) venir à bout de leur énergie ; les Safeney, avec Sarah l'allergologue qui guérira Mathis de son atopie (pas de pression) et Paul, mon futur référent cardio à la Pitié et semble-t-il chevalier qui prendra Mathis comme écuyer ; Chloé et Adrien (Chlodri), toujours disponibles pour parler de nos atermoiements médicaux à propos de Mathis, et Léo et Gabriel, avec qui Mathis a beaucoup partagé de vêtements ; Ombeline, avec qui je finirai peut-être par élever des poules un jour et Vivien, le passionné de la recherche ; Adèle, Camille et Clément, mes futurs chefs lors de mes prochains stages (Adèle on y est presque), fournisseurs d'activités culturelles (Clément) et sauveurs de parents en détresse avec la veilleuse (excellent choix Camille) ; Juliette, la pédiatre baroudeuse qu'il ne faut pas contrarier ; et Côme, réanimateur néphrologue de formation mais surtout excellent ténor à la chorale du conservatoire du XIIe.

Pour terminer, je veux te remercier Marie pour ton soutien, ta patience et ta compréhension, surtout vu ce que tu as dû endurer pendant ces derniers mois (à charge de revanche si tu décides d'en faire une !). Heureusement, Mathis est arrivé juste à temps pour illuminer nos journées et nos nuits pendant cette fin de thèse. Cette thèse vous est dédiée, ainsi qu'à Manon.

Table of Contents

Introduction 1

I. The peripheral nervous system 3

1. Organisation of the peripheral nervous system 3

1.1. Overview of the nervous system 3

1.1.1. Nervous system 3

1.1.2. Central nervous system 4

1.1.3. Peripheral nervous system 5

1.2. Neuronal diversity in the peripheral nervous system 7

1.2.1. Somatic sensory neurons 7

1.2.2. Motor neurons and proprioceptive innervation 9

1.2.3. Cutaneous sensory innervation 10

1.3. Glial diversity within the peripheral nervous system 11

1.3.1. Schwann cells 11

1.3.2. Glial satellite cells 14

1.3.3. Endo-, epi- and perineurial fibroblasts 15

2. Development of the peripheral nervous system 16

2.1. Peripheral nervous system stem cells 16

2.1.1. What is a stem cell? 16

2.1.2. Embryonic stem cells 16

2.1.3. Multipotent stem cells in the adult peripheral nervous system 18

2.2. The neural crest: key multipotent stem cells during development 18

2.2.1. The neural crest and advances in developmental biology 18

2.2.2. Neural crest specification and migration 19

2.2.3. Neural crest differentiation 22

2.3. The peripheral nervous system derives from the neural crest 25

2.3.1. Sensory neurons 25

2.3.2. Schwann cells 28

2.3.3. Satellite glial cells 35

3. Boundary cap cells 35

3.1. Boundary cap cells origin and markers 35

3.1.1. Anatomical position and origin 35

3.1.2. Boundary cap cells markers 36
3.1.3. BC cells heterogeneity 36
3.2. Boundary cap cells functions 37
3.2.1. Gatekeepers for motor neurons cellular bodies 37
3.2.2. Stem cells for the developing peripheral nervous system 39
3.3. Boundary cap cells in disease: type 1 neurofibromatosis 40
II. The cardiovascular system 43
1. Organisation of the cardiovascular system 43
1.1. Overview of the circulatory system 43
1.2. Blood vessels 44
1.2.1. Macrovasculature 44
1.2.2. Microvasculature 45
1.3. Cellular diversity within the blood vessels 45
1.3.1. Endothelial cells 45
1.3.2. Mural cells 47
1.3.3. Perivascular fibroblast-like cells 51
2. Development of the vascular system 52
2.1. Vasculogenesis 52
2.1.1. Angioblast specification 52
2.1.2. Primitive vascular network 53
2.1.3. Arteriovenous fate acquisition 54
2.2. Angiogenesis 55
2.2.1. Sprouting angiogenesis 55
2.2.2. Common neurovascular guidance cues 57
2.3. Mural cells development 58
2.3.1. Origin of mural cells 58
2.3.2. Mural cell development 60
3. Nerve role in vascular maturation 62
3.1. Peripheral nerves are aligned with arteries 62
3.2. Peripheral nerves direct blood vessel patterning 63
3.3. Peripheral nerves promote arterial differentiation 63
III. Presentation and aims of my thesis work 67

Results 69

Article one 71

Boundary caps give rise to neurogenic stem cells and terminal glia in the skin

Article two 105

Derivatives of neural tube-associated boundary caps migrate along peripheral nerves to give rise to a major part of skin vasculature mural cells

Discussion 131

1. Contribution of boundary cap cells during development 134

1.1. Glial derivatives 134

1.1.1. Schwann cell heterogeneity 134

1.1.2. Subepidermal glia 134

1.2. Perivascular derivatives 135

1.2.1. Redundancy of mural cell recruitment during development 135

1.2.2. Mural cells heterogeneity 136

1.3. On the glial to vascular switch 138

2. Origins of boundary cap cells 139

2.1. About Schwann cell precursors 139

2.2. Boundary cap cells and the neural crest 140

2.3. Boundary cap cells and Schwann cell precursors 141

3. Boundary cap cells heterogeneity 142

General conclusions 145

Appendix 149

Unpublished results 151

Skin progenitor cells do not have the potential to generate functional cortical-like neurons

Article three 171

Development and use of a 3D macroporous polysaccharide-based scaffold for neuronal culture

Bibliography 195

Table of Figures

Figure 1. The nervous system. 3
Figure 2. Neuronal polarity and conduction. 4
Figure 3. The spinal nerve. 5
Figure 4. Organisation of the peripheral nervous system. 6
Figure 5. Different types of sensory neurons. 8
Figure 6 Muscle innervation. 9
Figure 7. The cutaneous innervation. 11
Figure 8. Schwann cells. 13
Figure 9. Glial satellite cells. 14
Figure 10. Peripheral nerve anatomy. 15
Figure 11. The stem cell concept. 17
Figure 12. Cre-LoxP tracing system. 19
Figure 13. Neural crest development. 20
Figure 14. Trunk neural crest migration. 21
Figure 15. Regions of the chick neural crest. 22
Figure 16. Factors involved in trunk neural crest differentiation. 23
Figure 17. Neural crest progressive lineage restriction model. 24
Figure 18. Sensory neurogenesis. 25
Figure 19. Sensory neurons specification. 26
Figure 20. The Schwann cell lineage. 29
Figure 21. Changes in phenotypic profile in the embryonic Schwann cell lineage. 30
Figure 22. Schwann cell differentiation. 33
Figure 23. Boundary cap cells. 35
Figure 24. Boundary cap cells markers. 36
Figure 25. Boundary cap cells confine the cellular bodies of motor neurons. 37
Figure 26. Fate-mapping of Krox20-traced boundary cap cells and their derivatives. 38
Figure 27. Conditional NF1 loss in Prss56-expressing boundar cap (BC) cells gives rise to paraspinal (plexiform) and cutaneous (diffuse) neurofibromas. 40
Figure 28. Schematic representation of the circulatory system. 43
Figure 29. Organization of the vasculature. 44
Figure 30. Mural cell continuum along the microvascular tree. 48

Figure 31. Vasculogenesis and arteriovenous fate. 53
Figure 32. Sprouting angiogenesis.. 56
Figure 33. Endothelial and mural cells have muvltiple origins within the same tissue. 59
Figure 34. Parallels in vessel and nerve patterning. 62
Figure 35. Schematic representation of the nerve-mediated vascular branching and arterial differentiation in the developing skin. 64
Figure 36. Schematic representation of *Krox20*- and *Prss56*-traced boundary cap cell derivatives in the trunk.. 133
Figure 37. *Prss56*-, *Krox20*- and *Dhh*-traced derivatives in the adult skin. 135
Figure 38. Genetic ablation of *Krox20*-traced boundary cap cells. 136
Figure 39. Trajectories reconstruction of BC cell derivatives in E12.5 dorsal skin 137
Figure 40. *Krox20*-traced BC derivatives express *Robo3* before detaching. 138
Figure 41. Schwann cell precursors, a « neural crest in disguise ». 139
Figure 42. On the origin of boundary cap cells. 141
Figure 43. Boundary cap cells, the neural crest and Schwann cell precursors. 142
Figure 44. scRNA-seq of traced cells from E11.5 *Krox20*^{Cre}, *Rosa26*^{tdTomato} meninges. 143

Table of Abbreviations

aGPCR	Adhesion G protein-coupled receptor
AJ	Adherens junctions
Alk	Activin receptor-like kinase
Ang1	Angiopoietin-1
ANS	Autonomic nervous system
BBB	Blood brain barrier
BDNF	Brain-derived neurotrophic factor
bHLH	Basic helix-loop-helix (bHLH)
BL	Basal lamina
BM	Basement membrane
BMP	Bone morphogenic protein
CADASIL	Cerebral autosomal-dominant arteriopathy with subcortical infarcts and leukoencephalopathy
cAMP	Cyclic adenosine monophosphate
CCL2	CC chemokine ligand 2
cNF	Cutaneous neurofibroma
CNS	Central nervous system
Col1a1	Collagen1α1
Coup-TFII	Chicken ovalbumin upstream promoter–transcription factor II
CSF	Cerebro-spinal fluid
CTF	C-terminal fragment
Cxcl12	CXC motif chemokine ligand 12
Cxcr4	CXC motif chemokine receptor 4
DCC	Deleted in colorectal cancer
Dhh	Desert hedgehog
Dll1/4	Delta-like ligand 1/4
DREZ	Dorsal root entry zone
DRG	Dorsal root ganglia
E	Day of embryonic life
EC	Endothelial cell
ECM	Extracellular matrix
Edn(r)	Endothelin (receptor)
EMP	Erythro-myeloid progenitor
EMT	Epithelial to mesenchymal transition
ESC	Embryonic stem cell
Etv2	E-26 variant 2 transcription factof
FACS	Fluorescence activated cell sorting
FGF	Fibroblast growth factor
FNE	Free nerve endings
GDNF	Glial cell-derived neurotrophic factor
GLAST	Glutamate-aspartate transporter
Hh	Hedgehog
HIF-1	Hypoxia-inducible factor 1
hPLAP	Human placental alkaline phosphatase
HTMR	High-threshold mechanoreceptor
ICAM-1	Intercellular adhesion molecule
ICM	Inner cellular mass
IGF2	Insulin-like growth factor 2
IL-1	Interleukine 1
iPSC	Induced pluripotent stem cell
ISC	Immature Schwann cell
ISE	Immature Schwann cell element
LTMR	Low-threshold mechanoreceptor
MEP	Motor exit points
MN	Motor neurons
MP	Myeloid progenitor
MSE	Myelinating Schwann cell element
NC	Neural crest
NCSC	Neural crest-derived stem cell
NF1	Neurofirbomatosis type 1
NGF	Nerve growth factor
Ngn1/2	Neurogenin 1/2
NMJ	Neuro-muscular junction
NO	Nitric oxyde
NPB	Neural plate border
Nrg1-III	Type III Neuregulin 1
Nrp1	Neuropilin 1
NT	Neural tube
NT3	Neurotrophin 3
Nte	Neuropathy target esterase
NTF	N-terminal fragment
PAF	Platelet activating factor

PDGF(R) Platelet-derived growth factor (receptor)
PGI_2 Prostacyclin
PI_3K Phosphatidylinositol-3-kinase
PLC-g Phospholipase C-g
pNF Plexiform neurofibroma
PNS Peripheral nervous system
PVF Perivascular fibroblast-like cell
RA Retinoic acid
Rgs5 Regulator of G protein signalling 5
Robo Roundabout guidance receptor
RSC Remak Schwann cell
S1P Sphingosine-1-phosphate
SC Schwann cells
SCP Schwann cell precursor
SKP Skin progenitor cell
scRNAseq Single cell RNA sequencing
Sema Semaphorin
SGC Satellite glial cells
Shh Sonic hedgehog
SLI Schmidt-Lanterman incisures
SM-MHC Smooth muscle-myosin heavy chain
SN Sensory neurons
SNS Somatic nervous system
TACE TNFα-converting enzyme
TGFβ Transforming growth factor beta
TJ Tight junctions
TNFα Tumor necrosis factor α
tPA Tissue plasminogen activator
Trk Tropomyosin-receptor-kinase
UMAP Uniform mannifold approximation and projection
VE-cadh Vascular endothelial cadherin
VEGF Vascular endothelial growth factor
VENT Ventrally emigrating neural tube cells
vSMC Vascular smooth muscle cell
vWF von Willebrand factor
Wnt Wingless-type MMTV integration

Introduction

I. The peripheral nervous system

1. Organisation of the peripheral nervous system

1.1. Overview of the nervous system

1.1.1. Nervous system

The nervous system is responsible for transmitting information throughout the body. It collects and integrates signals from the environment, and it programs and coordinates their motor response. In vertebrates, it is divided in two parts that are in continuity (Figure 1), the central nervous system (CNS) and the peripheral nervous system (PNS). At the cellular level, it is composed of two broad cell categories, neurons and glial cells.

Neurons are polarised cells, consisting of a cellular body called soma and cellular processes called dendrites, that remain near the soma, and axons that can extend over long distances to connect their target (Figure 2). There is a wide diversity of neurons, depending on their polarity or neurotransmitter. They are electrically excitable cells that convert stimuli into electrical signals, called action potentials, that they can conduct through their axons. An action potential is generated when the axonal membrane is depolarized beyond the threshold necessary for voltage-gated sodium channels to open. The intracellular influx of positive charges spreads and depolarizes the adjacent segment of membrane, until it triggers another action potential hence conducting the signal without any decrement. They can communicate with other neurons using neuro-transmitters through connections called synapses.

Glial cells support neural functions in several ways, and differ between the CNS and PNS. They maintain homeostasis, protect neurons and myelinate axons. The myelin sheath consists of multiple layers of cell membrane wrapped around the axon. It is a vertebrate evolutionary acquisition that enabled the development of large and

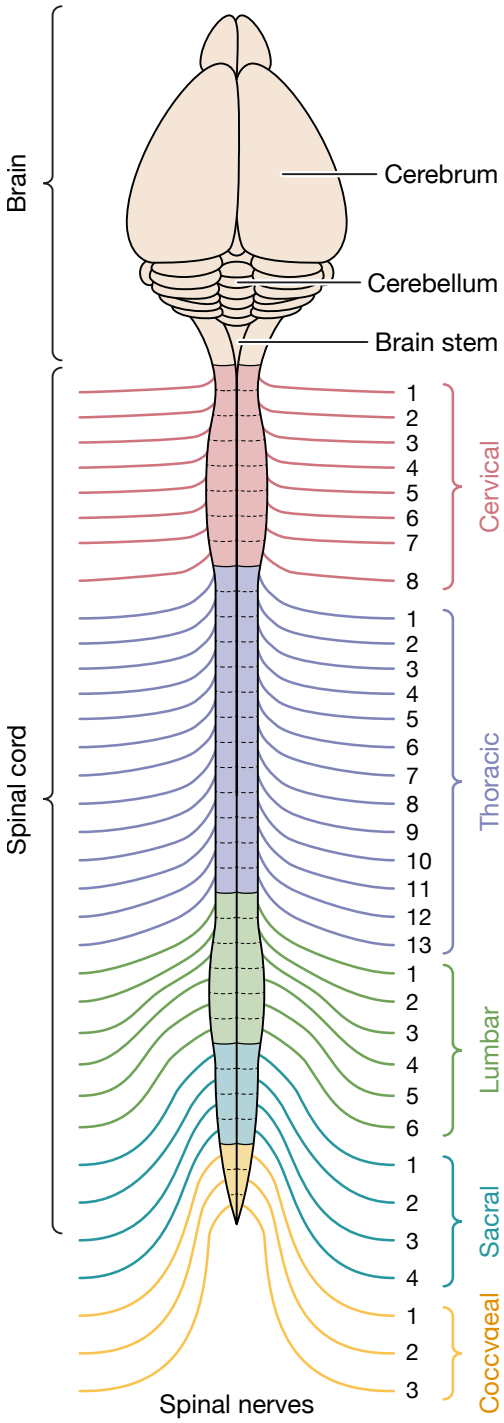

Figure 1. The nervous system. The central nervous system is made of the brain and spinal cord. The spinal cord is segmented and spinal nerves are named for their spinal cord level and are numbered in order from rostral to caudal. Along with cranial nerves and the autonomic nervous system (not shown), they make the peripheral nervous system. Adapted from *Neuroscience, Exploring the Brain, Fourth Edition* (2016) and *The Mouse Nervous System, First Edition* (2012).

complex nervous systems by enabling rapid and efficient nerve conduction (Figure 2). It does not cover the whole axonal length, with breaks in the insulation every 0.2 to 2 mm called Ranvier nodes, where voltage-gated cross the membrane to generate action potentials. This is called saltatory conduction, as the action potential "jumps" between each node instead of slowly spreading along the whole axonal length.

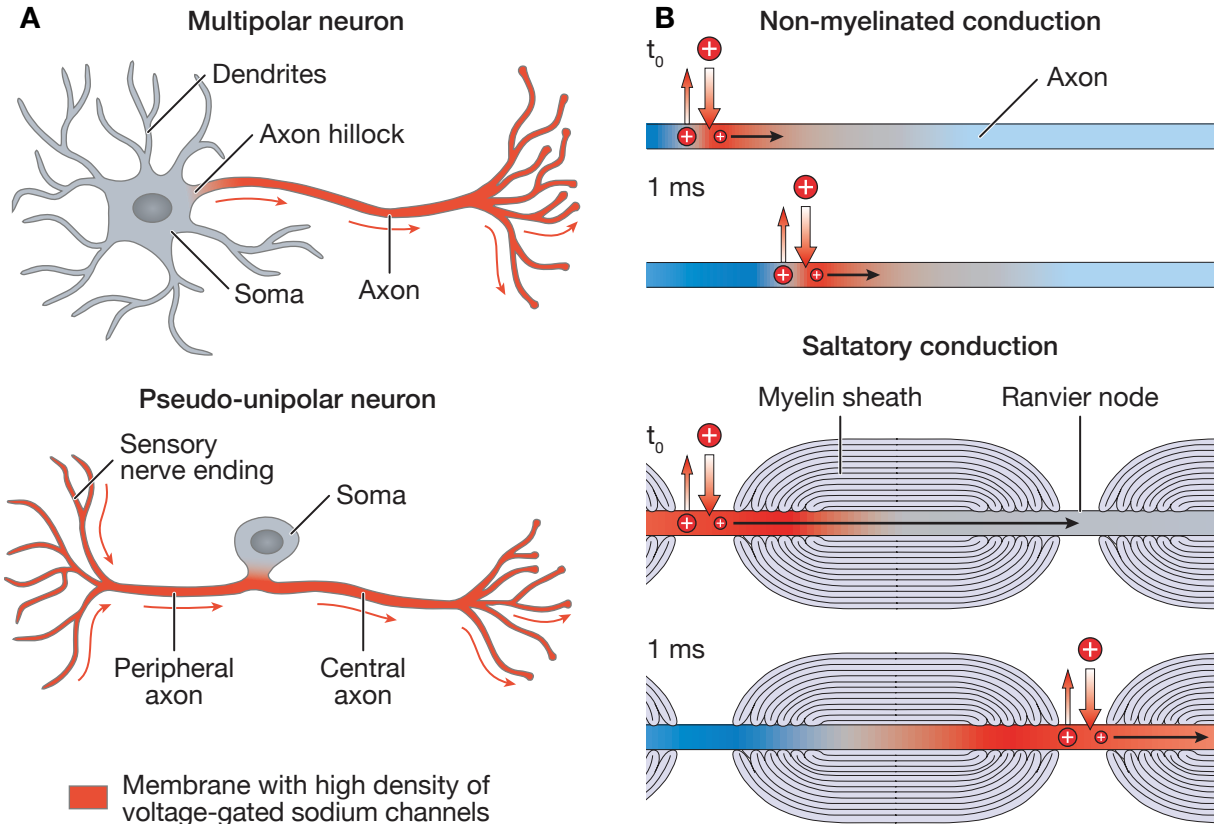

Figure 2. Neuronal polarity and conduction. (**A**) Lower motor neurons in the spinal cord are multipolar neurons, and peripheral sensory neurons are pseudo-unipolar. The high density of voltage-gated sodium channels in the axonal membrane enables axons to generate and conduct action potentials (arrows indicate the normal direction). (**B**) In non-myelinated conduction, the entry of positive charges during the action potential causes the membrane just ahead to depolarize to threshold. In saltatory condution, myelin allows current to spread farther and faster between nodes, thus speeding action potential conduction. Adapted from *Neuroscience, Exploring the Brain, Fourth Edition* (2016).

1.1.2. Central nervous system

The CNS is composed of the brain and the spinal cord (Figure 1). The brain is formed by complex neural networks, receiving neural projection from and sending projections to the spinal cord. It is responsible for data integration, motor action coordination, emotion and cognition. The spinal cord conveys and modulates information between the brain and the PNS. The CNS has multiple layers of protection. It is encased in the skull and vertebral column for physical protection. It is surrounded by the meninges, whose role is to protect the CNS and under which flows the cerebro-spinal fluid (CSF). And finally at the cellular level, the blood-brain barrier (BBB) tightly controls the movement of bloodborne substances to the CNS.

In the CNS, glial cells include oligodendrocytes, astrocytes, ependymal cells and microglia. Oligodendrocytes are myelinating cells that can wrap around multiple axons. Astrocytes fill most of the space that isn't occupied by neurons or blood vessels. They regulate the chemical content of the extracellular space, such as the synaptic junctions, and participate to the formation of the BBB. Ependymal cells line CSF-filled ventricles in the brain and central canal in the spinal cord. They are ciliated cells that produce (in the choroid plexuses), regulate and direct the flow of CSF. Finally, microglia are resident macrophage-like cells in the CNS. They are key to its immune defence and also its maintenance by removing debris left by dead or degenerating cells.

1.1.3. Peripheral nervous system

The PNS connects the CNS with the rest of the body, and is composed of the somatic (SNS) and autonomic nervous systems (ANS). The SNS includes the cranial nerves III to XII and thirty four pairs of spinal nerves that innervate the skin, muscle and joints under voluntary control (Watson, 2012). Each spinal nerve is connected to the spinal cord by a ventral and dorsal root (Figure 3). Lower somatic MN are multipolar neurons whose cell

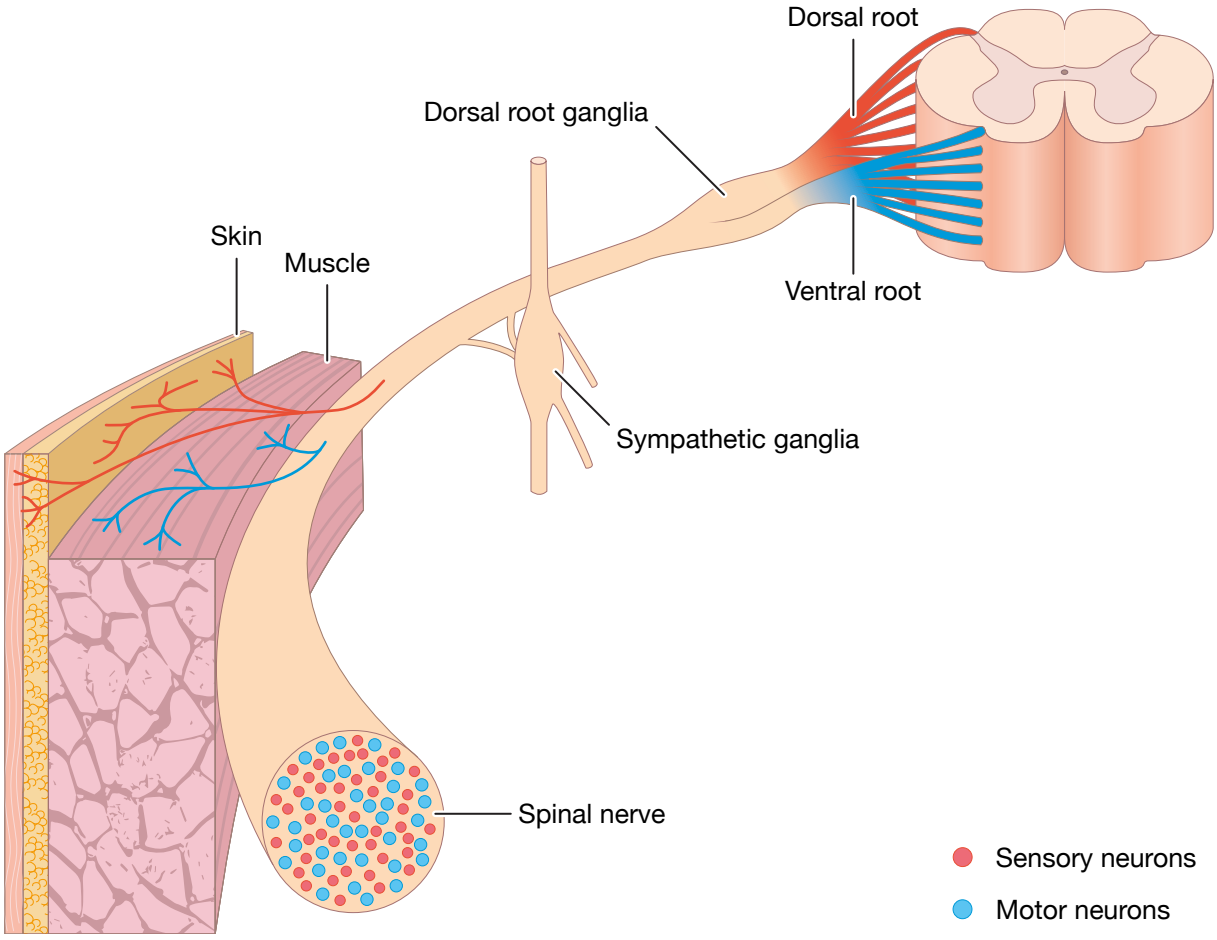

Figure 3. The spinal nerve. Thirty-four pairs of nerves leave the spinal cord in mice to supply the skin and the muscles. Incoming sensory fibers (red) and outgoing motor fibers (blue) divide into spinal roots where the nerves connect to the spinal cord. The ventral roots contain only motor fibers and the dorsal roots contain only sensory fibers. Adapted from *Neuroscience, Exploring the Brain, Fourth Edition* (2016).

bodies are located in the anterior horn of the brainstem and spinal cord, but their axons exit through the ventral roots to extend in the PNS (Stifani, 2014). They receive glutamatergic input from upper MN, whose cell bodies are located in the pre- and primary motor regions of the cerebral cortex. Somatic sensory neurons (SN) are pseudo-unipolar neurons whose cell bodies are located outside the spinal cord, in dorsal root ganglia (DRG). They have one axonal branch that reaches the periphery to connect its targets, and another branch that projects into the spinal cord and forms synapses with second-order neurons in the grey matter. Notably, SN do not form synapses with one another within the DRG (Pannese, 2010).

The ANS innervates glands, smooth muscle and cardiac muscle (Figure 4). Thus, it targets almost every organ in the body. It coordinates vegetative functions such as the cardiac rhythm, arteries and intestines contraction and relaxation, and the secretory function of various glands. It includes the sympathetic and parasympathetic divisions, which have antagonistic actions. The sympathetic division mobilizes the body in stressful situations (physical activity, fear or anger) by increasing the heart and respiratory rate, or the blood flow to skeletal muscles. On the contrary, the parasympathetic division acts mainly in a resting situation to reduce energy consumption while maintaining vital functions. Contrary to lower somatic motor neurons, the cellular bodies of all lower autonomic neurons are clustered outside the CNS in autonomic ganglia and are called post-ganglionic neurons. They are driven by pre-ganglionic neurons, whose cell bodies are within the CNS and which send their axons through the ventral roots. Sympathetic ganglia are either in the sympathetic chain, which lies next to the spinal column, or within collateral ganglia in the abdominal cavity. Parasympathetic ganglia are typically

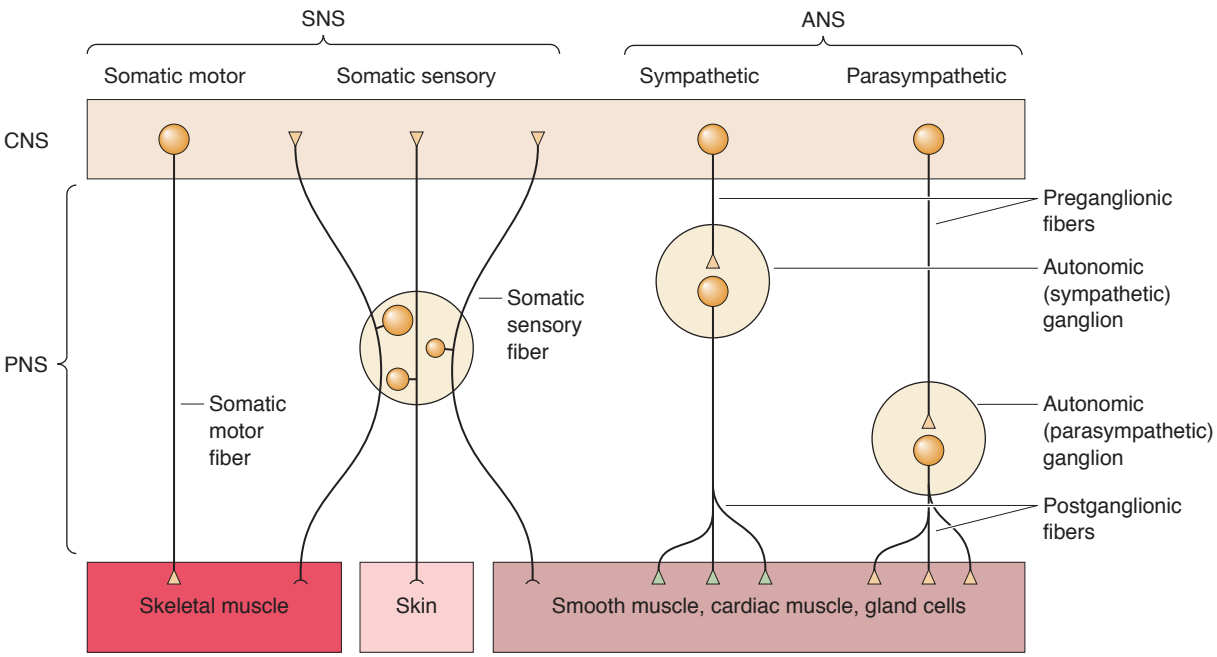

Figure 4. Organisation of the peripheral nervous system. Lower spinal somatic motor neurons are in the ventral horn control skeletal muscle. Peripheral sensory neurons, whose cell bodies are in dorsal root ganglia, innervate skeletal muscle, skin and viscerae. Visceral functions depend on the sympathetic and parasympathetic divisions of the ANS, whose lower motor neurons are in autonomic ganglia. Adapted from *Neuroscience, Exploring the Brain, Fourth Edition* (2016).

located close to, on, or in their target organ. In the remainder of my introduction, I will focus on the structure, function and development of the SNS.

In the adult PNS, there are only two types of glial cells. Schwann cells (SC), which can be myelinating or non-myelinating, provide support to peripheral axons. Glial satellite cells wrap around the cellular bodies of sensory, sympathetic and para-sympathetic neurons. Similarly to astrocytes in the CNS, they supply nutrients to neurons and regulate their micro-environment. I will further discuss their properties later in my introduction.

1.2.Neuronal diversity in the peripheral nervous system

1.2.1. Somatic sensory neurons

The somatic sensory system is responsible for the senses other than seeing, hearing, tasting, smelling and balance. They are three main somatic senses: touch, pain and body position. Contrary to the other systems, its receptors are disseminated through the body. SN are a very diverse population, and a combination of morphological, molecular and functional properties are used to characterize each type (Figure 5). SN can be classified morphologically according to their soma size, axon diameter, degree of myelination and spinal cord projections (Bear et al., 2016; Lallemend and Ernfors, 2012). Aα SN have large cell bodies and thick heavily myelinated axons with the fastest conduction velocities (80–120 m.s-1). Aβ SN have medium cell bodies and myelinated axons with fast conduction velocities (35–75 m.s-1). Aδ SN have small cell bodies and lightly myelinated processes with intermediate conduction velocities (5–30 m.s-1). Finally, C-type SN have the smallest cell bodies and thin unmyelinated axons with slow conduction velocities (0.2–2 m/s). SN form unmyelinated nerve endings with specific ion channels, and depending on their stimuli they can be can classified as mechano-, proprio- or nociceptors. Aα (or type I) SN are proprioceptors of skeletal muscle, responsible for the sense of body position. Aβ and a subset of Aδ and C fibers are low-threshold mechanoreceptors (LTMR) of the skin, responsible for the sense of light-touch. Most Aδ and C SN are high-

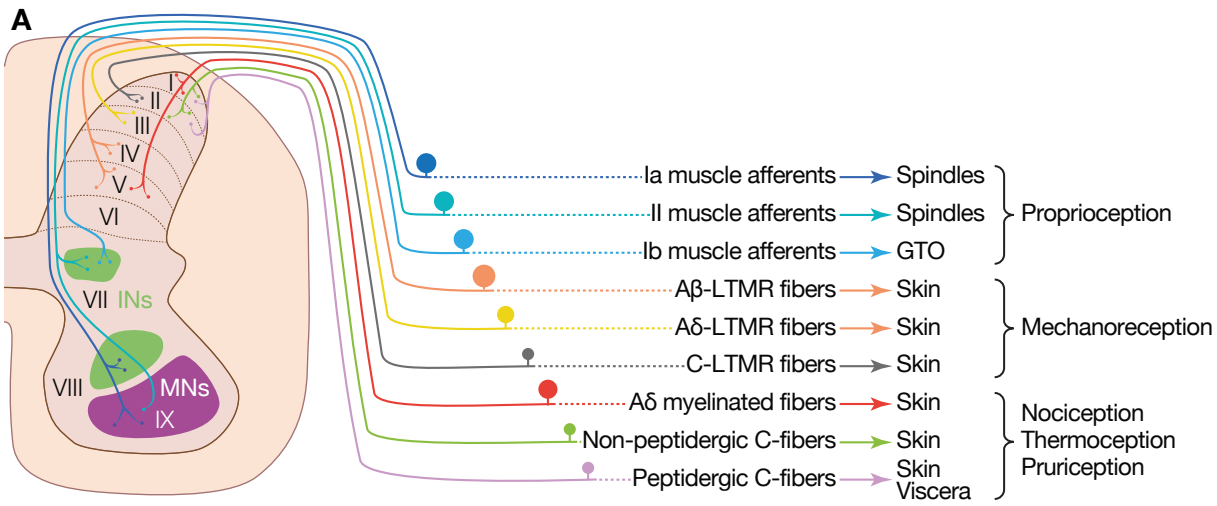

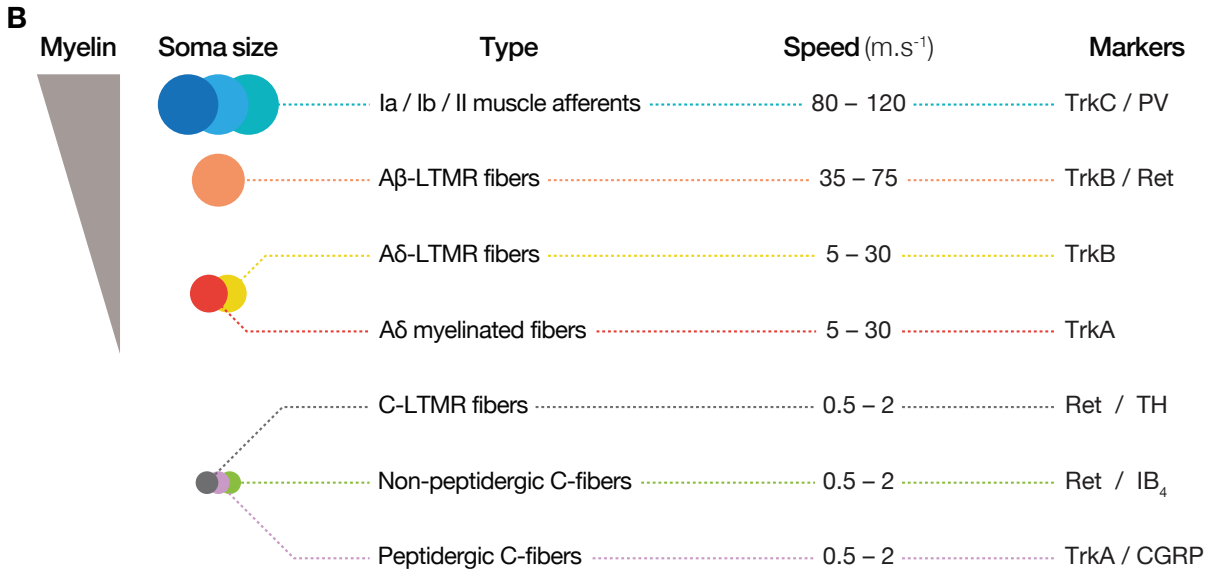

Figure 5. Different types of sensory neurons. (**A**) Central termination patterns of different classes of DRG neuron. The group Ia and II afferents that innervate muscle spindles in the periphery project into the ventral spinal cord to connect motor neurons directly. Group Ib afferents,which innervate golgi tendon organs, as well as group II afferents, connect interneurons at the intermediate zone of the spinal cord, whereas group Ia afferents terminate more ventrally. The C-, Aδ- and Aβ-low-threshold mechanoreceptors (LTMR) project to the dorsal horn, where they occupy distinct but partially overlapping laminae. Hence, C-LTMR endings terminate in lamina IIi and overlap with the Aδ-LTMR fibers that end partly within lamina IIi and mainly in lamina III. The Aβ-LTMR fibers terminate in laminae III through V. The Aδ myelinated fibers innervate laminae I and V and peptidergic and non-peptidergic neurons, laminae I and II. Nociceptive, thermoceptive and pruriceptive neurons are either unmyelinated (C-fiber) or lightly myelinated (Aδ) sensory neurons. Peripherally, all types except types Ia, Ib and II afferents, innervate the skin and, unlike peptidergic neurons, non-peptidergic neurons terminate only in cutaneous fields and do not contribute to deep innervation. (**B**) Sensory neurons can be classified by their soma size and/or axon diameter. Type Ia/b, II and Aβ fibers are highly myelinated, while Aδ fibers are lightly myelinated, with lower conduction velocities. Sensory neurons can also be classified by their expression of different molecular markers, such as TrkA, TrkB, TrkC, Ret, parvalbumin (PV), tyrosine hydroxylase (TH) or isolectin-B4 (IB4). Adapted from Lallemend and Ernfors (2012), Le Pichon and Chesler (2014) and *Neuroscience, Exploring the Brain, Fourth Edition* (2016).

threshold mechanoreceptors (HTMR), thermal or chemical nociceptors. They extend free nerve endings (FNE) in the skin and most organs, with the notable exception of the brain. Because Aδ and C fibers have different conduction velocities, nociception first produces a fast and sharp pain (Aδ) followed by a duller and longer lasting second pain (C). Finally, SN can be classified molecularly by their expression of neurotrophic factors receptors (Lai et al., 2016; Lallemend and Ernfors, 2012; Le Pichon and Chesler, 2014). Tropomyosin-receptor-kinase A (TrkA), TrkB, TrkC and the receptor tyrosine kinase Ret are receptors for the neurotrophins NGF (nerve growth factor), BDNF (brain-derived neurotrophic factor), NT3 (neurotrophin-3) and GDNF (glial cell-derived neurotrophic factor) family ligands respectively (Bourane et al., 2009; Gascon et al., 2010; Luo et al., 2009; Marmigère and Ernfors, 2007). Their expression is crucial for SN target selection, survival and proper differentiation. Large diameter proprioceptive SN express TrkC, while LTMR express TrkB and/or Ret and nociceptive SN express TrkA or Ret (Averill et al., 1995; Lallemend and Ernfors, 2012).

1.2.2. Motor neurons and proprioceptive innervation

Motor neurons

The SNS controls skeletal muscle and is responsible for voluntary movements. Such movements need to be extremely precise, requiring a fine sense of each muscle's position, also known as proprioception. Each skeletal muscle is formed by hundreds of muscle fibers, enclosed in a collagen sheath that forms, at its extremities, the tendons which connect it to the bones. As their functions need to be exerted in a coordinated manner, lower somatic MN are spatially grouped into columns and pools (Dasen, 2009; Kanning et al., 2010). They are grouped in columns along the anterior-posterior axis, that each have specific molecular profiles (Dasen, 2009; Romanes, 1951). Within a given column, the group of MN that innervate a single skeletal muscle is defined as a motor pool (Dasen, 2009; Kanning et al., 2010; Stifani, 2014). A motor unit is composed of a single MN and all the muscle fibers it innervates. There are three kinds of MN defined by the muscle fiber type they innervate: alpha (α), gamma (γ) and beta (β) MN (Hunt and Kuffler, 1951; Kuffler et al., 1951). α-MN only innervate extrafusal fibers, located outside the muscle spindle, and are responsible for muscle contraction (Figure 6). γ-MN innervate the intrafusal muscle fibers at the two ends of the muscle spindle (Burke et al., 1977; Westbury, 1982). During muscle contraction, their co-activation induces a retraction of its two poles, keeping the spindle taut which allows the continuous firing of alpha MN. β-MN are smaller and less abundant than the other MN subtypes (Stifani, 2014). They innervate both intra and extrafusal fibers, and mostly modulate the activity of sensory neurons. α-MN receive input from three sources: motor input from the upper MN that is the basis for the initiation and control of voluntary movement, sensory input from the proprioceptive neurons and excitatory or inhibitory input from interneurons. The identity of these different MN subtypes of motor neurons is characterized by the position of their cellular bodies both on the antero-posterior

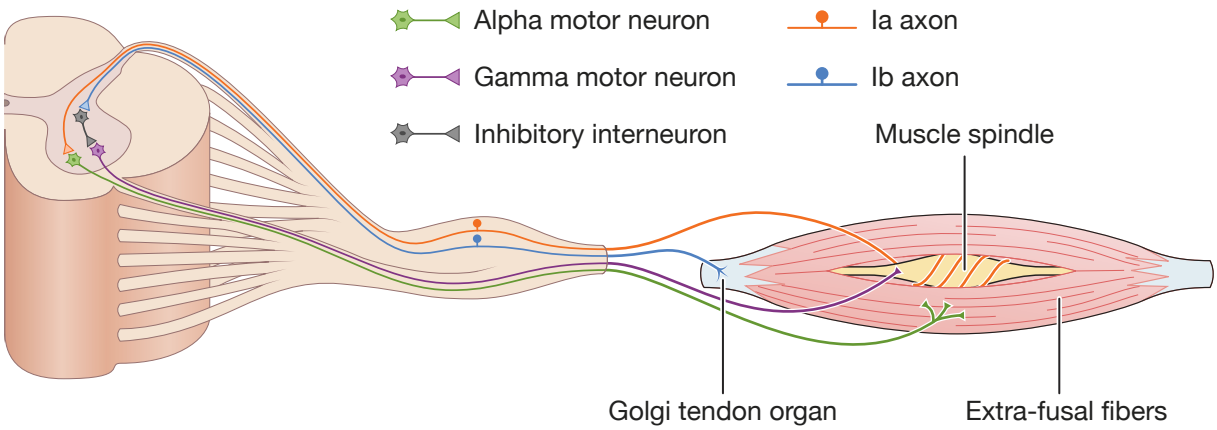

Figure 6 Muscle innervation. Type Ia and Ib SN provide the proprioceptive input from skeletal muscle. Ia fibers innervate the muscle spindle, which is a strech detector that informs of the muscle length. Ib fibers innervate the Golgi tendon organs, which monitor muscle tension. Ia SN project in the ventral horn and made direct contact with alpha-MN. Ib SN connect interneurons in the intermediate zone. Alpha-MN innervate extrafusal muscle fibers and are responsible for muscle contraction. Gamma-MN innevate contractile fibers within the muscle spindle, in order to keep it taut during contraction. Together these neurons form mono- or poly-synaptic arc reflexes that are necessary for proper muscle contraction. Adapted from *Neuroscience, Exploring the Brain, Fourth Edition* (2016).

and dorso-ventral axis, and by the specific expression of homeo-domain transcription factors of the LIM family (Kanning et al., 2010; Stifani, 2014).

Proprioception

Each muscle provides two kinds of proprioceptive input: length and tension (Figure 6). The muscle spindle monitors muscle length and is formed by several types of specialized muscle fibers contained in a fibrous capsule, deep within the muscle. It is innervated in its noncontractile equatorial region by sensory Ia neurons that wrap their nerve endings around its fibers (Brown et al., 1967; Proske and Gandevia, 2012). When stretched, their mechanosensitive ion channels are activated and action potentials can be triggered. The Golgi tendon organs are located at the muscle-tendon junction, and monitors muscle tension (Bianconi and van der Meulen, 1963; Proske and Gandevia, 2012). They are innervated by thin axon branches of sensory Ib neurons that entwine among the coils of collagen fibrils. During muscle contraction, the tension increase straightens them and make them squeeze the Ib axons, which triggers action potentials. Proprioceptive neurons enter through the dorsal root to make projections into the intermediate and ventral spinal cord. Their information is relayed to the brain through the dorsal column medial lemniscus pathway. However, they also connect motor neurons directly or indirectly through inhibitory or excitatory interneurons, forming mono- or polysynaptic reflex arcs that are necessary for proper muscle contraction (Bear et al., 2016).

1.2.3. Cutaneous sensory innervation

The skin protects the body from the external environment and helps maintain body homeostasis by regulating its temperature and fluids evaporation. But it is also where the sense of touch begins, making it the largest sensory organ in the body (Abraira and Ginty, 2013; Rice and Albrecht, 2008; Zimmerman et al., 2014). It is composed of an outer layer called epidermis and an inner layer called dermis (Figure 7). The subcutaneous tissue, called hypodermis, attaches it to the underlying bones and muscle and supplies it with blood vessels and nerves. There are two types of skin, hairy and glabrous (hairless). LTMR that innervate the skin are distinguished by the cutaneous end organs they associate with: Pacinian corpuscles, Meissner corpuscles (only in glabrous skin), Ruffini endings, Merkel's discs and hair follicles. Each have their specific stimuli and properties. Pacinian corpuscles are onion-like structures composed of multiple, fairly loose concentric layers of Schwann cell lamellae enclosed within a dense outer capsule. Meissner's corpuscles are supplied by LTMR that terminate as stacks of multiple disks alternating with terminal Schwann cells in the upper dermis of glabrous skin. Both detect vibrations of different frequencies. Ruffini endings are stretch receptor located deep in the dermis. Merkel cells are located in the epidermis, and they actively participate to mechano-transduction (Woo et al., 2014). Lanceolate endings are elongated flattened blade-

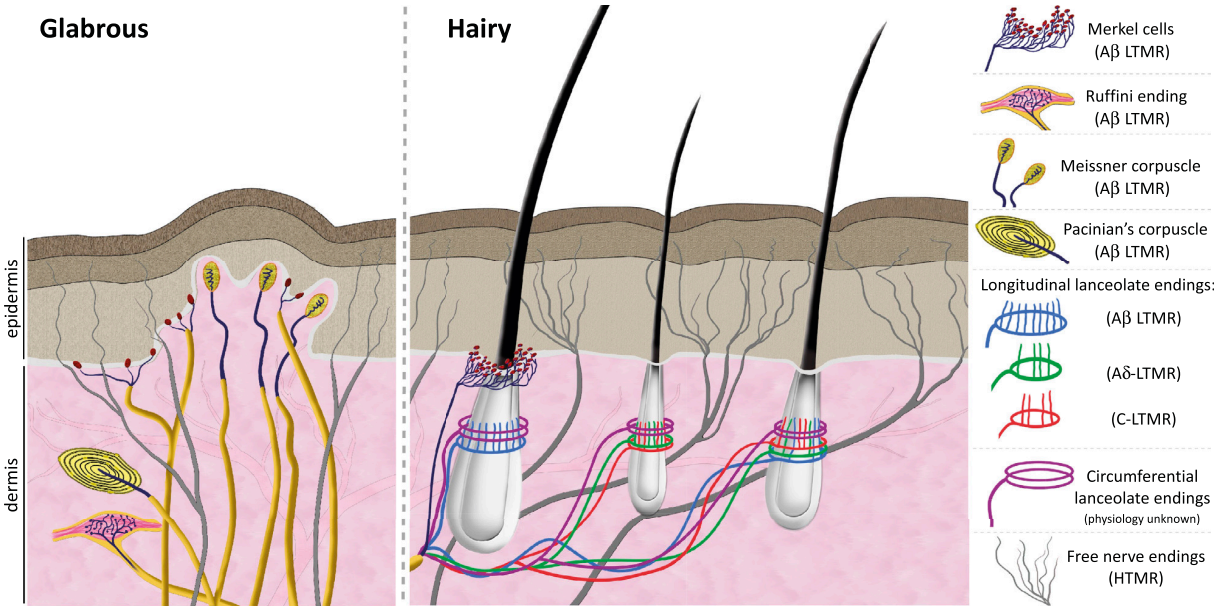

Figure 7. The cutaneous innervation. Innocuous touch information is processed by both glabrous hairless and hairy skin. (**A**) In glabrous skin, innocuous touch is mediated by four types of mechanoreceptors. The Merkel cell-neurite complex is in the basal layer of the epidermis and consists of clusters of Merkel cells making synapse-like associations with enlarged nerve terminals branching from a single Aβ fiber. This provides acute spatial images of tactile stimuli. Meissner corpuscles are localized in the dermal papillae and consist of horizontal lamellar cells embedded in connective tissue. They detect movement across the skin. Ruffini endings are localized deep in the dermis and are morphologically similar to the Golgi tendon organ, a large and thin spindle-shaped cylinder composed of layers of perineural tissue. Their exact role remains debated. Lastly, Pacinian corpuscles are located in the dermis of glabrous skin where their characteristic onion-shaped lamellar cells encapsulate a single Aβ ending. They detect high-frequency vibration. (**B**) In hairy skin, tactile stimuli are transduced through hair follicles, some associated with touch domes at the apex and Aβ-LTMR longitudinal lanceolate endings at the base, others triply innervated by C- LTMR, Aδ-LTMR, with or without Aβ-LTMR longitudinal lanceolate endings. In addition, all three hair follicle types are innervated by circumferential lanceolate endings whose physiological properties remain unknown. Noxious touch is detected by free nerve endings found in the epidermis of both glabrous and hairy skin and are characterized by both Aδ- and C-HTMR responses. Adapted from and Abraira and Ginty (2013).

like structures that are typically oriented parallel to the long axis of the hair follicles. They function as velocity detectors for the deformation of hair. Aδ and C fibers form free nerve endings (FNE) in the skin, mostly in the epidermis and around hair follicles.

1.3.Glial diversity within the peripheral nervous system

1.3.1. Schwann cells

All peripheral axons are covered by glial cells called Schwann cells (SC), named after physiologist Theodor Schwann who first described them (Schwann, 1839). SC can be myelinating or non-myelinating (Figure 8). Both insulate peripheral axons from each other and provide key metabolic support to maintain axonal integrity (Nave, 2010; Viader et al., 2011). Both SC types derive from a common progenitor called SC precursor (SCP) via successive steps of embryonic development, but retain an unusual plasticity (Jessen and Mirsky, 2005; Jessen et al., 2015). Indeed, seminal studies have shown that when nerve segments containing mostly myelinating SC are grafted into a largely unmyelinated nerve, these SC do not myelinate (Aguayo et al., 1976b). Conversely, non-myelinating SC are capable of generating myelin

when sections of predominately unmyelinated nerve are grafted into a primarily myelinated nerve (Aguayo et al., 1976a). More recently, it has been shown that this plasticity is of critical importance after a peripheral nerve injury. After an injury, SC dedifferentiate back into their immature stage before differentiating into a specific repair SC, that promote and guide axon regrowth in coordination with fibroblasts, macrophages and blood vessels (Cattin et al., 2015; Parrinello et al., 2010).

Myelinating Schwann cells

Myelinating SC wrap around and myelinate a single large axon (Salzer, 2015). They are radially and longitudinally polarized into distinct membrane domains with specific properties (Figure 8). Longitudinally, they are divided into nodal, paranodal and juxtaparanodal compartments near the Ranvier nodes, and the internodal compartment in between (Arroyo and Scherer, 2000; Ozcelik et al., 2010; Pereira et al., 2012; Salzer, 2003). Radially, they are defined by their inner (adaxonal) and outer (abaxonal) membrane surfaces. The adaxonal membrane is separated from the axon by a 15 nm gap, the peri-axonal space. It is enriched in receptors and adhesion molecules, such as MAG proteins (Myelin-Associated Glyco-protein) to interact with the axon. The abaxonal membrane is adjacent to the basal lamina (Figure 8). The myelin sheath membranes are located between these two domains. Their architecture, function and integrity are based on interactions between the axon and SC (heterotypic), and between the membranes of the same SC (homotypic). They result from the presence of different types of adhesion, scaffolding and cytoskeleton proteins. The internode myelin sheath is mostly compact, due to the adhesion of the successive membrane layers that form homotypic contacts. Myelin has a high lipid content and is enriched in cholesterol, which plays an important role in its assembly and insulating properties (Saher et al., 2009). Compact myelin is also enriched in adhesion molecules, the most abundant being P0, a transmembrane adhesion molecule which promotes compaction via homophilic adhesion of its extracellular domain (Arroyo and Scherer, 2000). Compact myelin is interrupted along the internode by the Schmidt-Lanterman incisures, which are stacks of non-compacted myelin that spiral around the axon to ensure rapid communication between the ad- and abaxonal regions and myelin maintenance (Figure 8). The nodal, paranodal and juxtaparanodal compartments have non-compact myelin and contain particular sets of ion channels, adhesion molecules and cytoplasmic proteins. The Ranvier node is a specialized axonal region, enriched in voltage-gated sodium channels. The paranodal loops correspond to the lateral edges of the myelin sheath, that act as a strong diffusion barrier through axoglial junctions (Poliak and Peles, 2003). The juxtaparanodal compartment is an intermediate region between the paranode and the internode. This area is characterized by an enrichment in specific potassium channels (Peles and Salzer, 2000; Salzer, 2003).

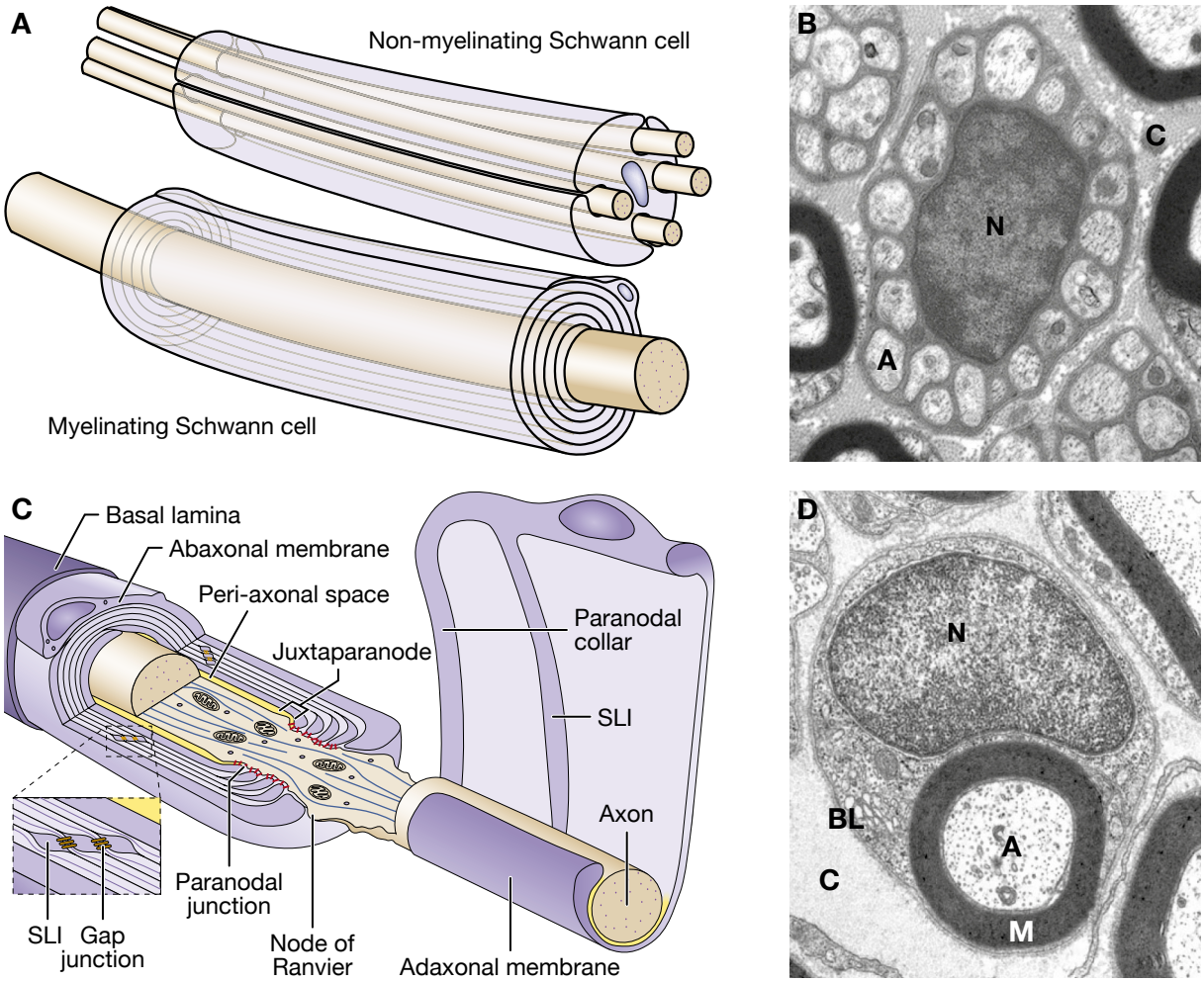

Figure 8. Schwann cells. (**A**) The most common type of non-myelinating Schwann cells (SC) are Remak SC, which ensheath multiple small caliber axons. Myelinating SC ensheath in a 1:1 ratio a large caliber axon. (**B**) Electron micrograph of transverse sections of adult mouse sural nerve (10 weeks of age). Magnification 25 000X. Typical Remak bundle in which each unmyelinated axon (A) is separated by SC cytoplasm and are of similar sizes around the nucleus (N). Collagen (C) fibrils are abundant in the peri-neural space. (**C**) Hypothetical drawing depicting a myelinated axon with the unrolled sheath of a SC shown on the right. Compacted myelin (pale purple) serves as an insulator that inevitably deprives the axoplasm (brown) of free access to nutrients in the extracellular milieu, except for at widely spaced short gaps (nodes of Ranvier). Non-compacted myelin defines a channel system (purple) that is continuous with the glial cytoplasm and brings cellular metabolites close to the periaxonal space (yellow). Schmidt-Lanterman incisures (SLI) are stacks of non-compacted myelin that spiral around the axon to ensure rapid communication between the ad- and abaxonal regions. They are linked by gap junctions when stacked. Around the SC is the basal lamina (dark purple). (**D**) Electron micrograph of a myelinating SC from a 21-day-old rat sciatic nerve. Magnification 25 000X. Myelinating (M) SC ensheath a single axon (A) and are surrounded by a basal lamina (BL). Collagen (C) fibrils are abundant in the peri-neural space. Adapted from Nave and Schwab (2005) and Nave (2010). EM pictures from Fricker et al. (2009) and Kidd, Ohno and Trapp (2013).

Non-myelinating Schwann cells

In peripheral nerves, non-myelinating SC, also called Remak SC (RSC), ensheath multiple small-caliber axons in "Remak bundles" (Figure 8). RSC are not as well characterized as their myelinating counterpart (Harty and Monk, 2017). They are the most common type of non-myelinating SC, but several others have been described at the peripheral nerve endings. For instance, perisynaptic SC cap motor nerve terminals at the neuromuscular junction (NMJ) (Auld and Robitaille, 2003; Balice-Gordon, 1996; Ko and Robitaille, 2015). They regulate the plasticity of the NMJ and modulate synaptic transmission through their specific expression

of ion channels and neurotransmitter receptors, and bidirectional interactions via trophic-related factors (Auld and Robitaille, 2003; Ko and Robitaille, 2015). In addition to RSC, several types of terminal non-myelinating SC have been described in the skin. Hair follicle-associated glia unsheathes lanceolate nerve endings, and is involved in the maintenance of the lanceolate complex (Li and Ginty, 2014). It could also modulate the activity of SN endings through calcium signalling (Takahashi-Iwanaga, 2005). Sub-epidermal glia is associated with nociceptive FNE, which contrary to what their name suggest are covered by terminal SC. Little is known about these cells beyond electron microscopy studies that revealed a peculiar morphology, with numerous cytoplasmic protrusions covering axons at the dermis/epidermis boundary (Cauna, 1973). Similarities with the morphology of perisynaptic SC questions whether these cells could also play a modulating role in nociception, but their exact function remains unknown (Reinisch and Tschachler, 2012). More recently, our lab has shown that these cell are the likely candidate for the cellular origin of cutaneous neurofibromas in neurofibromatosis type 1 (NF1) disease (Radomska et al., 2019). Finally, other terminal SC are present within Meissner or Pacinian corpuscles, and the arrector pili muscle. Although these cells are likely to have specific molecular properties and functions, they still remain unknown.

1.3.2. Glial satellite cells

Satellite glial cells (SGC) are located in the PNS sensory and autonomic ganglia (Pannese, 2010). They tightly wrap around the neuronal soma, with only a 20 nm gap between them (Figure 9). In mice, 4 to 10 SGC ensheath an individual soma depending on its size, and form a distinct functional unit connected by Gap junctions (Hanani, 2005; Ledda et al., 2004). SGC express distinct glial markers such as S100 or Vimentin, pointing to an heterogeneity that may depend on the size and function of the SN they are associated with (Nascimento et al., 2008). SGC have similar functions to astrocytes, providing support to and modulating the activity of SN. Indeed, SGC express various neurotransmitter receptors, such as the purinergic P2 receptors, and can release neuroactive substances such as ATP (Gonçalves et al., 2018;

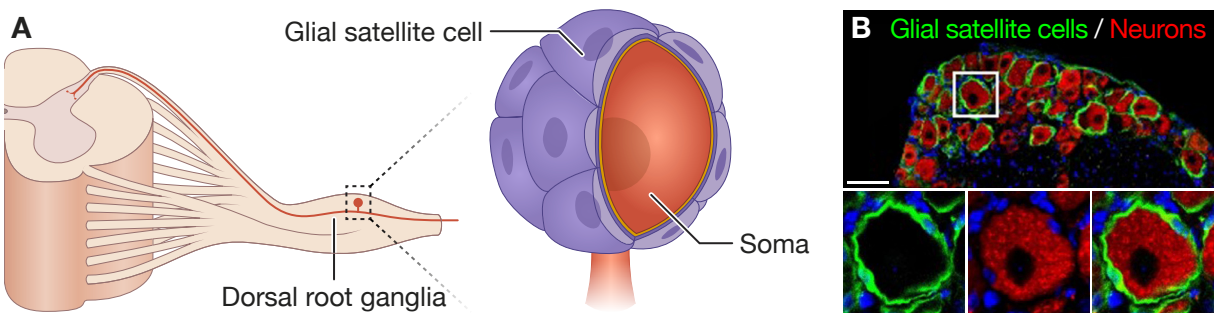

Figure 9. Glial satellite cells. (A) The soma of sensory neurons are located in the DRG. Each pseudo-unipolar neuron branches off with a peripheral process that connects with target tissues in the periphery and a central process that projects in the spinal cord dorsal horn. Its soma is covered by satellite glial cells (SGC). (B) Immunostaining of a mouse DRG section stained against the SGC marker glutamine synthetase in green and the purinoreceptor P2X7 in red, which is expressed in sensory neurons. Scale bar 50 µm. Adapted from Gonçalves et al. (2018). Immunostaining from Jager (2016).

Huang et al., 2013). In response to neural injury they can enter an « activated » stage, which they can transmit to other SCG through calcium signalling (Suadicani et al., 2010). Through this process, SGC help recruit other SN for the amplified response and may be implicated in the development of chronic pain (Hanani, 2012). Finally, a subpopulation of SGC might correspond to multipotent glial progenitors. In culture, they form self-renewing spheres, and generate SC, astrocytes and oligodendrocytes (Fex Svenningsen et al., 2004).

1.3.3. Endo-, epi- and perineurial fibroblasts

All peripheral nerves are protected by three fibroblastic layers: the epi-, peri- and endoneurium (Figure 10). Multiple axons and their surrounding SC lie within the endoneurium, which consists of extracellular matrix components, such as collagen, secreted by endoneurial fibroblasts (Kucenas, 2015). They are assembled in fascicles ensheathed by the perineurium, which is formed by highly compacted concentric rings of perineurial fibroblasts connected via tight junctions. They are a part of the blood-nerve barrier, which protects the interior of the nerve (Akert et al., 1976; Shanthaveerappa and Bourne, 1963). Finally, fascicles are bundled together by the epineurium into a single nerve structure. It is made of collagen secreted by epineurial fibroblasts and adipocytes. Peripheral nerves are highly vascularized, with blood vessels located both in the endo- and epineurium. Even though they play a key role in the architecture and homeostasis of the peripheral nerve, epi-, peri- and endoneurial fibroblasts are not classified as glial cells. Few endoneurial fibroblasts molecular markers have been described such as Platelet-derived growth factor receptor alpha (PDGFRα) or Thy1, and they

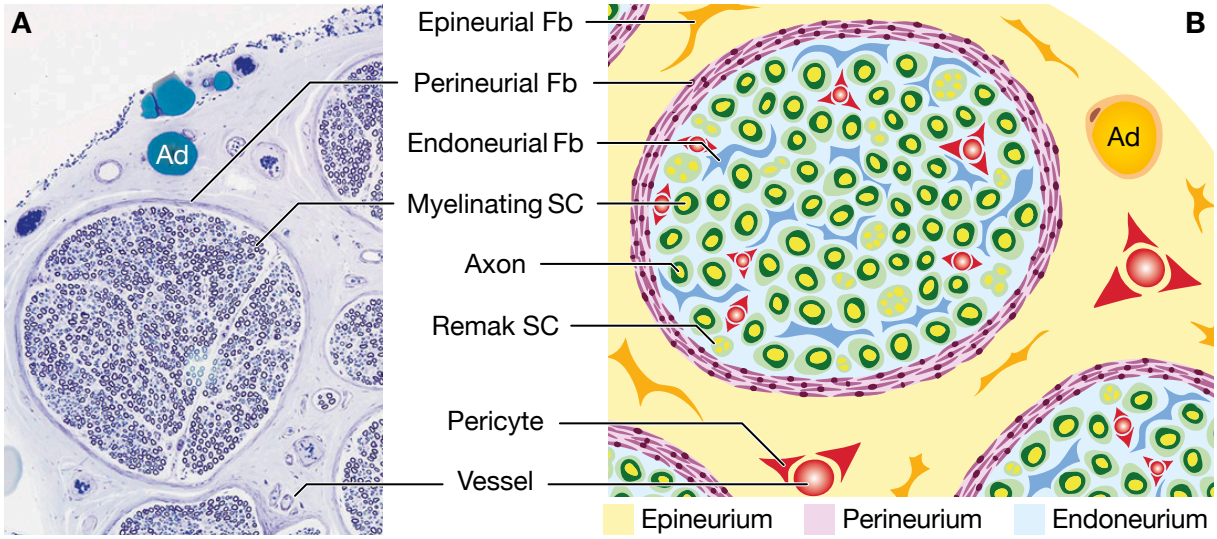

Figure 10. Peripheral nerve anatomy. (**A**) Toluidine blue-stained semithin cross section of an entire human sural nerve, composed of ten fascicles ensheathed by a thin perineurium, each surrounded by the epineurium. The large green epineurial bodies are adipocytes (Ad). (**B**) Perineurial cells form a sheath around the nerve that separates the endoneurial environment from the epineurial environment. Within the endoneurium, there are SC that myelinate single axons, non-myelinating SC that are associated with multiple axons, endoneurial fibroblasts and pericytes that surround small blood vessels. Perineurial cells are distinguished based on their position and their characteristic flattened morphology. Schwann cells are distinguished by their association with axons, their expression of glial markers and their basal lamina. Endoneurial fibroblasts lack a basal lamina, often have long interdigitating processes, are not associated with axons. Adapted from Joseph et al. (2004). Sural nerve section from *Biopsy Diagnosis of Peripheral Neuropathy, Second Edition* (2015).

don’t express SC markers such as S100β (Joseph et al., 2004; Richard et al., 2014). They synthesize collagen, which is necessary for SC to generate their basal lamina, they also play a role in myelin phagocytosis, inflammatory response and nerve regeneration (Parrinello et al., 2010; Richard et al., 2012). More recently, it has been shown that they may be mesenchymal precursor cells with the ability to regenerate tissues (Carr et al., 2019).

2. Development of the peripheral nervous system

2.1. Peripheral nervous system stem cells

2.1.1. What is a stem cell?

A stem cell is a cell that can replicate itself (self-renew) and has the ability (potency) to differentiate into multiple cell types, either directly or through terminal divisions (Gilbert, 2016; Siminovitch et al., 1963). When they are not quiescent, stem cells face at each division a choice between self-renewal and generating lineage-committed progenitor cells which is ensured by asymmetrical division (Figure 11). Asymmetrical division can either be at the single cell level, with one stem cell dividing into a stem cell and a progenitor cell, or at the population level, with subsets dividing symmetrically into either stem or progenitor cells (Simons and Clevers, 2011). This choice is highly influenced by the interaction between stem cells and their environment, called niche. Overall, these participate to the subtle equilibrium necessary to maintain the stem cell pool. Stem cell potency is defined by the cell type diversity they generate *in vivo*. Hence, a cell able to generate a both embryonic and extra-embryonic lineages is considered as *totipotent*, and only embryonic lineage *pluripotent*. *Multipotent* stem cells, often called somatic stem cells, are restricted to cell types specific to the tissue they reside in. Finally, *unipotent* stem cells only generate one cell type.

2.1.2. Embryonic stem cells

Embryonic development is a complex process during which a single cell will give rise to an entire organism made up of hundreds of cell types. In mice embryos, blastomeres are totipotent until the 16-cell stage (Baker and Pera, 2018; Tarkowski et al., 2010). At the 32-cell stage, the morula cavitates into the blastocyst, which consists of a spherical layer of trophectoderm cells around a fluid-filled cavity called blastocoel, with a cluster of approximately 12 cells, called the inner cell mass (ICM), adhering to one side (Fleming, 1987). The ICM then develops into the epiblast and hypoblast, a layer of primitive endoderm that separates it from the blastocoel. The epiblast will generate all the embryonic cell types, whereas the trophectoderm and primitive endoderm will give rise to the extraembryonic structures (Stephenson et al., 2012). When cultured, ICM cells generate pluripotent embryonic stem cells (ESC) that can self-renew indefinitely in proper culture conditions (Evans and Kaufman, 1981; Evans, 2011; Martin, 1981; Thomson et al., 1998). Over the last 30 years, advances in

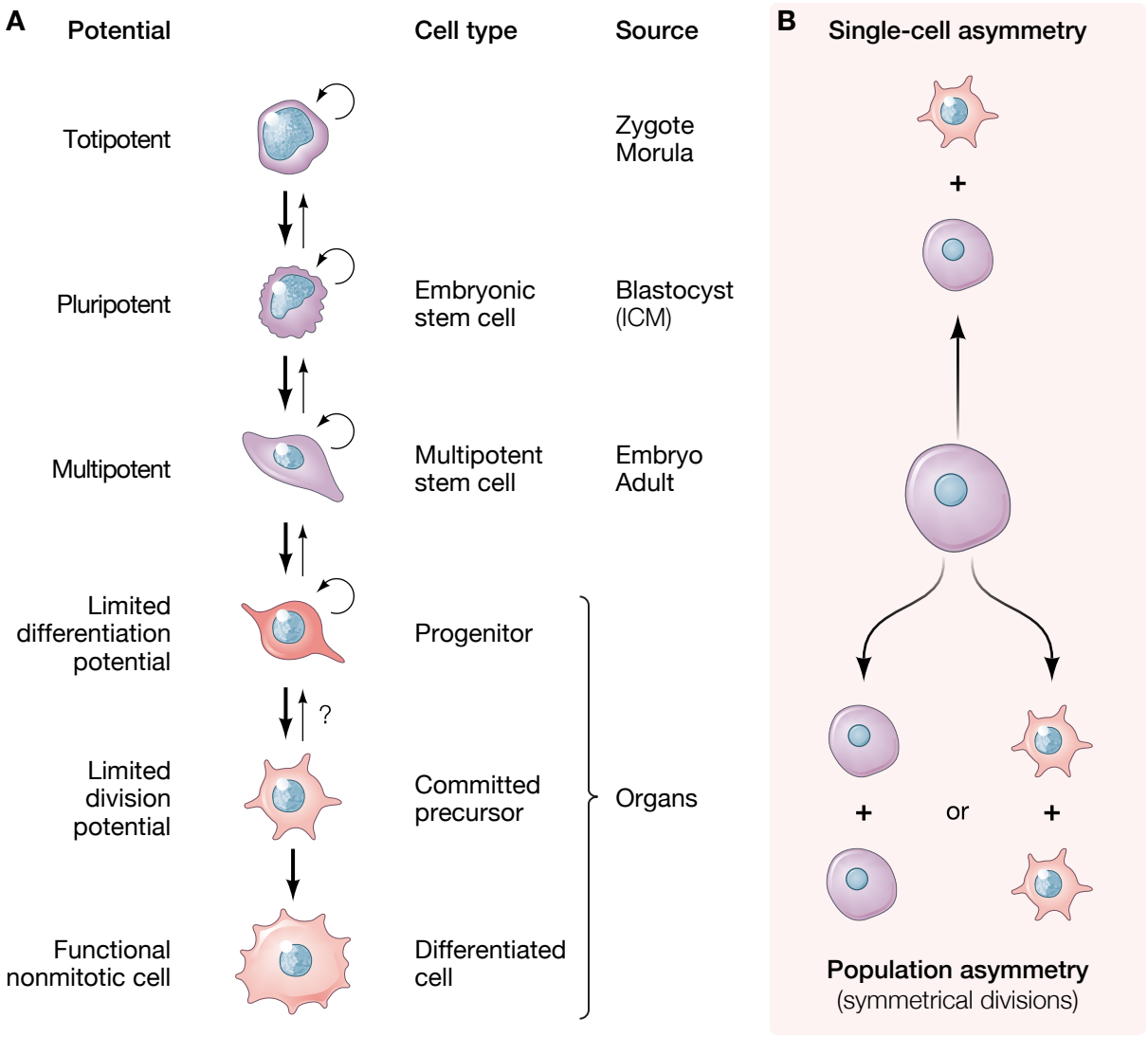

Figure 11. The stem cell concept. (**A**) The first defining stem cell property is their differentiation potential. Totipotent stem cells are capable of generating embryonic and extra-embryonic tissues, while pluripotent stem cells only embryonic. Multipotent stem cells that can generate several cell types exist in the embryo, an example being the neural crest, and in adult tissues (somatic stem cells). When differentiating, they can give rise to highly proliferative progenitors that will generate committed precursors which will finally differentiate in a nonmitotic functional cell. (**B**) The second defining stem cell property is their ability to self renew and give rise to committed cells through asymmetrical division. It can either take place at the single cell or at the population level, in which case there is a balance between groups of stem cells that either self renew or give rise to committed cells. Adapted from *Developmental Biology, Eleventh Edition* (2016).

developmental biology have provided important insights into ESC differentiation, with the identification of downstream multipotent stem cells committed to different lineages (Wu and Izpisua Belmonte, 2016). This has supported the development of protocols for the efficient *in vitro* generation of a wide diversity of cell types such as cardiomyocytes or neurons (Murry and Keller, 2008). Three transcription factors (Oct4, Nanog and Sox2) are necessary the ICM and epiblast to maintain their pluripotency (Shi and Jin, 2010). A decade ago, it was shown that retrovirus-mediated transfection of four transcription factors, Oct4, Sox2, c-Myc and Klf4 could induce the dedifferentiation of somatic cells into an ESC-like state (Takahashi and Yamanaka, 2006; Takahashi et al., 2007; Yu et al., 2007). The discovery of induced pluripotent stem cells (iPSC) opened a new field for stem cell research and cell therapies.

2.1.3. Multipotent stem cells in the adult peripheral nervous system

Somatic stem cells are essential for many adult tissues, both in normal conditions and during regeneration. Bone marrow transplantations in mice in the 1950s were the first demonstration supporting the existence of an adult hematopoietic stem cell at the origin of both lymphoid an myeloid lineages (Becker et al., 1963). Since then, adult somatic stem cells have been identified in most adult tissues including the brain, epidermis, hair follicles, muscle, and intestinal villi (Clevers and Watt, 2018; Goodell et al., 2015). Adult stem cells maintain their ability to self-renew and their multipotency on the long term. Each type is located in a tissue-specific stem cell niche that regulates their survival, self-renewal and differentiation potential (Simons and Clevers, 2011).

During embryonic development, the PNS derives from a population of multipotent stem cells called the neural crest (NC), which gives rise to a broad cell diversity. When entering their target tissues, most NC cells undergo progressive developmental restrictions. However, some instead retain their multipotency and form NC-derived stem cells in each tissue (NCSC) (Dupin and Sommer, 2012). Such NCSC have been described in the sciatic nerve, DRG and skin innervation (Bixby et al., 2002; Carr et al., 2019; Kruger et al., 2002; Morrison et al., 1999; Nagoshi et al., 2008; Wong et al., 2006). In proper conditions these cells can not only generate PNS cell types, but also other ecto- and mesodermic cell types. Somatic stem cells have a significant clinical potential for regenerative medicine, either as a putative source of cells for homologous transplantation or as a therapeutic target to improve tissue regeneration (Keller, 2005; Shevde, 2012).

2.2. The neural crest: key multipotent stem cells during development

2.2.1. The neural crest and advances in developmental biology

The neural crest (NC) is a key evolutionary acquisition of vertebrates (Gans and Glenn Northcutt, 1983; Glenn Northcutt, 2005; Sauka-Spengler et al., 2007). It was first described in the chick embryo by Wilhelm His as a strip of cells between the neural tube (NT) and dorsal ectoderm (His, 1868). It is a transient, multipotent and highly motile cell population that emerges from the dorsal portion of the NT, migrates towards the periphery and gives rise to numerous derivatives, such as peripheral neurons and glia, cartilage, bone and melanocytes (Le Douarin and Kalcheim, 1999). Almost fifty years ago, the development of "quail-chicken" grafts allowed to perform seminal discoveries in the NC field. It consisted in transplanting a quail embryo NT fragment into a chicken embryo before NC delamination, without altering its development nor inducing rejection. Hence, it allowed to trace quail cells and their derivatives thanks to their specific nuclear staining (Le Douarin and Kalcheim, 1999). Later, the development of dye injections or infection with a reporter-expressing virus allowed to follow single cells and their progeny during development. In mice, advances in genetic

manipulations were instrumental in developing the Cre-LoxP prospective cell-fate mapping system (Figure 12). It requires to cross two transgenic mice: one in which Cre recombinase expression is under the control of regulatory elements of a gene of interest; and one in which a Cre-inducible reporter gene, such as tandem dimeric tomato (tdTomato), is under the control of an ubiquitously active promoter such as Rosa26 (Madisen et al., 2010). When the gene of interest is expressed, it induces a Cre-mediated deletion of the STOP codon which switches on the reporter gene in the cell and all its derivatives. Several Cre-lines have been generated and used for NC cell-fate mapping: *HtPA-Cre* (*human tissue plasminogen activator*), *P0-Cre*, *Sox10-Cre* and *Wnt1-Cre* (Matsuoka et al., 2005; Pietri et al., 2003; Yamauchi et al., 1999). Genetic fate-mapping has allowed to successfully track NC derivatives during and beyond embryonic development to postnatal and adult stages.

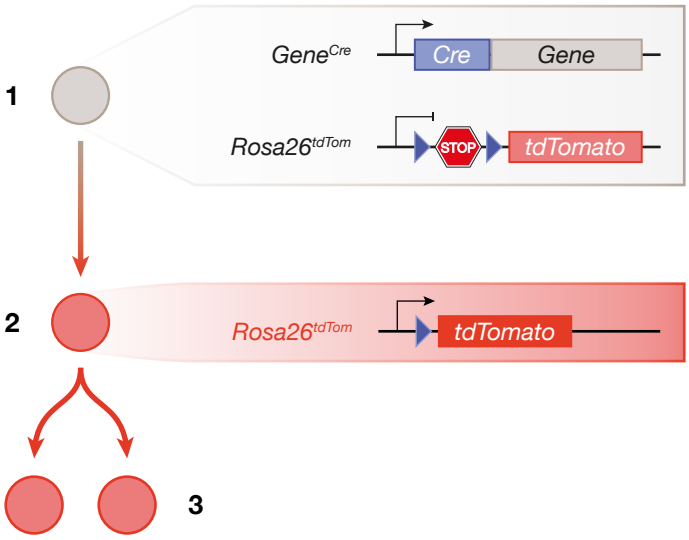

Figure 12. Cre-LoxP tracing system. The Cre-LoxP fate-mapping system requires to cross a mouse in which Cre recombinase expression is under the control of regulatory elements of a gene of interest, and one in which a Cre-inducible reporter gene such as tdTom is under an ubiquitously active promoter, such as Rosa26. Hence, when the gene of interest is expressed (1), Cre recombinase is expressed and activates the fluorescent reporter gene (2), which will make the cell, and all the cell that it will give rise to, fluorescent (3).

2.2.2. Neural crest specification and migration

After a specification phase during which they receive defining environmental cues (Figure 13), NC cells undergo an epithelial-to-mesenchymal transition (EMT) to exit the NT and migrate throughout the developing embryo along specific pathways. This process is subject to a fine spatial and temporal restriction. Indeed, the same transcription factor, patterning signal or guidance cue can have different, often opposite, effects at different times and/or sites.

Neural crest specification and delamination

NC specification begins during early gastrulation within the neural plate border (NPB) region, located between the future neural and epidermal domains (Figure 13). It is induced by a precise combination of Wingless-type MMTV integration (Wnt), bone morphogenetic protein (BMP), fibroblast growth factor (FGF), retinoic acid (RA) and Notch signals secreted by the ectoderm, the neuroepithelium and the underlying mesoderm (García-Castro et al., 2002; Groves and LaBonne, 2014; Milet and Monsoro-Burq, 2012). Its second step is the establishment of NC identity, defined by the expression of several key transcription factors such as Snail/Slug, Twist, FoxD3 and the SoxE genes that activate the EMT effector program (Khudyakov and Bronner-Fraser, 2009; Kos et al., 2001; Mayor and Theveneau, 2013; Simoes-

Costa and Bronner, 2015). It results from the concerted action of signalling pathways and medial NPB transcription factors such as Pax3/7, Msx1 and Zic1 (Grocott et al., 2012; Monsoro-Burq et al., 2005; Patthey et al., 2009). Then, NC cells undergo an EMT during which they detach from the neuroepithelium, lose their apicobasal polarity and modify their contacts with the ECM. The EMT effector program vary across the antero-posterior position and species, but the major common transcription factors are Snail/Slug, FoxD3 and Sip1 (Simoes-Costa and Bronner, 2015; Theveneau and Mayor, 2012). This process involves molecular switch between epithelial type 1 cadherins and type 2 cadherins, as well as the reorganization of the actin cytoskeleton that provides them particular adhesive and migratory properties (Szabó and Mayor, 2018; Taneyhill, 2008).

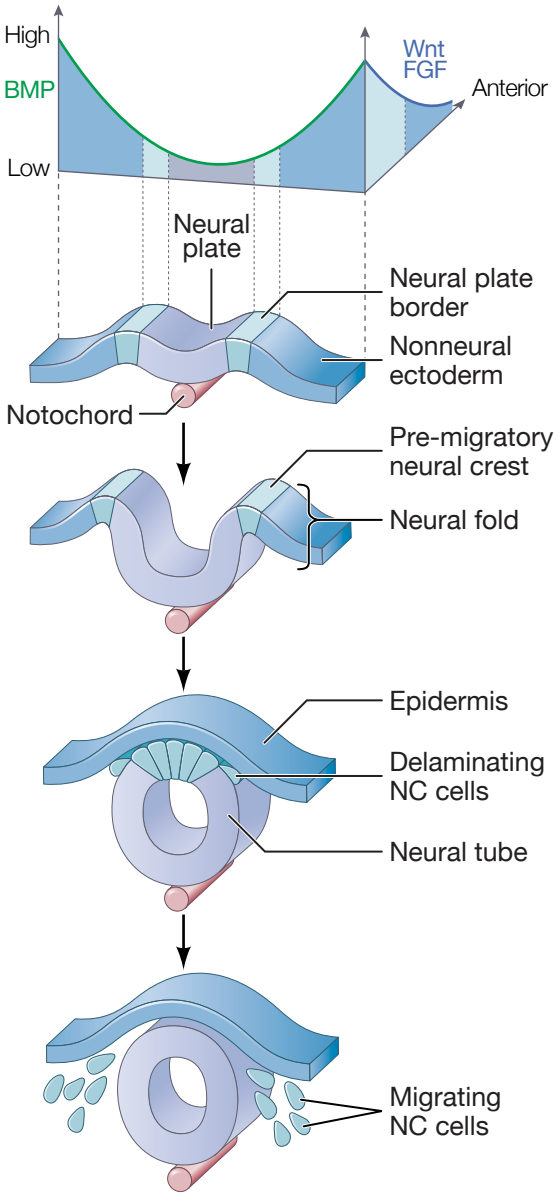

Figure 13. Neural crest development. First, neural crest (NC) cells are specified in the border plate region by a gradient of BMB, Wit and FGF signalling during early gastrulation. Then, when the neural tube (NT) folds, NC cells delaminate at the point of NT closure. Then, they migrate throughout the embryo to give rise to multiple cell types. Adapted from Developmental Biology, Eleventh Edition (2016).

Neural crest migration

After delamination, NC cells first migrate in the cephalic region between the epidermal and mesodermal layers as a continuous sheet, which subsequently splits into three streams. Next, trunk migration is initiated progressively along the antero-posterior axis in thin streams (Figure 14) that align as a chain with the somites (Le Douarin and Kalcheim, 1999). NC migration relies on permissive ECM molecules (fibronectin, laminins and some collagens) that line migration routes and is shaped by multiple negative and positive guidance cues (Harris and Erickson, 2007; Szabó and Mayor, 2018; Theveneau and Mayor, 2012). Three major receptor families are involved, and can have an attractive or repulsive effect with their ligands depending on the expressed subtype: neuropilin (Nrp) receptors to class 3 semaphorins (Sema3); tyrosine kinase-active erythropoietin-producing human hepatocellular (Eph) receptors to ephrins; and G-protein coupled endothelin (Edn) receptor B (EdnrB). In the head, Nrp2-expressing NC cells avoid Sema3A/D secreted by the surrounding tissues (otic vesicles, rhombomeres and eyes) and migrate alongside NC cells with compatible Eph/ephrin codes to

invade tissues with compatible Eph/ephrin profiles (Theveneau and Mayor, 2013). Trunk NC cells follow two distinct paths: (i) a ventromedial path along the NT and notochord, that will give rise to autonomic and enteric neurons, glia and adrenomedullary cells; (ii) a ventrolateral path, that will give rise to sensory neurons and glia; (iii) a dorsolateral path immediately below the dorsal ectoderm, that will give rise to the majority of skin melanocytes (Krull, 2001; Szabó and Mayor, 2018; Theveneau and Mayor, 2012). The choice between both pathways is an example of the opposite effects that ligands can have. Indeed in the dorsolateral path, ephrin-B1 and Edn3 attract NC cells that express EphB2 and EdnrB2 but repel NC cells that express EphB3 and EdnrB, which in turn are diverted to the ventromedial and ventrolateral paths (Harris and Erickson, 2007; Santiago and Erickson, 2002). In the latter, NC cells migrate initially between the somites but this path is quickly blocked by Sema3F, and the following cells are redirected through the somites. They are restricted to the rostral part of the somites by the expression of ephrin-B1, Sema3F and ECM components such as versicans that act as repulsive cues in their caudal segments (Harris and Erickson, 2007; Kalcheim and Teillet, 1989; Keynes and Stern, 1984).

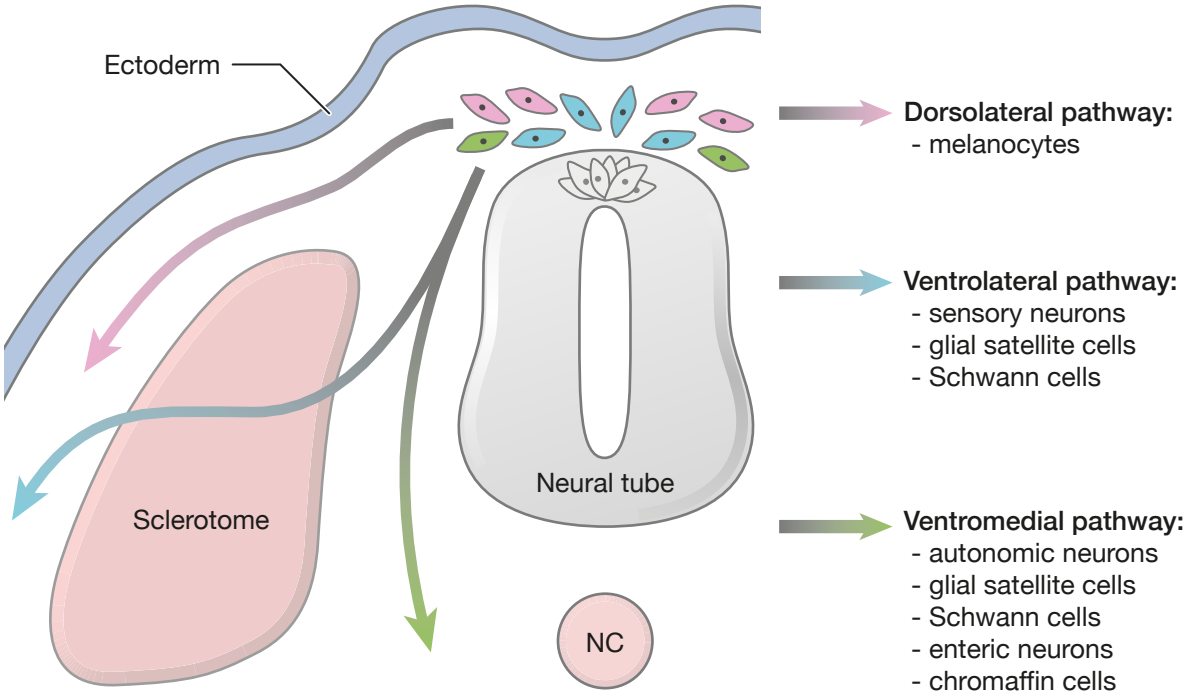

Figure 14. Trunk neural crest migration. Trunk neural crest (NC) cells migrate following three pathways. The dorsolalteral pathway, under the ectoderm, is followed by NC cells that will give rise to melanocytes. In the ventrolateral pathway, NC cells first migrate between the neural tube and the somites before migrating through their rostral parts. They give rise to sensory neurons, glial satellite cells and Schwann cells. Finally, some NC cells migrate ventrally to give rise to autonomic and enteric neurons, glial cells and adrenal chromaffin cells. Adapted from Szabo and Mayor (2018) and *Developmental Biology, Eleventh Edition* (2016).

2.2.3. Neural crest differentiation

Neural crest differentiation

NC cells differentiation is subject to a fine temporal and spatial restriction along the anterior-posterior axis (Figure 15). As a result, depending on their position on the anterior–posterior axis NC cells are subdivided in cranial, vagal, trunk, and sacral NC with different potentials (Dupin et al., 2018; Le Douarin and Kalcheim, 1999; Martik and Bronner, 2017). While NC cells at all axial levels contribute to melanocytes, sensory neurons only originate from the trunk NC, enteric neurons from the vagal and sacral NC, and bone and cartilage only the cranial NC (Dupin et al., 2018; Le Douarin and Kalcheim, 1999; Martik and Bronner, 2017). Their differentiation is controlled by multiple factors, including main signalling pathways (Figure 16), such as FGFs and sonic hedgehog (Shh) for skeletal fate (Abzhanov and Tabin, 2004; Ahlgren and Bronner-Fraser, 1999; Li et al., 2010), transforming growth factors (TGF) for smooth muscle cells (Shah et al., 1996), BMP2 and 4 for autonomous neurons (Shah et al., 1996; White et al., 2001) and Wnt/β-catenin signalling for SN and melanocytes (Lee et al., 2004). Environmental cues also play an essential role to regulate their differentiation, such as neuregulins for glial fate (Bhatt et al., 2013; Dupin et al., 2000; Leimeroth et al., 2002; Martinez-Morales et al., 2007; Shah et al., 1994). However, it has been demonstrated through heterotopic transplantation assays that NC cells of different regions are not fate restricted and that all populations exhibit comparable potentials (Le Douarin and Dupin, 2003). In addition, NC cells differentiation potential is also subject to a temporal restriction. For instance, although Wnt signalling is necessary for NC specification, it becomes after delamination the master signal for sensory neurogenesis (Lee et al., 2004).

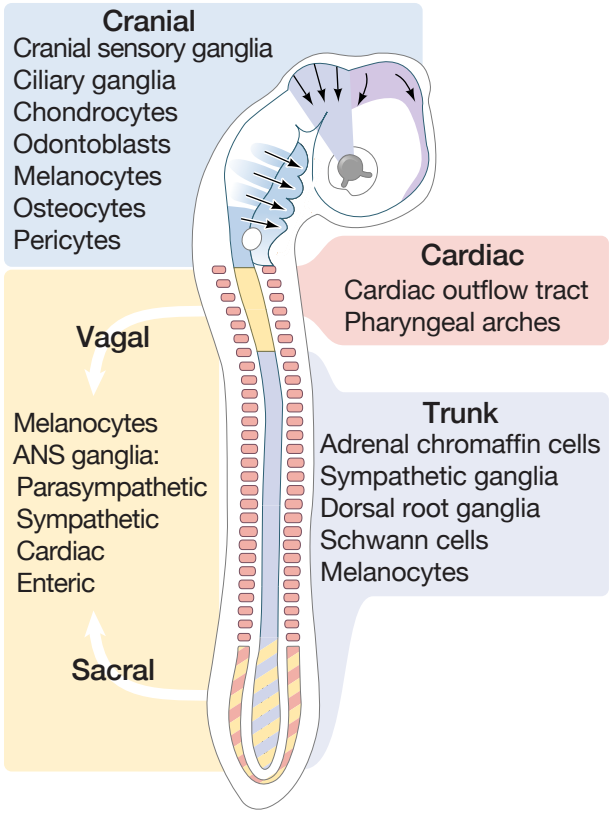

Figure 15. Regions of the chick neural crest. The cranial neural crest (NC) migrates into the pharyngeal arches and the face to form bones and cartilage, melanocytes and participate to the cranial nerves. It also gives rise to CNS pericytes. The vagal and sacral NC form the parasympathetic nerves of the gut. Cardiac NC cells are critical in making the division between the aorta and the pulmonary artery. Trunk NC cells make sensory and sympathetic neurons, melanocytes and a subset of them forms the medulla portion of the adrenal gland. Adapted from Martik and Bronner (2017) and *Developmental Biology, Eleventh Edition* (2016).

Neural crest multipotency

Over several decades, there has been a considerable controversy on how NC cells give rise to such a vast lineage repertoire (Dupin and Sommer, 2012). One model proposes that all NC derivatives arise from a single type of multipotent stem cells, akin to the hematopoietic model (Figure 17). In this model, initial multipotent NC stem cells would gradually lose their differentiation potential to become tri- or bi-potent before being committed to one cell type (Le Douarin and Kalcheim, 1999). The other suggests that NC derivatives arise from a heterogeneous population of already committed precursors in the pre-migratory NC. Early studies in avian and mouse embryos, where individual NC cells were traced either with dye labelling or low-titer infection with a reporter-expressing virus, concluded that NC cells were multipotent in vivo (Bronner-Fraser and Fraser, 1988; 1989; Frank and Sanes, 1991). At the same time, in vitro clonal analysis of quail and rat NC cells also supported this hypothesis (Baroffio et al., 1988; 1991; Stemple and Anderson, 1992). However, other publications reported instead that NC cells were a heterogeneous population of restricted progenitors (Harris and Erickson, 2007; Henion and Weston, 1997; Luo et al., 2003). In particular, it was proposed that NC cells are already committed before delamination and organized according to a spatiotemporal pattern in the dorsal NT of chicken embryos (Krispin et al., 2010; Nitzan et al., 2013a). However, similar experiments performed afterwards instead suggested that NC

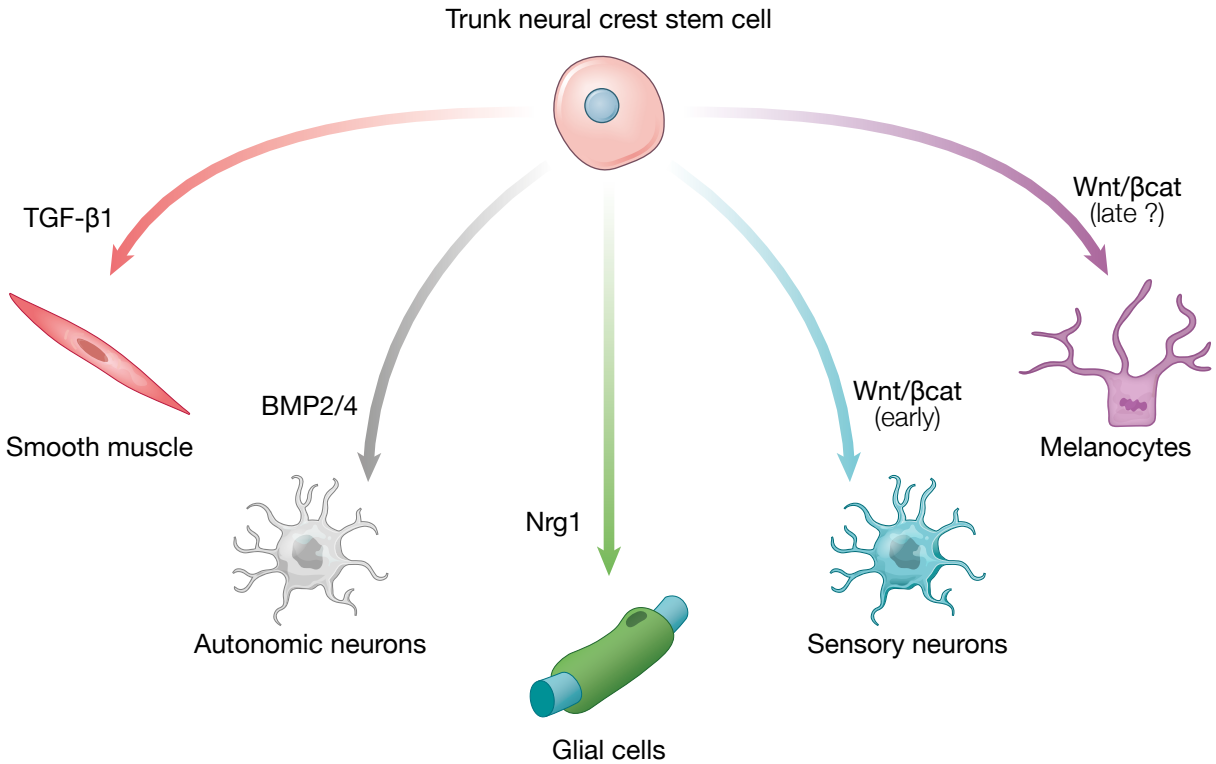

Figure 16. Factors involved in trunk neural crest differentiation. Based on in vitro and in vivo studies, the following factors are involved in the differentiation of the trunk neural crest (NC). However, the role of Wnt in melanocyte differentiation remains unclear in mice. Indeed, in absence of Wnt mice lack both sensory neurons and melanocytes, but constituve activation of the Wnt/β-catenin signalling pathway results in only sensory neurons. Recent studies have suggested that Wnt could play a role in melanocyte at a later time point, but it has yet to be proven. Adapted from Anderson (1997) and Lee et al. (2004).

cells can generate multiple differentiated cell types, regardless of their location within the neural tube or time of emigration (McKinney et al., 2013). More recently, new advances in the Cre-LoxP tracing system have allowed to use it as an *in vivo* clonal analysis assay to address the question of NC cells multipotency non-invasively. The R26R-Confetti allele acts as a multicolour Cre-inducible reporter that generates randomly nuclear green, cytoplasmic yellow or red, or membrane-bound blue cells in a stochastic manner (Snippert et al., 2010). This system was used with inducible reporter lines, *Wnt1-CreER*^{T} and *Sox10-CreER*^{T2}, at different time points to demonstrate that the vast majority of trunk NC cells are multipotent *in vivo* before delamination and during migration (Baggiolini et al., 2015). More recently, a similar approach with *Sox10-CreER*^{T2} and *PLP-CreER*^{T2} was used to study NC-derived clones during facial development. They showed that single NC cells give rise to a spatially defined clonal patches containing multiple ectomesenchymal lineages such as osteogenic, chondrogenic, adipogenic and odontogenic but not neural (Kaucka et al., 2016). Overall, these new studies show that the majority of NC cells are multipotent, both at the premigratory and migratory stage, and that lineage restriction occurs at a later time.

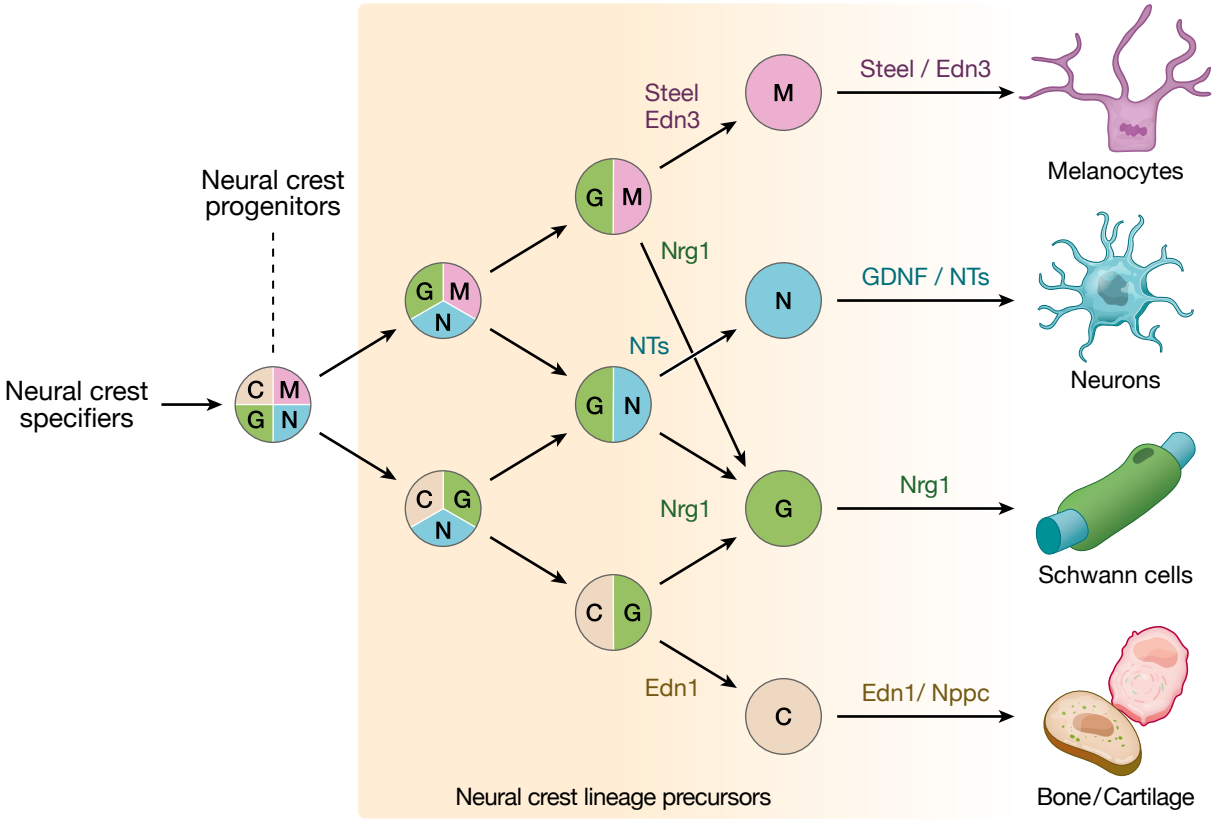

Figure 17. Neural crest progressive lineage restriction model. In this model, neural crest stem cells give rise to intermediate progenitor cells that are initially multipotent, and whith time are restricted until they give rise to committed precursors of cartilage/bone (C), glia (G), neurons (N), and melanocytes (M). The paracrine factors regulating these steps are shown in colored type. Abbreviations: Edn1/3, endothelin-1/3; GDNF, glial cell-derived neurotrophic factor ; Nrg1, neuregulin 1; NTs, neurotropins, Nppc, natriuretic peptide precursor. Adapted from Le Douarin and Dupin (2003) and Martinez-Morales et al. (2007).

2.3.The peripheral nervous system derives from the neural crest

2.3.1. Sensory neurons

Sensory neuron specification

Sensory neurogenesis occurs during NC cells ventromedial migration in two successive and overlapping waves (Figure 18) that have been described both in chick and mouse embryos (Frank and Sanes, 1991; Lawson and Biscoe, 1979; Ma et al., 1999; Marmigère and Ernfors, 2007). In mice, they respectively take place between E9.5 to E11.5 and E10.5 to E13.5 (Figure 19). They are under the control of the Wnt/β-catenin signalling pathway, which promotes the expression of two essential basic helix-loop-helix (bHLH) transcription factors, neurogenin-1 (Ngn1) and Ngn2 (Hari et al., 2002; Lee et al., 2004; Ma et al., 1999). Neurogenins bias NC cells to the sensory as opposed to the autonomic lineage, which is induced by Achaete-scute homolog 1 (Ascl1), another bHLH transcription factor (Bertrand et al., 2002; Guillemot et al., 1993). Ngn2 expression begins in a subset of migratory NC cells close to the dorsal NT, that will aggregate to form the DRG (Ma et al., 1999; Marmigère and Ernfors, 2007). This first Ngn2+ wave gives rise to SN-committed cells that express the forkhead transcription factor Foxs1 and will differentiate into TrkB+ mechanoreceptive and TrkC+ proprioceptive SN (Figure 19; Frank and Sanes, 1991; Ma et al., 1999; Marmigère and Ernfors, 2007; Montelius et al., 2007). However, a subset of Ngn2+ cells do not express Foxs1 and remain Sox10+ uncommitted NC cells in the nascent DRG. These cell will either give rise to GSC or, with other NC cells, participate to the second Ngn1+ neurogenesis wave that takes place within the DRG and produces small TrkA+ nociceptive and TrkB+/TrkC+ SN (Montelius et al., 2007;

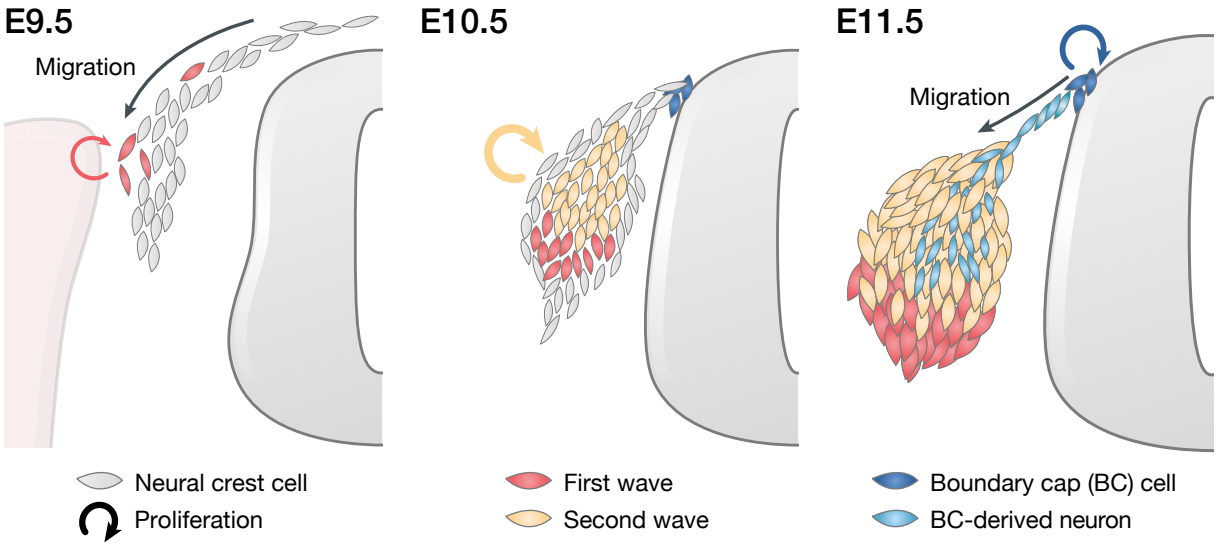

Figure 18. Sensory neurogenesis. During development, dorsal root ganglion (DRG) sensory neurons (SN) arise from two overlapping waves of neurogenesis. The first wave takes place between embryonic day (E)9.5 and E11.5. Multipotent neural crest (NC) cells migrate at the level of the rostral part of the dorsal somitic lip. They contribute to large mechanoreceptive and proprioceptive SN in the DRG. The second wave occurs between E10.5 and E13.5 in post-migratory cells in the DRG, and results in all SN subtypes. Boundary cap (BC) cells can be identified at E10.5 in the spinal cord dorsal root entry zone. Their derivatives migrate into the DRG and give rise to small nociceptive neurons. Thickness of curved arrows indicates different rates of proliferation. Adapted from Marmigeres and Ernfors (2007).

Zirlinger et al., 2002). Indeed, in the absence of Ngn2, Ngn1 is sufficient to generate all types of SN but in the absence of Ngn1 TrkA+ SN do not develop (Ma et al., 1999).

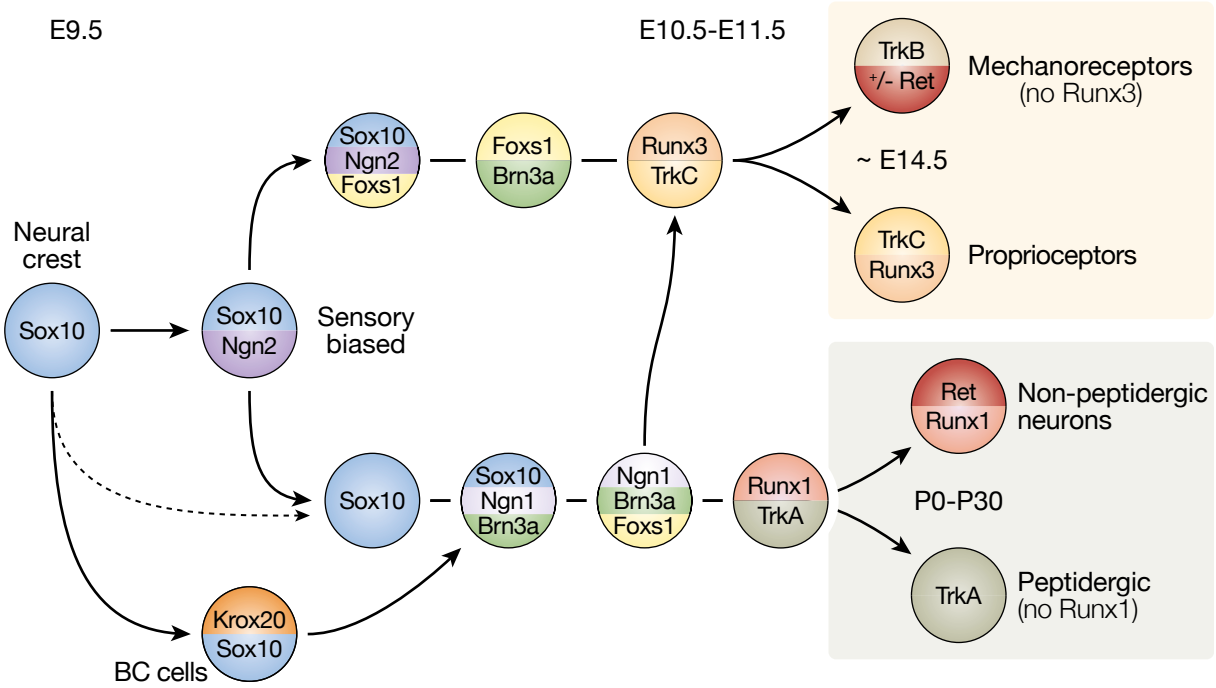

Figure 19. Sensory neurons specification. In the first wave, Sox10-positive cells migrate and express Neurogenin 2 (Ngn2), which biases them towards a sensory fate. Cells with high levels of Ngn2 subsequently commit to a sensory neuron (SN) fate as defined by the expression of the forkhead transcription factor Foxs1 during migration. Other cells with low or no Ngn2 remain uncommitted. Neurons of the first wave express Brn3a and form large proprio- and mechanoreceptive neurons expressing runt-related transcription factor 3 (Runx3) and neurotrophic tyrosine receptor kinase C (TrkC) at early developmental stages. In the second neurogenesis wave, Sox10-positive cells within the dorsal root ganglia start to express Foxs1, Brn3a and Ngn1, before they express Runx factors. They can give rise to both TrkA+ and TrkC+ SN by expressing Runx1 or Runx3, respectively. Sox10- and Krox20-positive boundary cap (BC) cells contribute to the Runx1/TrkA nociceptive neuronal population in addition to glia. Finally, Runx expression levels control SN diversification into different cell types. Indeed, maintained Runx3 expression promotes the proprioceptive fate, while continuous TrkA expression promotes the peptidergic fate. E, embryonic day; P, postnatal day. Adapted from Marmigeres and Ernfors (2007).

It is crucial for proper PNS development that all NC cells that migrate through the nascent DRG do not commit to the SN lineage and give rise for instance to glial cells. Two mechanisms other than Wnt/β-catenin have been shown to play key roles in this finely tuned balance between neurogenesis and gliogenesis: Notch and Sox10. Indeed, Notch activation by it ligand delta-like 1 (Dll1), which is expressed by SN, has been shown *in vitro* to inhibit neurogenesis and increase gliogenesis (Kubu et al., 2002; Morrison et al., 2000; Wakamatsu et al., 2000). Hence, newly formed SN inhibit neurogenesis in their adjacent cells. While it has been shown *in vitro* that Sox10 expression maintains NC cells pluripotency, recent studies in zebrafish embryos have identified Sox10 as an active promoter of sensory neurogenesis (Carney et al., 2006; Delfino-Machín et al., 2017). Indeed, they have shown that Sox10 drives Ngn1 expression and that a single amino acid substitution in its DNA binding high mobility group (HMG) domain induces the loss of all glial cells while retaining neurogenesis. Given the multiple functions of Sox10 during NC specification but also during melanogenesis and

gliogenesis, it is likely to function in a combinatorial fashion (Aoki et al., 2003; Britsch et al., 2001).

Sensory neuron maturation

The earliest SN subtypes markers are the TrkA, TrkB and TrkC neurotrophins receptor for NGF, BDNF and NT3 respectively, that play several roles during SN development (Figure 19; Lallemend and Ernfors, 2012; Marmigère and Ernfors, 2007; Mu et al., 1993; Sommer, 2013). First, neurotrophins act as long range cues that participate to axonal guidance (Bibel and Barde, 2000; Marmigère and Ernfors, 2007). Second, they control cell survival during the naturally occurring cell death that is a part of normal development. Indeed in mice, loss of function of each of these receptors leads to the disappearance of their corresponding SN populations (Klein et al., 1994; 1993; Smeyne et al., 1994). Similarly, NT3 inactivation in mice results in significant neuronal loss (Fariñas et al., 1994; Lee et al., 1994). Finally, they direct phenotypic maturation by regulating peptides an ion channels expression (Bibel and Barde, 2000; Marmigère and Ernfors, 2007). Indeed, it was shown in knock-in mice that replacing TrkA with TrkC induces a fate switch of some TrkA-expressing nociceptors into proprioceptive neurons (Moqrich et al., 2004). Two other genes, runt-related transcription factor 1 (Runx1) and Runx3 (Figure 19) play an important role in DRG SN diversification (Kramer et al., 2006; Marmigère and Ernfors, 2007). Runx transcription factors are key regulators of lineage-specific gene expression in major developmental pathways such as neuronal differentiation or osteogenesis (Levanon and Groner, 2004). *Runx1* and *Runx3* are differentially expressed in SN in a non-overlapping manner, respectively in TrkA+ and TrkC+ SN. Interestingly, both shape their respective lineages by switching from being transcriptional activators at earlier stages to acting as repressors later (Kramer et al., 2006; Marmigère et al., 2006). Indeed, *Runx3* expression starting at E10.5 is necessary for the establishment of an early TrkC+ population from which will arise both TrkB+ LTMR and TrkC+ proprioceptive SN. However between E11.5 and E13.5, its continuous expression downregulates TrkB and consolidates the proprioceptive lineage (Kramer et al., 2006). In a similar fashion, Runx1 initially activates TrkA expression but at late embryonic and postnatal stages its continuous expression represses TrkA and consolidates the non-peptidergic Ret+ nociceptor lineage (Chen et al., 2006; Kramer et al., 2006; Marmigère et al., 2006).

Axonal guidance

Finally, another key aspect of SN development is their ability to direct their axons towards and reach the appropriate targets in the spinal cord and the periphery. An interesting example is the TrkC+ proprioceptive SN development, which involves both extrinsic environmental guidance cues such as NT3 and Sema3A, and cell-intrinsic factors such as Runx3. Indeed, NT3 acts as a long range guidance cue that is essential for their ability to reach the muscle and induce the formation of their sensory end-organs, the GTO and the muscle spindle (Kucera et al., 1995; Lee et al., 1994). Once innervated, these end-organs start expressing NT3 which in return promotes the survival of their innervating TrkC+ proprioceptive SN and their proper afferent projections. Indeed, when their axons reach the spinal cord dorsolateral margin, they are initially repelled by the presence of Sema3A through its interaction with Nrp1-plexinA4/3 (Masuda et al., 2003; Yaron et al., 2005). Sema3A is then progressively downregulated in the dorsal spinal cord, allowing the entry of sensory axons, but its expression is maintained in the ventral horn (Fu et al., 2000). At this stage, contrary to the other SN, TrkC+ SN downregulate Nrp1, which allows them to project appropriately in the ventral horn (Pond et al., 2002). Finally, several studies have shown that Runx3 plays a specific role in the establishment of terminal contact patterns in the spinal cord, mediated only partly by TrkC (Chen et al., 2006; Levanon et al., 2002). Although its role could be due to its influence on other unknown axon guidance cues, the fact that *Runx1* overexpression *in vitro* in a serum-free medium induces neurite outgrowth in a dose-dependent manner suggests that Runx3 could act cell-autonomously to drive axonal growth (Marmigère et al., 2006).

2.3.2. Schwann cells

Schwann cell precursors

NC cells generate SC in three successive steps (Figure 20): between E10.5-13.5, they generate SC precursors (SCP); around E14.5-15.5 SCP convert into immature SC (ISC); and finally around birth, ISC either become myelinating or non-myelinating SC depending on the diameter of the axon they randomly associate with (Jessen and Mirsky, 2005; Jessen et al., 2015; Woodhoo and Sommer, 2008). At E12.5, embryonic nerves are still compact axon bundles, intimately associated with SCP who depend on them for their survival, and do not yet contain blood vessels or connective tissue (Jessen et al., 1994; 2015). SCP play several key functions beyond their role as an intermediary stage in SC development. They provide necessary trophic support to the developing sensory and motor neurons (Garratt et al., 2000; Riethmacher et al., 1997). SCP ensheath axon growth cones and in their absence, developing nerves reach their target fields but are defasciculated distally and present abnormal branching and terminal sprouting (Grim et al., 1992; Jessen et al., 2015; Wanner et al., 2006; Woldeyesus et al., 1999). Finally, recent studies have shown that SCP are a multipotent stem cell population that gives rise to several cell types (Figure 20) such as endoneurial fibroblasts, melanocytes,

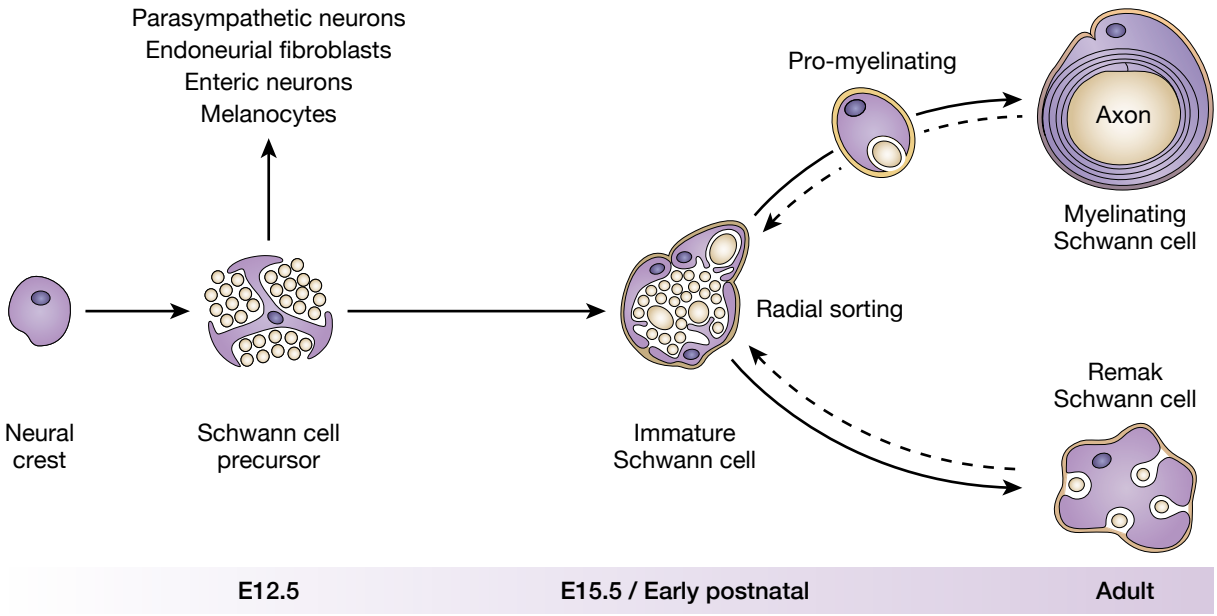

Figure 20. The Schwann cell lineage. The embryonic phase of Schwann cell (SC) development involves three transient cell populations: first, migrating neural crest cells; second, Schwann cell precursors (SCP); third, immature Schwann cells (ISC). All ISC cells have the same developmental potential, and their fate is determined by the axons with which they associate. Myelination occurs only in SC that by chance envelop large diameter axons. SC that ensheath small diameter axons become mature non-myelinating SC. Dashed arrows indicate the reversibility of the final transition. Adapted from Jessen, Mirsky and Lloyd (2015).

adrenergic chromaffin cells, parasympathetic and enteric neurons (Adameyko et al., 2009; Britsch et al., 2001; Dyachuk et al., 2014; Espinosa-Medina et al., 2014; Furlan et al., 2017; Joseph et al., 2004; Petersen and Adameyko, 2017; Uesaka et al., 2015). It is unclear at this point if these multipotent SCP are only a transient population or if they do exist in the adult nerve, in a similar fashion to adult NCSC.

Compared with sensory neurogenesis, transcription factors actively promoting gliogenesis have not been identified so far. Two transcription factors expressed by early NC cells, FoxD3 and Sox10, are involved in NC gliogenesis. Gain- and loss-of-function experiments have shown that FoxD3 acts as a fate switch by inhibiting neuro- and melanogenesis in NC cells while being permissive for glial differentiation (Nitzan et al., 2013a; 2013b). Sox10 inactivation *in vivo* leads to the absence of SC and SGC (Britsch et al., 2001; Kim et al., 2003; Paratore et al., 2001). However, given the multiple roles of Sox10 in NC ontogeny, it is likely that its pro-gliogenic effect depends on the presence of extracellular cues. One could be the Nrg1 signalling pathway, as Sox10 drives the expression of its receptor ErbB3 (Britsch et al., 2001). Two signalling pathways, Nrg1 and Notch, are involved in early NC cells differentiation into SCP. Nrg1 is an epidermal growth factor-like ligand that interacts with ErbB receptor tyrosine kinases (Birchmeier and Nave, 2008; Garratt et al., 2000; Nave and Salzer, 2006). Due to extensive alternative RNA splicing, there are numerous Nrg1 isoforms categorised in six major classes, the most common being types I-III. Following proteolytic cleavage, type I and II Nrg1 are released from the cell surface and function as a paracrine signal, but because of a second anchoring domain, type III Nrg1 (Nrg1-III) remains tethered to the cell surface and

acts as a juxtacrine signal (Mei and Xiong, 2008; Nave and Salzer, 2006; Wang et al., 2001). Neuronal expression of Nrg1-III is essential for the survival, proliferation and migration of SCP, through its interaction with ErbB2/3 heterodimers (Birchmeier, 2009; Lyons et al., 2005; Morris et al., 1999; Nave and Schwab, 2005; Riethmacher et al., 1997; Woldeyesus et al., 1999). Indeed, ErbB2/3 inactivation leads to the absence of SCP and a subsequent massive death of SN and motor neurons. However, it may not be necessary for SCP/SGC specification: *in vitro*, Nrg1-III inhibit neurogenesis but NC cells can give rise to SC in its absence; *in vivo*, SCP are formed in the absence of ErbB3 in zebrafish and SGC appear normally in the absence of Nrg1-III (Garratt et al., 2000; Lyons et al., 2005; Shah et al., 1994). As mentioned earlier, it has been shown *in vitro* that Notch activation inhibits neurogenesis in NC cells and increases the number SC (Kubu et al., 2002; Morrison et al., 2000; Wakamatsu et al., 2000). Interestingly, conditional inactivation in NC cells of its canonical pathway effector, Rbp/d, only blocks the formation of SGC, while SC formation along peripheral nerves is not affected (Taylor et al., 2007). There is also evidence that Notch activation, like Nrg1, stimulates ISC formation from SCP and ISC proliferation (Woodhoo et al., 2009). Overall, it is not yet clear whether Nrg1-III and Notch act instructively on NC cells to promote gliogenesis.

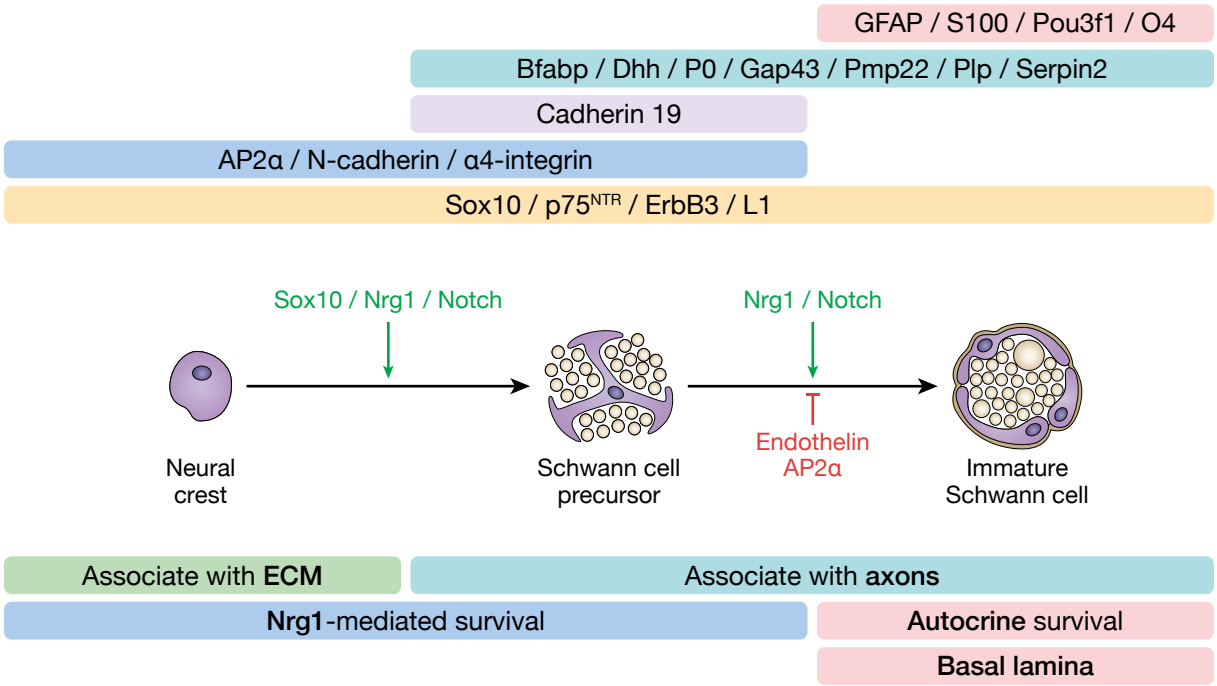

Figure 21. Changes in phenotypic profile in the embryonic Schwann cell lineage. The boxes above the lineage drawing indicate the changes in gene expression that take place during embryonic Schwann cell (SC) development. Each developmental stage also involves characteristic relationships with surrounding tissues, and distinctive cell signalling properties (boxes below lineage drawing). For instance, while neural crest (NC) cells migrate through the extracellular matrix (ECM), SCP and immature SC (ISC) are embedded among axons with minimal extracellular spaces separating them. Basal lamina is absent from migrating NC cells and SCP, but appears on ISC. Finally, *in vitro* Neuregulin 1 (Nrg1) only supports NC cells survival in the presence of an ECM, although this is not required for the NRG1-mediated survival of SCP. ISC have autocrine survival circuits that are absent from SCP. Adapted from Jessen and Mirsky (2005) and Jessen, Mirsky and Lloyd (2015).

Immature Schwann cells

In mice, SCP mature into ISC around E14.5–E15.5 (Figure 21), when axons reach their peripheral targets, and undergo coordinated changes in molecular expression and signal responses (Jessen and Mirsky, 2005; Jessen et al., 2015; Woodhoo and Sommer, 2008). ISC envelop groups of axons to form irregular axon/ISC families, each covered by a nascent basal lamina and surrounded by ECM that has now formed within the nerve (Webster et al., 1973). Their apparition correlates with the development of the endo- and perineurium as well as the intra-neural vascular plexus. ISC secrete Desert hedgehog (Dhh) that interacts with its receptor, Patched/Smoothened, which is expressed by fibroblasts surrounding the nerve (Parmantier et al., 1999). A key ISC acquisition is the establishment of an autocrine loop that allows them to survive in the absence of neurons or Nrg1-III (Figure 21). Unlike SCP, they can support their own survival by secreting a cocktail of survival factors that include insulin-like growth factor 2 (IGF2), NT3, platelet-derived growth factor-β (PDGFB), leukaemia inhibitory factor (LIF) and lysophosphatidic acid (LPA) (Dowsing et al., 1999; Meier et al., 1999; Weiner and Chun, 1999). The SCP-ISC transition is under the control of positive axonal signals, such as Nrg1 and Notch1-ligand Jagged1, and negative signals such as Edn. Indeed, it has been shown *in vitro* that Nrg1-III induces the differentiation of SCP into ISC (Dong et al., 1995; Leimeroth et al., 2002). Similarly, Notch1 activation by axonal Jagged1 also drives the differentiation of SCP into ISC, in part by elevating ErbB2 receptor levels and their responsiveness to Nrg1-III (Woodhoo et al., 2009). Conversely, its inactivation *in vivo* leads to a delayed maturation SCP into ISC. Two negative regulators of ISC differentiation have been described, Edn and adaptator protein complex 2 alpha (AP2α). Edn slows the differentiation of SCP into ISC *in vitro*, and *in vivo* SC form prematurely in rats with defective EdnrB (Brennan et al., 2000). AP2α is the only transcription factor whose inhibitory role in the SCP-ISC transition has been demonstrated (Figure 21). It is downregulated during ISC differentiation, and if maintained its expression delays ISC differentiation (Stewart et al., 2001). Transforming growth factor (TGF)-β plays a very specific role to adjust the SC pool to the number of axons in the developing nerve. Indeed, in vitro experiments as well as loss of function mutants have shown that it can induce both proliferation in ISC with tight axonal contacts and cellular death in cells with less effective axonal contacts (D'Antonio et al., 2006; Einheber et al., 1995; Parkinson et al., 2001; Ridley et al., 1989). *In vitro* data suggests that this dual effect results from a cooperation with the Nrg1 signalling (D'Antonio et al., 2006).

Radial sorting

As they differentiate around birth into myelinating and non-myelinating SC, ISC extend cytoplasmic processes into groups of axons and progressively segregate them (Harty and Monk, 2017; Jessen et al., 2015; Salzer, 2015). All ISC have a similar myelination potential, and their commitment to myelination is under axonal control (Jessen and Mirsky, 2005;

Nave and Salzer, 2006). At the end of this process, called radial sorting, pro-myelinating SC establish a 1:1 relationship with large-diameter axons (> 1 μm), while future non-myelinating SC continue to be associated with multiple small-diameter axons (Figure 22). It has been known for more than 30 years that radial sorting and myelination are deeply connected to basal lamina development around SC, and are highly dependent on interactions with ECM molecules such as laminins and collagens (Bunge et al., 1986; Chernousov et al., 2008). Indeed, it has been shown that laminin α2β2γ1 (laminin-211) is a key radial sorting and myelination regulator through its interactions with its abaxonal receptors β1-integrins and α-dystroglycan and their effector Fak (Berti et al., 2011; Feltri et al., 2002; McKee et al., 2012; Pellegatta et al., 2013; Pereira et al., 2017; Yu et al., 2005). More recently, adhesion G protein-coupled receptor (aGPCR) Gpr126, that is expressed by ISC, has been identified as an essential radial sorting and myelination regulator (Monk et al., 2009; 2011). aGPCR are a newly defined receptor family that, when activated, can undergo autoproteolysis resulting in an extracellular N-terminal fragment (NTF) and a seven-transmembrane-containing C-terminal fragment (CTF; Langenhan et al., 2013). Importantly, key amino-acids at the CTF extracellular end can act as a tethered agonist, while the cleaved NTF remains noncovalently associated at the cell-membrane and can either modulate CTF signalling or function independently from it (Langenhan et al., 2013; Liebscher et al., 2014; Prömel et al., 2012). Indeed, it has been shown that the interaction between laminin-211 and the NTF of Gpr126 is necessary and sufficient for radial sorting, and at low concentrations inhibits CTF signalling which is involved later in myelination (Petersen et al., 2015).

Myelinating Schwann cells

Myelination is the result of complex molecular changes induced by extrinsic signals that trigger in turn significant transcriptional changes (Glenn and Talbot, 2013a; Jessen and Mirsky, 2005; Nave and Salzer, 2006; Nave and Schwab, 2005; Salzer, 2015). Two major extrinsic signals are presented by the axon and ECM, respectively Nrg1-III and laminin-211 (Figure 22). Nrg1-III is expressed by axons in amounts proportional to their diameters (Taveggia et al., 2005). The level of Nrg1-III expression in axons regulates the initiation of myelination as well as myelin sheath thickness (Michailov et al., 2004; Taveggia et al., 2005). Indeed, overexpressing Nrg1-III in sympathetic neurons that are normally not myelinated leads to their myelination (Taveggia et al., 2005). Nrg1-III signalling activates several downstream pathways in SC, such as the phosphatidylinositol-3-kinase (PI3K), the MEK/ERK and the phospholipase C-g (PLC-g) calcium signalling pathway (Nave and Salzer, 2006; Pereira et al., 2012). Indeed, several studies have shown that signalling downstream of PI3K and MEK/ERK positively regulates myelination and myelin sheath thickness *in vivo* (Cotter et al., 2010; Goebbels et al., 2010; Ishii et al., 2013; Newbern et al., 2011; Sherman et al., 2012). Finally, Nrg1-III signalling is modulated depending on which protease cleaves it. Indeed, β-secretase (BACE1) cleaving promotes myelination and mice lacking BACE1 have abnormally thin

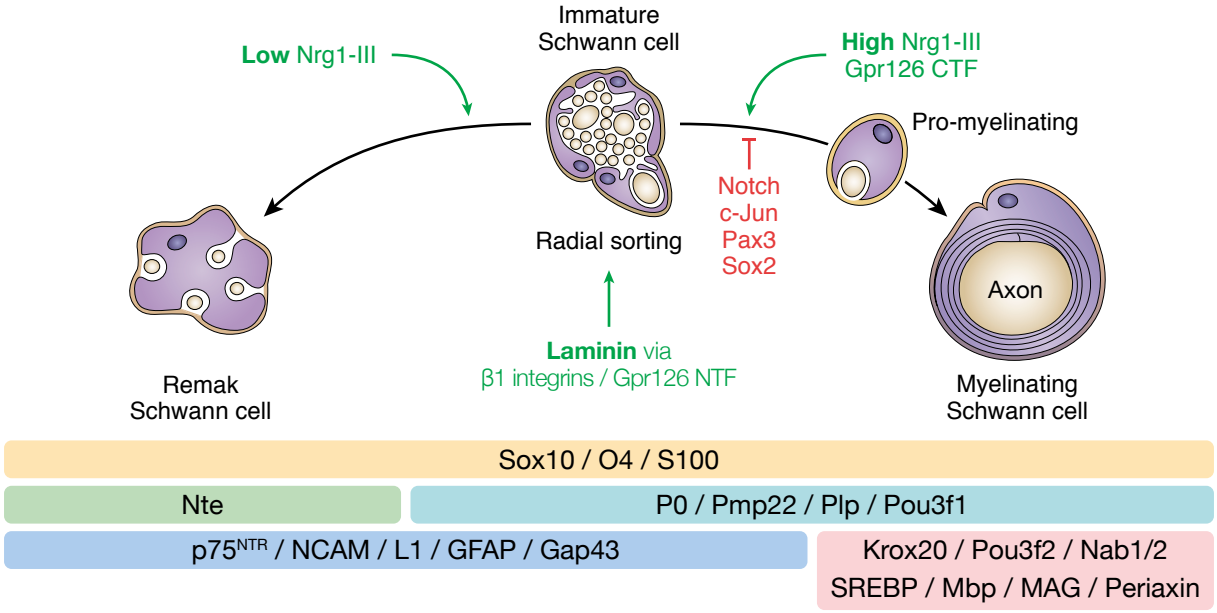

Figure 22. Schwann cell differentiation. The boxes under the lineage drawing indicate the changes in gene expression that take place during Schwann cell (SC) development. Green arrows show positive regulation, red arrows inhibition.Laminin signalling through β1 integrins and Gpr126 N-terminal fragment (NTF) is essential for radial sorting, during which immature SC (ISC) associate either with a single large axon or mutliple small diamater axons. Myelination is promoted by high axonal levels of type III neuregulin 1 (Nrg1-III) and Gpr126 C-terminal fragment signalling. Oppositely, in presence of low levers of Nrg1-III SC do not myelinate. Notch, c-Jun, Pax3 and Sox2 oppose myelination. Adapted from Jessen and Mirsky (2005) and Jessen, Mirsky and Lloyd (2015).

myelin sheaths, while tumor necrosis factor-α-converting enzyme (TACE/ADAM17) cleaving represses myelination and TACE mutants exhibit hypermyelination in peripheral nerves (La Marca et al., 2011; Willem et al., 2006). In addition to its role in radial sorting, laminin is also essential to initiate myelination. When laminin-211 concentrations increases in the ECM, it promotes CTF signalling which drives the expression of promyelinating transcription factor Pou3f1 (Oct6) by elevating cAMP levels (Glenn and Talbot, 2013b; Monk et al., 2009; Petersen et al., 2015). Indeed, in Gpr126 mutants transient cAMP increase restores myelination while Nrg1-III overexpression is insufficient (Glenn and Talbot, 2013b). Moreover, *in vitro* experiments suggest that cAMP may amplify the strength of Nrg1 signals and modulate SC response to Nrg1-III from proliferation to myelination (Arthur-Farraj et al., 2011; Monje et al., 2006).

During development, SC myelination is under the control of pro-myelinating and demyelinating transcription factors (Pereira et al., 2012; Svaren and Meijer, 2008). The main pro-myelinating transcription factors are Sox10, Pou3f1 (Oct6), Pou3f2 (Brn2) and Krox20 (Egr2; Figure 22). They are organised in a feed-forward loop, in which Sox10 expression at the ISC stage activates Pou3f1/Pou3f2 during the promyelinating stage before activating Krox20 in synergy with them at the myelinating stage (Ghislain et al., 2002; Kuhlbrodt et al., 1998; Svaren and Meijer, 2008). Pou3f1/Pou3f2 are downregulated at the myelinating stage, at which point Sox10 and Krox20 act in synergy to drive the transcription of myelin structural proteins and biosynthetic components of myelin lipid synthesis (Kuhlbrodt et al., 1998;

Svaren and Meijer, 2008). The POU homeo-domain transcription factors Pou3f1 and Pou3f2 are cell autonomous regulators of the timing and rate of the promyelinating-myelinating SC transition, whose deletion results in hypomyelination and the persistence of promyelinating SC into adulthood (Bermingham et al., 1996; Jaegle et al., 1996; 2003). *Krox20* is considered a master regulator of PNS myelination. From E10.5 to E15.5, its expression is restricted to boundary cap (BC) cells at the CNS/PNS interface. Around E15.5, it is expressed in all pro-myelinating ISC (Topilko et al., 1994). After birth, its continuous expression along with Sox10 is necessary to promote and then to maintain the myelinating phenotype (Decker et al., 2006; Topilko et al., 1994). Its inactivation blocks SC at the promyelinating stage. Analysis of cis regulatory sequences directing Krox20 expression in SC have identified two distinct elements (Ghislain et al., 2002). The first ISC element (ISE) is active between the E15.5 and E18.5 stages in ISC while the myelinating SC element (MSE) is activated at E18.5 and is maintained in myelinating cells. These pro-myelinating genes are counterbalanced during SC development by the transcription factors c-Jun, Sox2 and Pax3 (Jessen and Mirsky, 2008; Svaren and Meijer, 2008). They are expressed by ISC during development and need to be downregulated before myelination (Figure 22), and also play a crucial role in nerve regeneration (Jessen and Mirsky, 2008). c-Jun is a key component of the AP-1 transcription factor complex, which has been shown to inhibit the induction of myelin genes by *Krox20* and cAMP, maintain SC proliferation and induce demyelination when overexpressed in uninjured adult nerves (Fazal et al., 2017; Jessen et al., 2015; Parkinson et al., 2008). Finally, Notch signalling also acts as a negative regulator of myelination after birth. It is selectively suppressed in cells that initiate myelination, and similarly to c-Jun its expression in uninjured adult nerves induces demyelination (Jessen and Mirsky, 2008; Woodhoo et al., 2009).

Non-myelinating Schwann cells

The mechanisms underlying the different types of non-myelinating SC differention are not as well understood as those regulating the myelination process. This may be in part because these cells maintain a molecular profile closer to ISC than myelinating SC (Jessen and Mirsky, 2008; Woodhoo and Sommer, 2008). Among them, advances have been made in the field of RSC differentiation (Harty and Monk, 2017). Indeed, the two main pathways involved in myelination, Nrg1-III/ErbB2/3 and laminin-211/Gpr126, are also involved in the proper development of RSC. Indeed, targeted loss of Nrg1-III in non-myelinated SN results in Remak bundles with many more axons, and dramatically reduced RSC axon ensheathment (Fricker et al., 2009). Loss of laminin-211/Gpr126 signalling results in naked small caliber axons in adults (Mogha et al., 2013; Petersen et al., 2015). Specific pathways involved in RSC differentiation are still unknown. However, *Neuropathy target esterase* (*Nte*) has recently been identified as specifically necessary to RSC maturation (Figure 22). Indeed, targeted deletion of *Nte* in ISC results in incomplete ensheathment of unmyelinated axons followed by their degeneration, without affecting myelinating SC (McFerrin et al., 2017).

2.3.3. Satellite glial cells

The sequences of SGC development remain poorly characterized compared to SC. Although both types derive from NC cells, developing SGC and SCP differ in several ways (Woodhoo and Sommer, 2008; Woodhoo et al., 2004). SGC development occurs earlier than SCP, in terms of autocrine survival mechanisms and expression of markers such as S100b and Fabp7. They do not require similar factors, as for instance IGF1 that only promotes the survival of SGC. In mice mutants for Nrg1 components, SGC remain unaltered contrary to SCP (Garratt et al., 2000; Woodhoo and Sommer, 2008). On the contrary, conditional inactivation of the Notch pathway in vivo blocks the formation of SGC but not SCP (Taylor et al., 2007). Given these differences, it has been suggested that GSC and SC glial lineages segregate at an early developmental stage, supported by fate-mapping experiments showing that Ngn2+ NC cells only give rise to SN and SGC but not SC (Woodhoo and Sommer, 2008; Zirlinger et al., 2002). However, our lab has shown that BC cells, which appear at E10.5, give rise to a subpopulation of SN, SGC and SC (Gresset et al., 2015; Maro et al., 2004). Another way to explain these results could be the presence of a heterogenous SGC population, which remains to be determined.

3. Boundary cap cells

3.1. Boundary cap cells origin and markers

3.1.1. Anatomical position and origin

During development, the NC also gives rise to a multipotent cell population called boundary cap (BC) cells, which has been described in birds, rodents and human embryos. BC cells form transient clusters of rapidly proliferating cells located at the dorsal root entry zone (DREZ) and ventral motor exit points (MEP) of all cranial and spinal nerves (Figure 24; Altman and Bayer, 1984; Niederländer and Lumsden, 1996; Vermeren et al., 2003; our unpublished results). The NC origin of dorsal BC cells has been well established by several fate-mapping studies with quail-chick grafts or NT electroporation (Niederländer and Lumsden, 1996; Radomska and Topilko, 2017; Woodhoo and Sommer, 2008). On the contrary, the origin of ventral BC cells is still controversial (Erickson and Weston, 1999). Indeed, retroviral labelling studies of the ventral NT have suggested the existence of a group of ventrally emigrating NT (VENT) cells that colonize the ventral root and give rise to multiple neuronal and non-neuronal cell types (Dickinson et al., 2004; Sohal et al., 1999). However, *in vivo* ventral NT fate-mapping at the hindbrain level by electroporating a GFP expression vector before to the putative

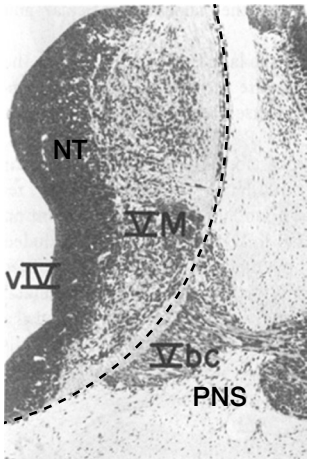

Figure 23. Boundary cap cells. Boundary cap cells (Vbc) were first described by Altman and Baier in 1984 as clusters of proliferating cells located at the dorsal entry root zone and ventral motor exit points of all cranial and spinal nerves in the rat. Abbreviations: NT, neural tube; PNS, peripheral nervous system.

VENT cells migration did not identify such cells (Yaneza et al., 2002). This data supports the hypothesis that most ventral BC cells, at least in the head, originate from the NC.

3.1.2. Boundary cap cells markers

Thirty years ago, our lab identified *Krox20* (*Egr2* in humans) as a BC cell marker in mouse embryos (Schneider-Maunoury et al., 1993; Wilkinson et al., 1989). Since then, the discovery of such BC-specific markers has allowed to expand our knowledge on this population through fate-mapping and functional studies. Our group and others have characterized additional BC markers such as *Cdh7*, *Sema3B* and *Sema3G* in chick embryos, and *Cxcr4* and *Netrin 5* in mouse embryos (Bron et al., 2007; Niederländer and Lumsden, 1996; Zhu et al., 2015). With a global gene expression profiling of BC cells versus SCP and NC cells in mouse embryos, our lab has also identified several new BC markers (Figure 24), including *Prss56*, Wnt inhibitor (*Wif1*) and *Hey2* (Coulpier et al., 2009). The detailed expression pattern analysis of *Krox20* and these new markers suggests that BC clusters form in mice around E10.5 simultaneously in both DREZ and MEP (Coulpier et al., 2009; Topilko et al., 1994). Indeed, their expression is initiated at E10.5 and persists until E14.5, after which none of them are expressed. This supports the idea that BC cells persist at least until that developmental time, before either undergoing profound molecular changes, emigrating from the CNS/PNS boundary, or dying (Radomska and Topilko, 2017).

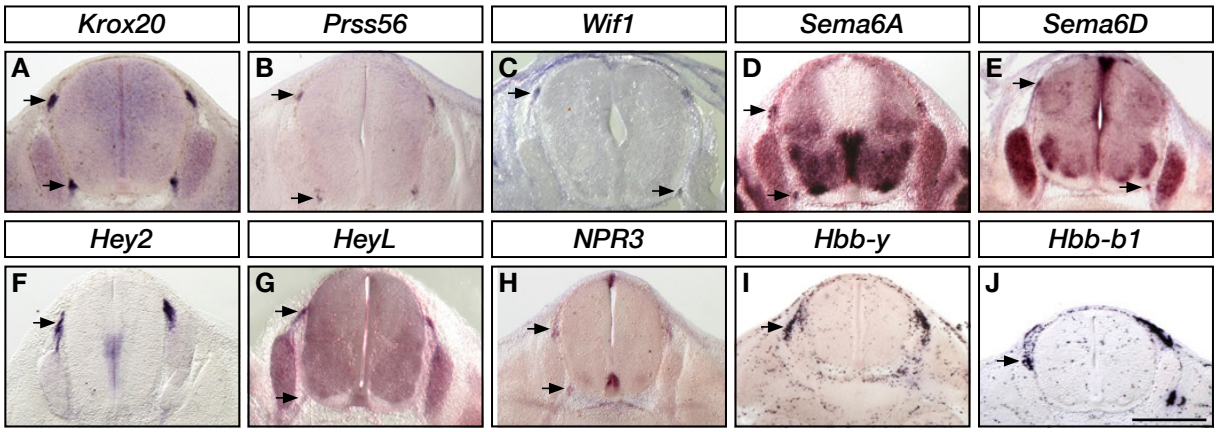

Figure 24. Boundary cap cells markers. Expression patterns of BC cells and nerve root markers at E12.5. The expression of the indicated genes was analyzed by *in situ* hybridization on transverse vibratome sections of E12.5 mouse embryonic spinal cords at the thoracic level. Arrows point to expression in the BC cells or nerve roots. Left and right roots are not always present in the section. Scale bar: 500 µm. Adapted from Coulpier et al. (2009).

3.1.3. BC cells heterogeneity

The situation is different in zebrafish embryos, that do not have proper BC cells. Although Nkx2.2-expressing cells have been described in the ventral NT to migrate to the periphery along the motor roots, they differ in several ways with BC cells (Fontenas and Kucenas, 2017; Kucenas et al., 2008). First, they do not stop at the PNS/CNS interface and keep migrating along motor nerves. Second, they give rise to a proximal part of the

perineurium, but not to peripheral glia. More recently, a distinct population of CNS-derived progenitors, localized at MEP and expressing Olig2 and Wif1, has been identified in zebrafish (Fontenas and Kucenas, 2018; Smith et al., 2014). These cells generate glial cells that, in a similar manner to ventral BC derivatives, exclusively ensheath ventral root motor axons. When taking in account our unpublished observations of significant discrepancies between *Wnt1*^{Cre} and *Krox20*^{Cre} fate-mapping in mice, and the expression of Wif1 in Krox20-traced BC, these results raise the possibility that ventral BC cells may have an heterogenous NC/CNS origin (Coulpier et al., 2009; Radomska and Topilko, 2017). This exciting hypothesis remains to be tested experimentally.

3.2. Boundary cap cells functions

3.2.1. Gatekeepers for motor neurons cellular bodies

The fact that ventral BC clusters form in mice around E10.5, which is also the time when motor axons grow out of the NT, raised the question of their possible role in defining MEP. Surprisingly, the genetic ablation of Krox20-expressing BC cells by a targeted expression of diphtheria toxin did not affect MN axon outgrowth but resulted, in a sub-population, in the translocation of their somata out of the NT (Figure 25) followed by their death (Vermeren

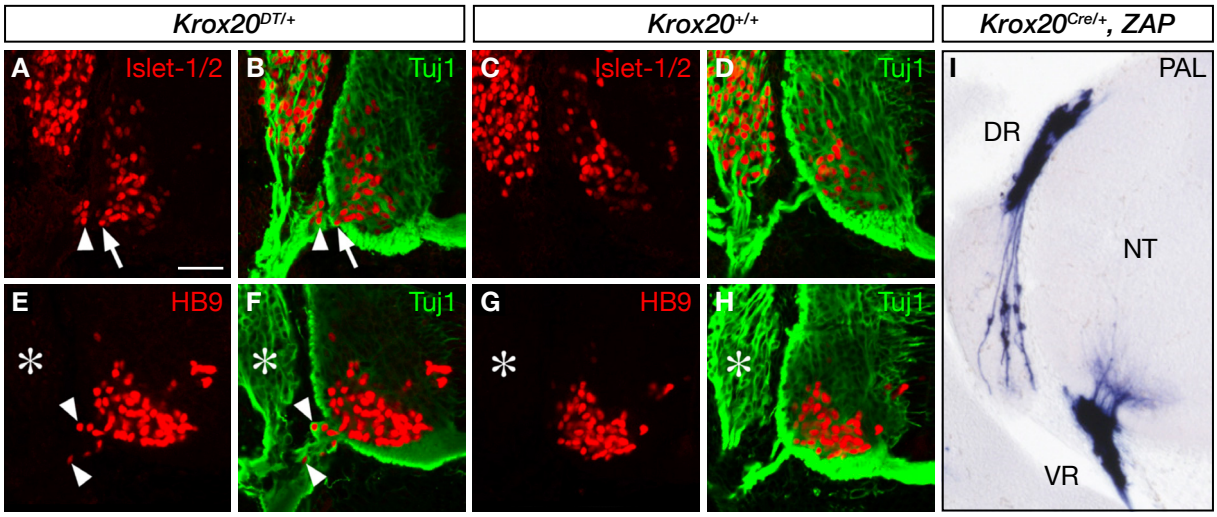

Figure 25. Boundary cap cells confine the cellular bodies of motor neurons. (**A–D**) Transverse sections of E11.5 *Krox20*$^{DT/+}$ (A-B) and wild-type (C-D) embryos immunostained with antibodies against the axonal marker β-III-tubulin (TuJ1, green) and Islet-1/2 (red), which labels both motor and sensory neurons. In the mutant, ectopic Islet-1/2-positive cells are frequently found in the marginal zone and within the ventral root (A-B, arrowheads), well separated from the dorsal root ganglia (DRG). Extraspinal Islet-1/2-positive neurons were never observed in wild-type embryos (C-D). (**E–H**) Transverse sections of E11.5 *Krox20*$^{DT/+}$ (E-F) and wild-type (G-H) embryos immunostained with antibodies against β-III- tubulin (TuJ1, green) and the motor neuron-specific marker HB9 (red), which is not expressed in DRG neurons (stars in E–F). In *Krox20*$^{DT/+}$ mutant embryos, HB9-positive neurons were observed in the marginal zone and within the ventral root (E-F, arrowheads), but not in wild-type embryos (G-H). (**I**) Transverse section of a E12.5 *Krox20*$^{Cre/+}$, *ZAP* embryo. ZAP encodes a Cre-inducible human placental alkaline phosphatase (hPLAP) providing high resolution staining of cell membranes. At the dorsal level, hPLAP-expressing cells are present at the CNS/PNS interface, along the dorsal root (DR) and in the DRG. At the ventral level, boundary cap cells form numerous cytoplasmic protrusions toward the ventral horn. Abbreviations: DR, dorsal root; VR, ventral root; PAL, alkaline phosphatase; NT, neural tube. Scale bar (A-H): 50 µm. Adapted from Vermeren et al. (2003) and Radomska and Topilko (2017).

et al., 2003). This observation supports that BC cells play a role in MN development by confining them to the CNS. Further studies have shown that this confinement is mediated in part by two signalling pathway, Sema6A and Netrin 5 (Bron et al., 2007; Mauti et al., 2007). BC cells membrane-attached Sema6A plays two roles in MN confinement. First, it aggregates BC cells at the CNS/PNS interface and then it confines MN somata to the ventral horn through its repellent effect, mediated by its MN-expressed receptors plexinA2 and/or Nrp2 (Bron et al., 2007). The involvement of Sema6A was surprising, since it requires direct contact between BC cells and MN cell bodies, which are about 100 µm apart. However, using a human placental alkaline phosphatase (hPLAP) reporter to label BC cells membranes, our lab has shown that some of them extend long cytoplasmic protrusions within the NT (Figure 25). They may ensheath MN axons up to their cell bodies, which could enable such an interaction (Radomska and Topilko, 2017). Netrins are a family of bifunctional axon guidance cues, capable of attracting or repelling axons when respectively binding a member of the deleted in colorectal cancer (DCC) or Unc5 receptor families (Tessier-Lavigne and Goodman, 1996). More recently, it was shown that the interaction between BC-expressed Netrin 5 and its MN-expressed DCC is also necessary to confine MN somata (Garrett et al.,

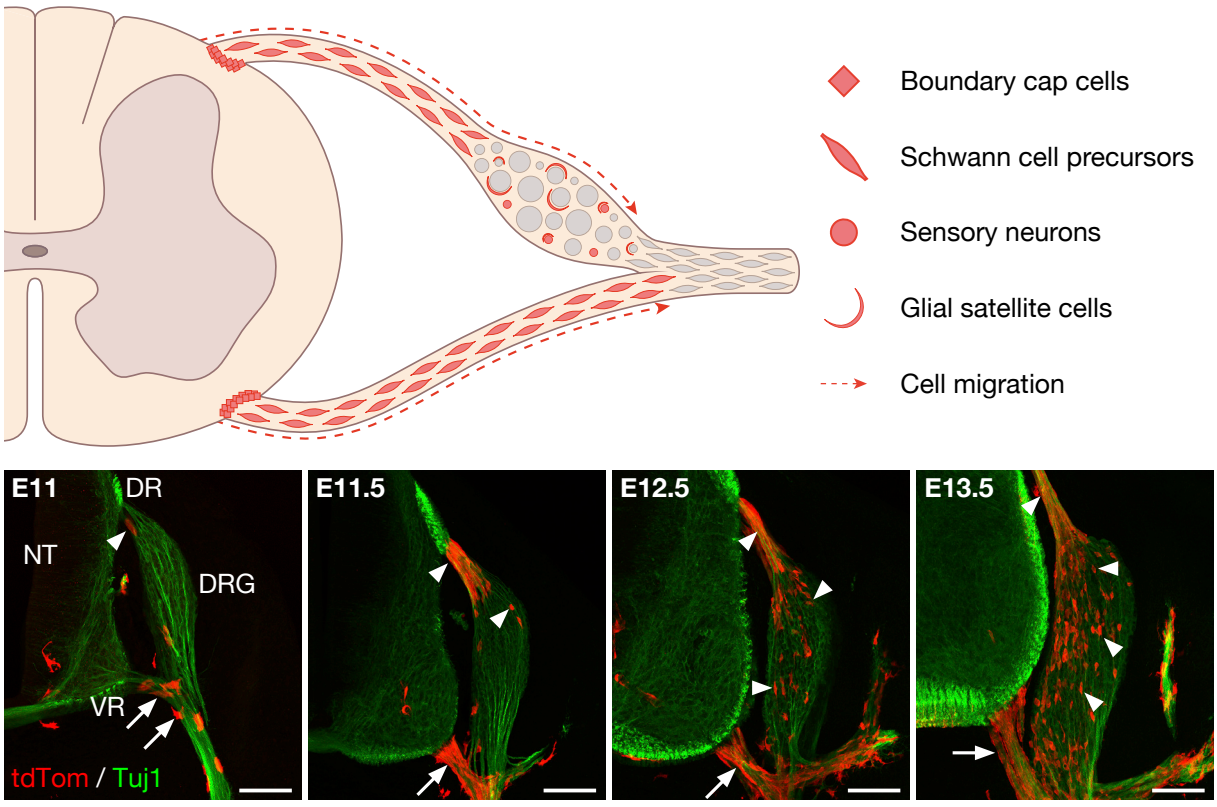

Figure 26. Fate-mapping of Krox20-traced boundary cap cells and their derivatives. Schematic representation of BC cell fate mapping in the trunk of a *Krox20*$^{Cre/+}$, *R26*^{tdTom} mouse embryo at E13.5. Clusters of BC cells reside transiently at the DR/VR entry/exit points and their derivatives populate the proximal (nerve roots and DRG) portions of peripheral nerves. Krox20-expressing BC cells (shown in red) give rise to Schwann cell precursors in the nerve roots, and a subset of sensory neurons and satellite glia in the DRG. Transverse sections of *Krox20*$^{Cre/+}$, *R26*^{tdTom} embryos between E11 and E13.5, immunostained against tdTom (red) and β-III-tubulin (Tuj1, green). Arrows and arrowheads indicate ventral and dorsal BC cells derivatives, respectively. Abbreviations: BC, boundary cap; DR, dorsal root; DRG, dorsal root ganglia; NT, neural tube; VR, ventral root. Scale bars: 100 µm. Adapted from Gresset et al. (2015).

2016). Interestingly, ectopic MN were observed in the posterior NT in the Sema6A/plexinA2 mutant embryos, whereas in Netrin 5/DCC mutants they were mostly observed in the anterior NT. These differences suggest that MN somata confinement is a complex process that differs depending on MN subtypes and the anterior-posterior axis.

3.2.2. Stem cells for the developing peripheral nervous system

To assess their contribution to the developing PNS, our lab has performed *in vivo* fate-mapping analysis of BC cells using mouse embryos carrying Cre recombinase under the control of Krox20 regulatory elements in combination with a Cre-inducible fluorescent reporter (Maro et al., 2004). Using this approach, we have shown that BC cells actively proliferate and emigrate from their initial position into the nerve roots and the DRG (Figure 26). In the dorsal and ventral nerve roots, BC derivatives correspond to most SC and a subpopulation of endoneurial fibroblasts. In the DRG, they give rise to a subpopulation of GSC and about 10% of TrkA+ nociceptive SN (Maro et al., 2004). The fact that the first Krox20-traced BC cells reach the DRG around E11.5 is likely to explain the absence of traced TrkB+ LTMR and TrkC+ proprioceptive SN. Indeed, at this time TrkB+/TrkC+ neurogenesis is ending and TrkA+ neurogenesis beginning, suggesting that the micro-environment is permissive for nociceptive SN development (Marmigère and Ernfors, 2007). This theory is supported by *in vitro* data and the fact that when transplanted into chicken DRG at an earlier stage, mouse BC cells also give rise to large-diameter SN (Hjerling-Leffler et al., 2005). Several studies have shown that BC cells are a multipotent stem cell population that can form spheres and self-renew *in vitro*, and differentiate into multiple cell types both in vitro and in vivo (Aquino et al., 2006; Hjerling-Leffler et al., 2005; Zujovic et al., 2010; 2011). Indeed, when transplanted after a focal spinal cord demyelination, BC cells isolated from embryonic nerve roots can migrate to the lesion site, proliferate and differentiate into mature myelinating SC and thus participate to the CNS remyelination with a higher efficiency than SC grafts (Zujovic et al., 2010). Moreover, when cultured in proper conditions or upon transplantation in the developing murine forebrain they can generate CNS cell types such as neurons, astrocytes and oligodendrocytes (Zujovic et al., 2011).

More recently, we have performed similar fate-mapping experiments using Cre recombinase under the control of Prss56 regulatory elements that I will detail in the results section (Gresset et al., 2015). Briefly, in addition to previously known derivatives, Prss56-traced BC cells also generate large-diameter SN and a subset of their ventral derivatives rapidly migrate along spinal nerves to reach the skin around E13.5. In the adult skin, Prss56-traced BC derivatives include non-myelinating and myelinating SC, terminal glia associated with lanceolate sensory endings, sub-epidermal glia unsheathing nociceptive fibres in the upper dermis and melanocytes (Gresset et al., 2015; Radomska and Topilko, 2017; Radomska et al., 2019). Fate-mapping of Krox-20 expressing BC cells in the postnatal skin was not possible

due to its expression in promyelinating SC at E15.5 and in the hair follicle and myelinating SC around birth (Gambardella et al., 2000; Topilko et al., 1994)

3.3.Boundary cap cells in disease: type 1 neurofibromatosis

Type 1 neurofibromatosis (NF1) is a common genetic disorder caused by mutations of a tumor suppressor gene encoding neurofibromin 1 (Nf1), that predisposes patients to develop benign peripheral nerve sheath tumors called neurofibromas (NF; Ratner, 2015). Almost all NF1 patients develop cutaneous NF (cNF) at nerve endings in the skin, and about a third develop in early infancy plexiform tumors (pNF) at the level of nerve roots and deep peripheral nerves that can progress into malignant peripheral nerve sheath tumors that are invariably lethal (Ratner, 2015). NF are complex tumors composed not only of SC but also axons, blood vessels, peri- and endoneurial fibroblasts, mastocytes and macrophages (Parrinello and Lloyd, 2009). NF are known to arise from the loss of NF1 heterozygosity in cells of the SC lineage, of the remaining functional copy of NF1 which results in the permanent hyperactivation of the Ras proto-oncogene. However, when and where the mutation occurs in the SC lineage cell type is still debated, ranging from NC stem cells to mature SC (Le et al., 2009; Mayes et al., 2011; Wu et al., 2008).

Given their position and progeny, BC cells represented an interesting putative cell at the origin of NF. However, conditional inactivation of Nf1 in Krox20-expressing BC gave rise only to paraspinal pNF, suggesting that pNF but not cNF could originate from them (Zhu et al., 2002). Nonetheless, this new Prss56-expressing BC cells population, with derivatives in both nerve roots and terminals in the skin, represented an interesting new candidate as a putative cell of origin for both pNF and cNF. Hence our lab had developed a mouse model of biallelic conditional inactivation of Nf1 in Prss56-traced BC cells and their derivatives, by introducing Cre recombinase under the control of Prss56 regulatory elements (*Prss56*^{Cre}) and a Cre-inducible fluorescent reporter (*Rosa26*^{tdTom}) into Cre-inducible *Nf1*$^{fl/fl}$ or *Nf1*$^{fl/-}$ backgrounds (Radomska et al., 2019). The resulting mice

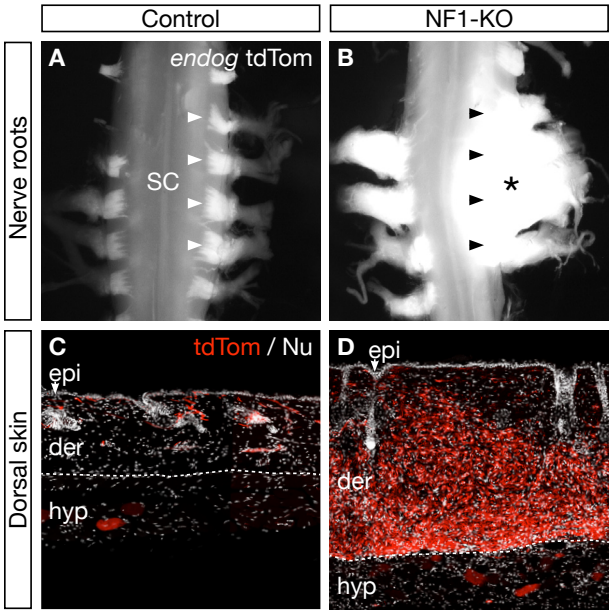

Figure 27. Conditional NF1 loss in Prss56-expressing boundar cap (BC) cells gives rise to paraspinal (plexiform) and cutaneous (diffuse) neurofibromas. (**A**, **B**) Cervical spinal cord comparison between control and Prss56^{Cre}, R26^{tdTom}, NF1$^{flox/flox}$ (NF1-KO) mice. There are multiple paraspinal neurofibromas (asterisk) encompassing nerve roots (arrowheads) and DRG, and compressing the spinal cord in the NF1-KO. All remaining roots show marked hyperplasia. (**C**, **D**) Dorsal skin sections from control and NF1-KO mice immunolabeled against tdTom (red). Note the accumulation of tdTom-traced cells in the NF1-KO dermis. The dermis-hypodermis boundary is indicated by dotted line. Abbreviations: SC, spinal cord; epi, epidermis; der, dermis; hyp, hypodermis; Nu, cell nuclei. Adapted from Radomska and Topilko (2017).

were the first animal model to faithfully recapitulate the human disease (Figure 27). This clearly indicates that Prss56-expressing BC cells and their derivatives are implicated in the development of pNF and cNF, but the specific cell type, especially in the skin, responsible for initiation and tumor progression remains to be determined. This new mouse model constitutes an exciting new genetic tool to better understand the mechanisms underlying disease progression, including at non-symptomatic stages and perform new therapeutic studies on NF1.

II. The cardiovascular system

1. Organisation of the cardiovascular system

1.1. Overview of the circulatory system

The circulatory system is responsible for distributing oxygen and nutrients to tissues, and removing and transmitting metabolic waste products, such as carbon dioxide, to the excretory organs (Carroll, 2007; Hall, 2016). It is subdivided into the blood-vascular and the lymphatic systems (Figure 28). The blood-vascular system is made of a muscle, the heart, which pumps a carrying fluid, the blood, throughout the body within blood vessels. In vertebrates, it is a closed circulatory system in which blood is confined to the vessels. Indeed, it first goes through the arterial system at high pressure to reach the capillary bed within each tissue, where exchanges occur, and it is then channelled through the venous system at low pressure back to the heart (Figure 28). In mammals, the heart is divided into its left and right sides, which are considered as two different synchronous pumps that propel blood into two circulations. In each, blood returning through veins arrives in a first chamber, the atria, before entering a second one, the ventricle, where it is pumped out into arteries. The right ventricle propels blood into the pulmonary circulation where it is oxygenated and which is connected to the left atria. Then, the left ventricle pumps it into the systemic circulation, which supplies blood to every organ, and is connected back to the right atria. The lymphatic system drains the extravasated fluid, called lymph, from the extracellular space and returns it to the venous circulation (Figure 28). Beyond the removal of waste products and cellular debris, it also plays an essential role in immune defence. Indeed, the lymphatic system includes multiple lymph nodes throughout the body, where lymphocytes are concentrated, and its associated organs, such as the spleen and thymus, are sites of lymphocyte production. In the remainder of my introduction, I will focus on the blood vessels.

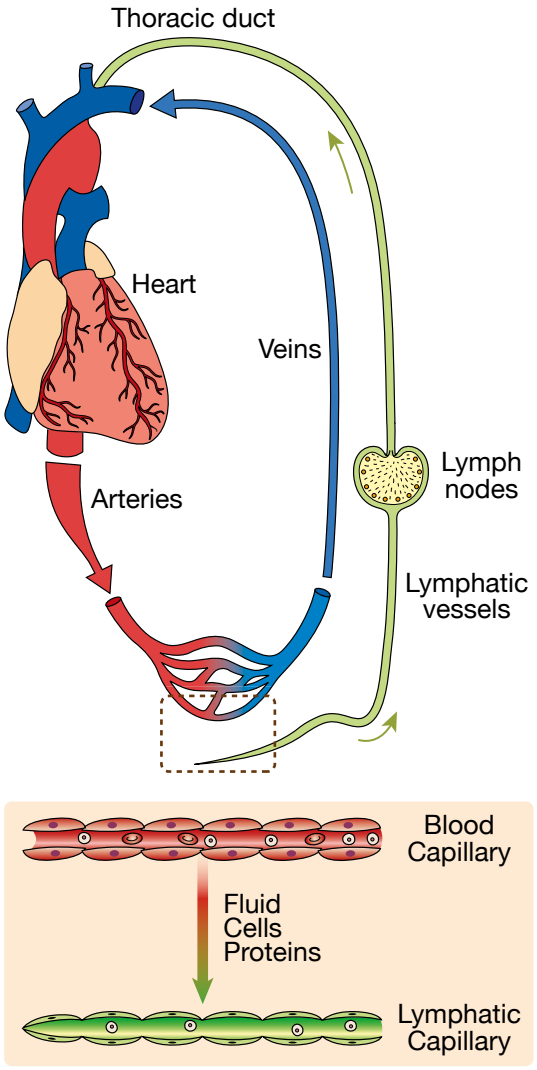

Figure 28. Schematic representation of the circulatory system. Blood is pumped from the heart through arteries, arterioles and capillaries to the tissues, where exchanges occur. Blood is returned to the heart via the venous circulation. The lymphatic system, composed of lymphatic capillaries and vessels, drains excess fluid, the lymph, containing proteins, lipids and immune cells, from the extracellular space and returns it to the venous circulation. Adapted from from Karkkainen et al. (2002).

1.2. Blood vessels

1.2.1. Macrovasculature

The macrovasculature is made of arteries and veins with a diameter of more than 100 µm (Carroll, 2007; Hall, 2016). They are composed of three concentric tissue layers around the lumen (Figure 29). The inner layer, or *tunica intima*, is in contact with blood and consists in a single layer of flat endothelial cells (EC), their basement membrane (BM) and the internal elastic lamina that circles it. Around it, the *tunica media* is made of a layer of vascular smooth muscle cells (vSMC), connective tissue and in large arteries it is delimited by the external elastic lamina. Finally, the outermost layer, the *tunica adventitia*, is made of connective tissue, immune cells and contains in the larger vessels the nerves and vessels that supply the vascular wall, called *vasa vasorum*. Blood vessels are organized in a sequence of vascular segments, each with specific properties and functions (Figure 29). The large vessels emerging from the heart are *elastic arteries*, whose media contains vSMC and numerous concentric lamellae of elastin and collagen. Their elasticity allows them to stretch in response to each pulse, which dampens blood pressure fluctuations over the cardiac cycle and maintains organ perfusion

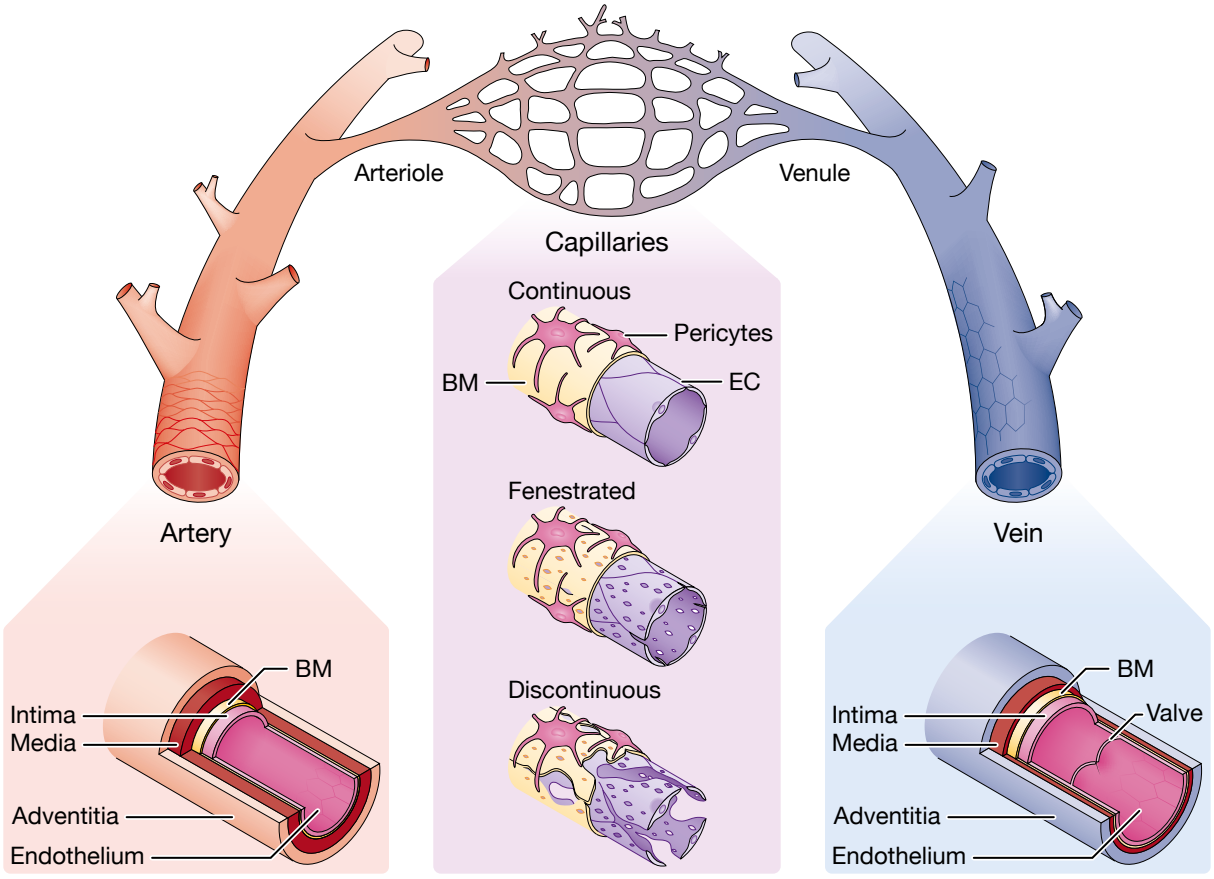

Figure 29. Organization of the vasculature. The vasculature is organized into hierarchical networks of arteries (red), veins (blue) and interconnected capillaries. Arterioles, capillaries and venules constitute the microvasculature. Large arteries and veins are characterized by a continuous lining of endothelial cells (EC), basement membrane (BM) and layers of smooth muscle cells (SMC). Blood capillary EC can be continuous, fenestrated or discontinuous, and they have a varying extent of BM and pericyte coverage. Adapted from Potente and Mäkinen (2017).

during the diastole. They are followed by *muscular arteries*, whose media contains many concentric layers of vSMC and fewer elastic lamellae. Their controlled contraction enables to regulate the blood flow entering into the microvasculature according to regional needs. Finally, the blood exiting the microvasculature goes back to the heart through *veins*, which have a thin media containing only a few layers of vSMC but a thick adventitia made of collagen and some longitudinal vSMC. Most veins have one-way valves that prevent the blood from going backwards.

1.2.2. Microvasculature

The microvasculature is organised in the following sequence (Figure 29): arterioles, capillaries, and venules (Carroll, 2007; Hall, 2016). First, the blood enters the microvascular tree through *arterioles*, whose media contains only one or two layers of vSMC, covered by a thin adventitia. They are the primary site of vascular resistance, and protect the capillaries by regulating the local blood pressure. Then, it reaches the *capillaries*, which are the smallest vessels with diameters ranging from 4 to 10 µm, and whose lumen allows the passage of cells in a single row. Their wall consists in EC and pericytes within their BM. Their endothelium can be continuous, as for instance in the skin, making them less permeable. Conversely, it can be discontinuous as in the liver, making them highly permeable. Intermediately, it can be discontinuous with a continuous BM, or fenestrated, in organs such as endocrine glands. Afterwards, the blood is drained by *venules* of increasing diameter, which are first covered by pericytes and then by few layers of vSMC, and a thin adventitia. Their endothelium has labile junctions, which can modulate their permeability during inflammation and allow the exit of immune cells (Girard et al., 2012).

1.3. Cellular diversity within the blood vessels

1.3.1. Endothelial cells

EC are a heterogeneous population with vascular segment-specific and organ-specific morphological and functional differences that allow the endothelium to adapt to regional needs (Aird, 2007a; 2007b; 2012; Chi et al., 2003; Cleaver and Melton, 2003). To highlight their heterogeneity, I will briefly present here several of their main functions except for angiogenesis and the arterio-venous identities, that I will discuss later in the section on the development of the vascular system.

Barrier function

EC are organised in a single-layer epithelium (Figure 29), linked together by adherens (AJ) and tight junctions (TJ), that acts as a size-selective and semipermeable barrier separating blood from the interstitium (Aird, 2007a; Komarova and Malik, 2010; Michiels, 2003). Fluids

and solutes smaller than 3 nm can move through a paracellular route, regulated by inter-endothelial AJ and TJ. Endothelial AJ, consisting in vascular endothelial (VE)-cadherin complexes with catenins, are the most frequent type among vascular beds. For instance during inflammation, EC increase vascular permeability by internalizing VE-cadherins, which destabilizes AJ (Dejana and Orsenigo, 2013; Komarova and Malik, 2010). By contrast, macromolecules move through a transcellular route via EC transcytosis. For instance, albumin and its ligands are transported from the luminal membrane by caveolae, formed by fission of plasma membrane macrodomains enriched with caveolin-1, to the basal membrane where they are released by exocytosis (Aird, 2007a; Komarova and Malik, 2010). Both routes are finely regulated to maintain the integrity of the endothelium, control tissue oncotic pressure and ensure the proper delivery of important blood-borne molecules such as hormones and albumin-bound ligands. They also differ in a segment-specific and organ-specific manner, illustrated by capillaries. Indeed, compared with other vascular segments, capillaries have a higher rate of transcytosis and looser inter-endothelial junctions to maximise exchanges (Aird, 2007b; 2012; Komarova and Malik, 2010). However, this is not the case in the brain with the BBB, where EC have few caveolae and form mostly TJ (Bendayan, 2002; Nitta et al., 2003; Simionescu et al., 2002).

Vascular tone

EC actively participate to the resting vascular tone by synthesizing nitric oxyde (NO) (Fleming et al., 1996; Furchgott and Zawadzki, 1980; Michiels, 2003; Palmer et al., 1987). Indeed, vSMC require a functional endothelium to relax properly in response to acetylcholine, and NO inhibition increases the basal blood pressure. EC also regulate the resting vascular tone by secreting prostacyclin (PGI_2) (Michiels, 2003; Moncada et al., 1976). In specific conditions, such as hypoxia, EC can also release the vasoconstrictive factor Edn (Kedzierski and Yanagisawa, 2001; Michiels, 2003; Yanagisawa et al., 1988). EC release Edn from their non-luminal surface, which induces vSMC contraction via EdnrA while simultaneously triggering the release of vasodilating NO/PGI_2 by EC via EdnrB to counteract it (Kedzierski and Yanagisawa, 2001).

Inflammation and immune response

EC play a significant role in inflammation, which can be summarized in the following sequence: increased blood flow by arterioles, capillaries and venules dilatation; fluid exsudation through increased permeability; and leukocytes extravasation (Aird, 2007a; Michiels, 2003; Nathan, 2002). Circulating cytokines such as TNF-α or interleukine (IL)-1 trigger a pro-inflammatory EC phenotype, which start secreting platelet-activating factor (PAF) which in turn stimulates neutrophil adhesion. Moreover, in post-capillary venules, EC express specific adhesion molecules such as E-, P-selectin, vascular cell adhesion molecule (VCAM)-1 and

intercellular adhesion molecule (ICAM)-1 that will recruit leukocytes and trigger diapedesis (Aird, 2012; Collins et al., 1995; Michiels, 2003; Muller, 2011). Diapedesis is a multistep process during which blood-borne leukocytes migrate through the endothelium towards the underlying tissue (Muller, 2011).

Haemostasis

All EC are actively involved in haemostasis, in which they can have a pro- or anti-thrombotic role. Indeed, quiescent EC secrete PGI_2 and NO, which prevent platelet aggregation (Michiels, 2003; Moncada et al., 1976; Palmer et al., 1987). Oppositely when activated, either by a vascular injury or circulating cytokines, they can promote platelet activation by secreting PAF, and coagulation by releasing von Willebrand factor (vWF). Finally, during thrombosis EC initiate fibrinolysis by secreting of tissue-plasminogen activator (tPA) and urokinase that activate plasmin, which in turn degrades the clot.

1.3.2. Mural cells

Mural cells are a heterogeneous population of perivascular cells classically divided between pericytes that ensheath capillaries and vSMC that are found in arterioles, venules and larger vessels (Armulik et al., 2011; Holm et al., 2018; Krueger and Bechmann, 2010). However, this definition has been challenged recently by growing evidence instead of a mural cell continuum (Figure 30) with transitional phenotypes at pre-capillary arterioles and post-capillary venules (Armulik et al., 2011; Hartmann et al., 2015; Holm et al., 2018). In addition with the lack of specific markers, this may explain why their proper identification remains challenging.

Pericytes

Pericytes were first described 150 years ago as a population of contractile cells surrounding the endothelium of small blood vessels (Eberth, 1871; Rouget, 1873; Zimmermann, 1923). Interestingly, pericytes may not be limited to the microvasculature, as there have been observations of subendothelial pericyte-like cells in large vessels (Andreeva et al., 1998; Díaz-Flores et al., 2009). Nonetheless, pericytes are currently defined as cells embedded within the microvascular BM (Armulik et al., 2011; Daneman and Keller, 2015; Sims, 1986). Capillary pericytes have a rounded cell body and limited branching, while post-capillary venule pericytes have a flattened cell body and many thin, branching cellular processes in a stellate pattern (Figure 30). Although they are separated by the BM, pericytes and EC contact each other through multiple holes where they establish different types of junctions. The main type are peg-socket junctions, which consist in reciprocal interdigitating evaginations from each cell and are believed to be mediated by N-cadherin and anchor pericytes (Armulik et al., 2011; Daneman and Keller, 2015; Gerhardt and Betsholtz, 2003). Adherens and gap junctions

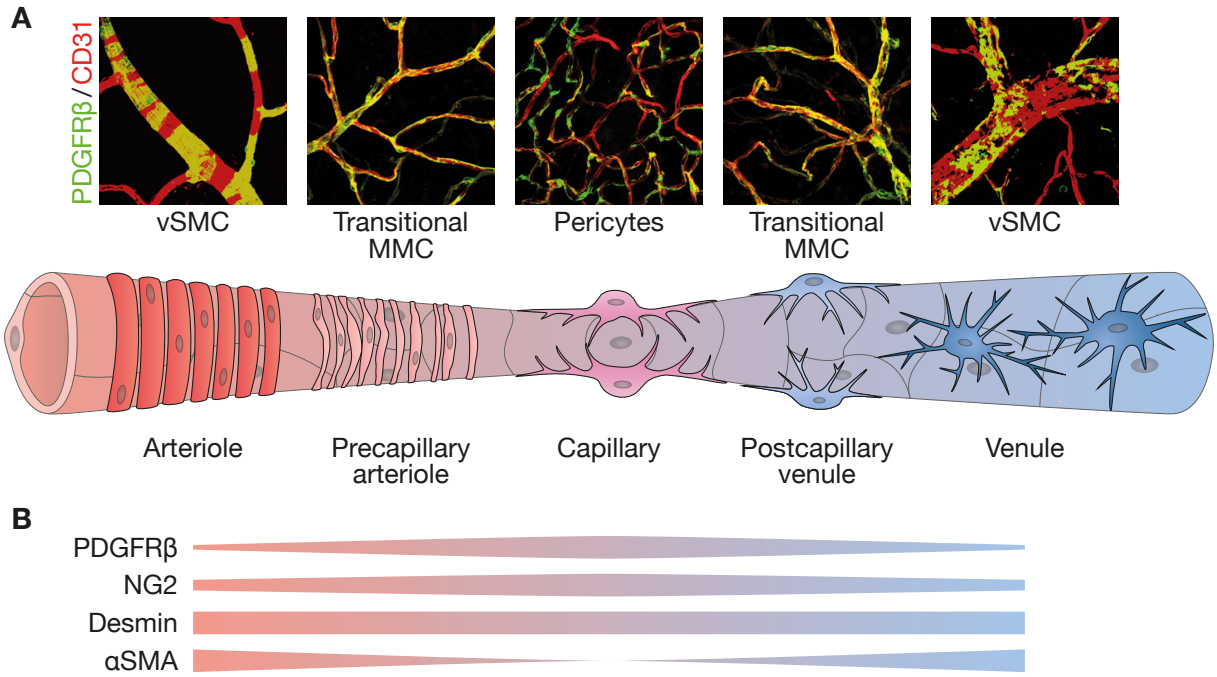

Figure 30. Mural cell continuum along the microvascular tree. (**A**) Confocal images of microvascular mural cells (MMC) of different vessel hierarchies labeled in *Pdgfrβ-mTmG* mice, with the coresponding schematic illustration. Arterioles are completely surrounded by a single layer of spindle-shaped vascular smooth muscle cells (vSMC). Precapillary arteriole coverage with transitional MMCs is loose. Pericytes covering the mid-capillary bed exhibit a round cell body and processes spanning over several endothelial cells (EC). Transitional MMC along the postcapillary venule are characterized by flattened cell bodies and multiple processes. Venule vSMC are large stellate cells not fully ensheathing the endothelium. (**B**) Mural cells express different combinations of markers such as platelet-derived growth factor receptor β (PDGFRβ), Neural/glial antigen 2 (Ng2), desmin, and α smooth muscle actin (αSMA) depending on their location along the microvasculature. Adapted from Holm, Heumann and Augustin (2018).

have also been described (Armulik et al., 2011; Ivanova et al., 2017). The most commonly used pericyte marker is PDGFRβ, which is involved in pericyte recruitment, and more recently other markers have been identified, such as neural/glial antigen 2 (Ng2), desmin, Cd13, α-smooth muscle actin (SMA), endosialin, regulator of G protein signalling 5 (Rgs5) or Tbx18 (Guimarães-Camboa et al., 2017). However, none of these markers is specific as they are expressed in multiple other cell types. The EC-to-pericyte ratio in normal tissues varies between 1:1 and 10:1, and their EC abluminal surface coverage ranges from 70% to 10%, primarily along endothelial cell-cell junctions and branch points (Ando et al., 2016; Armulik et al., 2011; Daneman and Keller, 2015; Sims, 1986). Their density is inversely correlated with vessel wall permeability and EC turnover rate (Armulik et al., 2011; Daneman and Keller, 2015; Díaz-Flores et al., 2009). This led to the hypothesis that pericytes promote endothelial stability and limit permeability, which has been supported by the analysis of knockout mice lacking pericytes (Hellström et al., 2001; Lindahl et al., 1997). Moreover, recent CNS pericytes live imaging has shown that while their cell body is static, they dynamically extend and retract their processes over days (Berthiaume et al., 2018). Interestingly, they negotiate their territory with one another as the ablation of a single pericyte leads to the robust extension of processes from adjacent pericytes (Berthiaume et al., 2018).

Pericytes regulate several of the vascular functions discussed earlier, in coordination with EC. For instance, they regulate the barrier function in several ways. First, they are necessary for the production and maintenance of a proper BM, and in their absence although EC secrete BM proteins they are not properly deposited (Armulik et al., 2010; Stratman et al., 2009; 2017; 2010). Moreover, recent studies on the BBB have shown that pericytes limit CNS vascular permeability by inhibiting the rate of transcytosis (Armulik et al., 2010; Daneman et al., 2010). Although it was their first suggested function, whether pericytes regulate blood flow remains an open question. Indeed, in vitro experiments have shown that pericytes express contractile proteins and can respond to vasodilative and vasoconstrictive agents (Daneman and Keller, 2015; Kennedy-Lydon et al., 2013; Rucker et al., 2000). However, *in vivo* experiments have yielded conflicting results, as for instance on their ability to regulate cerebral blood flow (Berthiaume et al., 2018; Hall et al., 2014; Hill et al., 2015). Over the last decade, several reports have detailed how pericytes positively regulate neutrophil transmigration through venular walls in the muscle and skin. Indeed, neutrophils exit the endothelium at permissive points without pericyte coverage and with different BM components, which is facilitated by the expansion of pericyte gaps (Ayres-Sander et al., 2013; Daneman and Keller, 2015; Proebstl et al., 2012; Voisin et al., 2010; Wang et al., 2012; 2006). Then, they crawl along pericytes via an interaction between the neutrophil-expressed Macrophage-1 antigen and ICAM-1 (Proebstl et al., 2012). Finally, it has been reported that after neutrophils exit venules, they are attracted by capillary pericytes, which control their activation status and survival (Stark et al., 2013). However, it has been reported in the CNS that pericytes downregulate leukocyte transmigration, suggesting a more complex and context-dependant role (Daneman et al., 2010). They also play a role in stabilizing blood vessels and promoting their maturation, which I will discuss in the development section. Finally, pericyte also regulate organ-specific functions such as the establishment of the BBB in the brain, the egress of T cells from the thymus or the storage of retinol in the liver (Armulik et al., 2010; Blomhoff and Blomhoff, 2006; Daneman and Keller, 2015; Daneman et al., 2010; Zachariah and Cyster, 2010).

Vascular smooth muscle cells

Although vSMC are highly specialized cells whose main function is contraction, they retain a remarkable plasticity which allows them to take on other roles in physiological and pathological vascular remodelling (Alexander and Owens, 2012; Owens et al., 2004; Rensen et al., 2007; Wang et al., 2015). Indeed, the vast majority of normal adult blood vessels vSMC display a contractile phenotype, but can reversibly switch to a synthetic phenotype depending on their environment (Alexander and Owens, 2012; Rensen et al., 2007). Contractile vSMC are elongated and spindle-shaped cells (Figure 30) that have been characterized by the presence of contractile proteins, ion channels, and signalling molecules necessary for their function (Owens, 1995; Owens et al., 2004). They are structurally different from other myocytes, as myosin and their surrounding actin filaments are joined together and anchored by dense

bodies within the cell or dense bands on the inner cell surface (Klabunde, 2011). Similarly to cardiomyocytes, vSMC are electrically connected by gap junctions, which allow propagated responses along the vessel. Several markers are commonly used to characterise them, although none is specific: α-SMA, smooth muscle-myosin heavy chain (SM-MHC), calponin, SM22α and desmin (Owens et al., 2004). Contractile vSMC are always in partially contracted state, which determines the resting blood vessel tone and diameter, and by modulating it they regulate the blood pressure and blood flow distribution (Klabunde, 2011; Owens et al., 2004). Vasoconstrictive signals are mediated by sympathetic adrenergic nerves, circulating hormones such as epinephrin and also EC-secreted Edn. Oppositely, they receive vasodilative signals from the circulation and their environment such as NO and PGI_2 from EC (Klabunde, 2011).

Synthetic vSMC have an epithelioid morphology and are characterized by a reduced expression of contractile vSMC differentiation markers, such as SM-MHC, and an increased proliferation rate, motility, and ECM components synthesis (Alexander and Owens, 2012; Owens et al., 2004). The current paradigm, in which contractile vSMC switch to a synthetic phenotype, was founded on multiple studies who demonstrated the conversion of contractile vSMC to a less differentiated, proliferative and migratory cell type in culture (Alexander and Owens, 2012; Owens, 1995; Owens et al., 2004). Two fate-mapping studies based on different Cre-inducible mouse lines have supported this hypothesis, and shown that vSMC down-regulate α-SMA, proliferate and contribute to neointima formation after a vascular injury (Herring et al., 2014; Nemenoff et al., 2011). More recently, this theory has been challenged by a report in which the authors used a *SM-MHC-Cre* mouse for lineage tracing and found that contractile vSMC are incapable of proliferating either *in vitro* or *in vivo* in response to injury (Tang et al., 2012). Instead, they identified a small population (<10%) of multipotent vascular stem cells by their expression of several markers, including Sox17, Sox10 and S100β, which proliferated to completely reconstitute medial vSMC in response to vascular injury. Hence, the *in vivo* plasticity of vSMC remains debated.

A source of multipotent stem cells?

Ten years ago, pericytes were reported to be mesenchymal stem cells (MSC) that could be expanded *in vitro* for multiple passages and give rise to cells of the osteo-, chondro- and adipogenic lineages (Crisan et al., 2008). Since then, several *in vivo* fate-mapping studies concurred that pericytes were progenitors of white adipocytes, follicular dendritic cells and skeletal muscle (Dellavalle et al., 2011; 2007; Krautler et al., 2012; Tang et al., 2008). It was also reported that CNS pericytes were able *in vitro* to generate neurons, oligodendrocytes and astrocytes (Dore-Duffy et al., 2006). However, a recent study has challenged the view of endogenous pericytes as multipotent tissue-resident progenitors (Guimarães-Camboa et al., 2017). The authors argued that most experiments were either based on artefactual *in vitro* cell culture and/or graft experiments which were not conclusive, or fate-mapping with the

PDGFRβ-*Cre* mouse line which is not specific enough. Indeed, using more specific *Tbx18-H2B-GFP* and *Tbx18-Cre-ERT2* mice line, they reported that while GFP+ Tbx18-expressing cells from adult mice behaved as MSC *in vitro*, Tbx18-traced pericytes and vSMC cells did not significantly contribute to other cell lineages in normal and pathological conditions (Guimarães-Camboa et al., 2017). Although these results strongly support that pericyte *in vitro* multipotency is due to their manipulation, the lack of a specific pan-pericyte marker means that it cannot be fully excluded that different subpopulations were studied. Similarly, the presence of multipotent stem cells within the vascular media has also been reported (Sainz et al., 2006; Tang et al., 2012). However, these claims are based on *in vitro* experiments and should be taken with caution in the absence of supporting *in vivo* experiments.

1.3.3. Perivascular fibroblast-like cells

In parallel to the studies which reported pericytes to be mesenchymal stem cells, others implicated them as the potential cell of origin for myofibroblasts, which are responsible for fibrosis after a lesion in the CNS, kidney and lung (Armulik et al., 2011; Daneman and Keller, 2015; Greenhalgh et al., 2013; Ren and Duffield, 2013). In the spinal cord, using a *glutamate-aspartate transporter (GLAST)-Cre* mouse line, it was reported that a GLAST-positive pericyte subpopulation was at the origin of scar tissue after a spinal cord injury (Göritz et al., 2011). More recently, it was shown that targeting this subpopulation to reduce its derived scarring promoted recovery after a spinal cord injury (Dias et al., 2018). However, another lineage-tracing study has demonstrated that a population of Collagen1α1 (Col1a1) and PDGFRα-expressing positive perivascular fibroblast-like cell (PVF) were actually at the origin of the fibrotic scar tissue (Soderblom et al., 2013). Similarly, more recent studies have shown in the kidney and lung that PVF and not pericytes are the major source of myofibroblasts (Hung et al., 2013; LeBleu et al., 2013). Finally, PVF could correspond to a population recently described in the skin and muscle of PDGFRα/β-expressing perivascular cells that transiently express Adam12 following injury and are the main source of myofibroblasts (Dulauroy et al., 2012). These examples show the challenge of properly defining pericytes and PVF, as well as the need for additional specific markers. Single-cell transcriptomic analysis (scRNA-seq) are likely to play a key role in the coming years to decipher the heterogeneous populations that are pericytes, vSMC and the newly defined PVF, as two recently published studies illustrate. Indeed, scRNA-seq of the brain vasculature has confirmed the existence of a Col1a1- and PDGFRα-positive population of PVF, and provided several other markers such as ECM components Lumican and Decorin (Vanlandewijck et al., 2018). Moreover, a second study has shown that following brain infection, PVF and Rgs5-expressing pericytes were the early source of the CC chemokine ligand 2 (CCL2), which in turn increases total neuronal excitability (Duan et al., 2018).

2. Development of the vascular system

As the diffusion distance of molecules is limited, the establishment of a functional circulatory system is necessary for the embryonic development. First during vasculogenesis, new vessels are assembled *de novo* by mesoderm-derived endothelial precursors (angioblasts) that differentiate into a primitive vascular network (Eichmann et al., 2005; Risau and Flamme, 1995; Swift and Weinstein, 2009). Then during angiogenesis, this network is organized into arteries and veins through vessel sprouting and remodeling (Adams and Alitalo, 2007; Herbert and Stainier, 2011; Potente and Mäkinen, 2017; Potente et al., 2011). Finally, the recruitment of mural cells that ensheath nascent EC tubules provides stability and regulates perfusion (Armulik et al., 2011; Jain, 2003). The vascular endothelial growth factor (VEGF) signaling pathway is essential during vascular development. In mammals, the VEGF family is composed of six secreted dimeric glycoproteins (A, B, C, D, E, and placenta growth factor) . There are three tyrosine kinase receptors, Fms-related tyrosine kinase 1 (Flt1/VEGFR1), fetal liver kinase 1 (Flk1/VEGFR2) and Flt4 (VEGFR3). VEGFA is the type most involved in vascular development, and while it also interacts with VEGFR1, VEGFR2 is the main mediator of VEGFA signaling (Apte et al., 2019; Blanco and Gerhardt, 2013; Olsson et al., 2006; Simons et al., 2016).

2.1. Vasculogenesis

2.1.1. Angioblast specification

Angioblast specification begins during early gastrulation (Figure 31), in posterior lateral plate mesoderm cells leaving the primitive streak (Drake and Fleming, 2000; Gilbert, 2016; Potente and Mäkinen, 2017; Risau and Flamme, 1995; Vokes and Krieg, 2015). They express VEGFR2 but not PDGFRα, and give rise to endothelial and hematopoietic cells during development (Eichmann et al., 1993; 2005). VEGFA/VEGFR2 plays a crucial role during early vasculogenesis, as heterozygous VEGFA or homozygous VEGFR2 mutants fail to develop a vasculature and die *in utero* (Carmeliet et al., 1996; Ferrara et al., 1996; Shalaby et al., 1995). However, the fact that angioblasts form in its absence supports that it is not necessary for their specification (Kelly and Hirschi, 2009; Marcelo et al., 2013; Shalaby et al., 1995). The first step in angioblast specification (Figure 31) is the transient expression of the E-26 variant 2 (Etv2) transcription factor, which is induced by a combination of BMP4, FGF2, Wnt and Notch signals (Eliades et al., 2016; Lee et al., 2008; Marcelo et al., 2013). At this stage, the transcription factor Runx1 acts as a fate switch between the hematopoietic and endothelial lineages (Figure 31). Indeed, it has been shown that Runx1 silencing by Bmi1 restrains the hemogenic potential of these progenitors (Eliades et al., 2016). The relationship between the hematopoietic and endothelial lineages has been controversial, with the question of a common bipotent progenitor called hemangioblast (Vokes and Krieg, 2015). However, recent data from genetic fate-mapping and *in vitro* experiments supports that the branching of both lineages takes place much earlier, while progenitors are still in the primitive streak

(Ditadi et al., 2015; Swiers et al., 2013; Ueno and Weissman, 2006).

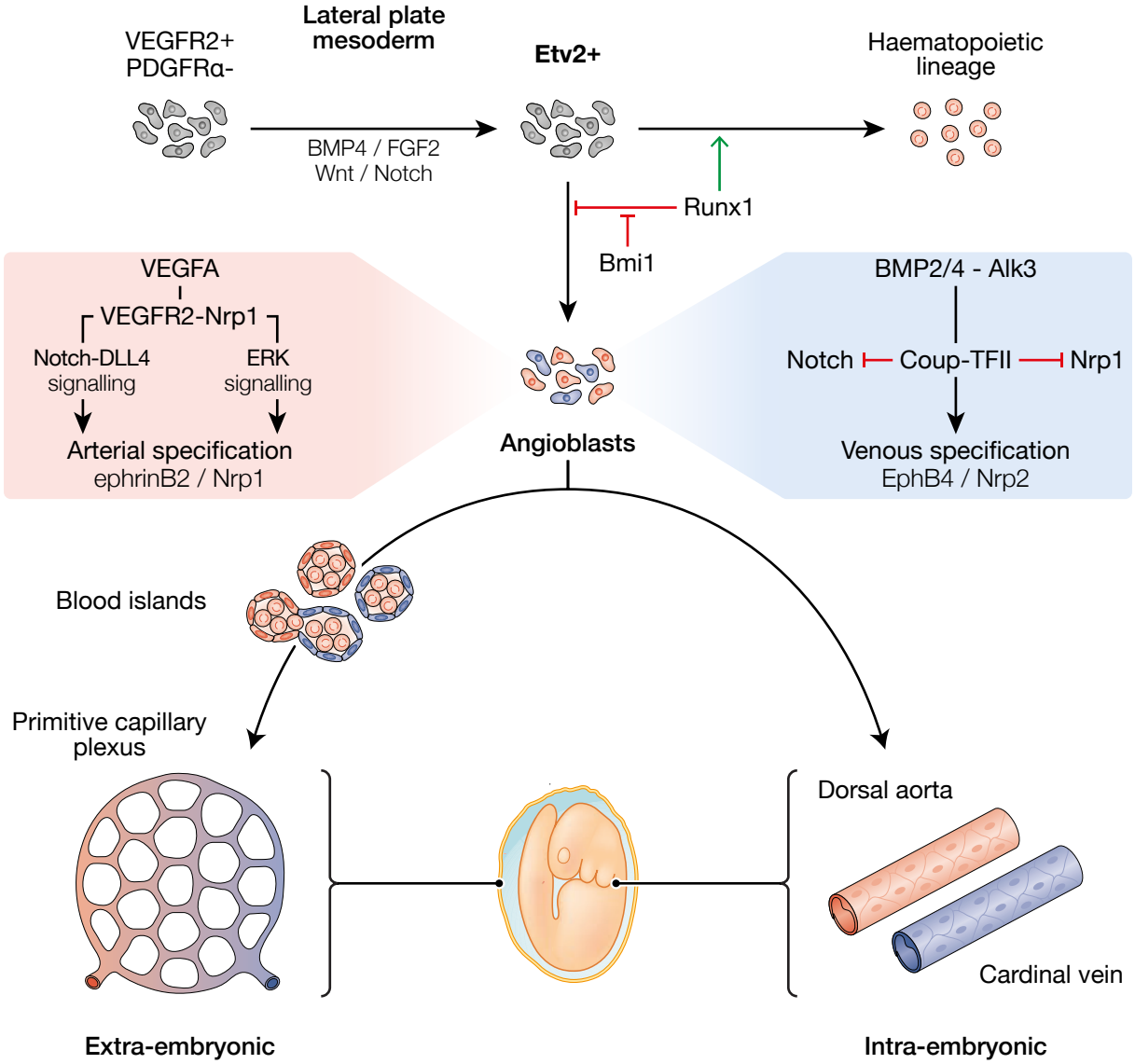

Figure 31. Vasculogenesis and arteriovenous fate. Endothelial progenitor cells (angioblasts) are specified within the lateral plate mesoderm by a combination of BMP4, FGF2, Wnt and Notch signalling that induces the expression of the E-26 variant 2 (Etv2) transcription factor, and Runx1 inhibition by Bmi1. Then, they acquire arterial or venous fate, and assemble into the first embryonic blood vessels: the dorsal aorta and cardinal vein. In the extra-embryonic yolk sac, angioblasts first assemble into blood islands that fuse to form a primary vessel network. The main signalling pathways and transcriptional programs that control the arteriovenous fate are detailed in the red and blue boxes. Adapted from Marcelo et al. (2013) and Potente and Mäkinen (2017).

2.1.2. Primitive vascular network

In mice, angioblasts reach at E6.5 the extra-embryonic yolk sac (Figure 31), where they form with blood islands with hematopoietic progenitors, and later at E7.5 the embryo (Drake and Fleming, 2000; Pardanaud and Dieterlen-Lièvre, 1993; Risau and Flamme, 1995). VEGFA/VEGFR2 signalling is crucial for their proper migration, proliferation and survival, and in its absence blood islands do not form (Marcelo et al., 2013; Shalaby et al., 1997). In the yolk sac, blood islands connect each other to form a primitive vascular plexus, while in the embryo angioblasts aggregate directly into the dorsal aorta or cardinal vein (Chung

and Ferrara, 2011). During this process, angioblasts initially form primitive tube-like vessels, before differentiating into EC with a basal lamina while forming the vascular lumen (Herbert and Stainier, 2011; Patel-Hett and Damore, 2011). Interestingly, in addition to angioblast it has recently been shown that erythro-myeloid progenitors (EMP) that are born in the yolk sac contribute to EC (Plein et al., 2018). Using an inducible *Csf1r-iCre* mouse line (*Csf1r* is a myeloid lineage gene), the authors have revealed that EMP give rise to EC in two waves, first in the yolk sac and then in the embryo where they persist into adulthood (Figure 33). While they have shown that this process is dependent on *Hoxa* cluster genes, the underlying mechanisms remain unknown. Their contribution is proportionally smaller than angioblasts in most organs, such as the brain, heart and lung, except in the liver where they represent 60% of EC.

2.1.3. Arteriovenous fate acquisition

Arteriovenous fate acquisition begins during vasculogenesis (Figure 31), before the onset of blood flow (Herbert and Stainier, 2011; Herzog et al., 2005; Marcelo et al., 2013; Swift and Weinstein, 2009). One of the first fate markers are ephrinB2 in artery-fated EC and EphB4 in their vein-fated counterparts (Wang et al., 1998). Their repulsive signalling allows the proper segregation of both EC types and is crucial for proper vascular development. Indeed, ephrinB2 knockout mice display severe vasculogenic defects (Wang et al., 1998). Whether arterial- and venous-fated angioblasts assemble into common precursor vessels before segregating, or arise from different pools of angioblasts defined by environmental cues, such as VEGF and Hedgehog (Hh), is still being investigated (Herbert et al., 2009; Kohli et al., 2013; Potente et al., 2011). At the end of this process, the primitive vascular plexus in the yolk sac and the cardinal vein and dorsal aortae in the embryo anastomose and connect to the developing heart prior to the first heartbeat, which occurs around E8 (Chong et al., 2011; Risau and Flamme, 1995).

The establishment of arterial identity is induced by two interrelated signalling pathways, VEGFA and Notch (Figure 31). VEGFA, whose expression is under the control of the Shh signalling pathway, induces arterial fate by binding to VEGFR2 and its co-receptor Nrp1 in two ways (Lanahan et al., 2013; Lawson et al., 2002). First, it activates Notch signalling by upregulating Dll4 and Hey2 through its downstream effectors Forkhead box C1 and C2 (Foxc1/2; Gu et al., 2003; Hayashi and Kume, 2008). Indeed, mice lacking Foxc1/2 lack arteries but display normal venous markers. More recently, it has been shown that VEGFA also activates Erk signalling, which is the key driver of arterial fate (Lanahan et al., 2010; 2013; Potente and Mäkinen, 2017; Sakurai et al., 2005; Simons and Eichmann, 2015). Notch-Dll4 signalling promotes ephrinB2 expression and supresses EphB4, which is key for arterial differentiation as *in vivo* inhibition of Notch results in an arterial to venous fate switch (Lawson et al., 2001). However, the relationship between Notch and VEGF signalling is likely

to be more complex. Indeed, while Notch-Dll4 signalling is considered to be downstream of VEGFA, a more recent report has shown that Notch1 activation by its ligand Dll1 is essential for arteriogenesis by upregulating of VEGFR2 and Nrp1 (Sörensen et al., 2009). The establishment of venous identity is induced by BMP signalling (Figure 31) and its inactivation *in vivo* resulted in the loss of venous identity (Neal et al., 2019). BMP2/4 binding to its activin receptor-like kinase (Alk)3 type I receptor, through the phosphorylation of SMAD1/5, upregulates Ephb4 and chicken ovalbumin upstream promoter–transcription factor II (Coup-TFII) expression. Indeed, Coup-TFII is known to repress Nrp1 and its downstream Notch signalling to induce vein identity, as EC acquire an arterial identity in its absence (You et al., 2005).

2.2. Angiogenesis

2.2.1. Sprouting angiogenesis

Angiogenesis is the process of expanding blood vessels (Figure 32), either by sprouting new branches or by intussusception, that subsequently remodel them into a functional vascular circuit (Risau, 1997). During angiogenic growth, some EC are selected to lead the growing sprout in order to maintain vascular integrity. They are called tip cells, and the EC following them stalk cells (Gerhardt et al., 2003). The main signalling pathway involved in sprouting angiogenesis is VEGFA/VEGFR2 (Adams and Alitalo, 2007; Blanco and Gerhardt, 2013). In response to high levels of VEGFR2, tip cells modify their cellular junctions, secrete matrix metalloproteases that degrade their surrounding basement membrane and acquire an extensively invasive and motile behaviour. They also start to express Dll4 which activates Notch1 signalling in the adjacent EC. Through the downregulation of VEGFR2 and the upregulation of VEGFR1, which acts as a decoy receptor that sequesters VEGF, Notch1 induces stalk cell behaviour (Blanco and Gerhardt, 2013; Hellström et al., 2007; Noguera-Troise et al., 2006; Ridgway et al., 2006). In addition, circulating BMP9/10 also support the stalk cell specification by upregulating Notch signalling upon binding their receptor Alk1 (Ricard et al., 2012). During sprouting, there is a dynamic tip and stalk cell shuffling, where one can become the other and vice versa (Jakobsson et al., 2010). This phenomenon was initially thought to be mostly the result of fluctuating levels of VEGF signalling, but recent studies have shown that the stalk cell phenotype must be actively repressed for a stalk cell to become a tip cell (Aspalter et al., 2015; Moya et al., 2012). This repression is mediated by Nrp1, which induces a differential responsiveness to BMP signalling which in turns downregulates Notch signalling.

In order to guide the emerging sprouts properly, tip cells extend multiple dynamic filopodial extensions (Figure 32) that sense and respond to attractive or repulsive guidance cues within their environment (De Smet et al., 2009; Gerhardt et al., 2003). Consequently, they

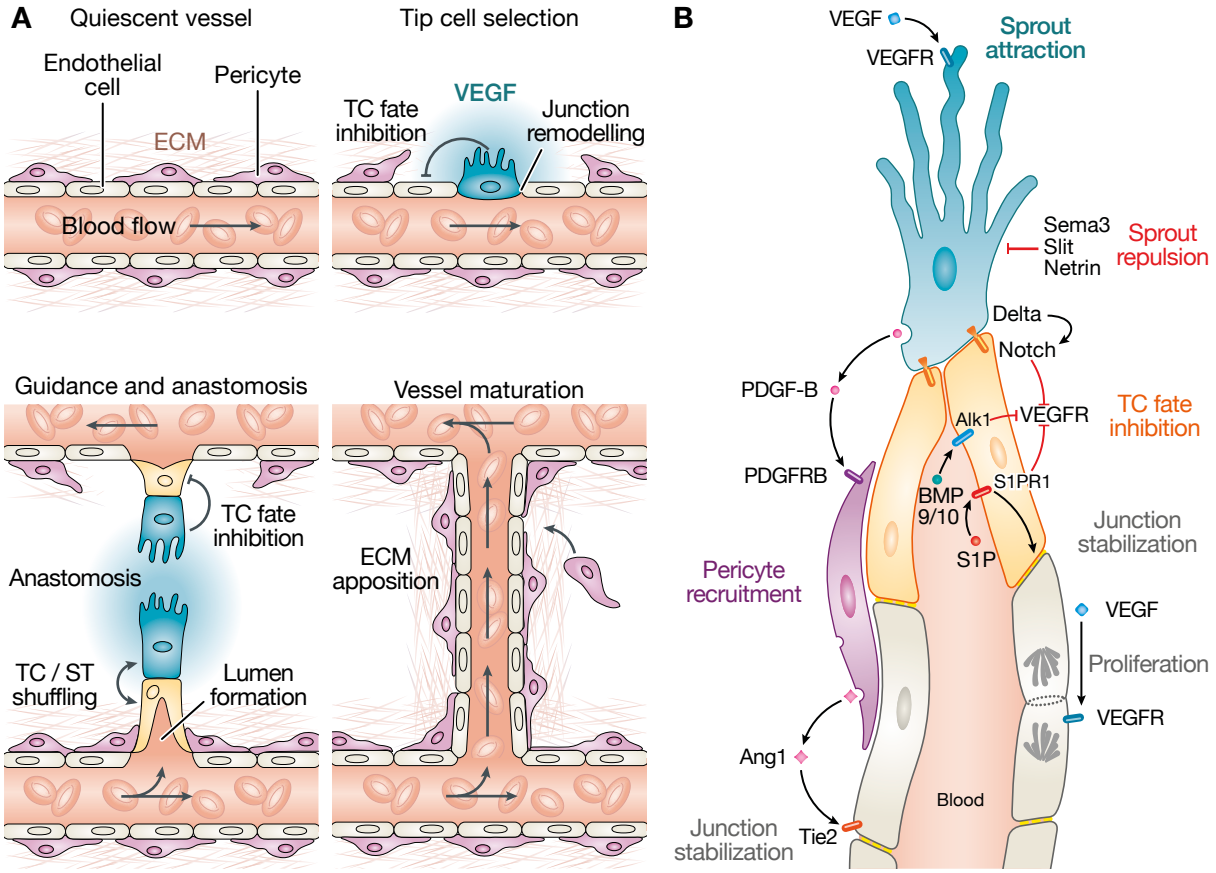

Figure 32. Sprouting angiogenesis. (**A**) In the absence of pro-angiogenic stimuli, endothelial cells are maintained in a quiscent state. During angiogenesis, high levels of exogenous pro-angiogenic factors such as VEGFA and of VEGF receptor 2 (VEGFR2) signalling select « tip cells » (TC) for sprouting, which inhibit the TC fate laterally in adjacent EC. TC sprouting behaviour is facilitated by the loosening of EC–EC junctions, the degradation of the extracellular matrix (ECM) and the detachment of pericytes (purple). Then, invasive TC sprouting is guided by gradients of pro-angiogenic growth factors and various environmental guidance cues. During sprout elongation, TC are trailed by endothelial 'stalk cells' (SC; yellow), which maintain connectivity with parental vessels and initiate vascular lumen morphogenesis. While TC inhibit the TC fate in adjacent EC, TC and SC may also shuffle and exchange positions during angiogenic sprouting. Finally, upon contact with other vessels, TC behaviour is repressed and vessels fuse by the process of anastomosis. Nascent perfused vessels are subsequently stabilized by the recruitment of supporting pericytes, the strengthening of EC–EC contacts and the deposition of an ECM to re-establish a quiescent endothelial phenotype. (**B**) Detailed representation of the signalling pathways involved, with their functions indicated in color. VEGFA attracts tip cells, while Sema3A, Slits and Netrins repel them. Stalk cell fate is maintained by a combination of Delta-like 4 (Dll4)–Notch signalling by the tip cell, and BMP and Sphingosine-1-phosphate (S1P) signalling from the circulating blood. VEGFA also stimulates stalk cell proliferation. Pericytes are recruited by the EC secretion of platelet-derived growth factor B (PDGFB), but also other signalling pathways such as TGFβ (not shown). In return, they express Angiopoietin 1 which binds to its receptor Tie2 and stabilizes EC-EC junction, in addition to S1P signalling. Adapted from Herbert and Stainier (2011) and Betsholtz (2018).

present many morphological and functional similarities with axonal growth cones (Adams and Eichmann, 2010; Carmeliet and Tessier-Lavigne, 2005). VEGFA is the main chemoattractive cue in tip cell guidance, which strongly express VEGFR2 in their filipodiae (Gerhardt et al., 2003). However, tip cells also express several receptors for axon-guidance cues that I will further discuss later in my introduction. During angiogenesis, stalk cells need to create a lumen to establish blood vessels. Two mechanisms, cell hollowing and cord hollowing, have been described respectively in small and large vessels (Iruela-Arispe and Davis, 2009; Potente et al., 2011; Zeeb et al., 2010). In cell hollowing, EC create the lumen by coalescing intracellular

vacuoles together within and between neighbouring EC. In cord hollowing, EC rearrange their junctions, define an apical-basal polarity before expressing on the apical membrane negatively charged glycoproteins that act as a repulsive signal and open the lumen (Strilic et al., 2009; Zeeb et al., 2010). Finally during anastomosis, new vessels fuse together as tip cells of two sprouting vessels first establish contacts and then consolidate their connection through the expression of VE-cadherin (Potente et al., 2011). Interestingly, it has been reported that macrophages can accumulate and interact with the filipodiae of neighbouring tip cells to facilitate the process (Fantin et al., 2010). Several processes then occur to stabilise the new vessel: EC generate their BM and recruit mural cells; the onset of blood flow activates the shear stress-responsive transcription factor Krüppel-like factor 2 (Klf2) that induces vessel remodelling; and the delivery of oxygen and nutrients reduces VEGF expression, promoting a quiescent EC phenotype (Nicoli et al., 2010; Potente et al., 2011).

Finally, the vascular network can be locally extended by a process called intussusception, during which the blood vessel is split by the insertion of tissue pillars (Adams and Alitalo, 2007; Djonov et al., 2000). Although this process has been well described during development, little is known about the molecular regulation of intussusception beyond the possible involvement of COUP-TFII (Hlushchuk et al., 2017; Mentzer and Konerding, 2014).

2.2.2. Common neurovascular guidance cues

Tip cells present many morphological and functional similarities with axonal growth cones and express several receptors for axon-guidance cues: EphB4, which bind ephrinB2; Nrp1/2 and plexinD1, which bind semaphorins; Unc5b, which binds netrins; and roundabout guidance receptors (Robo), which bind slit proteins (Adams and Eichmann, 2010; Carmeliet and Tessier-Lavigne, 2005; Larrivée et al., 2009).

EphB4 – ephrinB2

As mentioned earlier, artery-fated EC express ephrinB2 while vein-fated express EphB4 which is key for their proper segregation. In addition, it has recently been shown in tip cells that reverse ephrinB2 signalling, via VEGFR2 internalization, is necessary for the VEGF-induced filopodial extension (Sawamiphak et al., 2010; Wang et al., 2010).

Nrp – Sema3E

Contrary to other semaphorins, Sema3E binds directly plexinD1 to act as a repulsive cue in a Nrp-independent manner (Gu et al., 2005). Indeed, contrary to Sema3e and plexinD1 mouse mutants, double-mutant mice deficient for Sema3e binding sites in Nrp1/2 do not display severe vascular defects. Nrp1 involvement in vascular development seems restricted to its role as a VEGF co-receptor (Gerhardt et al., 2004; Jones et al., 2008).

Unc5B - Netrin

It has also been shown that the netrin receptor Unc5b is expressed in arterial EC, sprouting capillaries and tip cells where it represses angiogenic growth (Adams and Eichmann, 2010; Carmeliet and Tessier-Lavigne, 2005; Lu et al., 2004; Suchting et al., 2007). Indeed, *Unc5b*$^{-/-}$ tip cells display uncontrolled filopodial extensions, and Unc5b knockout mice excessive vascular branching (Lu et al., 2004). Whether this effect is mediated by Netrin 1 remains uncertain with several conflicting studies (Larrivée et al., 2007; Lu et al., 2004; Serafini et al., 1996). It has proposed that Unc5B may, in the absence of a ligand, induce EC apoptosis (Castets et al., 2009). However, recent reports have pointed towards an interaction with Robo4, that I will detail in the next paragraph (Koch et al., 2011; Zhang et al., 2016).

Robo - Slit

Robo is a single-pass transmembrane receptor which was first identified as the mediator of axonal repulsion during midline crossing in the CNS upon binding to its ligand Slit (Brose et al., 1999; Kidd et al., 1999). Since then, four Robo (Robo1-4) and three Slit genes (Slit1-3) have been identified in vertebrates (Blockus and Chédotal, 2016; Chédotal, 2007). Robo4, which is selectively expressed by EC, and more recently Robo1/2 have been reported to have different roles in angiogenesis (Bedell et al., 2005; Blockus and Chédotal, 2016; Dubrac et al., 2016; Huminiecki et al., 2002; Jones et al., 2009; Rama et al., 2015). Indeed, Robo1/2 receptors and Slit2 have been shown to promote endothelial cell motility and polarity during angiogenesis, in cooperation with VEGFA signaling (Dubrac et al., 2016; Rama et al., 2015). Oppositely, Robo4 has been reported to promote vascular stability and inhibit angiogenesis (Bedell et al., 2005; Jones et al., 2009). Although its function was initially linked to Slit binding, recent reports support that this is not the case (Enomoto et al., 2016; Fritz et al., 2015; Jones et al., 2009; Koch et al., 2011; Rama et al., 2015; Yu et al., 2014; Zhang et al., 2016). Instead, two studies have shown that Robo4 binds Unc5b in neighbouring cells via its extracellular domain to inhibits angiogenesis and vessel permeability by counteracting VEGF signalling independently of Slit2 (Koch et al., 2011; Zhang et al., 2016).

2.3.Mural cells development

2.3.1. Origin of mural cells

Depending on their location, mural cells have many different developmental origins (Armulik et al., 2011; Daneman and Keller, 2015; Holm et al., 2018). The earliest studies have shown that mesodermal angioblasts coalesce around endothelial tubes and give rise to both EC and mural cells (Clark and Clark, 1925; Drake et al., 1998; Hungerford and Little, 1999; Kumar et al., 2017; Yamashita et al., 2000). Additional mesodermal origins have been described since then. Indeed, aortic mural cells derive from somites caudal to the

pharyngeal arches in its descending thoracic segment, while in in the abdomen they derive from splanchnic mesoderm (Christ et al., 2004; Majesky, 2007). Moreover, cells within the pleural and peritoneal mesothelium undergo an EMT, migrate and give rise to mural cells and fibroblasts in the lung, gut and liver (Asahina et al., 2011; Que et al., 2008; Wilm et al., 2005). In the heart, coronary mural cells derive from the epicardial mesothelium (Volz et al., 2015; Zhou et al., 2008). Finally, the NC has been shown to give rise to mural cells in the CNS, the head and neck regions, the thymus and, via the secondary heart field, the ascending and arch portions of the aorta and the base of the pulmonary trunks (Bergwerff et al., 1998; Etchevers et al., 2001; Korn et al., 2002; Majesky, 2007; Müller et al., 2008; Trost et al., 2013). To add to this complexity, recent studies have shown that in addition to this tissue-dependant heterogeneity, mural cells are also heterogeneous within each tissue (Dias Moura Prazeres et al., 2017; Yamazaki and Mukouyama, 2018). Indeed, it was first reported that about a fifth of cardiac mural cells derive from cardiac EC and not epicardial cells (Chen et al., 2016). More recently, it has been demonstrated that tissue-localized myeloid progenitors contribute to pericyte development in the embryonic skin (Figure 33) and brain vasculature (Yamamoto et al., 2017; Yamazaki et al., 2017).

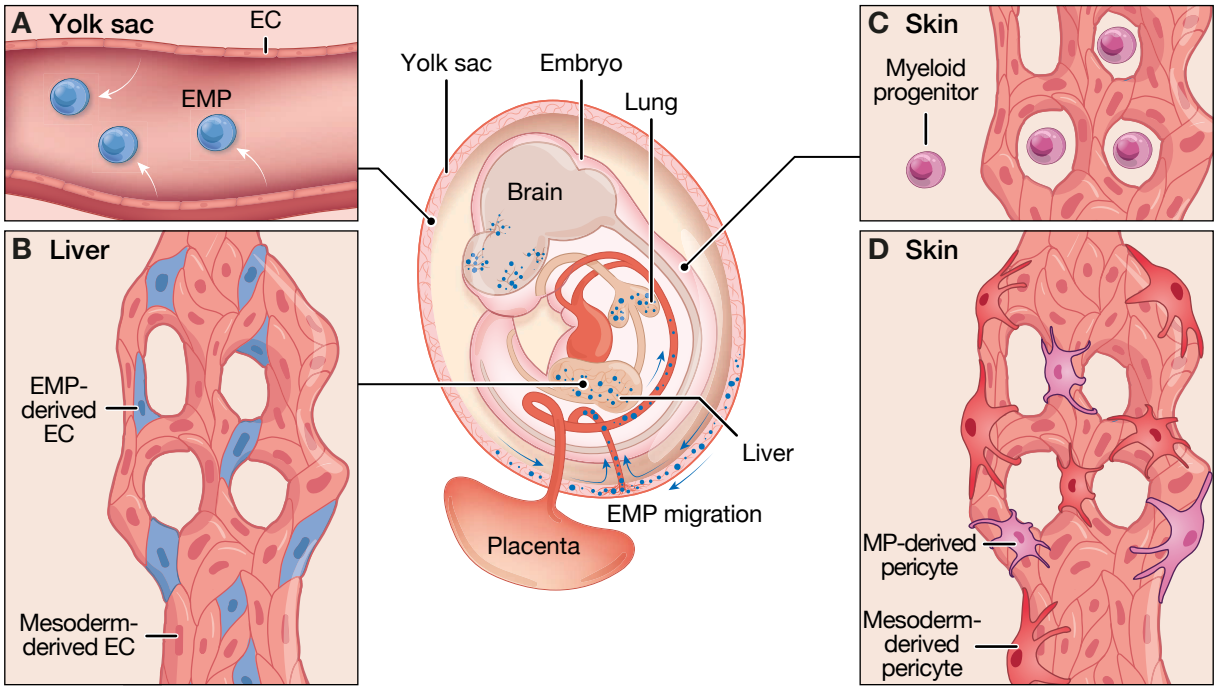

Figure 33. Endothelial and mural cells have multiple origins within the same tissue. (**A-B**) Endothelial cells (EC) were assumed until recently to solely derive from angioblasts. But it has recently been shown in several organs such as the brain, liver and lungs that some EC derive from erythro-myeloid progenitors (EMP) that migrate into the embryo from the yolk sac. (**C-D**) Altgough mural cells are known to have different origins between tissues, it was assumed that within a single one they had the same origin. However, it has also been shown in the skin vasculature that in addition to mesoderm-derived mural cells, a subpopulation actually derives from tissue-resident myeloid progenitors, under the influence of TGFβ signalling. Adapted from Iruela-Arispe (2018).

2.3.2. Mural cell development

Mural cell development begins with their recruitment by EC of the vascular plexus during angiogenesis (Figure 32). Then, in response to specific environmental cues, they can either proliferate and migrate or become quiescent, differentiate and by their interactions with EC promote the maturation and stabilization of the blood vessels.

Mural cell recruitment

The PDGFB/PDGFRβ signalling pathway is crucial for mural cell recruitment during development (Armulik et al., 2011; Daneman and Keller, 2015; Gaengel et al., 2009). Indeed, knockouts of each gene in mice resulted in perinatal death from vascular dysfunction due to a global lack of mural cells (Levéen et al., 1994; Soriano, 1994). In addition, PDGFB has been shown to induce mural cell fate in undifferentiated mesenchymal cells, an promote vSMC proliferation (Gaengel et al., 2009). During angiogenesis, tip cells release PDGFB, which binds to the PDGFRβ expressed by developing mural cells and attracts them towards the angiogenic sprout (Gerhardt and Betsholtz, 2003; Lindahl et al., 1997). Once secreted, PDGFB is bound to heparan sulfate proteoglycans either on the cell surface of in the ECM, which is critical for its bioavailability and function (Abramsson et al., 2007; Lindblom et al., 2003). Indeed, genetically-modified mice in which PDGFB could not bind to the ECM displayed a reduced number of pericytes (Lindblom et al., 2003). Nonetheless, the fact that pericyte recruitment in the liver and thymus was unaffected in both knockout mice suggest that other signalling pathways are involved, at least in specific organs (Hellström et al., 1999; Lindahl et al., 1997). Indeed, several signalling pathway have been suggested to regulate mural cell recruitment in cooperation with PDGFB/ PDGFRβ: heparin-binding EGF via its receptor ErbB1/2; ephrin-B2, which regulates PDGFRβ internalization in mural cells; Shh signalling via its receptor Patched, in the choroid plexus; and possibly TGFβ and Notch, which are also involved in pericyte differentiation (Cappellari et al., 2013; Foo et al., 2006; Iivanainen et al., 2003; Jakobsson and van Meeteren, 2013; Nakayama et al., 2013; Nielsen and Dymecki, 2010; Stratman et al., 2010).

Mural cell differentiation

TGFβ is an important signalling pathway involved in pericyte differentiation and blood vessel maturation (Armulik et al., 2011; Dijke and Arthur, 2007; Gaengel et al., 2009). Indeed, knockouts of most of the TGFβ signalling pathway genes in mice lead to embryonic death at mid-gestation with severe vascular abnormalities and mural cell defects (Jakobsson and van Meeteren, 2013). Two type I TGFβ receptors, Alk1 and Alk5, are expressed by both EC and mural cells, and appear to induce opposing cellular effects. Alk1 activation triggers Smad1/5 phosphorylation, which promotes cell proliferation and migration, and inhibit vessel maturation. Oppositely, Alk5 activation triggers Smad2/3 phosphorylation, which promotes

cell quiescence and differentiation (Chen et al., 2003; Goumans et al., 2002; Ota et al., 2002). Overall, TGFβ signalling is the result of a complex interplay, in which Alk1 signalling inhibits Alk5 but also requires it, and differential responses of both receptors to TGFβ (Gaengel et al., 2009; Goumans et al., 2002). Hence, in presence of a strong and prolonged TGFβ stimulation Alk1 signal decreases over time and is overcome by Alk5, which promotes cell differentiation vessel maturation. Moreover, a recent study has shown that TGFβ signalling, through its receptor Tgfbr2, promotes the differentiation of embryonic myeloid progenitors into pericytes (Yamazaki et al., 2017). Finally, it has also been reported in EC that TGFβ and Notch signalling cooperate to promote vessel stabilization by upregulating N-cadherin expression via direct interactions between their effectors, Smad4 and RBP/J, on its promoter (Daneman and Keller, 2015; Li et al., 2011).

In addition to its role in arteriogenesis and angiogenesis, Notch signalling is also involved in the interactions between EC and mural cells. Indeed, Notch3 mutations are responsible in humans for the cerebral autosomal-dominant arteriopathy with subcortical infarcts and leukoencephalopathy (CADASIL) syndrome, which is the most common form of hereditary stroke disorder (Joutel et al., 1996; Ruchoux et al., 1995). Analyses of Notch3 knockout mice have shown an abnormal maturation of arterial vSMC, with a reduced expression of several arterial vSMC markers such as PDGFRβ (Domenga et al., 2004; Jin et al., 2008; Krebs et al., 2003). More recently, a study based on brain autopsies from CADASIL patients has reported the presence of pericyte degeneration, suggesting the involvement Notch3 signalling in their survival (Dziewulska and Lewandowska, 2012). The Notch ligand involved is Jagged-1 (Jag1), which is expressed both in EC and pericytes, in which it is part of an auto-regulatory loop (Liu et al., 2009). Jag1 has also been shown to be essential for vSMC in vivo (High et al., 2008).

Blood vessel maturation

Contrary to PDGFB/PDGFRβ, in the angiopoietin-1 (Ang1)/Tie2 signalling pathway the ligand, Ang1, is expressed by mural cells and its receptor, Tie2, is expressed on EC (Armulik et al., 2011; Davis et al., 1996; Dumont et al., 1993; Sundberg et al., 2002). Although initial analyses of knockout mice for both genes reported that they lacked mural cells, a more recent study has demonstrated that this phenotype is due to flow-dependent defects and could be replicated by the cardiac-specific deletion of Ang1 (Jeansson et al., 2011; Patan, 1998; Suri et al., 1996). Moreover, several studies have shown that Ang1/Tie2 is not required for pericyte recruitment (Jeansson et al., 2011; Jones et al., 2001; Tachibana et al., 2005). Instead, Ang1 over-expression studies have supported a role for Ang1 in blood vessel maturation and stability, as they resulted in an increased vascular branching and remodelling (Armulik et al., 2011; Gaengel et al., 2009; Thurston et al., 1999; Uemura et al., 2002). Interestingly, Ang1 expression in hematopoietic cells has also been reported to have a critical role in angiogenesis and vascular stabilization (Goossens et al., 2011; Takakura et al., 2000).

Sphingosine-1-phosphate (S1P) is a blood-borne bioactive lipid that binds to its EC G-protein-coupled receptor S1P1, which has been shown to be essential for proper vessel maturation (Allende and Proia, 2002). Indeed, upon binding S1P1 it activates, via Rac, VE-cadherin assembly into adherens junctions (Lee et al., 1999). Moreover, it is also involved with TGFβ and Notch in the proper trafficking of N-cadherin to cell adhesions between EC and mural cells (Paik et al., 2004).

3. Nerve role in vascular maturation

3.1. Peripheral nerves are aligned with arteries

Although the similarities between the vascular and nervous arborizations have been known for centuries (Figure 34), the underlying mechanisms have only been recently discovered (James and Mukouyama, 2011; Vesalius, 1543). Early studies in embryonic chick limb skin reported that while major nerves and large vessels were indeed aligned, their spatial organization was independently controlled (Martin and Lewis, 1989). However, the question of smaller-diameter vessel branching could not be addressed at the time as it was difficult to detect. Over the last 15 years, three studies have demonstrated how peripheral nerves play an essential role in directing blood vessel patterning and promoting arterial differentiation (Mukouyama et al., 2005; 2002; Yamazaki et al., 2017). To analyze this complex and dynamic process, they focused on the mouse embryonic limb skin, which has a highly stereotypic and recognizable vascular branching pattern (Mukouyama et al., 2002). In the embryonic skin, the

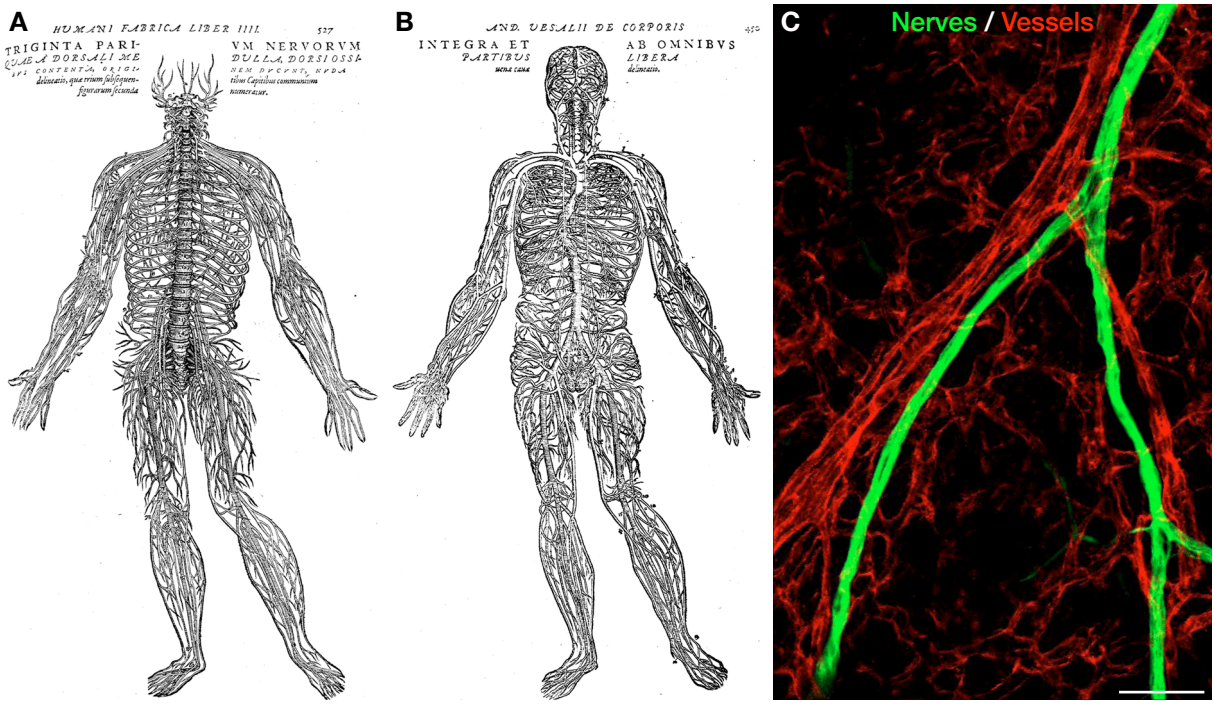

Figure 34. Parallels in vessel and nerve patterning. (**A-B**) Drawing by the Belgian anatomist Andreas Vesalius (1543) highlighting the similarities in the arborization of the vascular and nervous networks. (**C**) Wholemount immunostaining of E15.5 embryonic skin immunostained against PECAM (blood vessels, red) and β-III-tubulin (nerves, green). Vessels and nerves track together towards their targets. Scale bar: 50 µm. Adapted from Carmeliet and Tessier-Lavigne (2005).

primary vascular plexus is established around E11.5, followed at E12.5 by the invasion of peripheral nerves, which show no alignment with blood vessels. However, following vascular remodeling blood vessels align at E14.5 with peripheral nerves. After aligning, some associated blood vessels start expressing arterial markers, such as ephrin-B2 and Nrp1, and by E15.5 most of them do (Mukouyama et al., 2002). Finally, vSMC cover associated blood vessels after they start expressing arterial markers.

3.2.Peripheral nerves direct blood vessel patterning

The first question that arose from these observations was whether peripheral nerves were responsible for the vascular alignment which occurs during remodeling. To answer it, the authors analyzed the embryonic limb skin of several knockout mouse lines. First, they used *Sema3A*$^{-/-}$ mutants in which the peripheral nerve pattern is disrupted (Taniguchi et al., 1997). In these mice, vascular remodeling did occur and blood vessels associated with the disorganized nerves, supporting that peripheral nerves directed vascular patterning. Then, they compared *Ngn1*$^{-/-}$, *Ngn2*$^{-/-}$ double homozygous mutants, which lacked peripheral SN and their accompanying SC, and *ErbB3*$^{-/-}$ mutants which only lacked SC (Ma et al., 1999; Riethmacher et al., 1997). Strikingly at E15.5, while vascular remodeling was mildly affected in *Ngn1*$^{-/-}$, *Ngn2*$^{-/-}$ mice, blood vessel association with peripheral nerves was greatly reduced in *ErbB3*$^{-/-}$ mutants limb skin, which suggested that SC were directly involved in vascular patterning (Mukouyama et al., 2002). More recently, another study has revealed that this mechanism is mediated via the activation of the CXC motif chemokine receptor Cxcr4, which is expressed by EC, by its peripheral nerve/SC-derived soluble ligand Cxcl12 (SDF1), which was already known to influence angiogenesis (Li et al., 2013; Tachibana et al., 1998). The authors used *Cxcl12*$^{-/-}$ and *Cxcr4*$^{-/-}$ mutants which displayed similar phenotypes consisting in a disturbed nerve-vessel alignment and a lack of arteriogenesis (Nagasawa et al., 1996; Tachibana et al., 1998). However, using *in vitro* assays they decoupled this process and demonstrated that peripheral nerve- or SC-expressed Cxcl12 recruits blood vessels via EC-expressed Cxcr4 (Figure 35), but is not directly involved in the arteriogenesis that follows (Li et al., 2013). While these two studies strongly suggest that SC are responsible via Cxcl12 secretion for the vascular patterning, a SC-specific Cxcl12 knockout would be necessary to confirm it.

3.3.Peripheral nerves promote arterial differentiation

The second question was whether peripheral nerves were responsible for the arterial differentiation which occurs within the aligned blood vessels. Interestingly, in *Ngn1*$^{-/-}$, *Ngn2*$^{-/-}$ mutants the expression of arterial markers and vSMC coverage was greatly reduced in smaller-diameter vessels (5 to 15 μm), contrary to larger-diameter vessels (30 to 100 μm) which appeared unaffected. Similarly, SC-depleted *ErbB3*$^{-/-}$ mutants also displayed a significant reduction in the expression of arterial markers and vSMC coverage. Moreover, the authors reported that

peripheral nerves and SC expressed VEGFA *in vivo*, and that *in vitro* VEGFA could induce arteriogenesis. Taken together, these results supported that both peripheral nerves and SC were involved in arteriogenesis, and suggested the involvement of VEGFA (Mukouyama et al., 2002). In a second report, the authors studied the role of VEGFA *in vivo*, avoiding the early embryonic lethality of VEGFA mutants by generating conditional knockout mice in motor, sensory neurons and SC (Carmeliet et al., 1996; Ferrara et al., 1996; Mukouyama et al., 2005). Indeed, combined VEGFA knockout in these three cell types resulted in total loss of VEGFA expression in peripheral nerves, which disrupted arteriogenesis, but not blood vessel alignment. This result was corroborated by the conditional inactivation of VEGFR2 and Nrp1 in EC, which resulted in an even more severe arteriogenesis defect, without affecting blood vessel alignment. Taken together, these results show that after recruiting blood vessels through the Cxcl12-Cxcr4 pathway, peripheral nerves and SC promote arteriogenesis by secreting VEGFA (Figure 35), which binds to VEGFR2 and its co-receptor Nrp1 on EC (Li et al., 2013; Mukouyama et al.,

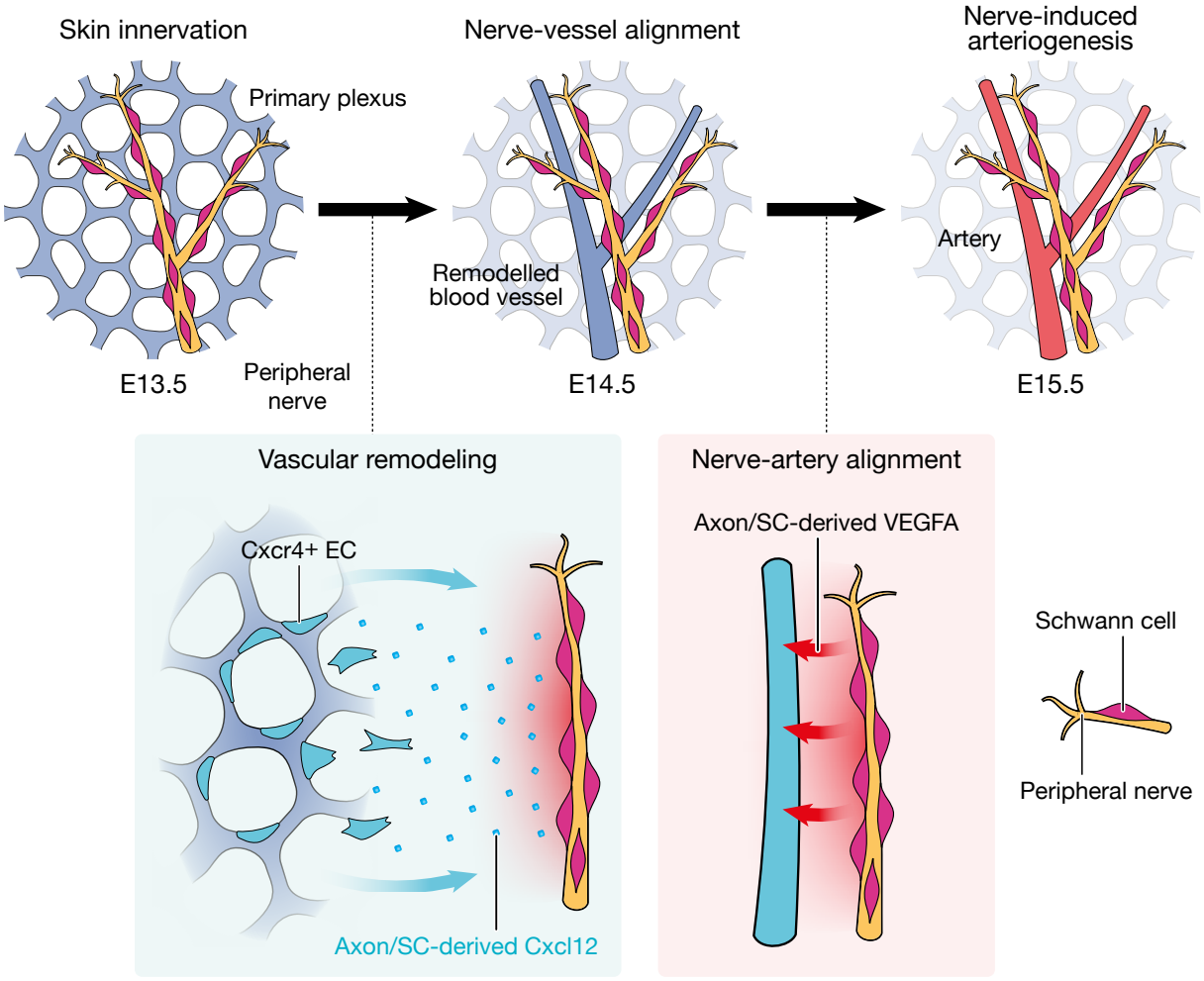

Figure 35. Schematic representation of the nerve-mediated vascular branching and arterial differentiation in the developing skin. The primary capillary plexus is established at E11.5, and by E13.5 peripheral nerves have invaded the skin. Subsequently, oxygen-deprived nerves may induce Cxcl12 and VEGFA expression through the activation of HIF-1 prior to vascular remodeling. Cxcl12-Cxcr4 signalling functions as a long-range chemotactic guidance cue to recruit vessels to align with nerves (blue box). Nerve-derived VEGFA instructs arterial differentiation in the nerve-associated vessels (red box). Arterial differentiation presumably requires a local action of VEGFA to induce arterial marker expression. As a result, the congruence of arteries and nerve patterns is established in the skin. Adapted from Li et al. (2013).

2005). Finally, to explain how these two signals are coordinated, the authors have suggested that they could be secreted by oxygen-deprived nerves. Indeed, it has been shown that hypoxia, via the activation of the transcription factor hypoxia-inducible factor 1 (HIF-1), can induce Cxcl12 and VEGFA expression (Ceradini et al., 2004; Forsythe et al., 1996). While this represents an interesting hypothesis, it has yet to be proven. Hence, how these two signals are coordinated remains for now an open question.

III. Presentation and aims of my thesis work

In the first report (Gresset et al., 2015), our group has shown that in addition to nerve root Schwann cells (SC) and dorsal root ganglia (DRG) sensory neurons, a subset of Prss56-traced BC derivatives migrates along peripheral nerves to the skin and gives rise to SC, terminal glia and stem-like skin progenitor cells (SKP). My contribution in this study, in which I am the third author, was to develop and use an experimental in vivo DRG graft model to confirm the neurogenic potential of BC-derived SKP. Although the experiments took place in the summer of 2013, before I began my neurology residency, I chose to include this article here as it laid the foundations for my thesis work. Indeed, following this study my thesis work revolved around two main questions:

- What is the contribution of Krox20-expressing BC cells to the developing trunk skin?

- What is the regenerative potential of naïve and pre-differentiated SKP transplanted in the central nervous system?

To answer the first question, we performed fate-mapping of BC cells expressing Krox20, which revealed their implication in the development of the vascular network. These findings are at the origin of the manuscript currently in preparation, in which I am the co-first author. In this study, we have characterized successive steps of the "glial to vascular switch" of Krox20-traced BC derivatives, and then studied its underlying mechanisms by performing global and single-cell transcriptomic analyses. This led us to discover that BC cells derivatives already activate mural cell differentiation program while they are still on nerves, and to highlight this glial population as a major source of mural cells.

To address the second question, I used several in vitro differentiation protocols and developed an experimental ischemic stroke model to perform in vivo grafts, that are detailed in the Appendix. Disappointingly, I have shown that SKP do not have the potential to generate functional neurons in vitro and in vivo when grafted in the injured brain parenchyma. However, I observed that explants or cell suspension of embryonic sensory cortex, when grafted after a stroke, integrate efficiently with the host, validating the feasibility of such an approach. Finally, during this study I initiated a collaboration that led to the development and use of a polysaccharide-based scaffold for culturing and manipulating embryonic neurons in vitro. A manuscript describing this study, in which I am first author, is being submitted for publication.

Results

Article one

Boundary caps give rise to neurogenic stem cells and terminal glia in the skin

The first *in vivo* fate-mapping of boundary cap (BC) cells was performed by our team using a mouse line carrying Cre under control of BC specific marker *Krox20* (Maro et al., 2004). This study revealed that BC-derivatives constitute a major source of nerve root Schwann cells (SC) and a subpopulation of glial satellite cells (GSC) and sensory neurons in the dorsal root ganglia (DRG). However, in this case, contribution of Krox20-expressing BC cells to the development of distal part of peripheral nervous system was not explored. The identification of another BC-marker, *Prss56* allowed us to perform lineage-tracing experiments of BC cells using a $Prss56^{Cre}$ allele (Gresset et al., 2015). We have shown that Prss56-traced BC cells also give birth to nerve root SC and DRG sensory neurons and GSC. Surprisingly, we also discovered that a subset of Prss56-traced BC derivatives, from the ventral root, migrates rapidly along peripheral nerves to the skin, where it provides plethora of glial cell types (myelinating and non-myelinating SC, lanceolate and terminal glia) and stem-like skin progenitor cells (SKP). Indeed, we have shown that BC-derived SKP can be self-renewed in sphere culture, while preserving a broad differentiation potential *in vitro* where they provide SC, neurons, melanocytes and adipocytes. Moreover, once transplanted in the adult mouse DRG they give rise to mature sensory neurons.

Please cite this article in press as: Gresset et al., Boundary Caps Give Rise to Neurogenic Stem Cells and Terminal Glia in the Skin, Stem Cell Reports (2015), http://dx.doi.org/10.1016/j.stemcr.2015.06.005

Stem Cell Reports
Article

OPEN ACCESS

Boundary Caps Give Rise to Neurogenic Stem Cells and Terminal Glia in the Skin

Aurélie Gresset,[1,4] Fanny Coulpier,[1,4] Gaspard Gerschenfeld,[1,3] Alexandre Jourdon,[1,3] Graziella Matesic,[1] Laurence Richard,[2] Jean-Michel Vallat,[2] Patrick Charnay,[1,*] and Piotr Topilko[1]

[1]Ecole Normale Supérieure, Institut de Biologie de l'ENS (IBENS), and INSERM U1024, and Centre National de la Recherche Scientifique (CNRS) UMR 8197, Paris 75005, France

[2]National Reference Centre "Rare Peripheral Neuropathies" Department of Neurology, Centre Hospitalier Universitaire de Limoges, 87042 Limoges, France

[3]Sorbonne Universités, UPMC Université Paris 06, IFD, 4 Place Jussieu, 75252 Paris Cedex 05, France

[4]Co-first author

*Correspondence: patrick.charnay@ens.fr

http://dx.doi.org/10.1016/j.stemcr.2015.06.005

SUMMARY

While neurogenic stem cells have been identified in rodent and human skin, their manipulation and further characterization are hampered by a lack of specific markers. Here, we perform genetic tracing of the progeny of boundary cap (BC) cells, a neural-crest-derived cell population localized at peripheral nerve entry/exit points. We show that BC derivatives migrate along peripheral nerves to reach the skin, where they give rise to terminal glia associated with dermal nerve endings. Dermal BC derivatives also include cells that self-renew in sphere culture and have broad in vitro differentiation potential. Upon transplantation into adult mouse dorsal root ganglia, skin BC derivatives efficiently differentiate into various types of mature sensory neurons. Together, this work establishes the embryonic origin, pathway of migration, and in vivo neurogenic potential of a major component of skin stem-like cells. It provides genetic tools to study and manipulate this population of high interest for medical applications.

INTRODUCTION

The neural crest (NC) is an embryonic, multipotent cell population that migrates extensively through the periphery and gives rise to various cell lineages, including most of the glial and neuronal components of the peripheral nervous system (PNS). NC cell settlement is normally accompanied by restriction to particular cell fates (Le Douarin and Dupin, 2003). However, recent studies have identified stem cell-like populations within adult NC targets, which show developmental potentials resembling those of NC cells (Dupin and Sommer, 2012; Le Douarin and Dupin, 2003). Among these populations, adult multipotent skin stem cells have attracted particular attention because they are easy to access, which would facilitate their use in regenerative medicine.

Fate-mapping studies have revealed the existence of different types of trunk skin stem cell populations that possess neurogenic and gliogenic potential, with both NC and non-NC origins. Stem cells confined to the dermal papillae of hair follicles originate from the mesoderm, whereas populations restricted to the glial and melanocyte lineages are derived from the NC (Dupin and Sommer, 2012; Jinno et al., 2010; Wong et al., 2006). These different cell populations can be cultured as floating spheres and generate neurons and Schwann cells under differentiation conditions (Biernaskie et al., 2006; Wong et al., 2006). However, a lack of specific markers has prevented their detailed localization and further characterization and purification.

Another type of NC-derived stem cell-like population has been identified in the embryo at the interface between the CNS and PNS. These cells form the so-called boundary caps (BCs), which are transiently observed at the nerve root entry/exit points along the neural tube (Niederländer and Lumsden, 1996). Fate analyses, taking advantage of BC-specific expression of the *Krox20* (also known as *Egr2*) transcription factor gene and available knockins at this locus (Vermeren et al., 2003; Voiculescu et al., 2000), have established that BC cells give rise to the Schwann cell component of the nerve roots and, in the dorsal root ganglia (DRGs), to nociceptive neurons as well as glial satellite cells (Maro et al., 2004). Furthermore, in culture, BC cells can generate Schwann cells, myofibroblasts, astrocytes, and neurons (Zujovic et al., 2011), and, when grafted into the lesioned spinal cord, efficiently migrate toward the lesion and differentiate into functional myelinating Schwann cells (Zujovic et al., 2010). Together, these studies indicate that BC cells have a broad differentiation potential and suggest that they constitute multipotent stem cells in the embryo.

These fate analyses relied on the restriction of *Krox20* expression to BC cells during early PNS development. However, from embryonic day 15.5 (E15.5), *Krox20* also is expressed in Schwann cells (Topilko et al., 1994), thereby preventing later analysis of BC derivatives. To circumvent this problem, we have generated a Cre recombinase knockin in a novel BC-specific marker, *Prss56,* previously known as *L20* (Coulpier et al., 2009), and we used it to trace

Please cite this article in press as: Gresset et al., Boundary Caps Give Rise to Neurogenic Stem Cells and Terminal Glia in the Skin, Stem Cell Reports (2015), http://dx.doi.org/10.1016/j.stemcr.2015.06.005

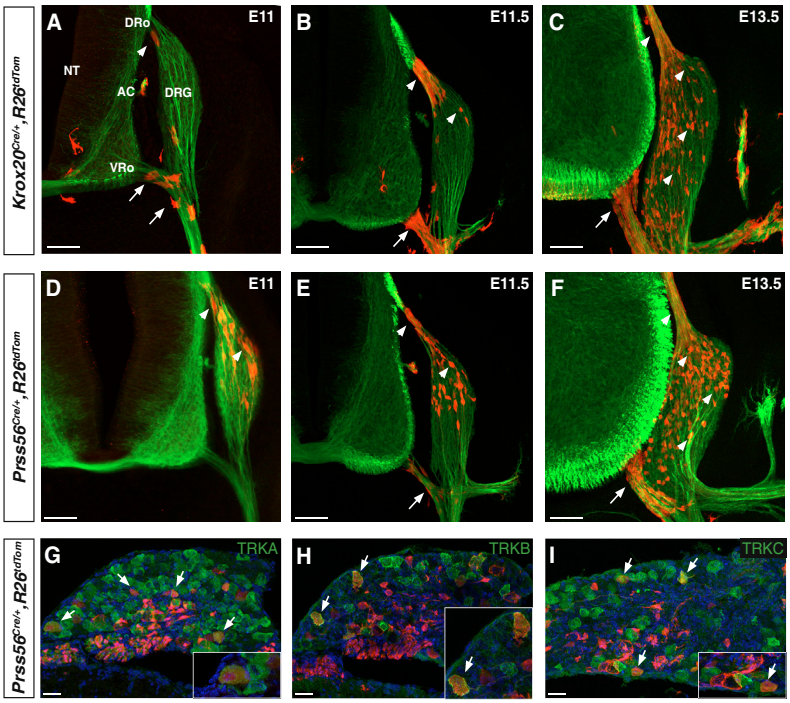

Figure 1. Tracing of *Krox20*- and *Prss56*-Expressing BC Cells along the Nerve Roots and in the DRG

(A–F) Transverse sections of $Krox20^{Cre/+}$, $R26^{tdTom}$ (A–C) and $Prss56^{Cre/+}$,$R26^{tdTom}$ (D–F) embryos, between E11 and E13.5 as indicated, were analyzed by immunocytochemistry using antibodies against tdTOM (red) and βIII-tubulin (green). Arrows and arrowheads indicate ventral and dorsal BC derivatives, respectively.

(G–I) Sections through the DRG from E18.5 $Prss56^{Cre/+}$,$R26^{tdTom}$ embryos were analyzed by immunocytochemistry using antibodies against tdTOM (red) and neuronal markers (TRKA, TRKB, and TRKC, green), as indicated. Insets show higher magnifications of the corresponding figures.

NT, neural tube; DRo, dorsal root; VRo, ventral root; AC, accessory nerve; DRG, dorsal root ganglion. Scale bars, 100 μm (A–F) and 50 μm (G–I). See also Figure S2.

BC cell derivatives in the embryo and the adult. *Prss56* encodes a trypsin-like serine protease and its mutation in the retina has been associated with microphtalmia in humans and mice (Nair et al., 2011). In this study, we show that, during embryogenesis, some of the BC derivatives rapidly migrate along the peripheral nerves and settle in the skin, where they provide terminal glia as well as multipotent progenitors that have broad differentiation capacities in culture and after transplantation into adult mice. This work, therefore, reveals the embryonic origin, pathway of migration, and in vivo neurogenic potential of a multipotent stem cell-like population in the skin.

RESULTS

Dorsal BC Cells Are Heterogeneous and Give Rise to the Different Neuronal Subtypes in the DRGs

Analysis of *Prss56* expression by in situ hybridization on whole embryos indicated that it is restricted to BC cells between E10.5 and E13.5 (Coulpier et al., 2009; Figures S1A, S1B, S3A, and S3B). Furthermore, apart from BC cells, no expression was detected outside of the CNS until E17.5 (Coulpier et al., 2009). On this basis, we generated a Cre knockin in *Prss56* to perform BC derivative tracing studies (Figure S1C). The pattern of expression of *Prss56* was not affected in heterozygous mutants, whereas *Prss56* mRNA was completely absent from homozygous mutants (Figures S1B and S1D), indicating that the mutation represents a null allele for *Prss56*. Homozygous mutant animals did not show any obvious phenotype in the PNS.

In an initial series of experiments, we compared expression and tracing patterns obtained with the *Prss56* and *Krox20* markers. To this end, we first performed in situ hybridization for *Prss56* mRNA on $Krox20^{lacZ}$ knockin embryos, in which β-galactosidase activity faithfully recapitulates *Krox20* expression (Maro et al., 2004). We found that, between E11.5 and E13.5, *Krox20* and *Prss56* showed overlapping patterns of expression at the levels of both dorsal and ventral roots (Figure S2A). To compare the progeny of *Krox20*- and *Prss56*-expressing BC cells, we combined the $Krox20^{Cre}$ (Voiculescu et al., 2000) or $Prss56^{Cre}$ alleles with the $R26^{tdTom}$ locus, in which Cre recombination leads to permanent activation of the tandem dimer tomato (tdTom) fluorescent reporter (Madisen et al., 2010; Figure S1E). We searched for labeled cells in the nerve roots and DRGs between E11 and E13.5. Using the $Krox20^{Cre}$ driver, we confirmed that the first traced cells appeared in the ventral root before E11 (Figure 1A; Coulpier et al., 2009), whereas labeled cells appeared in the dorsal root around that stage and in the DRGs later on (Figures 1A–1C; Maro et al., 2004). In contrast, in $Prss56^{Cre/+}$,$R26^{tdTom}$ embryos, the first labeled cells appeared in the dorsal root and in the dorsal part of the DRGs around E11 (Figure 1D).

Please cite this article in press as: Gresset et al., Boundary Caps Give Rise to Neurogenic Stem Cells and Terminal Glia in the Skin, Stem Cell Reports (2015), http://dx.doi.org/10.1016/j.stemcr.2015.06.005

Labeled cells along the ventral root only appeared at later stages (Figures 1E and 1F). In the nerve roots, labeled cells from both tracing systems gave rise to SOX10-positive Schwann cell precursors (Figure S2B; Maro et al., 2004). Similarly, in the DRGs, both types of traced cells gave rise to putative neurons with extending axons (Figure S2C).

Neurogenesis in the DRGs involves two phases, with mechanoceptive and proprioceptive neurons emerging first, followed by nociceptors (Marmigère and Ernfors, 2007). We have shown previously that the only neurons generated by *Krox20*-expressing BC cells in the DRGs are nociceptors (Maro et al., 2004). To identify the neuronal derivatives of the *Prss56*-expressing BC cell population, we analyzed DRG sections from E18.5 $Prss56^{Cre/+}$,$R26^{tdTom}$ embryos by co-immunostaining them with antibodies against the tracer tdTOM and TRKA (nociceptive), TRKB (mechanoceptive), or TRKC (proprioceptive) neurotrophic receptors. We found that traced cells included all three types of neurons (Figures 1G–1I). Quantification indicated that they represented 9.8% ± 1.9%, 6.3% ± 2.8%, and 13.3% ± 4.6% of the TRKA-, TRKB-, and TRKC-positive neuronal populations, respectively. The observation of mechanoceptive and proprioceptive neurons among BC derivatives traced with the *Prss56* driver is consistent with the presence of traced cells in the DRGs from E11 (Figure 1D), when these neuronal types are generated (Marmigère and Ernfors, 2007). In double-traced $Krox20^{Cre/+}$, $Prss56^{Cre/+}$,$R26^{tdTom}$ embryos, labeled cells represented 9.2% ± 1.1% of the TRKA-positive neurons. This proportion is similar to those obtained with each tracing individually, suggesting that *Krox20*- and *Prss56*-expressing BC cell populations overlap.

Together, these data suggest the existence of heterogeneity within BC cells, with *Krox20* and *Prss56* being expressed in distinct, although overlapping subpopulations. In contrast to what was thought previously, dorsal BC cells give rise to the different neuronal subtypes in the DRGs.

Ventral Root BC Derivatives Migrate along the Peripheral Nerves to the Skin

We noticed that, from E11.5 in $Prss56^{Cre/+}$,$R26^{tdTom}$ embryos, some labeled cells were located in the proximal part of the ventral ramus (VR) (Figure 2A), suggesting that the migration of ventral BC derivatives may extend beyond the root. To investigate this possibility, we immunostained transverse sections from $Prss56^{Cre/+}$,$R26^{tdTom}$ embryos at brachial, thoracic, and lumbar levels for tdTOM and βIII-tubulin, a neuronal/axonal marker, at successive stages of development (Figure 2). At E11.5, labeled cells were present in the ventral root and in the proximal part of the VR of all spinal nerves (Figure 2A). At E11.75, labeled cells had accumulated in the distal part of the elongating VR and a few traced cells were detected in the proximal segment of the growing dorsal ramus (DR) (Figure 2B). At E12–E12.5, sparse labeled cells were present along the extending spinal nerves (Figures 2C and 2D). From E12.5–E13, labeled cells were observed at the level of the skin (Figures 2D and 2E). Subsequently, their number considerably increased in the cutaneous nerves in both the dorsal (Figure 2F) and ventral (Figure 2G) skin. From these stages, labeled cells were concentrated at both extremities of the somatosensory nerves (root and cutaneous segments) and had almost disappeared from the central segments (Figures 2F and 2G).

The spatial-temporal distribution of the labeled cells along spinal nerves suggests a wave of migration from the BCs to the skin along the peripheral nerves, between E11.5 and E13. To rule out the possibility that some cells in the skin might activate *Prss56* de novo, we performed in situ hybridization and RT-PCR analyses on skin preparations at E13.5, when a large number of labeled cells had accumulated in the skin. At this stage, *Prss56* mRNA was restricted to the BCs and was not detected in the skin by either procedure (Figures S3A–S3C). These results further support the idea that the labeled skin cells are derived from the BCs by migration along the nerves.

Skin BC Derivatives Include Different Types of Schwann-like Cells

To investigate the distribution and identity of BC derivatives in the trunk skin after birth, we first performed a whole-mount immunohistochemistry analysis of $Prss56^{Cre/+}$, $R26^{tdTom}$ newborn dorsal skin preparations, staining for tdTOM and βIII-tubulin. This revealed a dense network of traced cells exclusively associated with the nerves in the hypodermis and dermis (Figure 3A). In the subcutaneous nerves, some of the traced cells expressed the myelin marker MBP (Figure 3B), indicating that they were myelinating Schwann cells.

Staining of transverse sections for βIII-tubulin and PGP9.5, an axonal marker present in terminal endings, confirmed the systematic association of the labeled cells with dermal nerves (Figures 3C and 3D). In the dermis, these traced cells were positive for the marker $P75^{NGFR}$ (Figure 3E), which is expressed in NC-derived, embryonic and adult stem cells and in immature and adult, non-myelinating Schwann cells (Jessen et al., 2015). In addition, they expressed the Schwann cell marker S100 (Figure 3F), but not the myelin marker MBP (Figure 3B), and were, therefore, immature/non-myelinating Schwann cells. They could be classified into three categories as follows: (1) those associated with dermal nerve fibers (Figures 3A and 3E, closed arrows), (2) lanceolate endings around hair follicles (Figures 3C, 3D, and 3F, empty arrowheads), and (3) free nerve endings of nociceptive fibers (Figures 3C, 3D, and 3G, closed arrowheads). Lanceolate endings are circumferential structures that surround the hair follicle and are composed of

Please cite this article in press as: Gresset et al., Boundary Caps Give Rise to Neurogenic Stem Cells and Terminal Glia in the Skin, Stem Cell Reports (2015), http://dx.doi.org/10.1016/j.stemcr.2015.06.005

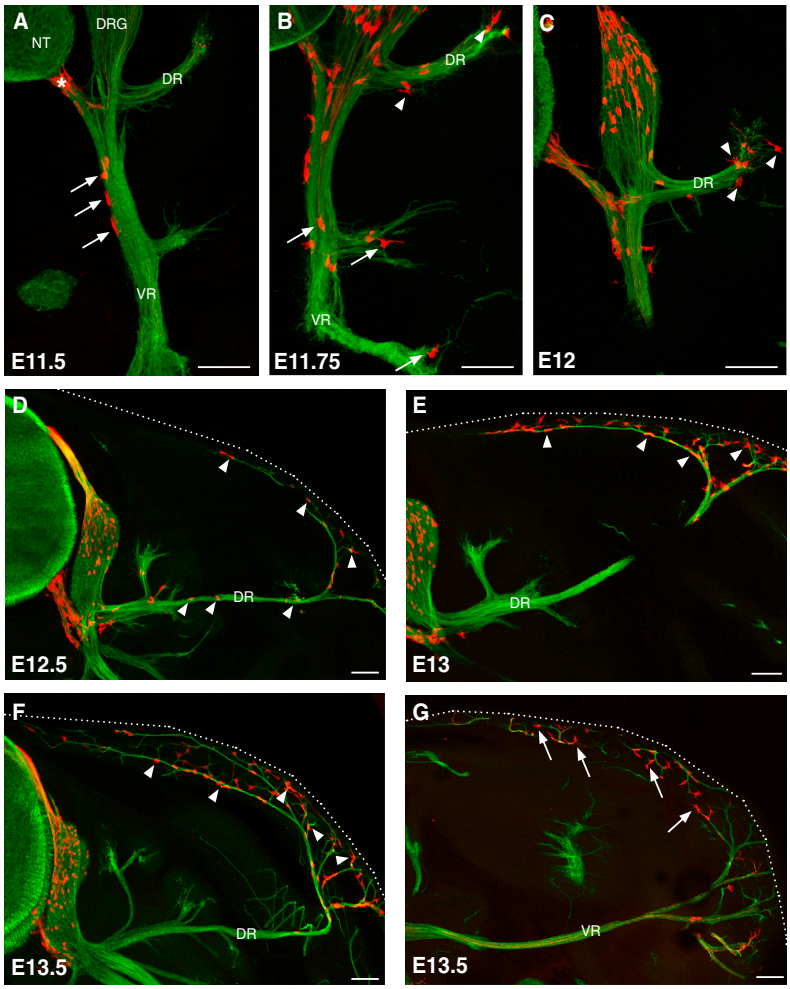

Figure 2. BC Derivatives Migrate along the Peripheral Nerves to the Skin

Transverse sections through the trunk of *Prss56*$^{Cre/+}$,*R26*^{tdTom} embryos, between E11.5 and E13.5 as indicated, were analyzed by immunocytochemistry using antibodies against tdTOM (red) and βIII-tubulin (green).

(A) At E11.5, tdTOM-positive cells are present along the ventral nerve root (asterisk) and the proximal part of the ventral ramus (VR) (arrows).

(B and C) Between E11.75 and E12, traced cells are detected along the VR (arrows) and the extending dorsal ramus (DR) (arrowheads).

(D) At E12.5, isolated traced cells are present along the entire trajectory of the nerve (arrowheads).

(E–G) From E13, tdTOM-positive cells are observed at cutaneous nerves in the dorsal (arrowheads) and ventral (arrows) skin. Dotted lines mark the embryo.

NT, neural tube; DRG, dorsal root ganglia. Scale bars, 100 μm. See also Figure S3.

mechanoreceptive nerve fibers and their associated terminal Schwann cells (Li and Ginty, 2014). Traced cells at the free nerve endings of nociceptive fibers showed an atypical morphology, with the soma localized in the upper part of the dermis, close to the epidermis, while a dense network of cytoplasmic protrusions penetrated the dermis and epidermis and followed the path of nerve terminals (Figure 3G). These cytoplasmic protrusions are often in close contact with blood vessels in the dermis (Figure 3H). These cells are likely to correspond to the teloglia, which was once described by Cauna, but not further investigated (Cauna, 1973). Interestingly, while some traced cells associated with the lanceolate endings expressed the progenitor/stem cell marker nestin, this was not the case for any of those associated with the free nerve endings (Figure 3I).

In the adult skin, the distribution and immunohistological signature of traced cells along the neuronal cutaneous network were comparable to that of newborns (Figures S4A–S4C). We further characterized adult BC derivatives in the hypodermis using electron microscopy. For this purpose, we used *Prss56*$^{Cre/+}$,*R26*^{lacZ} animals, where Cre recombination leads to permanent expression of β-galactosidase, which can convert the Bluogal substrate into electron-dense precipitates (Maro et al., 2004). Analysis of subcutaneous nerves confirmed that the majority of the labeled cells were non-myelinating Schwann cells (Figure S4D), but also identified a few myelinating Schwann cells (Figure S4D), as observed in the newborn (Figure 3B), and endoneurial fibroblasts, characterized by the absence of basal lamina (Figures S4D and S4E).

Together, our data indicate that BC cell derivatives in neonatal and adult skin consist mainly of Schwann cells, most of them non-myelinating, and some endoneurial fibroblasts. Among the Schwann cells, some are associated with the dermal nerve fibers and others with nerve terminals, either lanceolate or free endings.

Please cite this article in press as: Gresset et al., Boundary Caps Give Rise to Neurogenic Stem Cells and Terminal Glia in the Skin, Stem Cell Reports (2015), http://dx.doi.org/10.1016/j.stemcr.2015.06.005

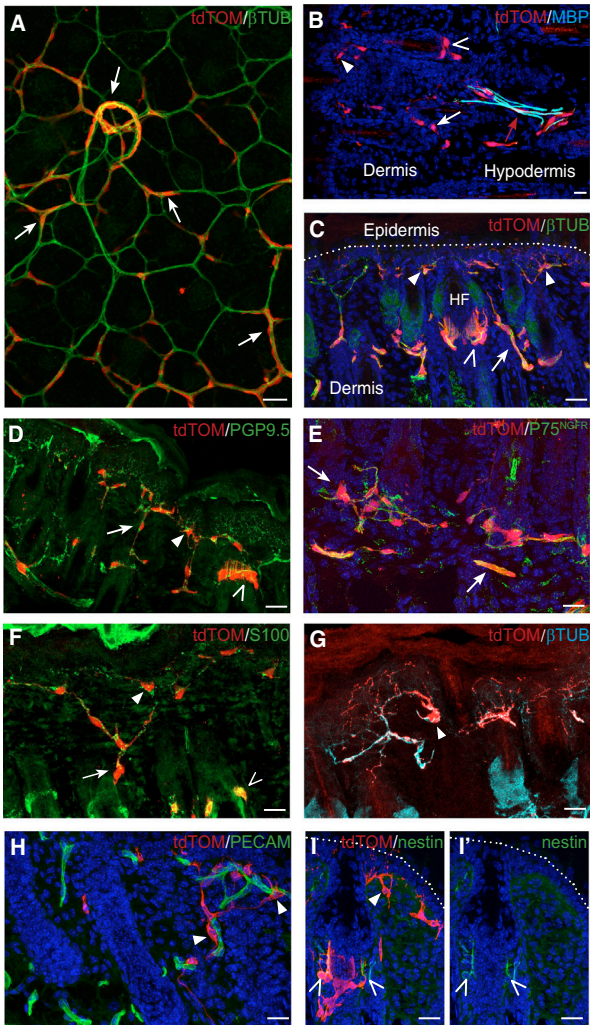

Figure 3. Identities of BC Derivatives in the Neonatal Skin

(A) Whole-mount immunostaining of newborn skin from *Prss56*$^{Cre/+}$, *R26*^{tdTom} animals for tdTOM and βIII-tubulin, viewed from the hypodermal side. Most traced cells are in contact with the subcutaneous or dermal nerves (arrows).

(B–I) Transverse sections of the skin from *Prss56*$^{Cre/+}$,*R26*^{tdTom} newborn animals labeled with the indicated antibodies. In the hypodermis, traced cells are associated with the cutaneous nerves and some express the myelin marker MBP (B, red arrow). In the dermis, tdTOM-positive cells are localized along βIII-tubulin-positive axons (C) and PGP9.5-positive terminal nerve fibers (D), and they express the NC stem cell/immature glial marker P75^{NGFR} (E) and the Schwann cell marker S100 (F), but not the myelin marker MBP (B, white arrow and open and closed arrowheads). These Schwann-like cells are associated with dermal nerves (A and C–F, arrows), free nerve endings (C, D, and F–I, closed arrowheads), or lanceolate endings of hair follicles (C, D, F, and I, open arrowheads). The cells associated with free nerve endings are highly ramified and are often in direct contact with blood vessels (G and H, arrowheads). Some of the traced cells at lanceolate endings express nestin (I and I′, empty arrowheads).

Scale bars, 50 μm. See also Figure S4.

Dermal BC Derivatives Can Be Propagated in Sphere Cultures and Are Multipotent

NC-derived progenitor/stem cells that express P75^{NGFR} and SOX10 have been described in the mouse and human skin (Wong et al., 2006). These characteristics are similar to those of skin BC derivatives (Figure 3E; Figure S3D) and led us to investigate whether some BC derivatives show stem cell-like properties. For this purpose, we performed floating sphere cultures from the back skin of *Prss56*$^{Cre/+}$, *R26*^{tdTom} newborn mice (Biernaskie et al., 2006; Wong et al., 2006). Numerous floating spheres were observed after 7–10 days in culture and could be propagated for at least 11 passages (Figure 4A). We used our tracing system to monitor BC derivatives over time in these cultures. While tdTOM-positive cells only represented 0.1% of the cells recovered after skin dissociation, their proportion increased during successive passages to reach approximately 80% of the sphere population at passage 10 (P10) (Figures 4A and 4B).

The rapid increase in the proportion of tdTOM-positive cells during the early passages might reflect either a proliferative advantage of traced cells or a de novo activation of the *Prss56* locus in previously unlabeled cells. *Prss56* expression was not detected by RT-PCR in cells freshly isolated from newborn skin or maintained in sphere culture for two, four, eight and 11 passages (Figure S5A). To avoid a possible dilution of the RT-PCR signal from rare stem cells at early culture stages, we enriched the initial culture in tdTOM-positive stem cells by immuno-panning, taking advantage of the fact that they derive from P75^{NGFR}-positive cells (see below). Once again, no *Prss56* expression was observed either immediately after immuno-panning or after 36 hr culture in sphere conditions (Figure S5B). Together, these data are not consistent with de novo activation of *Prss56* in culture conditions and suggest a proliferative advantage for the traced cells. In agreement with this interpretation, immunostaining analysis with the mitotic marker phospho-histone H3 showed that more than 97% of the floating tdTom-positive cells expressed this marker after 36 hr in culture (Figure S5C), indicating that these cells are highly proliferative.

We next characterized tdTOM-positive cells from spheres. Staining of P2 spheres indicated that tdTOM-positive cells express immature glial/neural stem cell markers, including P75^{NGFR}, vimentin, fibronectin, nestin, and SOX2, but not the CNS progenitor marker OLIG2 (Figure 4C). Further characterization was performed by RT-PCR on cells isolated from freshly dissociated skin

Please cite this article in press as: Gresset et al., Boundary Caps Give Rise to Neurogenic Stem Cells and Terminal Glia in the Skin, Stem Cell Reports (2015), http://dx.doi.org/10.1016/j.stemcr.2015.06.005

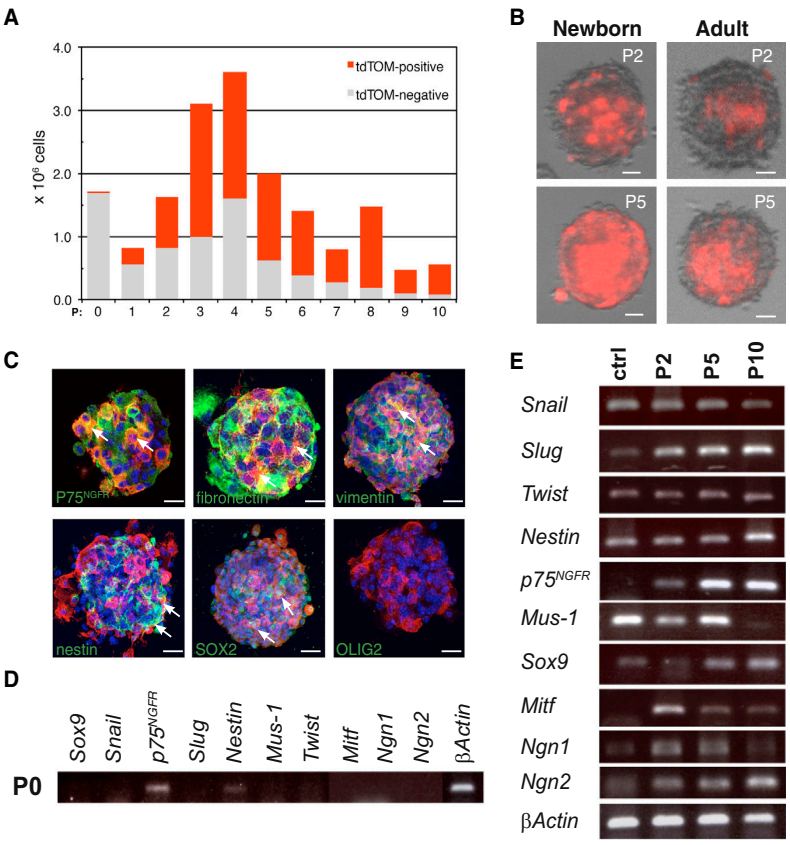

Figure 4. In Vitro Characterization of Skin BC Derivatives

(A) Evolution in the numbers of tdTOM-positive and -negative cells at successive passages (P) in sphere cultures from *Prss56*$^{Cre/+}$,*R26*^{tdTom} newborn skin is shown.

(B) Examples of spheres generated from newborn and adult skin at P2 and P5 show the content in traced cells (red).

(C) Characterization of tdTOM-positive cells (red) from P2 spheres with glial and stem/progenitor markers (green). Arrows point to traced cells positive for the indicated marker.

(D and E) RT-PCR analysis of the expression of NC and stem/progenitor-specific genes in newborn skin cells immediately after dissociation (D) or cultured in sphere-forming medium at the indicated passage (E). In (E), the control (ctrl) corresponds to RNA extracted from the neural tube of E8.5 embryos.

Scale bars, 100 μm (B) and 50 μm (C). See also Figure S5 and Table S1.

(P0) or maintained in sphere culture for two, five, and ten passages. Dissociated cells from back skin expressed *p75*^{NGFR} and low levels of *nestin* (Figure 4D). Exposure to sphere-forming culture conditions led to increases in the levels of expression of several NC (*Snail*, *Slug*, and *Twist*) and immature cell (*nestin*, *p75*^{NGFR}, and *musashi-1*) markers (Figure 4E), presumably reflecting the increasing proportion of tdTom-positive cells. The spheres also expressed early markers of NC-derived lineages, including chondrocytes (*Sox9*), melanocytes (*Mitf*), and neurons (*Ngn1* and *Ngn2*) (Figure 4E).

We next analyzed the differentiation potential of cultured tdTOM-positive cells. Cells from neonatal *Prss56*$^{Cre/+}$,*R26*^{tdTom} skin were maintained in culture for two or five passages, mechanically dissociated, and cultured for 2 additional weeks in the presence of serum, which promotes their spontaneous differentiation. They were then analyzed according to their morphology and by immunostaining with antibodies against tdTOM and neuronal (βIII-tubulin), Schwann cell (S100), and myofibroblast (SMA) markers. In both P2 and P5 cultures, numerous neurons, myofibroblasts, as well as rare Schwann cells and adipocytes were observed among the traced population (Figures 5A–5E). We also investigated the response of these dermal BC-derived cells to lineage-specific factors added to the differentiation medium. The addition of forskolin and heregulin greatly enhanced the capacity of spheres to differentiate into Schwann cells (Figure 5F). The addition of stem cell factor (SCF) and endothelin-3 promoted the generation of melanocytes (Figure 5G), while ascorbic acid and bone morphogenetic protein 2 (BMP2) favored the generation of chondrocytes (Figure 5H). These results are consistent with the expression of early markers of NC-derived lineages in spheres (Figure 4E). We also assessed the capacity of spheres to differentiate into a lineage that is not derived from the NC. Inhibition of BMP and Shh signaling enabled the generation of OLIG2-positive immature oligodendrocytes, a CNS glial cell type (Figure 5I). Finally, as the spheres obtained from back skin were initially heterogeneous and contained BC derivatives as well as other skin stem cell-like cells, it was important to isolate the BC derivatives as early as possible to investigate their stem cell properties. For this purpose, newborn skin was dissociated and cultured in sphere conditions for 10 days. tdTOM-positive cells were then purified by fluorescence-activated cell sorting (FACS) and cultured

Please cite this article in press as: Gresset et al., Boundary Caps Give Rise to Neurogenic Stem Cells and Terminal Glia in the Skin, Stem Cell Reports (2015), http://dx.doi.org/10.1016/j.stemcr.2015.06.005

A

	Newborn						Adult	
	P2			P5			P1	P5
	Total	P75^{NGFR}+	Thy1 +	Total	P75^{NGFR} +	Thy1 +	Total	Total
Neurons	+ +	+ +	-	+ +	+ +	-	+ +	+ +
Schwann	+	+	-	+	+	-	++	+
Myofibroblasts	++++	++++	++++	++++	++++	++++	++++	++++
Adipocytes	++	++	++	++	++	++	++	++

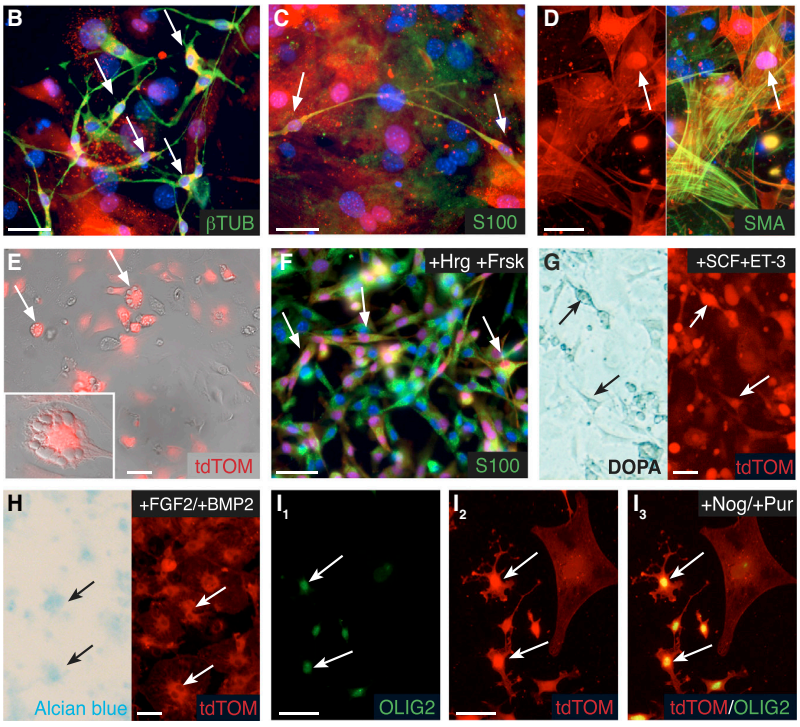

Figure 5. Pluripotency of Skin BC Derivatives In Vitro

(A) Cell type distribution of tdTOM-positive cells from newborn and adult skin cultured in spontaneous differentiation conditions after the indicated passage. Cultures were performed from the total skin population or P75^{NGFR}- or Thy1-positive subpopulation purified by immuno-panning. Cell types were identified by cell morphology and expression of specific markers (see B–E). Approximate distributions are indicated as follows: +, 0.1% to 1%; ++, 1% to 5%; +++, 5% to 15%; and ++++, 15% to 40%.

(B–I) Cell type identification of tdTOM-positive cells from newborn skin cultured in spontaneous (B–E) or induced (F–I) differentiation conditions. Immunolabeling identified the presence of neurons (B, βIII-tubulin positive), Schwann cells (C and F, S100 positive), and myofibroblasts (D, smooth muscle actin [SMA] positive). Cells with morphological features of adipocytes (E), characterized by the presence lipid droplets (inset), also were observed. The proportion of Schwann cells was increased upon the addition of forskolin and heregulins during differentiation (F). DOPA reaction and Alcian blue staining revealed the presence of tdTOM-positive melanocytes (G) and chondroncytes (H) after induced differentiation. Differentiation in the presence of noggin and purformamine led to the formation of immature oligodendrocytes (I_1–I_3, OLIG2 positive). Arrows point to traced cells expressing the indicated marker. Scale bars, 30 μm.

in sphere conditions. tdTOM-positive cells formed spheres that could be propagated for several passages (Figure S6A) and spontaneously differentiated into NC-derived lineages, including neurons, Schwann cells, and myofibroblasts (Figures S6B–S6D). Together, these results indicate that tdTOM-positive cells from back skin can be propagated in sphere culture, possess a broad differentiation potential in culture, and are plastic in their fate.

Finally, we investigated whether these BC derivatives with stem cell properties are maintained in the adult skin. Traced cells in the adult skin were slightly more abundant (0.6% of the total initial population) than in neonatal skin. Sphere cultures performed with adult skin showed similar proliferation and differentiation properties (Figures 4B and 5A). As skin BC derivatives comprise both glial and fibroblast cells, we wondered whether the stem cells belonged to one or the other population. By magnetic immuno-panning against P75^{NGFR} for immature glial cells and Thy1 for fibroblasts (Manent et al., 2003), we isolated each cell type, as well as the double-negative population, from newborn skin and performed sphere cultures. Spheres containing numerous traced cells were obtained from both glial and fibroblastic populations, but not from the double-negative fraction. In differentiation conditions, the P75^{NGFR}-positive population gave rise to a similar distribution of cell types as without fractionation, whereas neuronal and glial derivatives were absent from the Thy1-positive population (Figure 5A). To further identify the skin tissue layer housing the stem cells, we performed sphere cultures from the hypodermis of neonatal *Prss56$^{Cre/+}$,R26^{tdTom}* mice after magnetic fractionation with P75^{NGFR} antigens. This fraction failed to form spheres, suggesting that the P75^{NGFR}-positive stem cells were restricted to the dermis, since the epidermis was devoid of traced cells. Together, our results indicate that BC derivatives in neonatal skin include a dermal, P75^{NGFR}-positive

Please cite this article in press as: Gresset et al., Boundary Caps Give Rise to Neurogenic Stem Cells and Terminal Glia in the Skin, Stem Cell Reports (2015), http://dx.doi.org/10.1016/j.stemcr.2015.06.005

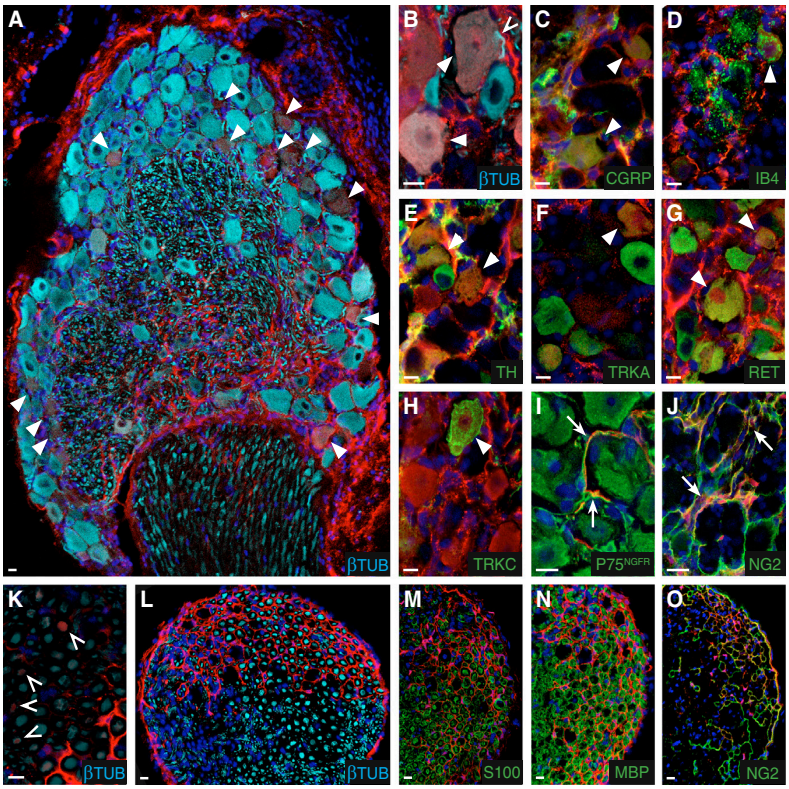

Figure 6. Skin BC Derivatives Give Rise to Various Types of Sensory Neurons upon Transplantation into the DRG

FACS-purified tdTOM-positive cells from skin cultures were injected into the DRGs of nude mice, which were analyzed by immunohistochemistry 30 days later.

(A–J) Transverse sections through the injected DRGs analyzed with antibodies against tdTOM and specific markers of neuronal, glial, or fibroblastic cell types according to the color code. Arrowheads and arrows indicate neuronal and non-neuronal traced cells, respectively.

(K–O) Transverse sections through the spinal nerve attached to the injected DRG. tdTOM-positive axons (empty arrowheads) were observed (K). Numerous traced cells encircled βIII-tubulin-positive axons (L). They were negative for immature (M) and myelinating (N) Schwann cell markers, but expressed NG2 (O), a marker of endo/perineurial fibroblasts.

Scale bars, 10 μm.

stem cell-like population that shows a broad differentiation potential and persists in the adult.

Skin BC Derivatives Grafted into the DRG Efficiently Differentiate into Sensory Neurons

To investigate the in vivo differentiation potential of skin BC derivatives, we first performed transplantations into adult DRGs. Newborn skin was dissociated and cultured in sphere conditions for 10 days. tdTOM-positive cells were then purified by FACS and injected into the L4 or L5 DRG of nude mice (2×10^4 traced cells/DRG). Mice were sacrificed 30 days after grafting and the injected DRGs were analyzed for the presence of tdTOM-positive cells. Of the 30 mice injected, 27 showed numerous tdTOM-positive cells in the injected DRGs. Within the successfully injected DRGs, most traced cells were positive for the neuronal marker βIII-tubulin (Figures 6A and 6B) and represented 12% ± 1.0% of all neurons in the DRG. Traced neurons were further characterized with markers of different categories of mature DRG neurons (Lallemend and Ernfors, 2012) and represented a large array of sensory neurons as follows: peptidergic (CGRP-positive, Figure 6C) and non-peptidergic (binding isolectin B4, Figure 6D) nociceptors; unmyelinated mechanoceptors (tyrosine hydroxylase-positive, Figure 6E); TRKA-positive neurons (Figure 6F), which include lightly myelinated nociceptors and a subpopulation of peptidergic nociceptors; RET-positive neurons (Figure 6G), which include myelinated mechanoceptors and a subpopulation of peptidergic and non-peptidergic nociceptors; and TRKC-positive neurons (Figure 6H), which include subpopulations of myelinated proprioceptors and mechanoceptors. Furthermore, immunostaining for βIII-tubulin in transverse sections through the dorsal root attached to the injected DRG revealed numerous tdTOM-positive axons (Figure 6K), indicating that at least some of the traced neurons had generated long projections. Together, these data indicate that the grafted cells efficiently differentiate into mature sensory neurons.

Other types of traced cells were observed within the DRG as follows: small, elongated $P75^{NGFR}$-positive cells in close contact with neuronal somata, which are glial satellite cells (Figure 6I); cells positive for the proteoglycan NG2 (Figure 6J), which is produced by perineurial and endoneurial fibroblasts in the rat adult sciatic nerve (Morgenstern et al., 2003); and a layer of cells surrounding the DRG, whose identity remains unknown (Figure 6A). Finally, numerous tdTOM-positive cells were observed in the dorsal root and spinal nerve attached to the injected DRG, indicating that injected cells had migrated away from the injection site (Figure 6L). These cells formed a dense network

Please cite this article in press as: Gresset et al., Boundary Caps Give Rise to Neurogenic Stem Cells and Terminal Glia in the Skin, Stem Cell Reports (2015), http://dx.doi.org/10.1016/j.stemcr.2015.06.005

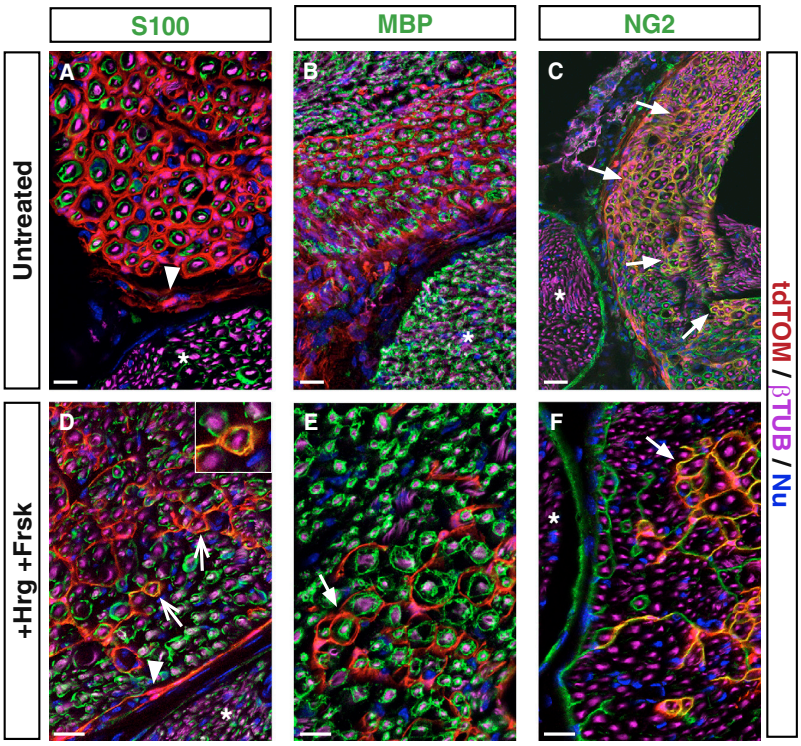

Figure 7. Skin BC Derivatives Give Rise to Peripheral Fibroblasts and Schwann Cells upon Injection into the Injured Sciatic Nerve

Newborn skin BC derivatives were cultured until P1, FACS purified (A–C; untreated) or treated with heregulin/forskolin (D–F; +Hrg+Frsk), and injected into injured sciatic nerves. Transverse sections of the grafted sciatic nerves were analyzed 6 weeks after grafting by immunohistochemistry with antibodies against tdTOM and the indicated neuronal, glial, and fibroblastic markers. Arrowheads point to perineurial cells, closed arrows to endoneurial cells, and open arrows to Schwann cells. Nu, nuclear staining. Ungrafted nerve bundles (asterisks) do not contain tdTOM-positive cells. Scale bars, 50 μm.

around the Schwann cell-axon bundles, and they were negative for immature (S100, Figure 6M) or myelinating (MBP, Figure 6N) Schwann cell markers, but were positive for NG2 (Figure 6O). Therefore, traced cells also differentiate into endo/perineurial-like fibroblasts in the dorsal root and the spinal nerve.

Together, our results indicate that, following injection into adult DRG, skin BC derivatives efficiently colonize the DRG and part of the spinal nerve and give rise to different cell types, including a variety of sensory neurons as well as glial cells and fibroblasts.

Skin BC Derivatives Grafted into Lesioned Peripheral Nerves Give Rise to Endo/Perineurial and Schwann Cells

To investigate whether skin BC derivatives also could differentiate in vivo into Schwann cells when provided with an appropriate environment, we performed transplantations into the cryo-lesioned sciatic nerves of nude mice (Stoll and Müller, 1999). Sciatic nerve lesions are known to enable recruitment of Schwann cells (Jessen et al., 2015). tdTOM-positive cells were prepared as for DRG transplantations and grafted into the lesion site. Six weeks later, numerous traced cells were observed within the lesion site (Figure 6A) as well as in the proximal part of the nerve, indicating that traced cells had efficiently colonized the lesioned nerve. Analyses of transverse and longitudinal nerve sections indicated that grafted traced cells were not in direct contact with the regenerated axons and were negative for markers for immature (S100, Figure 7A) and myelinating (MBP, Figure 7B) Schwann cells. Most traced cells appeared to wrap single axon/Schwann cell units (Figures 7A and 7B, closed arrows), in a manner similar to endoneurial fibroblasts (Morgenstern et al., 2003). Some traced cells were also at the level of the perineurium (Figure 7A, arrowheads), ensheathing fascicles composed of axons, their associated Schwann cells, and the surrounding endoneurium. Consistent with these observations, the traced cells were positive for the NG2 marker (Figure 7C). Thus, after transplantation into the injured sciatic nerve, tdTOM-positive cells do not engage into the glial pathway and differentiate preferentially into endo/perineurial-like fibroblasts.

We finally asked whether exposing tdTOM-positive cells to factors promoting a Schwann cell fate prior to transplantation would modify this situation. Skin-derived spheres were maintained for 2 weeks in the presence of forskolin and heregulin, then dissociated and injected into the injured sciatic nerve. Six weeks after transplantation, although most traced cells were NG2-positive fibroblastic cells (Figures 7D–7F), we observed some S100-positive Schwann cells (Figure 7D, open arrows), which had remained immature as they did not express the MBP myelin

Please cite this article in press as: Gresset et al., Boundary Caps Give Rise to Neurogenic Stem Cells and Terminal Glia in the Skin, Stem Cell Reports (2015), http://dx.doi.org/10.1016/j.stemcr.2015.06.005

marker (Figure 7E). Together, our results indicate that, in the lesioned sciatic nerve environment, grafted BC-derived skin stem cells mainly engage into an endo/perineurial fibroblastic fate, although in vitro treatment with Schwann cell fate-promoting factors redirects some of them toward the glial pathway.

DISCUSSION

This study builds on previous observations that the NC contribution to PNS formation occurs in two waves (Maro et al., 2004), with one population migrating directly to their target locations, while the other makes a stop at the level of the BCs. In contrast to what was previously thought (Maro et al., 2004), we establish that the two waves make similar qualitative contributions in terms of neuronal subtypes in the DRG. Along peripheral nerves of the trunk, the BCs provide the entire proximal Schwann cell nerve root component, as well as a large part of the glia covering the distal parts of skin nerves, whereas the direct NC contribution appears largely restricted to the intermediate part of the nerves. These distinct origins may underlie functional differences between glial populations at different levels along the nerves.

These data have to be considered in the context of recent studies that have shown that embryonic peripheral nerves contain progenitor cells with NC-like potential. Specifically, the early glial components of peripheral nerves, the Schwann cell precursors, possess extensive differentiation capacities as, in addition to Schwann cells (Jessen et al., 2015), they can give rise to melanocytes in the skin (Adameyko et al., 2009), parasympathetic neurons (Dyachuk et al., 2014; Espinosa-Medina et al., 2014), and mesenchymal derivatives in the tooth (Kaukua et al., 2014). However, BC cells appear distinct from these pluripotent glial populations by their location at the PNS/CNS boundary, the expression of specific markers such as *Krox20* and *Prss56* (Coulpier et al., 2009), and the identity of their derivatives. Furthermore, some BC derivatives maintain their pluripotency in adult tissues, while the pluripotency of Schwann cell precursors is restricted to a specific developmental period.

In the skin, we have shown that BC derivatives give rise to at least three glial populations as follows: Schwann cells (mainly non-myelinating) associated with subcutaneous and dermal nerves, and two types of terminal Schwann cells, associated with lanceolate endings or free nerve endings. Lanceolate endings are specialized sensory organs that detect hair movement (Abraira and Ginty, 2013). They form a palisade structure surrounding the hair follicle and are composed of terminal fibers carrying rapidly adapting low-threshold mechanoreceptors (Aβ, Aδ, and C) (Abraira and Ginty, 2013). The terminal Schwann cells are involved in the maintenance of the lanceolate complex (Li and Ginty, 2014) and could play a role in calcium signaling (Takahashi-Iwanaga et al., 2008).

Free nerve endings are non-specialized cutaneous sensory receptors that are involved in the perception of touch, pressure, and pain (Abraira and Ginty, 2013). In contrast to their name, free nerve endings also are associated with terminal Schwann cells. Terminal Schwann cells have been studied only by electron microscopy and present a very peculiar morphology, with numerous cytoplasmic protrusions covering the axons at the dermis/epidermis boundary (Cauna, 1973). We provide here a genetic marker that enables optical observations of these cells. Their morphology resembles that of perisynaptic Schwann cells (PSCs), which cap motor nerve terminals at the neuromuscular junction (Balice-Gordon, 1996). PSCs are involved in sensing and modulating synaptic transmission through the specific expression of neurotransmitter receptors and ion channels on their surface (Auld and Robitaille, 2003). Given their similarity with PSCs in terms of terminal location and morphology, we speculate that Schwann cells associated with free nerve endings might play a direct role in depolarizing axon membranes. The *Prss56*^{Cre} line allows easy identification of these atypical Schwann cells and should facilitate their detailed characterization.

In the dermis, the glial P75^{NGFR}-positive BC derivatives also include a neurogenic and gliogenic stem-like cell population. Multipotent stem-like cell populations have been described previously in the adult trunk skin, associated with the glial and melanocyte lineages and derived from the NC (Wong et al., 2006) or associated with hair follicle dermal cells and derived from the mesoderm (Biernaskie et al., 2009; Jinno et al., 2010). Our results indicate that the BC-derived population constitutes the major, but not single, component of skin stem-like cells detected in these culture conditions, as they represent approximately 80% of the sphere population at late passage. Our work is consistent with recent observations indicating that human adult skin stem cells with neurogenic potential express P75^{NGFR} and can be ascribed to the Schwann cell lineage (Etxaniz et al., 2014). Together, our results establish the precise origin of the large majority of the stem-like cells in the dermis and provide a unique and specific genetic tool for their identification, further study, and manipulation.

Most importantly, grafting experiments establish that this stem cell-like population can efficiently differentiate into various types of mature sensory neurons in the adult DRG. The differentiated neurons survive at least 2 months and many extend long axons in the dorsal root and spinal nerve, although it remains to be determined whether these axons cross the PNS/CNS boundary and establish connections in the spinal cord. Such a neurogenic potential has

Please cite this article in press as: Gresset et al., Boundary Caps Give Rise to Neurogenic Stem Cells and Terminal Glia in the Skin, Stem Cell Reports (2015), http://dx.doi.org/10.1016/j.stemcr.2015.06.005

never been reported for skin-derived stem cells and it raises the possibility that these cells may manifest an even broader plasticity (e.g., generation of central glia and neurons), if offered the appropriate cellular environment. The fact that these stem cells give rise to a very different distribution of cell types (only endo/perineurial fibroblasts and Schwann cells) upon transplantation into a lesioned sciatic nerve and that they can generate immature oligodendrocytes in vitro is consistent with such a possibility. However, in contrast to the glial character of most traced cells in the dermis, only a small number of Schwann cells are generated after their transplantation into the peripheral nerve. This could reflect differences in the differentiation potentials of BC and newborn skin-traced stem-like cells.

BC derivatives with self-renewal and neurogenic potential also have been identified in the mouse embryonic DRGs (Hjerling-Leffler et al., 2005; Li et al., 2007). In vitro, these stem-like cells re-express NC markers and differentiate efficiently into peripheral sensory neurons (Hjerling-Leffler et al., 2005). Recently, stem/progenitor cells were identified in the adult DRG (Vidal et al., 2015). However, their differentiation might be more restricted as, after transplantation into the lesioned spinal cord, they exclusively generated Schwann cells. It will be interesting to determine whether this population derives from BC cells.

In conclusion, our work opens the way for the detailed analysis of a major population of skin stem cells that are derived from the BCs, have powerful neurogenic potential, and, because of their accessibility, constitute valuable candidates for regenerative medicine. The specific genetic tools developed in the present study should be instrumental for further characterization and manipulation of this promising cell population.

EXPERIMENTAL PROCEDURES

Mouse Lines, Genotyping, and Ethical Considerations

All mouse lines were maintained in a mixed C57BL6/DBA2 background. We used the following alleles or transgenes that were genotyped as indicated in the original publications: *Krox20*^{Cre} (Voiculescu et al., 2000), *Rosa26*^{lacZ} (Soriano, 1999), *Rosa26*^{tdTom} (Madisen et al., 2010), and *Krox20*^{lacZ} (Schneider-Maunoury et al., 1993). *Prss56*^{Cre} was generated in this work (see Figure S1). Genotyping was performed by PCR on tail DNA using primers described in Table S1. Day of the plug was considered E0.5. Animals were sacrificed by decapitation (newborn) or cervical dislocation (adult) unless indicated otherwise. All animal manipulations were approved by a French Ethical Committee (Project Ce5/2012/115) and were performed according to French and European Union regulations.

FACS

tdTOM-positive cells were isolated from neonatal skin cell preparations and cultured as floating spheres. Primary spheres were mechanically dissociated and the resulting cell suspension (3×10^6 cells/ml) was purified on a FacsVantage (Becton Dickinson) equipped with an argon laser tuned to 561 nm. Dead cells and doublets were excluded by gating on a forward-scatter and side-scatter area versus width. Log RFP fluorescence was acquired through a 530/30 band pass. Internal tdTOM-negative cells served as negative controls for FACS gating. tdTOM-positive cells were sorted directly into culture medium until use in transplantation assays. For verification of the purity of the sorted cells, aliquots of the tdTOM-positive and tdTOM-negative fractions were sorted via FACS again with similar gating parameters and, in parallel, seeded onto coverslips and analyzed by immunohistochemistry with anti-tdTOM antibody.

Transplantations into the DRGs and Sciatic Nerve

Adult nude mice were anesthetized by intra-peritoneal injection of ketamine (Imalgene 500; 0.5 μl/g) and xylazine (Rompun 2%, 0.2 μl/g) before surgery. In addition, local anesthesia (lidocaine) was applied. The tdTOM-positive cells were prepared from neonatal skin, cultured for 10 days in sphere conditions, purified by FACS, and immediately injected. For transplantation into the DRG, the lower lumbar vertebral column was exposed by a midline incision of the skin and fascia, and the right L4 or L5 DRG was exposed via a hemi-laminectomy. A suspension containing 2×10^4 tdTOM-positive cells (10^4 cells/μl) was injected into the DRG. After 1 month, the animals were injected with a lethal dose of ketamine and xylazine and perfused with saline, followed by a fixative solution containing 4% paraformaldehyde (PFA) in PBS. The DRG with the attached nerve roots and spinal nerves was dissected, post-fixed in 4% PFA for 3 hr, and cryoprotected overnight in PBS containing 15% sucrose. Serial 14-μm cryosections were prepared and stored at −80°C until analysis. For transplantation into the sciatic nerve, the nerve was exposed and crushed four times for 10 s with forceps chilled in liquid nitrogen. A suspension containing 10^5 tdTOM-positive cells (5×10^4 cells/μl) was immediately injected into the lesion site as previously described (Stoll and Müller, 1999). After 6 weeks, the animals were sacrificed and the injected sciatic nerves were dissected, fixed in 4% PFA for 3 hr, and cryoprotected overnight. Serial 14-μm cryosections were prepared and stored at −80°C until analysis.

SUPPLEMENTAL INFORMATION

Supplemental Information includes Supplemental Experimental Procedures, six figures, and one table and can be found with this article online at http://dx.doi.org/10.1016/j.stemcr.2015.06.005.

AUTHOR CONTRIBUTIONS

A.G., F.C., P.T., and P.C. designed the experimental paradigm. A.G., F.C., G.G., A.J., G.M., L.R., and P.T. performed the experiments. A.G., F.C., G.G., J.-M.V., P.C., and P.T. analyzed the data. A.G., P.C., and P.T. wrote the paper.

ACKNOWLEDGMENTS

We thank Christo Goridis, James Cohen, and Pascale Gilardi for critical reading of the manuscript. We are grateful to the IBENS Imaging Facility, supported by grants from the Région Ile-de-France

DIM NeRF 2009; to the IBENS mouse facility; and to the cell sorting platform of the Curie Institute. Work in the P.C. laboratory has been supported by the INSERM, the CNRS, the Ministère de la Recherche et Technologie (MRT), the Fondation pour la Recherche Médicale (FRM DEQ20121126545), the Association Française contre les Myopathies, and the Association de Recherche sur le Cancer. A.G. has been supported by the Fondation Pierre Gilles de Gennes, FRM (SPF20101221087), MRT, and LABEX MemoLife.

Received: December 2, 2014
Revised: June 17, 2015
Accepted: June 17, 2015
Published: July 23, 2015

REFERENCES

Abraira, V.E., and Ginty, D.D. (2013). The sensory neurons of touch. Neuron *79*, 618–639.

Adameyko, I., Lallemend, F., Aquino, J.B., Pereira, J.A., Topilko, P., Müller, T., Fritz, N., Beljajeva, A., Mochii, M., Liste, I., et al. (2009). Schwann cell precursors from nerve innervation are a cellular origin of melanocytes in skin. Cell *139*, 366–379.

Auld, D.S., and Robitaille, R. (2003). Perisynaptic Schwann cells at the neuromuscular junction: nerve- and activity-dependent contributions to synaptic efficacy, plasticity, and reinnervation. Neuroscientist *9*, 144–157.

Balice-Gordon, R.J. (1996). Dynamic roles at the neuromuscular junction. Schwann cells. Curr. Biol. *6*, 1054–1056.

Biernaskie, J.A., McKenzie, I.A., Toma, J.G., and Miller, F.D. (2006). Isolation of skin-derived precursors (SKPs) and differentiation and enrichment of their Schwann cell progeny. Nat. Protoc. *1*, 2803–2812.

Biernaskie, J., Paris, M., Morozova, O., Fagan, B.M., Marra, M., Pevny, L., and Miller, F.D. (2009). SKPs derive from hair follicle precursors and exhibit properties of adult dermal stem cells. Cell Stem Cell *5*, 610–623.

Cauna, N. (1973). The free penicillate nerve endings of the human hairy skin. J. Anat. *115*, 277–288.

Coulpier, F., Le Crom, S., Maro, G.S., Manent, J., Giovannini, M., Maciorowski, Z., Fischer, A., Gessler, M., Charnay, P., and Topilko, P. (2009). Novel features of boundary cap cells revealed by the analysis of newly identified molecular markers. Glia *57*, 1450–1457.

Dupin, E., and Sommer, L. (2012). Neural crest progenitors and stem cells: from early development to adulthood. Dev. Biol. *366*, 83–95.

Dyachuk, V., Furlan, A., Shahidi, M.K., Giovenco, M., Kaukua, N., Konstantinidou, C., Pachnis, V., Memic, F., Marklund, U., Müller, T., et al. (2014). Neurodevelopment. Parasympathetic neurons originate from nerve-associated peripheral glial progenitors. Science *345*, 82–87.

Espinosa-Medina, I., Outin, E., Picard, C.A., Chettouh, Z., Dymecki, S., Consalez, G.G., Coppola, E., and Brunet, J.F. (2014). Neurodevelopment. Parasympathetic ganglia derive from Schwann cell precursors. Science *345*, 87–90.

Etxaniz, U., Pérez-San Vicente, A., Gago-López, N., García-Dominguez, M., Iribar, H., Aduriz, A., Pérez-López, V., Burgoa, I., Irizar, H., Muñoz-Culla, M., et al. (2014). Neural-competent cells of adult human dermis belong to the Schwann lineage. Stem Cell Reports *3*, 774–788.

Hjerling-Leffler, J., Marmigère, F., Heglind, M., Cederberg, A., Koltzenburg, M., Enerbäck, S., and Ernfors, P. (2005). The boundary cap: a source of neural crest stem cells that generate multiple sensory neuron subtypes. Development *132*, 2623–2632.

Jessen, K.R., Mirsky, R., and Lloyd, A.C. (2015). Schwann cells: development and role in nerve repair. Cold Spring Harb. Perspect. Biol., a020487.

Jinno, H., Morozova, O., Jones, K.L., Biernaskie, J.A., Paris, M., Hosokawa, R., Rudnicki, M.A., Chai, Y., Rossi, F., Marra, M.A., and Miller, F.D. (2010). Convergent genesis of an adult neural crest-like dermal stem cell from distinct developmental origins. Stem Cells *28*, 2027–2040.

Kaukua, N., Shahidi, M.K., Konstantinidou, C., Dyachuk, V., Kaucka, M., Furlan, A., An, Z., Wang, L., Hultman, I., Ährlund-Richter, L., et al. (2014). Glial origin of mesenchymal stem cells in a tooth model system. Nature *513*, 551–554.

Lallemend, F., and Ernfors, P. (2012). Molecular interactions underlying the specification of sensory neurons. Trends Neurosci. *35*, 373–381.

Le Douarin, N.M., and Dupin, E. (2003). Multipotentiality of the neural crest. Curr. Opin. Genet. Dev. *13*, 529–536.

Li, L., and Ginty, D.D. (2014). The structure and organization of lanceolate mechanosensory complexes at mouse hair follicles. eLife *3*, e01901.

Li, H.-Y., Say, E.H.M., and Zhou, X.-F. (2007). Isolation and characterization of neural crest progenitors from adult dorsal root ganglia. Stem Cells *25*, 2053–2065.

Madisen, L., Zwingman, T.A., Sunkin, S.M., Oh, S.W., Zariwala, H.A., Gu, H., Ng, L.L., Palmiter, R.D., Hawrylycz, M.J., Jones, A.R., et al. (2010). A robust and high-throughput Cre reporting and characterization system for the whole mouse brain. Nat. Neurosci. *13*, 133–140.

Manent, J., Oguievetskaia, K., Bayer, J., Ratner, N., and Giovannini, M. (2003). Magnetic cell sorting for enriching Schwann cells from adult mouse peripheral nerves. J. Neurosci. Methods *123*, 167–173.

Marmigère, F., and Ernfors, P. (2007). Specification and connectivity of neuronal subtypes in the sensory lineage. Nat. Rev. Neurosci. *8*, 114–127.

Maro, G.S., Vermeren, M., Voiculescu, O., Melton, L., Cohen, J., Charnay, P., and Topilko, P. (2004). Neural crest boundary cap cells constitute a source of neuronal and glial cells of the PNS. Nat. Neurosci. *7*, 930–938.

Morgenstern, D.A., Asher, R.A., Naidu, M., Carlstedt, T., Levine, J.M., and Fawcett, J.W. (2003). Expression and glycanation of the NG2 proteoglycan in developing, adult, and damaged peripheral nerve. Mol. Cell. Neurosci. *24*, 787–802.

Nair, K.S., Hmani-Aifa, M., Ali, Z., Kearney, A.L., Ben Salem, S., Macalinao, D.G., Cosma, I.M., Bouassida, W., Hakim, B., Benzina, Z., et al. (2011). Alteration of the serine protease PRSS56 causes angle-closure glaucoma in mice and posterior microphthalmia in humans and mice. Nat. Genet. *43*, 579–584.

Niederländer, C., and Lumsden, A. (1996). Late emigrating neural crest cells migrate specifically to the exit points of cranial branchiomotor nerves. Development *122*, 2367–2374.

Schneider-Maunoury, S., Topilko, P., Seitandou, T., Levi, G., Cohen-Tannoudji, M., Pournin, S., Babinet, C., and Charnay, P. (1993). Disruption of Krox-20 results in alteration of rhombomeres 3 and 5 in the developing hindbrain. Cell *75*, 1199–1214.

Soriano, P. (1999). Generalized lacZ expression with the ROSA26 Cre reporter strain. Nat. Genet. *21*, 70–71.

Stoll, G., and Müller, H.W. (1999). Nerve injury, axonal degeneration and neural regeneration: basic insights. Brain Pathol. *9*, 313–325.

Takahashi-Iwanaga, H., Nio-Kobayashi, J., Habara, Y., and Furuya, K. (2008). A dual system of intercellular calcium signaling in glial nets associated with lanceolate sensory endings in rat vibrissae. J. Comp. Neurol. *510*, 68–78.

Topilko, P., Schneider-Maunoury, S., Levi, G., Baron-Van Evercooren, A., Chennoufi, A.B., Seitanidou, T., Babinet, C., and Charnay, P. (1994). Krox-20 controls myelination in the peripheral nervous system. Nature *371*, 796–799.

Vermeren, M., Maro, G.S., Bron, R., McGonnell, I.M., Charnay, P., Topilko, P., and Cohen, J. (2003). Integrity of developing spinal motor columns is regulated by neural crest derivatives at motor exit points. Neuron *37*, 403–415.

Vidal, M., Maniglier, M., Deboux, C., Bachelin, C., Zujovic, V., and Baron-Van Evercooren, A. (2015). Adult DRG stem/progenitor cells generate pericytes in the presence of central nervous system (CNS) developmental cues, and Schwann cells in response to CNS demyelination. Stem Cells *33*, 2011–2024.

Voiculescu, O., Charnay, P., and Schneider-Maunoury, S. (2000). Expression pattern of a Krox-20/Cre knock-in allele in the developing hindbrain, bones, and peripheral nervous system. Genesis *26*, 123–126.

Wong, C.E., Paratore, C., Dours-Zimmermann, M.T., Rochat, A., Pietri, T., Suter, U., Zimmermann, D.R., Dufour, S., Thiery, J.P., Meijer, D., et al. (2006). Neural crest-derived cells with stem cell features can be traced back to multiple lineages in the adult skin. J. Cell Biol. *175*, 1005–1015.

Zujovic, V., Thibaud, J., Bachelin, C., Vidal, M., Coulpier, F., Charnay, P., Topilko, P., and Baron-Van Evercooren, A. (2010). Boundary cap cells are highly competitive for CNS remyelination: fast migration and efficient differentiation in PNS and CNS myelin-forming cells. Stem Cells *28*, 470–479.

Zujovic, V., Thibaud, J., Bachelin, C., Vidal, M., Deboux, C., Coulpier, F., Stadler, N., Charnay, P., Topilko, P., and Baron-Van Evercooren, A. (2011). Boundary cap cells are peripheral nervous system stem cells that can be redirected into central nervous system lineages. Proc. Natl. Acad. Sci. USA *108*, 10714–10719.

Stem Cell Reports

Supplemental Information

Boundary Caps Give Rise to Neurogenic Stem Cells and Terminal Glia in the Skin

Aurélie Gresset, Fanny Coulpier, Gaspard Gerschenfeld, Alexandre Jourdon, Graziella Matesic, Laurence Richard, Jean-Michel Vallat, Patrick Charnay, and Piotr Topilko

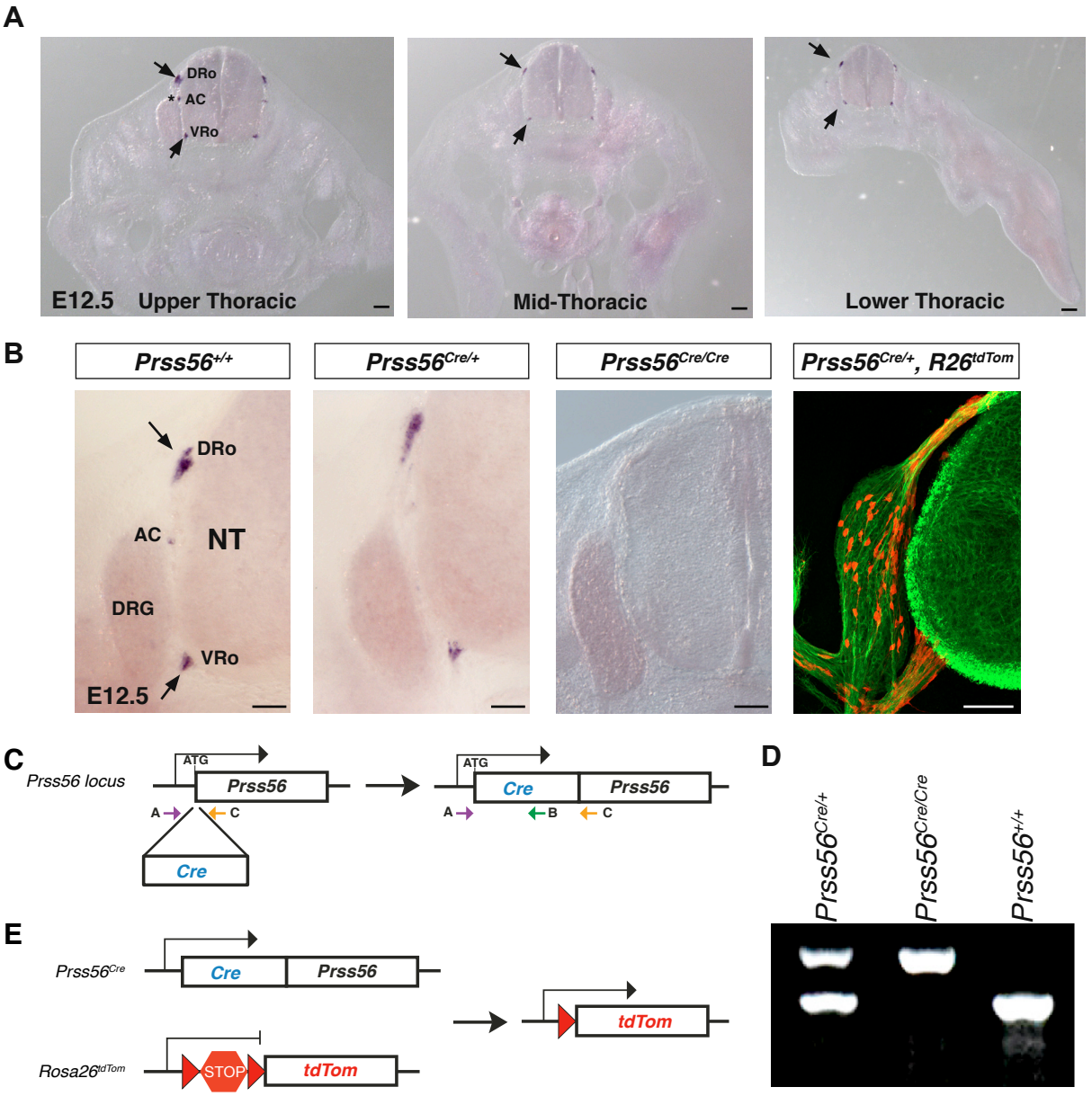
A
DRo
AC
VRo
E12.5 Upper Thoracic
Mid-Thoracic
Lower Thoracic
B
Prss56+/+
Prss56Cre/+
Prss56Cre/Cre
Prss56Cre/+, R26tdTom
DRo
AC
NT
DRG
VRo
E12.5
C
Prss56 locus
ATG
Prss56
A
C
Cre
ATG
Cre
Prss56
A
B
C
D
Prss56Cre/+
Prss56Cre/Cre
Prss56+/+
E
Prss56Cre
Cre
Prss56
Rosa26tdTom
STOP
tdTom
tdTom

Figure S1

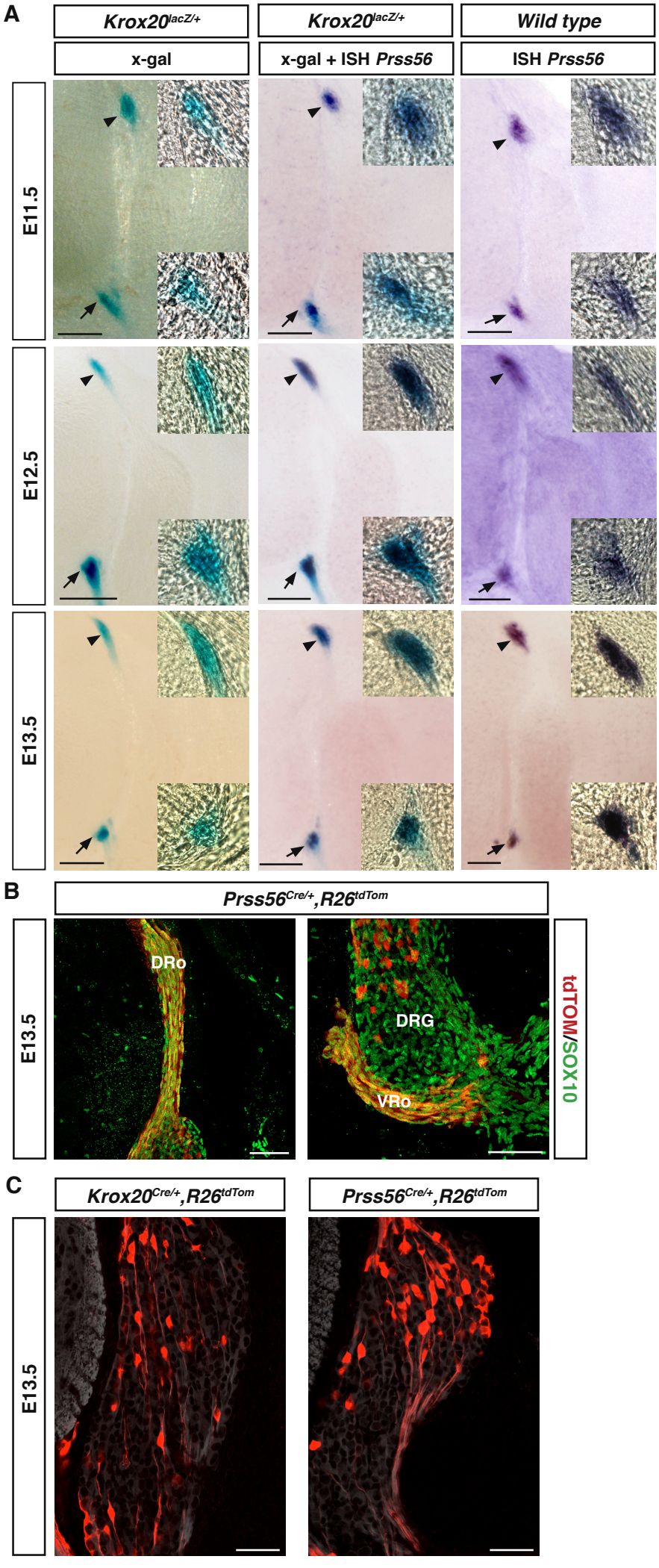
A
Krox20lacZ/+
x-gal
Krox20lacZ/+
x-gal + ISH Prss56
Wild type
ISH Prss56
E11.5
E12.5
E13.5
B
Prss56Cre/+,R26tdTom
E13.5
DRo
DRG
VRo
tdTOM/SOX10
C
Krox20Cre/+,R26tdTom
Prss56Cre/+,R26tdTom
E13.5

Figure S2

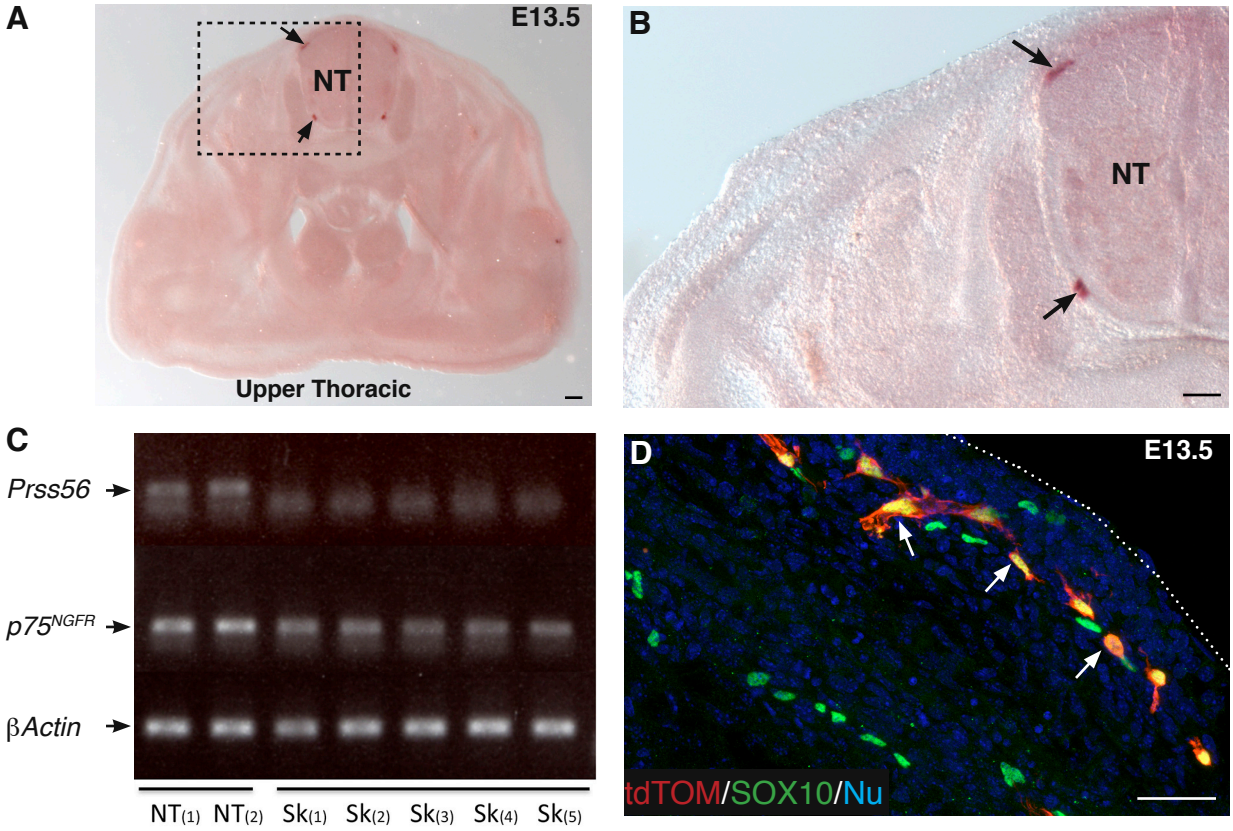
A
E13.5
NT
Upper Thoracic
B
NT
C
Prss56
p75NGFR
βActin
NT(1) NT(2) Sk(1) Sk(2) Sk(3) Sk(4) Sk(5)
D
E13.5
tdTOM/SOX10/Nu

Figure S3

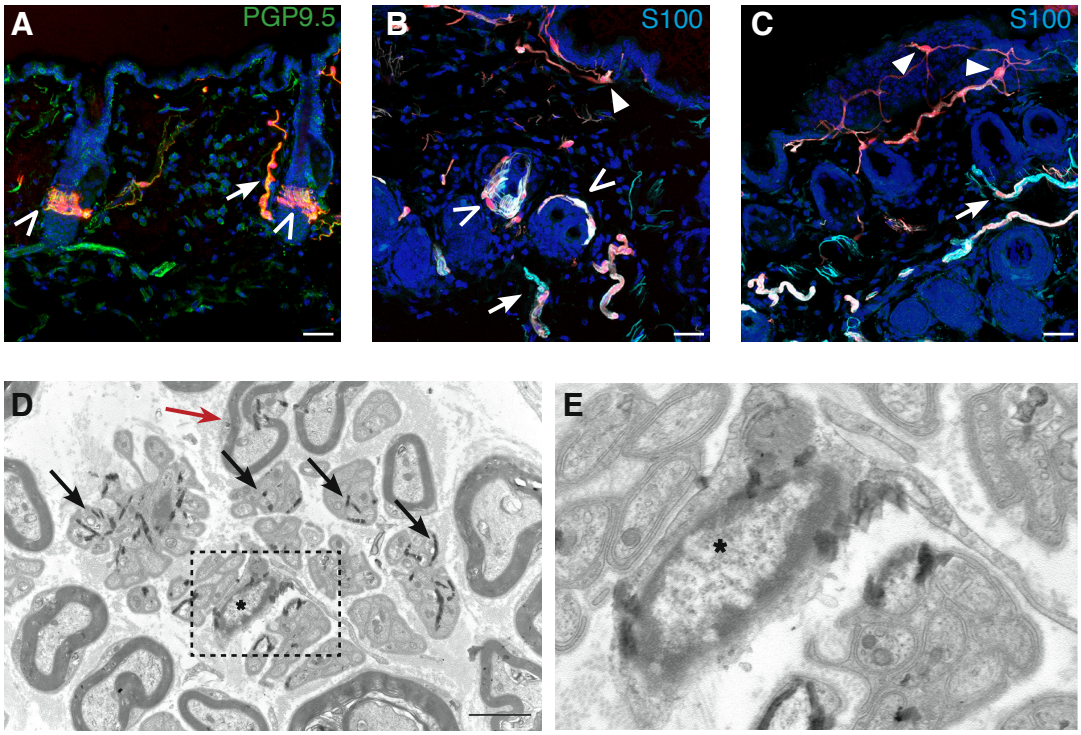

Figure S4

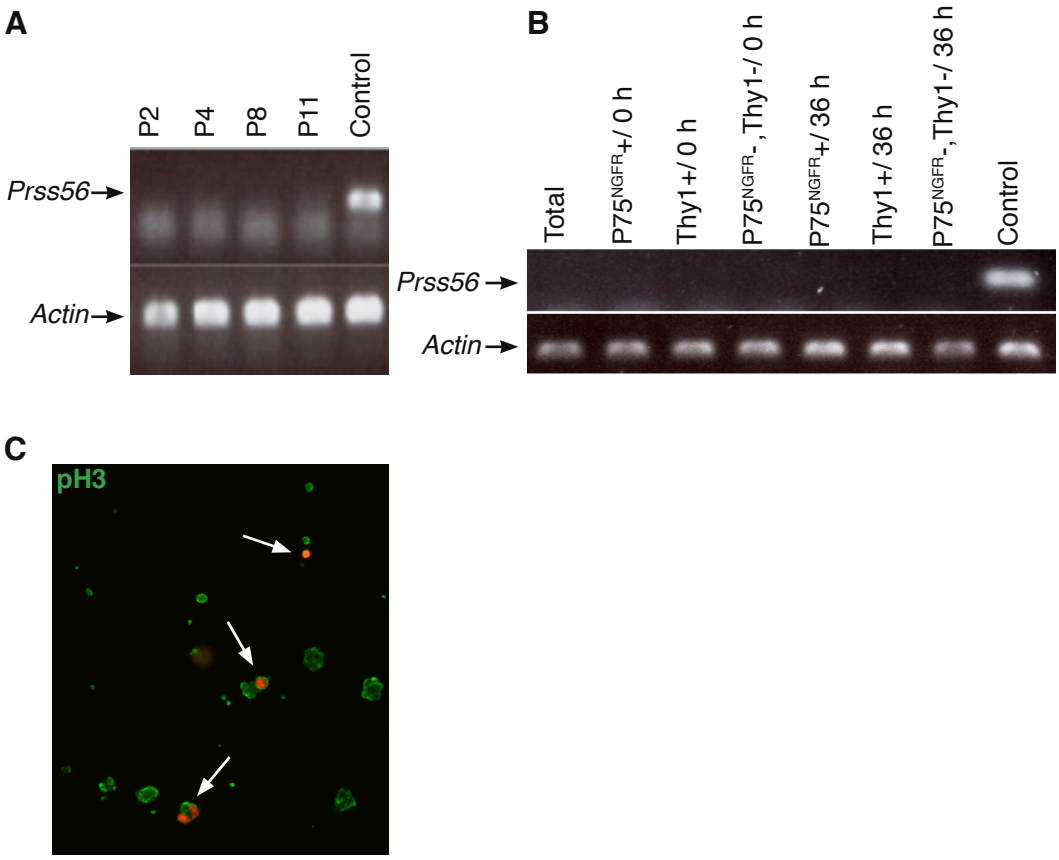
A
P2
P4
P8
P11
Control
Prss56
Actin
B
Total
P75NGFR+/ 0 h
Thy1+/ 0 h
P75NGFR-, Thy1-/ 0 h
P75NGFR+/ 36 h
Thy1+/ 36 h
P75NGFR-, Thy1-/ 36 h
Control
Prss56
Actin
C
pH3

Figure S5

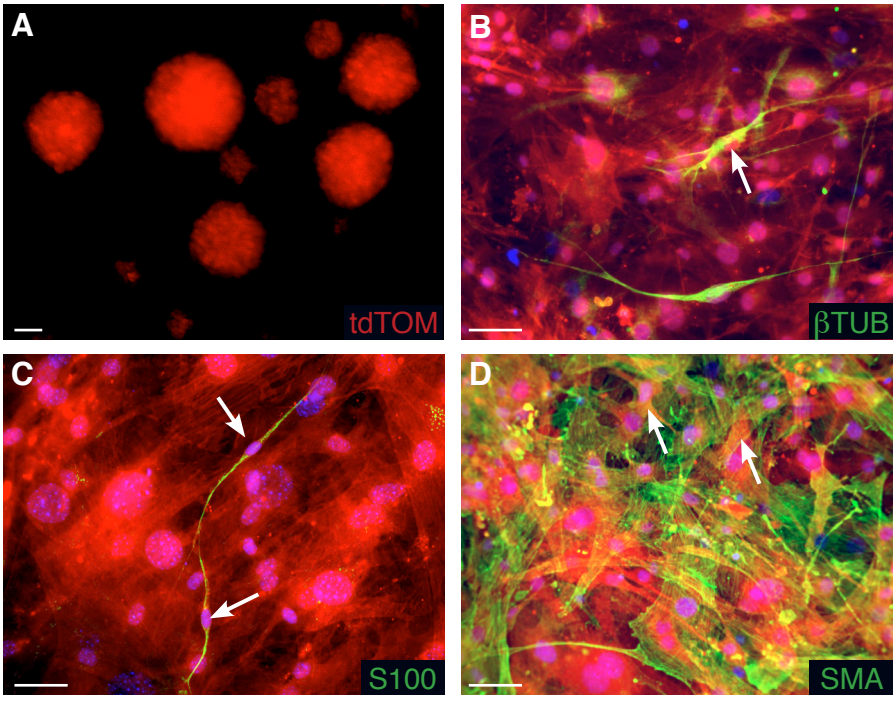

Figure S6

SUPPLEMENTAL INFORMATION

SUPPLEMENTAL FIGURE LEGENDS

Figure S1, related to Experimental Procedures and Figure 1. **Generation of a Cre knock-in at the *Prss56* locus and tracing of the derivatives of *Prss56*-expressing cells.** (A) Specific expression of *Prss56* in BC cells. Transverse vibratome sections at E12.5 covering the thoracic regions indicate that the presence of *Prss56* mRNA in the dorsal and ventral BCs, and along the accessory nerve (AC) in a wild type embryo. The expression in the BCs is maintained in sections covering the thoracic region (arrows) and no additional site of expression is observed. (B) Transverse sections from E12.5 wild type, $Prss56^{Cre/+}$, $Prss56^{Cre/Cre}$, and $Prss56^{Cre/+}$,$R26^{tdTom}$ mutant embryos at the upper thoracic level were subjected to in situ hybridization with a *Prss56* probe or immunolabeling with tdTOM (red) and βIII-tubulin (green) antibodies. The expression pattern described in (A) is conserved in $Prss56^{Cre/+}$embryos, whereas expression is completely lost in $Prss56^{Cre/Cre}$ embryos. tdTOM traced cells completely covers the nerve roots and are present within the DGR and along more distal regions of the nerve. (C) Schematic representation of the generation of the $Prss56^{Cre}$ knock-in allele by insertion of the *Cre* coding sequence at the *Prss56* initiation codon. The arrows underneath the gene indicate the positions of the primers used for PCR analysis. (D) Examples of embryo genotyping for the *Prss56* locus, performed by PCR analysis using the combination of primers A, B and C shown in panel (C). (E) Combining the $Prss56^{Cre/+}$ allele with the Cre-activable tandem dimer Tomato reporter $Rosa26^{tdTom}$ leads to permanent activation of the reporter in *Prss56*-expressing cells and their progeny. NT, neural tube. AC, accessory nerve, DRo, dorsal root; VRo, ventral root, DRG, dorsal root ganglia. Scale bar: 100 μm. See also Table S1.

Figure S2, related to Figure 1. **BC cells give rise to dorsal and ventral root Schwann cells and sensory neurons in the DRG.** (A) Transverse sections through the trunk of *Krox20*$^{lacZ/+}$ and wild type embryos, between E11.5 and E13.5 as indicated. *Krox20*$^{lacZ/+}$ embryos were subjected to X-gal staining to reveal β-galactosidase activity (first column), followed by in situ hybridization with a *Prss56* probe (second column). Wild type embryos were analyzed by in situ hybridization with a *Prss56* probe (third column). Note the intermediate color observed in the case of double labeling, indicating a large overlap between the domains of *Krox20* and *Prss56* expression in the BC populations of dorsal (arrowhead) and ventral (arrow) roots. (B) Transverse sections from E13.5 *Prss56*$^{Cre/+}$,*R26*^{tdTom} embryos show that most of the cells in the dorsal and ventral roots are positive for both the tracing marker tdTOM and the Schwann cell precursor marker SOX10. (C) In the DRG from E13.5 *Krox20*$^{Cre/+}$,*R26*^{tdTom} and *Prss56*$^{Cre/+}$,*R26*^{tdTom} embryos, most of the traced cells have a bipolar morphology. DRo, dorsal root; VRo, ventral root, DRG, dorsal root ganglia. Scale bars : 100 μm (A) and 50 μm (B-C).

Figure S3, related to Figure 2. **tdTOM-positive cells in the skin do not express *Prss56* and are SOX10-positive. (**A-B) In situ hybridization with a *Prss56* probe on a transverse section of a wild type E13.5 embryo. *Prss56* expression is detected in the BCs (arrows), but not in the skin. (B) Higher magnification of the area outlined in (A). (C) Analysis of *Prss56* expression by RT-PCR in the skin of wild type E13.5 embryos. $SK_{(1)}$-$SK_{(5)}$ correspond to skin preparations from different embryos. $NT_{(1)}$ and $NT_{(2)}$ are positive controls corresponding to the neural tube with attached BC cells from two of these embryos. A *Prss56*-specific band is observed with the NT samples (arrow), but not with the skin samples. (D) Transverse sections from E13.5 *Prss56*$^{Cre/+}$,*R26*^{tdTom} embryos analyzed by immunochemistry using antibodies against tdTOM (red) and peripheral glia (SOX10, green) markers. tdTOM-positive cells in the

skin express SOX10 (arrows). NT, neural tube; Nu, Hoechst 33342 labeling of nuclei. Scale bars: 100 μm in (A-B) and 50 μm in (C).

Figure S4, related to Figure 3. Identities of BC-derivatives in the adult skin. (A-C) Transverse sections of the skin from *Prss56*$^{Cre/+}$,*R26*^{tdTom} adult animals labeled with the indicated antibodies. In the dermis, BC derivatives (red) are localized along PGP9.5-positive terminal nerve fibers (A), express the Schwann cell markers S100 (B-C), and are associated with dermal nerves (A-C, arrows), free nerve endings (B,C, closed arrowheads) or lanceolate endings of hair follicles (A-C, open arrowheads). (D) Electron microscopy analysis of a transverse section through a subcutaneous nerve from adult *Prss56*$^{Cre/+}$,*R26*^{lacZ} animals. β-galactosidase-positive cells include myelinating (red arrow) and non-myelinating Schwann cells (black arrows), as well as endoneurial fibroblasts (star). (E) Higher magnification of the area outlined in (D). Scale bars: 50 μm in A-I and 5 μm in J.

Figure S5, related to Figure 4. Cultured skin cells do not express *Prss56* and are highly proliferative. (A) RT-PCR analysis of *Prss56* expression in newborn skin cells maintained in sphere culture conditions for 2, 4, 8 and 11 passages. (B) RT-PCR analysis of *Prss56* expression in total, P75^{NGFR}-positive, Thy1-positive and P75^{NGFR}-, Thy1-double negative skin cell fractions obtained by immuno-panning, freshly isolated (0 h) or maintained in culture for 36 h. *Prss56* expression is not observed in any of the skin-derived cell preparations, whereas it is easily detectable in control samples (Control) from an E13.5 neural tube with attached BC cells. (C) tdTOM-positive cells maintained in culture for 36 h express the mitotic marker pH3.

Figure S6, related to Figure 5. Purified skin tdTom-positive cells proliferate in culture and are multipotent. Newborn skin cells were maintained in sphere culture conditions until P1, FACS-sorted, and tdTOM-positive cells were returned to sphere culture conditions for several passages. (A) Examples of spheres, exclusively constituted of tdTOM-positive cells, indicating the proliferative capacity of BC derivatives. (B-D) Cell type identification of tdTOM-positive cells from newborn skin cultured in differentiation conditions after two passages, using the indicated antibodies. Immunolabeling identifies neurons (B, positive for βIII-tubulin), Schwann cells (C, positive for S100) and myofibroblasts (D, positive for SMA). Scale bars: 100 μm in (A) and 30 μm in (B-D).

SUPPLEMENTAL TABLE

mRNA or Gene	Primer sequence	Annealing temp (°C)	Expected product size (bp)
wild type Prss56	**A**: 5'-CAGGTGAGGTGCGGACCATT-3' **C**: 5'-AAACCACTGCCCACCGACAT-3'	65	588
Prss56^{Cre}	**A**: 5'-CAGGTGAGGTGCGGACCATT-3' **B**: 5'-ACGGAAATCCATCGCTCGACCAGTT-3'	65	851
β-actin	5'-TGTTACCAACTGGGACGACA-3' 5'-GGGGTGTTGAAGGTCTCAAA-3'	60	165
Prss56	5'-GGTCTTCAGTGGCCTAGTGG-3' 5'-AGCCTCTGTCCTTGATCAGC-3'	58	151
p75^{NGFR}	5'-CAGAGCGAGACCTCATAGCC -3' 5'-TGCAGCTGTTCCATCTCTTG -3'	60	180
Snail	5' -AAACCCACTCGGATGTGAAG- 3' 5' –GAAGGAGTCCTGGCAGTGAG-3'	60	184
Slug	5'-GCACTGTGATGCCCAGTCTA- 3' 5' -TTGCCACAGATCTTGCAGAC- 3'	60	130

Nestin	5'-CTCGAGCAGGAAGTGGTAGG- 3' 5'-GCCTCTTTTGGTTCCTTTCC-3'	55	140
Mush	5' -AGGAAAGCAAAGGGCTTCTC-3' 5'- GCCAGGTCTCACCTCATGTT-3'	60	166
Twist	5' -CTTTCCGCCCACCCACTTCCTCTT-3' 5'-GTCCACGGGCCTGTCTCGCTTTCT-3'	57	334
Sox9	5' -AGCTCACCAGACCCTGAGAA - 3' 5'- TCCCAGCAATCGTTACCTTC - 3'	59,6	200
Mitf	5' -TGTACCTTCAGCGTGCAGTA-3' 5' -ACCAGGAAATTGCCGCATTT- 3'	59	352
Sox2	5' –CCCAACTATTCTCCGCCAGA- 3' 5' –TCTAGTCGGCATCACGGTTT- 3'	59	380
Ngn1	5' –ACGCCCTGTTTCATCCCATA- 3' 5' –GTCTTCAGGGGCTCATCTGT- 3'	59	313
Ngn2	5' TCCACTTCACAGAGCAGAGG- 3' 5' –CACAGGGACCAGTTGCATTC- 3'	59	303

Table S1, related to Experimental Procedures and Figure 4. Primer sequences and PCR conditions for RT-PCR and genotyping analyses

SUPPLEMENTAL EXPERIMENTAL PROCEDURES

In situ hybridization and immunofluorescence

In situ hybridization on embryos was performed as previously described (Coulpier et al., 2009). For β-galactosidase and *Prss56* co-labeling, *Krox20*$^{lacZ/+}$ whole embryos were processed for β-galactosidase staining as described (Maro et al., 2004). Samples were then post-fixed overnight in 4% PFA before being serially sectioned (150 μm) and processed for in situ hybridization. Immunohistochemical analysis of embryos was performed on 100 μm transverse vibratome sections that were stored at -20°C in PBS including 30% glycerol and 30% ethylene glycol. Cryosection and immunolabeling were performed as described (Maro et al., 2004). Sections were mounted in Aqua poly/Mount (PolySciences) and optical sections of were obtained on a confocal microscope (SP5, Leica). The ImageJ software was used to generate Z-stacks and quantify tdTOM-positive cells. At least five areas per structure per animal were photographed and the number of tdTOM-positive cells relative to the total number of cells expressing a given marker was determined. The results are given as median ± standard error of the mean (s.e.m). The antibodies are described below. Nuclei were counterstained with Hoechst (33342, Sigma).

Antibodies

For immunofluorescence, the following primary antibodies were used: rabbit anti-tdTOM (1:400, Clontech #632496), mouse biotinylated anti-βIII-tubulin (1:800, R&D #BAM1195), rabbit anti-PGP9.5 (1:400; Abcam #AB137800), goat anti-SOX10 (1:100, Santa Cruz #sc-17342), mouse anti-nestin (1:100; Millipore #MAB353), rabbit anti-S100 (1:300, Dako #Z0311), rabbit anti-fibronectin (1:100, Millipore #AB2033), chicken anti-vimentin (1:100; Millipore #AB5733), rabbit anti-P75^{NGFR} (1:300; Abcam #AB8874), mouse anti-SMA (1:400, Sigma #A2547), rabbit anti-phospho-Histone H3 (1:100, Millipore #06-570), rabbit anti-

GFAP (1:300, Dako #ZO334), rabbit anti-TRKA (1:500, Millipore #06-574), goat anti-TRKB (1:500, R&D #AF1494), goat anti-TRKC (1:500, R&D #AF1404), goat anti-RET (1:20, R&D #AF482), mouse anti-CGRP (1:500, Millipore #MAB317), mouse anti-TH (1:1000, Millipore #MAB318), rat anti-MBP (1:100, Millipore #MAB386), IB4-A488 (1:200, Invitrogen #l21411) from *Griffonia simplicifolia*, rat anti-PECAM (1:100; BD Pharmigen #553370), rabbit anti-NG2 (1:200; Millipore #AB5320), and goat anti-SOX2 (1:200, R&D #AF2018). Fluorophore-conjugated secondary antibodies were from Jackson Immuno Research.

Cell culture and immuno-panning

Sphere cultures were performed from neonatal and adult (6-8-week old) $Prss56^{Cre/+},R26^{tdTom}$ mice as previously described (Biernaskie et al., 2007). Briefly, the back skin was carefully dissected free of other tissue and then digested with collagenase/dispase type I (Sigma/Roche) for 2 h at 37°C. Skin samples were then mechanically dissociated and the cell suspension was filtered. Dissociated cells were resuspended at $4x10^4$ cells/ml in DMEM-F12, 3:1 medium containing B-27 without vitamin A supplement (Invitrogen), 20 ng/ml EGF and 40 ng/ml bFGF (both from Sigma), referred to as proliferation medium. Cultures were fed every 4 days, by addition of 1/10 of fresh medium containing growth factors and supplements, and spheres were passaged every 7-10 days. For spontaneous differentiation, spheres were plated in differentiation medium (DMEM-F12, 3:1, containing 10% FBS) onto 4-well Nunc culture slides coated with poly-D-lysine/laminin, maintained two weeks, and the differentiation medium was changed every 2 days. For induced Schwann cell differentiation, spheres were plated in differentiation medium for three days. The medium was then changed to DMEM-F12, 3:1, 1% FBS, 1% N2 supplement (Invitrogen), 50 ng/ml heregulin (Sigma) and 4 μM forskolin (Sigma). For induced differentiation into chondrocytes and melanocytes, spheres were processed as previously described (Wong et al., 2006). Briefly, for chondrocytes

differentiation, spheres were plated in differentiation medium supplemented with 50 µg/ml ascorbic acid (Sigma). FGF2 (Sigma) was added for 9 days and then replaced with 10 ng/ml BMP2 (Sigma) for 3 days. For melanocytes differentiation, spheres were plated in differentiation medium containing 50 ng/ml SCF (Sigma) and 100 nM endothelin-3 (Sigma) for 9 days. Chondrocytes and melanocytes were revealed as previously described (Wong et al., 2006). For oligodendrocyte differentiation, spheres were maintained in proliferation medium for 24 h. The medium was then changed to a differentiation medium (DMEM/F12, 1:1, 1% N2, 2 µg/ml heparin (Sigma), 2% B-27) supplemented with 50 ng/ml Noggin, 10 µM SB431542, and 10 ng/ml FGF2 (all from Sigma). The cells were maintained in this medium for 3 days, and then the medium was changed to a differentiation medium supplemented with 5 mM Purmorphamine, and 100 nM retinoic acid (all from Sigma), where the cells were cultured for an additional day before immunohistochemical analysis. For immuno-panning, cell suspensions from neonatal back skin were prepared as described above. Dissociated cells were first purified by magnetic cell sorting using an antibody against $P75^{NGFR}$ (1:200, Abcam) as previously described (Manent et al., 2003). The negative fraction was collected and purified in the same way with an antibody against Thy1 (1:200, BD Pharmigen). After purification, the $P75^{NGFR}$- and Thy1-positive fractions were counted and resuspended in proliferation medium. Purified Schwann cells were obtained from 2-week old $Krox20^{Cre/+}$,$R26^{tdTom}$ mice. The sciatic nerves were collected, maintained in Wallerian degeneration conditions for 10 days in Schwann cell medium (DMEM, 10% FBS supplemented with 2 µm forskolin and 10 ng/ml heregulin), then dissociated for 3 h in digestion solution (collagenase type I, 130 U/ml; dispase type I, 2.5 mg/ml) on a rocking table at 37°C. The cells were then plated onto poly-L-lysin/laminin coated dishes and cultured in Schwann cell medium until purification by magnetic immuno-panning based on their specific expression of the $P75^{NGFR}$ antigen as above.

Electron microscopy

Subcutaneous nerves from adult (8-weeks) back skin were dissected and fixed for 2 h in 1% glutaraldehyde, 0.4% PFA in PBS, then washed in PBS and subjected to β-galactosidase staining as previously described (Maro et al., 2004). Nerves were osmificated for 1 h in 1% OsO_4 (Polysciences), rinsed in PBS, dehydrated in graded acetone, and embedded in Epon. Semi-thin sections (1 μm) were stained with toluidine blue. Ultra-thin sections (50 nm) were stained with uranyl acetate and lead citrate. The sections were observed with a Phillips electron microscope.

Semi-quantitative RT-PCR

Total RNA (100 ng) was isolated from embryonic skin, reverse transcribed using the pSuperscript III Rnase H reverse transcriptase (Invitrogen) and a mix of oligo-dT and random primers (Invitrogen), according to the manufacturer's instructions. PCR was performed as follows: 2 min at 94°C; 30 cycles of 2 min at 94°C, 1 min at the primer-specific annealing temperature, 30 s at 72°C. The primer sequences are shown in Supporting Information Table 1. For each RNA sample, two independent PCR amplifications were performed.

Article two

Derivatives of neural tube-associated boundary caps migrate along peripheral nerves to give rise to a major part of skin vasculature mural cells

More recently, we have explored the possibility that Krox20-expressing BC also migrate along peripheral nerves and participate to the skin development. Surprisingly, we discovered that a subpopulation of Krox20-traced BC-derivatives, detach from nerves and attach to the vascular plexus where they differentiate into pericytes and vascular smooth muscle cells (VSMC). In the trunk, this glial-to-vascular switch (GVS) occurs both near the ventral roots and in the skin. These observations are at the origin of my second article. In this study, we have shown that this GVS takes place between E12.5 and E13.5 in the skin, and is accompanied by extinction of glial markers and activation of a full set of mural cell markers such as PDGFRβ and SMA. Moreover, single-cell transcriptomic analysis of BC derivatives isolated from E12.5 skin revealed that while most cells remain attached to nerves, more than half of them already display a molecular signature of mural cell precursors. This study identified Krox20-expressing BC cells as major source of mural cells for the developing peripheral vasculature.

Derivatives of neural tube-associated boundary caps migrate along peripheral nerves to give rise to a major part of skin vasculature mural cells

Authors: Gaspard Gerschenfeld[1,2]†, Fanny Coulpier[1,3]†, Aurélie Gresset[1], Pernelle Pulh[1], Sophie Lemoine[3], Jules Gilet[4], Isabelle Brunet[5], Patrick Charnay[1] and Piotr Topilko[1]*

Affiliations:

[1] Ecole normale supérieure, PSL Research University, CNRS, Inserm, Institut de Biologie de l'Ecole normale supérieure (IBENS), Paris, France.

[2] Sorbonne Université, Collège Doctoral, F-75005 Paris, France.

[3] Genomic facility, Ecole normale supérieure, PSL Research University, CNRS, Inserm, Institut de Biologie de l'Ecole normale supérieure (IBENS), Paris, France.

[4] Inserm U932, PSL Research University, Institut Curie, Paris, France.

[5] Inserm U1050, Centre Interdisciplinaire de Recherche en Biologie (CIRB), Collège de France, Paris, France

* Correspondence to: topilko@biologie.ens.fr.

† These authors contributed equally to this work.

One Sentence Summary:

Nerve-associated boundary cap derivatives give rise to pericytes and smooth muscle cells of the peripheral vasculature

Abstract: Beside its essential functions in protecting and myelinating nerves, peripheral glia plays a key role in blood vessel development, providing diffusible factors that govern alignment with nerves and maturation. Here, we show that a specific peripheral glial population, derived from boundary cap (BC) cells, constitutes a major source of mural cells for the developing vasculature. Using Cre-based reporter tracing analyses, we show that BC cells generate derivatives that migrate along peripheral nerves before detaching and incorporating into the vascular plexus, and differentiating into pericytes and vascular smooth muscle cells. Switching from glial to mural molecular identities occurs while the cells are still associated with the nerves. This study highlights the plasticity of BC cells and identifies a novel origin for skin mural cells.

Main Text:

Peripheral blood vessels and nerves orchestrate body development and homeostasis by providing oxygen, nutriments and eliminating toxic compounds, while ensuring communication with the environment. Over the last decade, several developmental studies have revealed that nerve-associated Schwann cells precursors (SCPs) migrate along nerves to reach their targets, then detach from nerves and give rise to various cells types, including skin melanocytes, adrenal medulla chromaffin cells, tooth mesenchymal stem cells, and enteric and parasympathetic neurons (*1-6*). Peripheral nerves and SCPs have also been shown to play a key role in angiogenesis by secreting diffusible factors driving the alignment of blood vessels with nerves and promoting arteriogenesis (*7-9*). A possible cell contribution of SPCs to the endothelial or mural components of the developing vascular plexus has however not been investigated so far. Mural cells (MCs) include pericytes and vascular smooth muscle cells that cover capillaries and larger vessels, respectively, and play key roles in blood vessel remodelling and stabilization (*10*). MC origin differs depending on their location, as brain, facial and thymic MCs derive from the neural crest, whereas gut, lung and liver MCs are mesoderm-derived (*11-14*). In the skin, although it has recently been shown that a MC subset originates from myeloid progenitors, the other source(s) of MCs remain(s) unknown (*15*).

Boundary cap (BC) cells form transient aggregates during embryogenesis at the dorsal entry and ventral exit points of all cranial and spinal nerves. Most BC cells, if not all, express the genes *Krox20* (also known as *Egr2*) and/or *Prss56* (*16*, *17*), which have been used to characterise them. Reporter tracing experiments using a *Prss56*^{Cre} allele have recently revealed that Prss56-positive BC cell derivatives migrate between embryonic day (E) 11.5 and E13.5 along nerve roots into dorsal root ganglia (DRGs), where they give rise to Schwann cells (SCs) and a subpopulation of sensory neurons, and along spinal nerves to reach the skin, where they differentiate into SC, terminal glia and melanocytes (*18*, *19*). Additional tracing

experiments using a *Krox20*^{Cre} allele have revealed the existence of similar derivatives in nerve roots and DRGs (*20*). However, in this case, peripheral migration was not analysed. Here, we investigate the contribution of Krox20-positive BC cells to the developing trunk skin.

For this purpose, we crossed animals carrying *Krox20*^{Cre} and *Rosa26R*^{Tomato} alleles to perform tracing of Krox20-positive cells on the basis of Tomato-labelling in resulting *Krox20*$^{Cre/+}$, *Rosa26R*$^{Tomato/+}$ embryos. As previously reported, we found multiple Tomato-positive (traced) cells in the dorsal and ventral roots at E11.5 (Fig. 1A), as well as the DRGs at E12.5 (Fig. 1B). Labelled cells were also first detected in the proximal spinal nerve segment at E11.5 (Fig. 1A,D) and then at the levels of intermediate nerve segments at E12.5 (Fig. 1B,E) and of skin nerve terminals at E13.5 (Fig 1C,F). This time-course evolution of traced cell distribution along the proximo-distal parts of the nerves strongly supports their progressive migration along nerves. Surprisingly, we also noticed the presence of numerous labelled cells that were not in contact with nerves, initially near the ventral roots (Fig. 1A,B, arrows) and later in the skin (Fig. 1A,F, arrows). To ensure that all labelled cells were indeed traced from Krox-20-positive BC cells and not the result of *de novo Krox20* expression in other cells populations, we performed *in situ* hybridization with a *Krox20* probe on E12.5 embryos (Fig. S1A) and RT-PCR with Krox20 primers on dissociated E12.5 skin (Fig. S1B). None of these experiments revealed expression of *Krox20*. In conclusion, this analysis indicates that derivatives of Krox20-positive BC cells migrate along the nerves up into the skin and suggests that part of them detach from the nerves during their journey.

To further investigate the presence of derivatives of Krox20-positive BC cells in the skin, we performed wholemount immunohistochemistry analyses on E12.5 to E15.5 embryonic skin, stained for nerves (βIII-tubulin), blood vessels (PECAM) and traced cells (tdTom) in particular to determine whether traced cells were in contact with nerves or blood

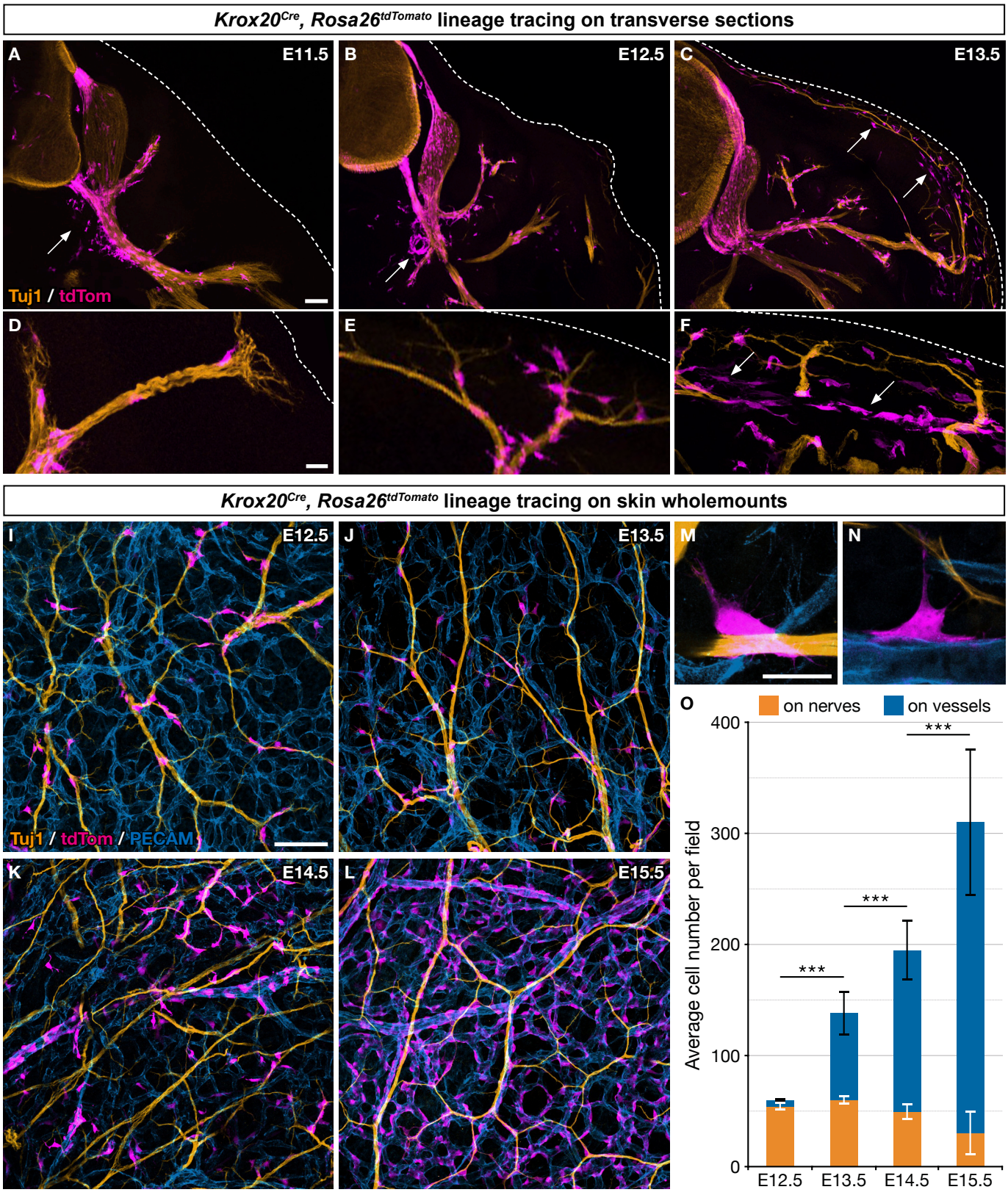

Figure 1. BC cell derivatives migrate along the nerves and incorporate into the vascular plexus. (A-F) Trunk transverse sections from *Krox20*$^{Cre/+}$,*Rosa26R*^{Tomato} embryos at the indicated stages, immunolabelled against Tomato (magenta) and Tuj1 (orange). Cells detached from the nerves (arrows) appear first near the ventral roots (A,B) and later the skin (C). (I-L) Whole-mount dorsal skin immunostained against Tomato (magenta), Tuj1 (orange) and PECAM (blue). (M, N) Higher magnifications showing cells in contact with both nerve and vessel. (O) Quantification of the number of labelled cells associated with nerve or vessel per field. Scale bars: (A-E,I-L) 100 µm; (D-F,M,N) 20 µm. *** = $P < 0.001$

vessels (Fig. 1I-O). While at E12.5 approximately 90% of the traced cells were in contact with nerves, this proportion decreased progressively with time to reach values in the order of 10% at E15.5 (Fig. 1I-L,O). In contrast, an increasing proportion of traced cells were found in contact with blood vessels, up to 90% at E15.5 (Fig. 1I-L,O). Traced cells attached to capillaries and larger vessels did not express the endothelial marker PECAM, suggesting that they might have an MC identity (Fig. 1L,N). This behaviour of Krxo20-positive BC cell derivatives differs dramatically from that of derivatives from Prss56-positive BC cells, which were not found associated with the vascular plexus (Fig. S1C-E, 18). Finally, at high magnification, a few traced cells straddling both nerves and vessels were observed (Fig. 1M,N). Together these data suggest that most derivatives from Krox20-positive BC cells having reached the skin after traveling along the nerve detach from them and are recruited within the vascular plexus.

To further characterize the identity of Krox20-positive BC cell derivatives settled in the skin, we used a combination of SCP and MC markers. We found that at E12.5 nerve-associated traced cells were positive for SCP markers, such as the transcription factor Sox10 and BFABP (Fig. 2A-C). Interestingly, at E13.5 the intensity of Sox10 immunolabelling was lower in cells with lose contact with the nerves and this marker was undetectable in cells associated with the vascular plexus (Fig. 2D-F). At E14.5 traced cells associated with the vascular plexus showed characteristic morphologies, covering small capillaries or wrapping around larger vessels, which were compatible with pericyte or vascular smooth muscle (VSM) cell identities. Consistently, these cells expressed several MC markers, such as NG2, PDGFRβ and SMA (Fig. 2G-I). Whole-mount analysis of newborn dorsal skin demonstrated the persistence of BC cell-derived MC on capillaries and larger diameter arteries and veins (Fig. S2A-D). Together these results indicate that Krox20-positive BC cells give rise to a major part of skin MCs and this component is maintained until birth at least. These MCs are

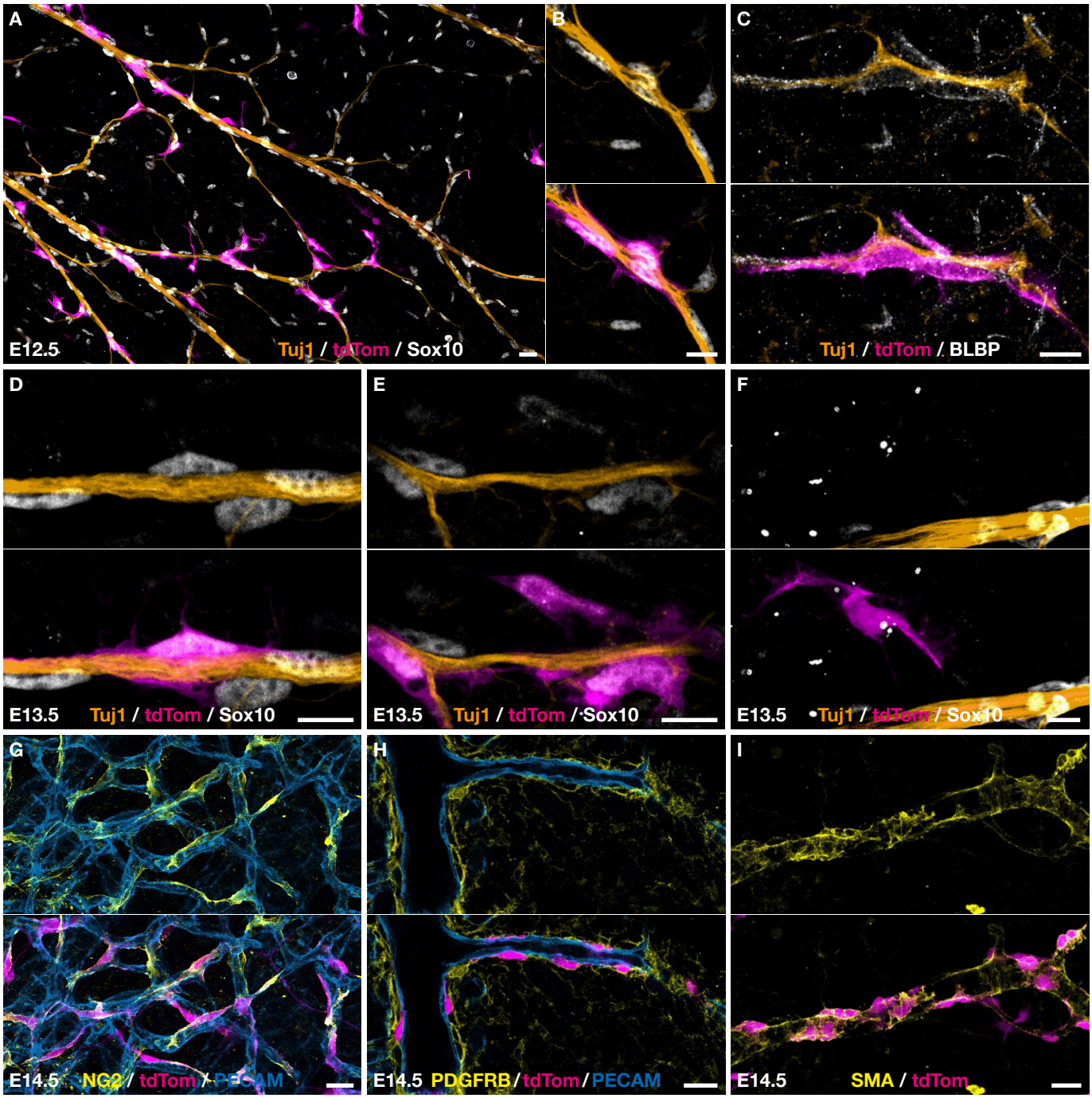

Figure 2. BC cell derivatives switch from SC precursor to MC identity. Whole-mount dorsal skin at the indicated stages, immunostained against Tomato (magenta), Tuj1 (orange), Sox10 or BLBP (white), PECAM (blue) and NG2, PDGFRβ or SMA (yellow). Nerve-associated BC cell derivatives express the SC precursor markers Sox10 (A,B) and BLBP (C). Sox10 is progressively downregulated during detachment (D-F). In the vascular plexus, Tomato-positive cells express MC markers NG2 (G), PDGFRβ (H) and SMA (I). Scale bars: (A,G-I) 20 µm; (D-F) 10 µm.

likely to be generated by detachment of cells associated with the nerves, which shut off the expression of initial glial markers and activate the expression of MC-specific ones, suggesting that they undergo a glial to vascular identity switch.

Relative quantification of traced cells in contact with nerves or blood vessels suggest that the glial to vascular switch occurs in the skin between E12.5 and E13.5 (Fig. 1O). To further characterize the extent of the switch, we performed a global, RNA-seq transcriptomic analysis, comparing traced cells purified by FACS from E12.5 and E13.5 dorsal skin. Significant up- or down-regulation was defined by variations of at least four-fold, with an adjusted *P*-value < 0.05. In these conditions, 269 genes were found up-regulated at E13.5 as compared to E12.5 and 280 were down-regulated. We crossed these data with the LungGENS dataset that repertories genes expressed in pericytes, vascular smooth muscle and matrix fibroblasts in the developing lung (*21*). Among the 269 up-regulated genes, 47 belonged to this category (Fig. 3). In contrast, only 5 down-regulated genes were found in the LungGENS database. We found no significantly downregulated SCP-related genes at E13.5, but a likely explanation is that half of the traced cells are still on nerves at this stage and only genes showing of at least four-fold variation were retained. Altogether, these data support the idea that, between E12.5 and E13.5, a number of traced cells undergo a major change in their pattern of gene expression, acquiring an MC identity.

Transcriptome analysis performed on bulk RNA preparations do not allow to assess the properties of individual cells. To perform a detailed analysis of the transcriptomic signature of single cells, we performed single-cell RNA sequencing (scRNA-seq) of traced cells purified by FACS from dissociated E12.5 skin. The choice of this stage was based on the conclusion of the bulk analysis suggesting that at E13.5 a large part of the traced cells have already undergone a glial to vascular switch. Analysing them at E12.5 might allow us to follow this process as it occurs. After filtering out low quality and Tomato-negative cells, we

A. Pericyte		
MGI	log2 FC	adj. *P*-value
Itga7	5.806	6.215E-06
Gm14005	4.899	5.391E-13
Abcc9	**4.429**	**2.434E-37**
Aspn	3.991	5.220E-04
Rgs5	3.924	4.861E-06
Itga1	3.880	6.582E-39
Gucy1a3	3.734	1.009E-17
Cspg4	**3.236**	**1.424E-18**
Kcnj8	2.855	4.477E-03
Notch3	2.652	2.588E-08
Rasl12	2.641	1.133E-11
Gucy1b3	2.570	4.523E-07
Crip1	2.493	4.809E-03
Kcnk3	2.382	5.310E-05
Col4a1	2.287	6.151E-09
Myh9	2.249	2.434E-07
Epas1	2.190	4.891E-06
Lrrc32	2.025	1.176E-05
Pdgfrb	**2.023**	**9.991E-10**

B. Smooth muscle/myofibroblast		
MGI	log2 FC	adj. *P*-value
Rgs5	3.924	4.861E-06
Gucy1a3	3.734	1.009E-17
Myh11	3.643	6.924E-09
Eln	3.461	1.220E-03
Myocd	3.440	1.277E-19
Abi3bp	3.236	1.436E-13
Triap1	3.026	4.547E-03
Col6a3	2.683	2.126E-02
Acta2	**2.487**	**1.981E-13**
Lmna	2.314	2.571E-05
Col6a2	2.146	2.843E-11
Col6a1	2.027	6.092E-07

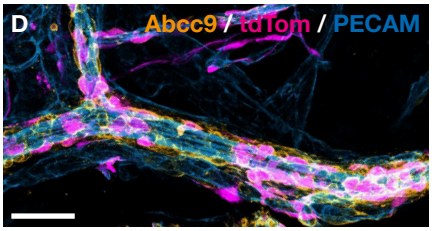

C. Matrix fibroblast		
MGI	log2 FC	adj. *P*-value
Itga1	3.880	6.582E-39
Xdh	3.813	3.369E-09
Eln	3.461	1.220E-03
Spry4	3.170	1.527E-08
Abca9	3.138	7.919E-07
Col6a3	2.683	2.126E-02
Rasl12	2.641	1.133E-11
Col14a1	2.592	1.685E-13
Slc7a10	2.369	2.385E-02
Htra3	2.326	1.195E-02
Lmna	2.314	2.571E-05
Col1a1	2.200	3.819E-09
Col6a2	2.146	2.843E-11
Tns1	2.143	1.802E-06
Col6a1	2.027	6.092E-07
Creb3l1	2.002	2.483E-08

Figure 3. Transcriptomic analysis of BC cell derivatives expression between E12.5 and E13.5. (A-C) Genes from the LungGENS dataset up-regulated in E13.5 versus E12.5 traced cells. The genes are classed according to their defined clusters of pericytes (A), smooth muscle cells (B) and fibroblasts (C). Genes highlighted in green have been validated by immunostainings. (D) At E14.5, many traced cells (tdTom) express Abcc9. Scale: 50 µm.

analysed 2355 single-cell transcriptomes with an average depth of 100,000 reads per cell (Fig. S3A). Cells had a median expressed-gene number of 4,696. Clustering analysis revealed two large clusters that, on the basis of preliminary analysis of specific markers, may correspond to SC and MC progenitors (see below), as well as three clusters that each represented approximately 1% of cells and presumably corresponding to myoblasts, endothelial and immune cells, and sensory neurons (Fig. S3B). It was very likely that these populations constituted contaminants for the following reasons: (i) in immunolabelling experiments, we never observed traced cells susceptible to correspond to immune, endothelial or skeletal muscle cells; (ii) contamination by a few sensory neurons is expected considering the way the dissection is performed (see Materials and Methods). These populations, which might distort the analysis, were therefore eliminated and the clustering analysis was repeated on the remaining 2223 cells. The data are presented in Fig. 4, as a uniform manifold approximation and projection (UMAP) plot (Fig. 4).

Three clusters can be identified. The first one contains 883 cells (40% of the total) that express Sox10, Erbb3, Ngfr and Plp1, in particular (Fig. 4B). These are typical markers of SC progenitors, suggesting that this cell population possesses this cellular identity. Analysis of additional genes allows to split this cluster in three sub-clusters (Fig. 4A). The largest cluster contains 1212 cells (54% of the total number). These cells express high level of fibroblast markers such as PDGFRα and Dlk1 and low levels of mural cell markers such as PGFRβ and Cd248 (Fig. 4C). Many of these cells also express markers like Col1a1 or Decorin (Fig. S3B,C), which have recently been associated with perivascular fibroblast-like cells (*22*). Together these data suggest that the large cluster correspond to mural cell precursors. This conclusion is further enforced by low-level expression in some of the cells of mature pericyte or VSM markers, like Tbx18 and SMA, respectively (Fig. 4D,E). This large cluster can be split into five sub-clusters considering the expression of other genes (Fig. 4A). Finally a small

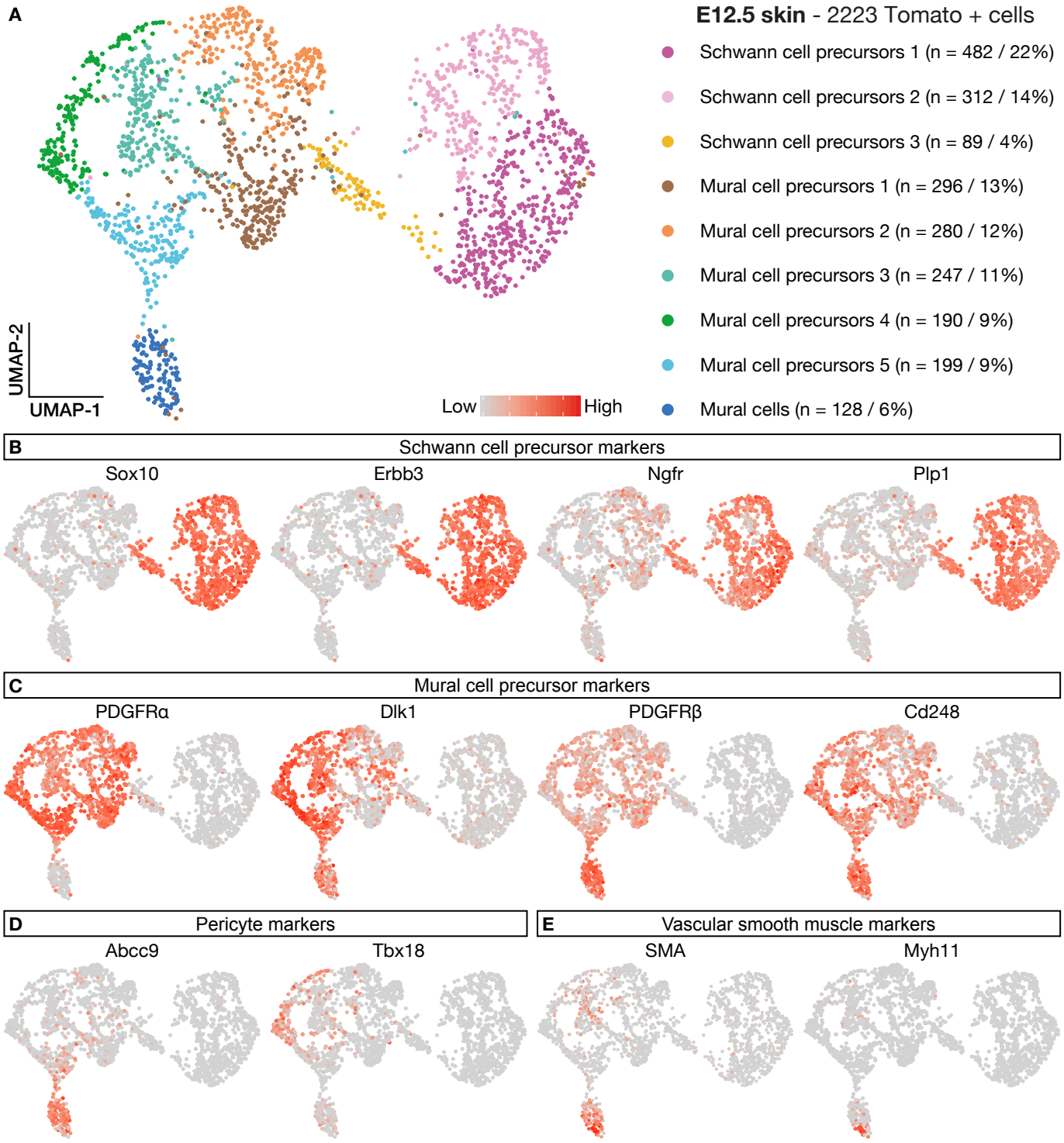

Figure 4. Identification of distinct cell populations within BC cell derivatives in E12.5 skin by cluster analysis of single cell transcriptomic data. Traced cells from E12.5 dorsal skin display molecular signatures corresponding to either SC precursors (A,B), MC precursors (A,C) or mature MCs. Cells are color-coded according to gene expression levels (gray = low, red = high).

cluster of 128 cells (6% of the total number) express markers of mature MC such as SMA, Abcc9 or Myh11 (Fig. 4D,E).

In conclusion, in accordance with our previous data indicating that Krox20-positive BC cell derivatives constitute a major source of MCs in the developing peripheral vasculature, this single-cell transcriptomic analysis reveals that, as early as E12.5, more than half of the derivatives having migrated into the skin are engaged into a MC pathway and that most of them correspond to MC precursors. A small proportion of these cells, corresponding to the third cluster, may have already reached a mature MC identity. The other traced BC cell derivatives show a molecular identity of SC precursors. The presence of bridges between the SC and MC precursor populations on the one side and between the MC precursor populations and the mature MCs on the other side (Fig. 4A, arrows) support the existence of a filiation between these populations. However, the very limited numbers of cells present in these bridges suggest that the transitions must occur very rapidly. Finally, it is striking to find such a proportion of traced cells engaged into the MC pathway in the skin at E12.5, whereas most of the cells are still associated with nerves (Fig. 1I). This indicates that the identity switch that most of these cells will undergo is initiated well before the cells detach from the nerve.

References and Notes:

1. I. Adameyko *et al.*, Schwann cell precursors from nerve innervation are a cellular origin of melanocytes in skin. *Cell*. **139**, 366–379 (2009).

2. V. Dyachuk *et al.*, Neurodevelopment. Parasympathetic neurons originate from nerve-associated peripheral glial progenitors. *Science*. **345**, 82–87 (2014).

3. I. Espinosa-Medina *et al.*, Neurodevelopment. Parasympathetic ganglia derive from Schwann cell precursors. *Science*. **345**, 87–90 (2014).

4. N. Kaukua *et al.*, Glial origin of mesenchymal stem cells in a tooth model system. *Nature*. **513**, 551–554 (2014).

5. T. Uesaka, M. Nagashimada, H. Enomoto, Neuronal Differentiation in Schwann Cell Lineage Underlies Postnatal Neurogenesis in the Enteric Nervous System. *J. Neurosci.* **35**, 9879–9888 (2015).

6. A. Furlan *et al.*, Multipotent peripheral glial cells generate neuroendocrine cells of the adrenal medulla. *Science*. **357** (2017), doi:10.1126/science.aal3753.

7. Y.-S. Mukouyama, D. Shin, S. Britsch, M. Taniguchi, D. J. Anderson, Sensory nerves determine the pattern of arterial differentiation and blood vessel branching in the skin. *Cell*. **109**, 693–705 (2002).

8. Y.-S. Mukouyama, H.-P. Gerber, N. Ferrara, C. Gu, D. J. Anderson, Peripheral nerve-derived VEGF promotes arterial differentiation via neuropilin 1-mediated positive feedback. *Development*. **132**, 941–952 (2005).

9. W. Li *et al.*, Peripheral nerve-derived CXCL12 and VEGF-A regulate the patterning of arterial vessel branching in developing limb skin. *Dev. Cell*. **24**, 359–371 (2013).

10. A. Holm, T. Heumann, H. G. Augustin, Microvascular Mural Cell Organotypic Heterogeneity and Functional Plasticity. *Trends Cell Biol.* **28**, 302–316 (2018).

11. H. C. Etchevers, C. Vincent, N. M. Le Douarin, G. F. Couly, The cephalic neural crest provides pericytes and smooth muscle cells to all blood vessels of the face and forebrain. *Development*. **128**, 1059–1068 (2001).

12. B. Wilm, A. Ipenberg, N. D. Hastie, J. B. E. Burch, D. M. Bader, The serosal mesothelium is a major source of smooth muscle cells of the gut vasculature. *Development*. **132**, 5317–5328 (2005).

13. J. Que *et al.*, Mesothelium contributes to vascular smooth muscle and mesenchyme during lung development. *Proc. Natl. Acad. Sci. U.S.A.* **105**, 16626–16630 (2008).

14. K. Asahina, B. Zhou, W. T. Pu, H. Tsukamoto, Septum transversum-derived mesothelium gives rise to hepatic stellate cells and perivascular mesenchymal cells in developing mouse liver. *Hepatology*. **53**, 983–995 (2011).

15. T. Yamazaki *et al.*, Tissue Myeloid Progenitors Differentiate into Pericytes through TGF-β Signaling in Developing Skin Vasculature. *Cell Rep*. **18**, 2991–3004 (2017).

16. C. Niederländer, A. Lumsden, Late emigrating neural crest cells migrate specifically to the exit points of cranial branchiomotor nerves. *Development*. **122**, 2367–2374 (1996).

17. F. Coulpier *et al.*, Novel features of boundary cap cells revealed by the analysis of newly identified molecular markers. *Glia*. **57**, 1450–1457 (2009).

18. A. Gresset *et al.*, Boundary Caps Give Rise to Neurogenic Stem Cells and Terminal Glia in the Skin. *Stem Cell Reports*. **5**, 278–290 (2015).

19. K. J. Radomska *et al.*, Cellular Origin, Tumor Progression, and Pathogenic Mechanisms of Cutaneous Neurofibromas Revealed by Mice with Nf1 Knockout in Boundary Cap Cells. *Cancer Discov*. **9**, 130–147 (2019).

20. G. S. Maro *et al.*, Neural crest boundary cap cells constitute a source of neuronal and glial cells of the PNS. *Nat. Neurosci.* **7**, 930–938 (2004).

21. Y. Du *et al.*, Lung Gene Expression Analysis (LGEA): an integrative web portal for comprehensive gene expression data analysis in lung development. *Thorax*. **72**, 481–484 (2017).

22. M. Vanlandewijck *et al.*, A molecular atlas of cell types and zonation in the brain vasculature. *Nature*. **554**, 1–35 (2018).

23. O. Voiculescu, P. Charnay, S. Schneider-Maunoury, Expression pattern of a Krox-20/Cre knock-in allele in the developing hindbrain, bones, and peripheral nervous system. *Genesis*. **26**, 123–126 (2000).

24. L. Madisen *et al.*, A robust and high-throughput Cre reporting and characterization system for the whole mouse brain. *Nat. Neurosci.* **13**, 133–140 (2010).

25. N. Renier *et al.*, Mapping of Brain Activity by Automated Volume Analysis of Immediate Early Genes. *Cell*. **165**, 1789–1802 (2016).

26. L. Jourdren, M. Bernard, M.-A. Dillies, S. Le Crom, Eoulsan: a cloud computing-based framework facilitating high throughput sequencing analyses. *Bioinformatics*. **28**, 1542–1543 (2012).

27. A. Dobin *et al.*, STAR: ultrafast universal RNA-seq aligner. *Bioinformatics*. **29**, 15–21 (2013).

28. H. Li *et al.*, The Sequence Alignment/Map format and SAMtools. *Bioinformatics*. **25**, 2078–2079 (2009).

29. A. Butler, P. Hoffman, P. Smibert, E. Papalexi, R. Satija, Integrating single-cell transcriptomic data across different conditions, technologies, and species. *Nat. Biotechnol.* **36**, 411–420 (2018).

30. C. Hafemeister, R. Satija, Normalization and variance stabilization of single-cell RNA-seq data using regularized negative binomial regression. *bioRxiv*. **3**, 576827 (2019).

Acknowledgments: We are grateful to the IBENS animal, Imaging and Genomic facilities. The IBENS imaging facility is a member of the national infrastructure France-BioImaging, supported by the French National Research Agency (ANR-10-INBS-04, ANR-10-LABX-54 MEMO LIFE, ANR-11-IDEX-0001-02 PSL* Research University «Investments for the future») and by the "Région Ile-de-France" (NERF N°2011-45, DIM Cerveau et Pensée "Alpins"). The IBENS Genomic Facility was supported by the France Génomique national infrastructure, funded as part of the "Investissements d'Avenir" program managed by the ANR (ANR-10-INBS-09); **Funding:** The Charnay laboratory was financed by INSERM, CNRS, MESRI and INCa. It has received support under the program "Investissements d'Avenir" launched by the French government and implemented by the ANR, with the references: ANR-10-LABX-54 MEMOLIFE and ANR-11-IDEX-0001-02 PSL* Research University; **Author contributions:** conceptualization: G.G., F.C., P.C., P.T.; funding acquisition: P.C., P.T.; project administration: P.C., P.T.; investigation: G.G., F.C., A.G., P.P, S.L.; software: G.G., F.C., S.L., J.G.; visualization: G.G., F.C.; writing, review, and/or revision of the manuscript: G.G., F.C., J.G., I.B., P.C., P.T.; **Competing interests:** Authors declare no competing interests; and **Data and materials availability:** Mouse strains *Krox20*^{Cre} and *Rosa26R*^{Tomato} are freely available from The Jacksons Laboratory (USA). *Prss56*^{Cre} will require MTA of future users. Bulk and single cell RNA-seq gene-expression data and raw Fastq files will be available on the GEO repository (www.ncbi.nlm.nih.gov/geo/). Single cell analysis R script will be available on GitHub.

Supplementary Materials:

Materials and Methods

Figures S1-S6

Supplementary Materials for

Derivatives of neural tube-associated boundary caps migrate along peripheral nerves to give rise to a major part of skin vasculature mural cells

Gaspard Gerschenfeld, Fanny Coulpier, Aurélie Gresset, Pernelle Pulh, Sophie Lemoine, Jules Gilet, Isabelle Brunet, Patrick Charnay and Piotr Topilko

Correspondence to: topilko@biologie.ens.fr

This PDF file includes:

Materials and Methods

Figs. S1 to S3

Materials and Methods

Mouse Lines, Genotyping, and Ethical Considerations

Mice used in this study were housed in a temperature- and humidity-controlled vivarium on a 12 h dark-light cycle with free access to food and water. All mouse lines were maintained in a mixed C57BL6/DBA2 background. We used the following alleles or transgenes that were genotyped as indicated in the original publications: *Krox20*^{Cre} (*23*), *Prss56*^{Cre} (*18*), *Rosa26R*^{Tomato} (*24*). Day of plug was considered E0.5. Animals were sacrificed by decapitation (newborn). All animal manipulations were performed according to French and European Union regulations.

In situ hybridization and immunofluorescence

In situ hybridization on embryo sections was performed as previously described (*17*). Briefly, samples were fixated overnight in 4% paraformaldehyde (PFA, Electron Microscopy Science) in 0.1M phosphate buffer (PBS) before being serially sectioned (150 µm) and processed for *in situ* hybridization. Embryonic immunohistochemical analysis was performed either on 50 µm transverse cryosections or embryonic skin wholemounts, both performed as previously described (*18*, *20*). Sections and embryonic skin wholemounts were stored at -20°C in 0.1M phosphate buffer (PBS) with 30% glycerol and 30% ethylene glycol. Briefly for wholemount immunolabelling, dorsal skins of E12.5 to E15.5 embryos were dissected after overnight fixation in 4% PFA. Samples were blocked overnight in 4% bovine serum albumin (BSA; Sigma Aldrich) in PBS containing 0.3% Triton-X-100 (PBST; Sigma Aldrich), then incubated for 3 days with the primary antibody/BSA/PBST solution at 4°C. After rinsing, secondary antibodies were applied overnight at room temperature. Samples were then washed and flat-mounted in Fluoromount-G (Southern Biotech). Antibodies are described below. Nuclei were counterstained with Hoechst (Life Technologies). Wholemount immunostaining and clarification of newborn skin was performed using the iDISCO+ method (*25*). Z-stacks were acquired using Leica TCS SP5 and TCS SP8 laser-scanning confocal microscopes and assembled in ImageJ.

Antibodies

For immunofluorescence, the following primary antibodies were used: rabbit anti-Tomato (1:500, Rockland #600-401-379), goat anti-Tomato (1:500, Sicgen, #AB0040-200), mouse biotinylated anti-βIII-tubulin (1:800, R&D Systems, #BAM1195), rabbit anti-βIII-tubulin (1:1000, BioLegend, #802001), rat anti-PECAM (1:100, BD Pharmigen, #553370), goat anti-PECAM (1:1000, R&D Systems, #AF3628), goat anti-Sox10 (1:200, SantaCruz Biotechnology, #sc-17342), rabbit anti-BLBP (1/250, abcam, #ab32423), rabbit anti-NG2

(1:200, Merck, #AB5320), mouse anti-SMA-Cy3 (1:400, Merck, #C6198), goat anti- PDGFRß (1:500, R&D Systems, # AF1042), rabbit anti-Abcc9 (1/100, ThermoFisher Scientific, # PA5-52413), goat anti-DLk1 (1:500, R&D Systems, #AF1144) and rabbit anti-Desmin (abcam, #ab15200). Fluorophore-conjugated secondary antibodies were from Jackson Immuno Research.

Cell quantification

Quantifications of labelled cells were performed on wholemount preparations of embryonic skin from three of E12.5, E13.5, E14.5 and E15.5 *Krox20*$^{Cre/+}$, *Rosa26R*$^{Tomato/+}$ embryos, labelled for Tomato, βIII-tubulin and PECAM. For each embryo, 5 z-stacks of different and non-overlapping fields of view were selected randomly and acquired using a Leica TCS SP5 laser scanning confocal microscope. The scanned surface area per field corresponds to 0.38 μm^2. All tomato-positive cells were counted, and those in contact with nerves, in each stack on the ImageJ software. Cells not in contact with nerves were considered to be on the vascular plexus. Results are given as an average ± one standard deviation. Statistical analyses of the "on nerve" / "on vessels" ratio between each time points were carried out using a chi-square test. *P* values considered significant are indicated by asterisks as follows: *, $P < 0.05$; **, $P < 0.01$; ***, $P < 0.001$. Statistical analyses were generated using the R software version 3.5.2 (R Core Team, 2018). Data are represented as mean values ± standard deviation.

Semi-quantitative RT-PCR

Total RNA (100 ng) was isolated from embryonic skin, reverse transcribed using the pSuperscript III RNAse H reverse transcriptase (Invitrogen) and a mix of oligo-dT and random primers (Invitrogen), according to the manufacturer's instructions. PCR was performed as follows: 2 min at 94°C; 35 cycles of 2 min at 94°C, 1 min at 58°C, 30 s at 72°C. Krox20 primer sequences were the following: (5'-3') GCAGAAGGAACGGAAGAGC; (3'-5') ACTGGTGTGTCAGCCAGAGC.

Skin dissection and fluorescence-activated cell sorting (FACS)

Embryos were selected by their Tomato expression under fluorescent stereomicroscope (Leica, Nussloch, Germany) and head and viscera were removed. The back skin was dissected from *Krox20*$^{Cre/+}$, *R26R*$^{Tomato/+}$ embryos at E12.5 or E13.5, and then digested with collagenase/dispase type I (Merck/Roche) for 15 min at 37°C. Digestion was stopped by adding 0.1 ml of Fetal Calf Serum (FCS). Skin samples were then mechanically dissociated and the cell suspension was filtered. Dissociated cells were then resuspended in PBS, 1% BSA. Tomato-positive cells were isolated from embryonic skin cell preparations by (FACS). Dead cells and doublets were excluded by gating on a forward-scatter and side-scatter area versus

width. Log RFP fluorescence was acquired through a 530/30 nm band pass. Internal Tomato-negative cells served as negative controls for FACS gating. Tomato-positive cells were sorted directly into lysis buffer for RT-PCR and bulk RNA sequencing experiments, or PBS, 0.04% BSA for single cell RNA sequencing experiments. To verify the purity of sorted cells, aliquots of the positive and negative fractions were sorted via FACS again with similar gating parameters, seeded onto coverslips and analyzed by immunohistochemistry with an anti-Tomato antibody.

Library preparation, RNA sequencing and data analysis

cDNA libraries, RNA sequencing library preparation and Illumina sequencing were performed at the Ecole Normale Supérieure genomic core facility (Paris, France). 5 ng of total RNA was amplified and converted to cDNA using SMART-Seq v4 Ultra Low Input RNA kit (Clontech). An average of 200 pg of amplified cDNA was used for library preparation using Nextera XT DNA kit (Illumina). Libraries were multiplexed by 12 on 1 high output flow cells. 75 bp sequencing reads were performed on a NextSeq 500 device (Illumina). The analyses were performed using the Eoulsan pipeline (*26*), including read filtering, mapping, alignment filtering, read quantification, normalization and differential analysis. Prior to mapping, poly-N read tails were trimmed, reads ≤40 bases and with mean quality ≤30 were discarded. Reads were then aligned against the Mus Musculus genome from Ensembl version 91 using STAR (version 2.5.2) (*27*). Alignments from reads matching more than once on the reference genome were removed using Java version of SamTools (*28*). To compute gene expression, Mus Musculus GFF3 genome annotation version 91 from Ensembl database was used. All overlapping regions between alignments and referenced exons were counted using HTSeq-count 0.5.3 (*26*). The sample counts were normalized, then statistically analyzed using DESeq2 (version 1.8.1). P-value <0.05 and Log2 FD > 2 were used as cutoffs criteria to select differentially expressed genes (DEGs).

Single cell RNA sequencing and data analysis

Tomato-positive cells were isolated by FACS from embryonic skin at E12.5. Around 10,000 cells were loaded into one channel of the Chromium system using the V3 single cell reagent kit (10X Genomics). Following capture and lysis, cDNA was synthesized, then amplified by PCR for 12 cycles as per the manufacturer's protocol (10X Genomics). The amplified cDNA was used to generate Illumina sequencing libraries that were each sequenced on one flow cell Nextseq500 Illumina. Cell Ranger 3.0.2 (10X Genomics) was used to process raw sequencing data. This pipeline converted Illumina basecall files to Fastq format, aligned sequencing reads to a custom mm10 transcriptome with added sequences for the Tomato and

Cre transgenes using the STAR aligner (*9*) and quantified the expression of transcripts in each cell using Chromium barcodes. We carried out analyses of processed scRNA-seq data in R version 3.5.2 (R Core Team, 2017) using the Seurat suite version 3.0 (*29*, *30*). Genes expressed in fewer than 3 cells were excluded from the analysis. Cells were excluded if they met one of the following parameters: expression of fewer than 3,000 genes; no Tomato expression; more than 10% of mitochondrial genes among expressed genes. Next, the data were log-normalized with a scale factor of 10^4. The graph-based method from Seurat was used to cluster cells. The PCA was selected as dimensional reduction technique to use in construction of Shared Nearest-Neighbor (SNN) graph, and we selected the first 15 PCs. A t-SNE clustering was performed on the scaled matrix with a 0.8 resolution to obtain a two-dimensional representation of the cell states with a resolution. Contaminating clusters were identified and removed from the dataset before repeating the analysis pipeline on the raw data. Only 81 cells expressed *Krox20*, at low levels and mostly in the SCP cluster. After log-normalization latent variables, defined as the number of UMI and the difference between the G2M and S phase scores, were regressed out using a negative binomial model. After selecting the first 12 PCs, clustering was performed with a 0.6 resolution. Uniform manifold approximation and projection (UMAP) was used to obtain a two-dimensional projection.

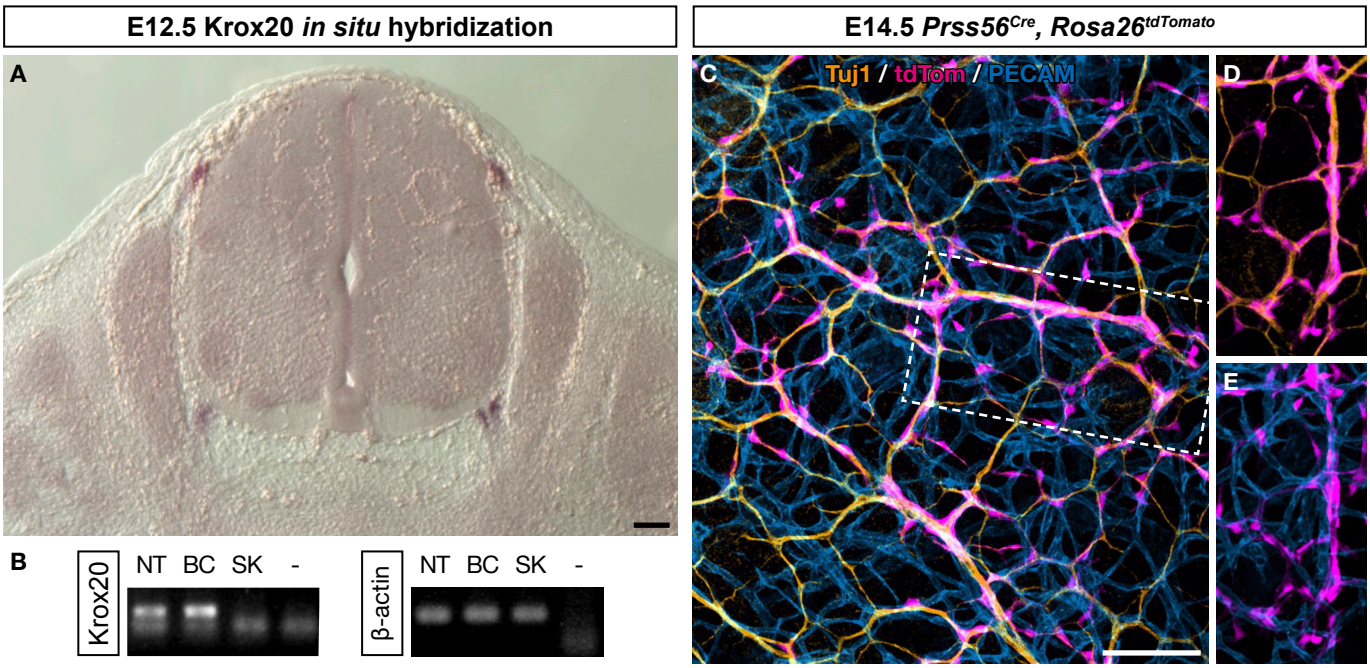

Figure S1. Tomato-positive cells are specific to *Krox20*^{Cre}, *Rosa26R*^{Tomato} tracing and are not due to a *de novo Krox20* activation. (A) *In situ* hybridization of a E12.5 mouse embryo with a Krox20 probe. BCC at the dorsal entry and ventral exit points express Krox20. There is no visible Krox20 expression near the ventral roots or in the skin, where Tomato-positive cells are observed. (B) Krox20 RT-PCR on dissociated E12.5 dorsal skin (SK), compared with neural tube (NT) and boundary caps (BC) as positive controls. (C-E) Dorsal skin wholemount immunostaining of a E14.5 *Prss56*$^{Cre/+}$, *Rosa26R*^{Tomato} embryo. All tomato-positive cells are attached to βIII-tubulin (Tuj1)-positive nerves and not to blood vessels (PECAM). Scale bar: (A) 200 µm; (C-E) 50 µm.

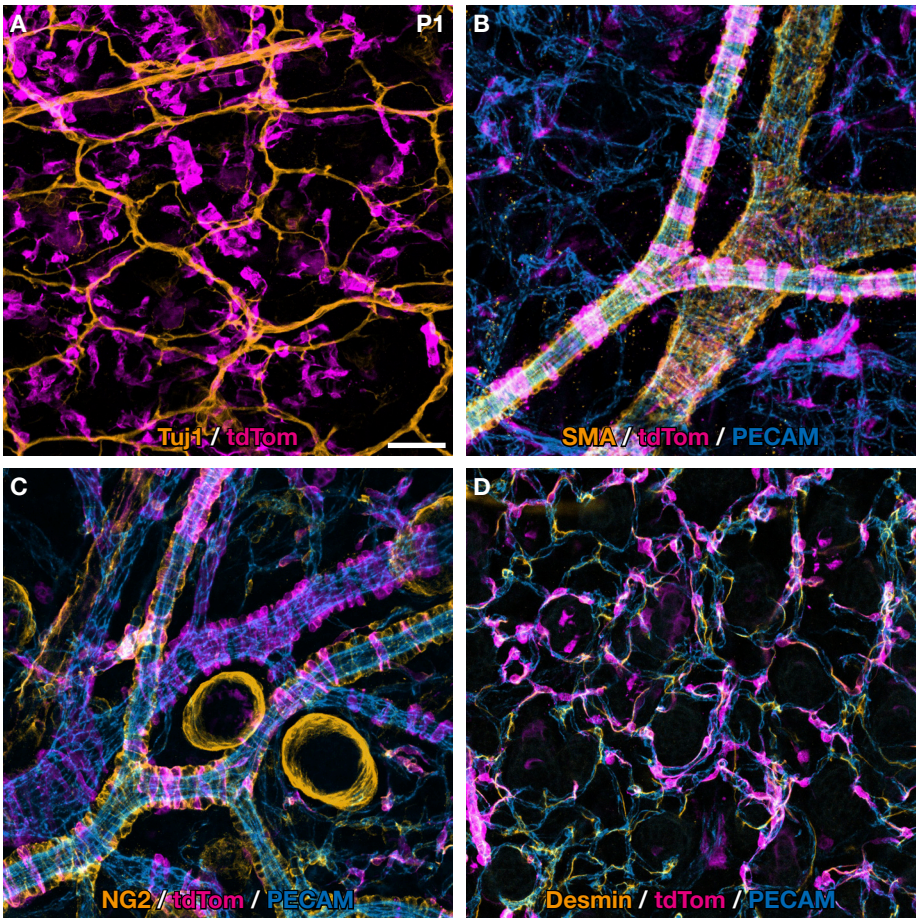

Figure S2. BC cell derivatives include pericytes, arterial and venous vascular smooth muscle cells in the newborn skin. *Krox20*$^{Cre/+}$, *Rosa26R*^{Tomato} newborn dorsal skin wholemount immunostainings. In the newborn skin, most Tomato-positive cells are detached from Tuj1-positive nerves (A). Venules differ from arterioles by their larger diameter and more irregular shape (B,C). Labelled cells express vascular smooth muscle markers smooth muscle actin (SMA, B), and when they are located on arterioles they are NG2-positive while on venules they are NG2-negative (C). Labelled cells also include capillary pericytes which are NG2 positive (C) and Desmin-positive (D). Scale bar: 50 µm.

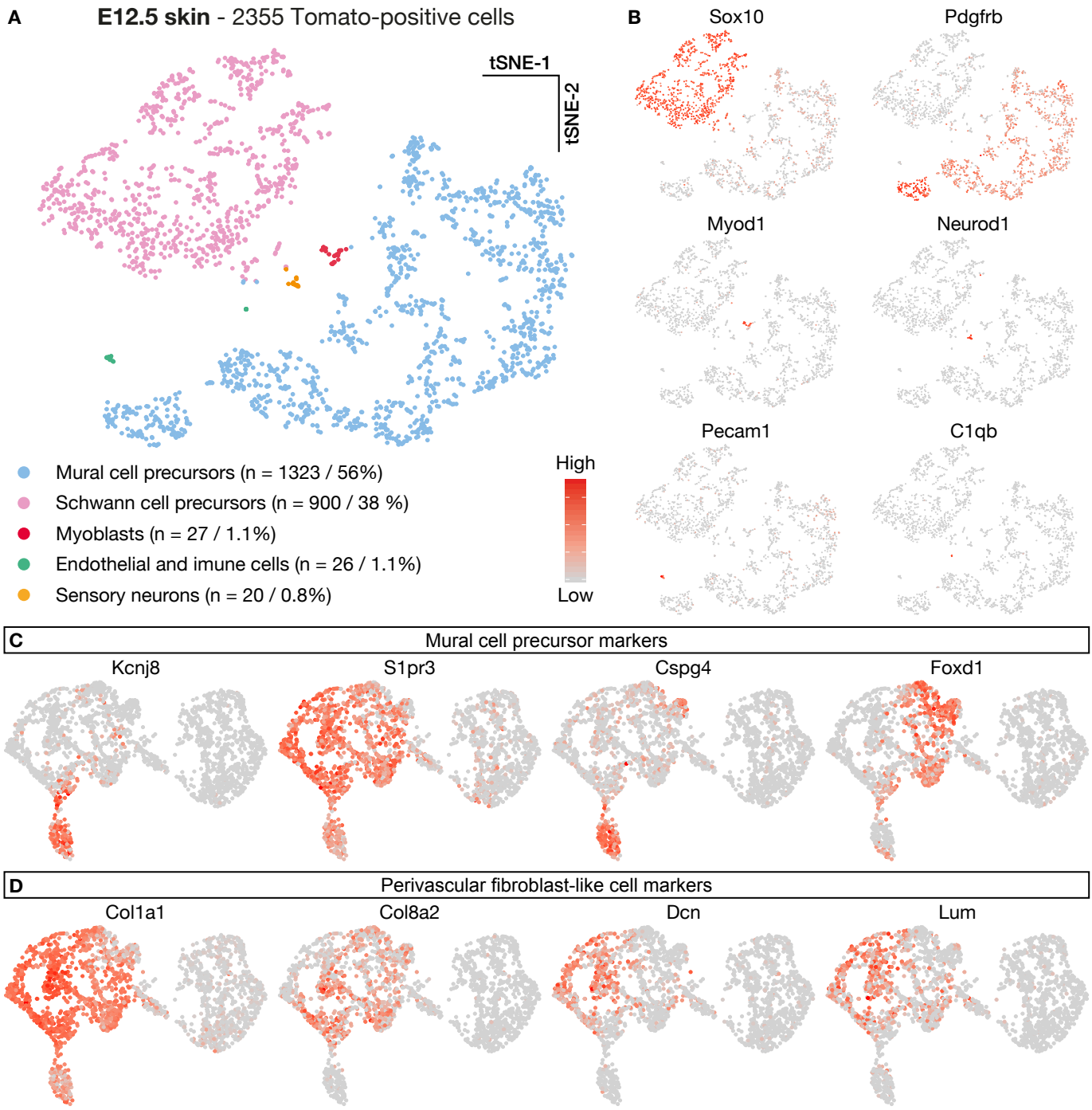

Figure S3. Single cell RNA sequencing of Tomato-positive cells from E12.5 *Krox20^{Cre}, Rosa26R^{Tomato}* dorsal skin. (A,B) t-SNE projection of all cells clusters. Schwann cell precursor (SCP, magenta) and mural cell precursor (MCP, blue) clusters have each been grouped according to their expression of Sox10 and PDGFRβ, respectively. Three contaminating clusters were detected: Myod1-positive myoblasts (red), Neurod1-positive sensory neurons (orange) and Pecam1 and C1qb-positive endothelial and immune cells (green). Each represented about 1% of total cells. (C,D) In addition to MC markers, MCP express markers of perivascular fibroblast-like cells. Cells are color-coded according to gene expression level (gray = low, red = high).

Discussion

During my PhD, I have worked on two projects focusing on the functional analysis of BC cells and their derivatives (Figure 36). In the first study, we have shown that in addition to nerve root Schwann cells and DRG neurons, a subset of Prss56-traced derivatives from the ventral roots migrates rapidly along peripheral nerves to reach the skin. In the adult skin, Prss56-traced BC derivatives correspond to a subpopulation of myelinating and Remak SC, sub-epidermal and lanceolate glia wrapping free nerve endings and hair follicles innervation, respectively. Moreover, they also give rise to SKP, a population of stem-like cells which can self-renew and have a broad differentiation potential *in vitro*, and *in vivo* after transplantation in the adult mouse DRG. In the second study, in addition to their previously reported nerve root and DRG derivatives, we have discovered that a ventral subset of Krox20-traced BC derivatives also migrates along spinal nerves, then detach and participate to the development of peripheral vasculature. Detachment from nerves takes place in two waves, between E10.5 and E11.5 under the neural tube, and between E12.5 and E13.5 in the skin. In newborn skin, a majority of Krox20-traced BC derivatives correspond to both capillary pericytes and arterial and venous

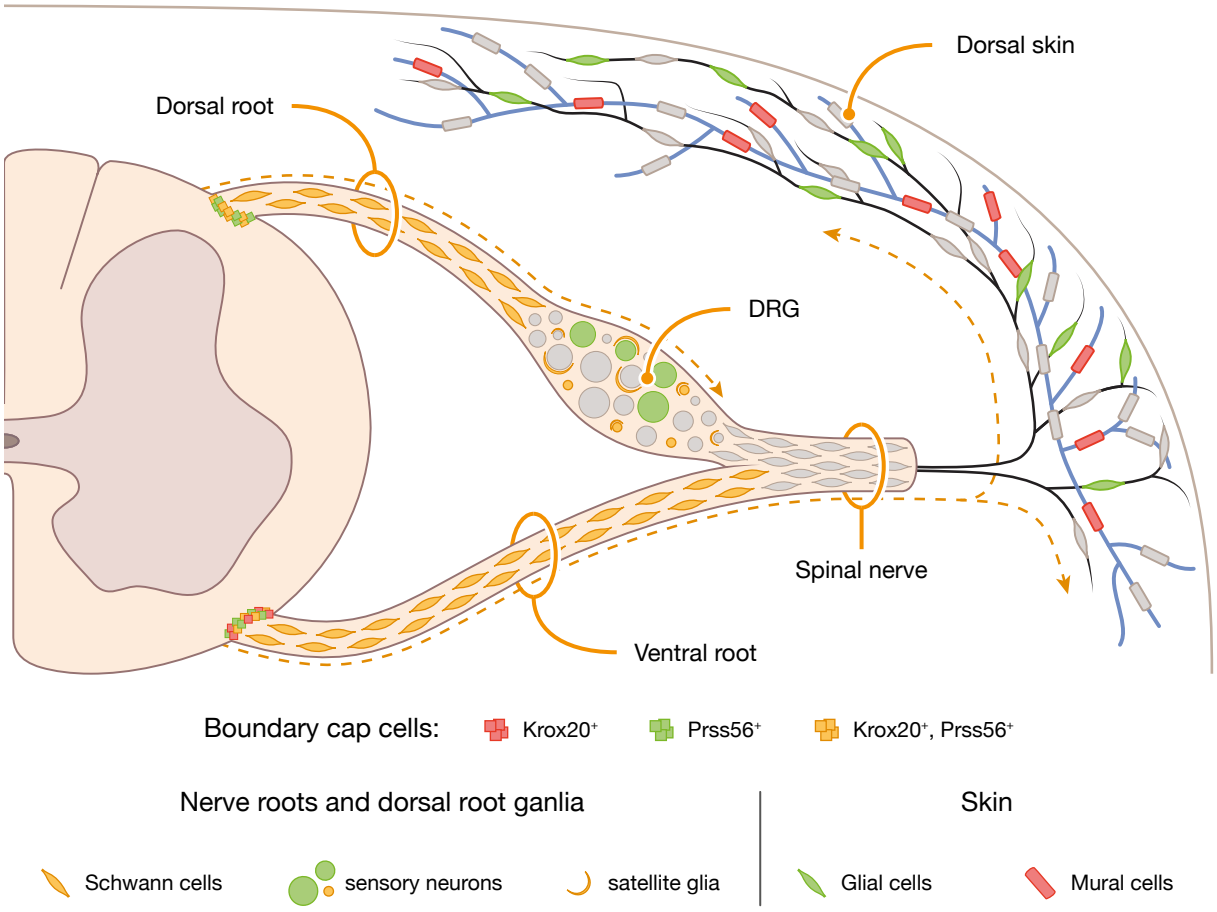

Figure 36. Schematic representation of *Krox20*- and *Prss56*-traced boundary cap cell derivatives in the trunk. Clusters of boundary cap (BC) cells reside transiently at the dorsal/ventral root entry/exit points and give rise to derivatives that populate nerve roots, dorsal root ganglia (DRG) and the skin. *Krox20*- and *Prss56*-expressing BC cells (orange) give rise to Schwann cell precursors (SCP) in the nerve roots, and a subset of sensory neurons and glial satellite cells in the DRG. Small fractions of ventral BC cell derivatives migrate along the nerves to the skin. *Prss56*-traced BC derivatives (green) remain in contact with axons and differentiate into mature glial cells (except for a small fraction that detaches and switch to melanocyte fate). Most, if not all, *Krox20*-traced BC derivatives (red) delaminate from nerves and integrate the vascular plexus as mural cells.

vSMC. Through wholemount immunostainings and bulk RNA-seq comparison of E12.5 versus E13.5 skin, we have found that detachment from nerves is accompanied by extinction of glial markers and expression of numerous mural cell markers. Strikingly, single-cell RNA-seq analysis of Krox20-traced cells from E12.5 skin, the period during which a majority of them remain attached to nerves, identified a mural transcriptomic signature suggesting that their specification takes place well before their detachment. After exposing the major aspects of my studies, I will discuss their implications regarding the origin and the heterogeneity of BC cells.

1. Contribution of boundary cap cells during development

1.1. Glial derivatives

1.1.1. Schwann cell heterogeneity

Our observations support the double embryonic origin of SC. Those of nerve roots and nerve endings in the skin derive from BC cells whereas the nerves in between are covered by NC- derived SC. Hence, the distribution of SC along peripheral nerves appears to be heterogeneous at least regarding their origin. Whether this heterogeneity is correlated with specific properties and/or functions remains undetermined so far. Interestingly, in patients with neurofibromatosis type 1 (NF1), benign nerve sheath tumors due to mutations of the *Nf1* gene in SC called neurofibromas (NF) are developing mainly at the level of nerve terminals and nerve roots, supporting the hypothesis of a SC functional heterogeneity and highlighting in the skin the role of BC-derived SC in this disease.

1.1.2. Subepidermal glia

Subepidermal glia is a poorly characterized cell population located on FNE in the mouse and human skin, and whose function remains largely unknown. We have shown that these cells originate from Prss56-expressing BC cells through the migration of their derivatives along nerves to the skin. Our recent observations suggest that most, if not all, of the subepidermal glia in the back skin derive from Prss56-expressing BC cells, since this population was not traced with the *Krox20*^{Cre} reporter line. Strikingly, subepidermal glia was not traced when the *Wnt1*^{Cre} (NC-specific Cre driver) and *Dhh*^{Cre} (SCP Cre driver) mice were used (Figure 37), suggesting their distinct origin (Radomska et al., 2019). The fact that among all the existing *Nf1* mouse models, *Prss56*^{Cre}*, Nf1*$^{fl/fl}$ mice are the only ones to develop diffuse cutaneous NF (cNF) points to subepidermal glia as the cell of origin of these tumors. Interestingly, topical treatment of *Nf1* KO mutant mice with inhibitor of RAS pathway (target of NF1) leads to the efficient elimination of cNF and subepidermal glial cells while myelinating SC cells remain insensitive to this treatment. This finding further supports the implication of subepidermal glia in the development of cNF. Moreover, their unique properties to ensheath nociceptive nerve endings in the skin raise the possibility of their implication in the nociception mechanisms.

However, such studies require the availability of specific markers to isolate and further characterize subepidermal glial cells. These studies are ongoing in our lab by performing single-cell RNA-seq of Prss56-traced cells isolated from postnatal skin. Such markers will allow us to isolate subepidermal glial cells from mouse and human skin and to initiate their functional characterization.

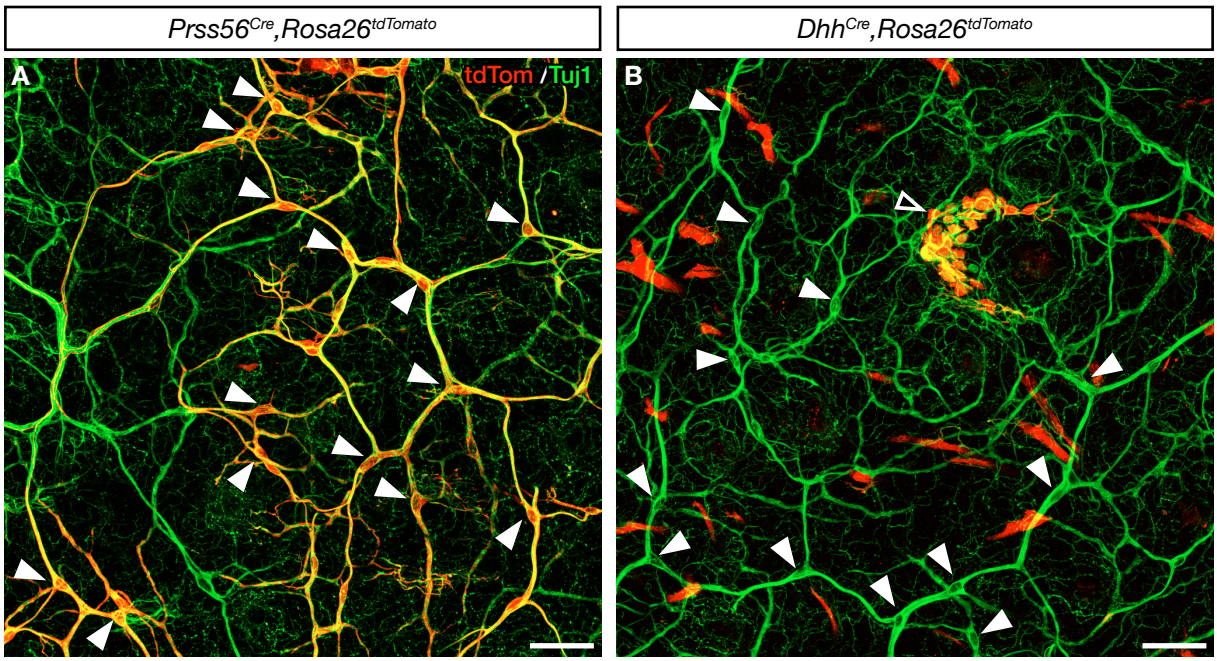

B

Cell type	*Prss56*^{Cre}	*Krox20*^{Cre}	*Dhh*^{Cre}
mSC	+	+	+
Remak SC	+	-	+
lanceolate glia	+	-	+
arrector pili glia	+	-	+
subepidermal glia	+	-	-
melanocytes	+	-	-
Merkel cells	-	-	+

Figure 37. *Prss56*-, *Krox20*- and *Dhh*-traced derivatives in the adult skin. Dorsal view of the subepidermal region from *Prss56*^{Cre},*Rosa26*^{tdTomato} (**A**) and *Dhh*^{Cre},*Rosa26*^{tdTomato} (**B**) adult skin. Numerous tomato-positive (red) Schwann cells associated with the subepidermal neuronal plexus (Tuj1, green) are present in the *Prss56*^{Cre},*Rosa26*^{tdTomato} dermis (**A**), while none are present at this level with the *Dhh*^{Cre} driver (**B**). Arrowheads point to cell bodies of subepidermal SC, empty arrowhead indicates traced Merkel cells. (**C**) Table summarizing the different derivatives present in the adult skin traced with the three Cre drivers. Scale bars: 50 µm.

1.2.Perivascular derivatives

1.2.1. Redundancy of mural cell recruitment during development

In this study, we have discovered that nerve-attached Krox20-traced BC cell derivatives constitute a major source of mural cells to the developing peripheral vasculature. Recent elegant studies point to myeloid progenitors (MP) as the cells at the origin of about half of mural cells in the skin. Here, we provide strong evidences that Krox20-traced BC derivatives are at the origin of the others (Yamazaki et al., 2017). Whether there are other, minor sources

of skin mural cells remains possible, as no double labelling study of BC cells and MP has been performed so far. In the myeloid progenitor study, it had been shown that their depletion did not significantly alter vascular development as their loss appeared to be compensated by other mural cells, probably BC-derived (Yamazaki et al., 2017). We also assessed whether BC-derived skin mural cells were necessary for vascular development and performed a genetic ablation of Krox20-expressing BC cells by targeted expression of diphtheria toxin. (Figure 38). Similarly to what was reported for MP, we did not detect any significant vascular phenotype at E15.5 and concluded that MP-derived mural cells compensate the loss of BC-derived mural cells. However, the fact that the BC-ablated embryos die around E15.5 without *Krox20* being expressed in other tissues beside rhombomeres 3 and 5, suggests the important role of Krox20-expressing BC derivatives during embryonic development (Vermeren et al., 2003). Altogether, these results suggest that mural cell recruitment during vascular development is a dynamic process in which at least two cell populations can participate and compensate each other in pathological situations.

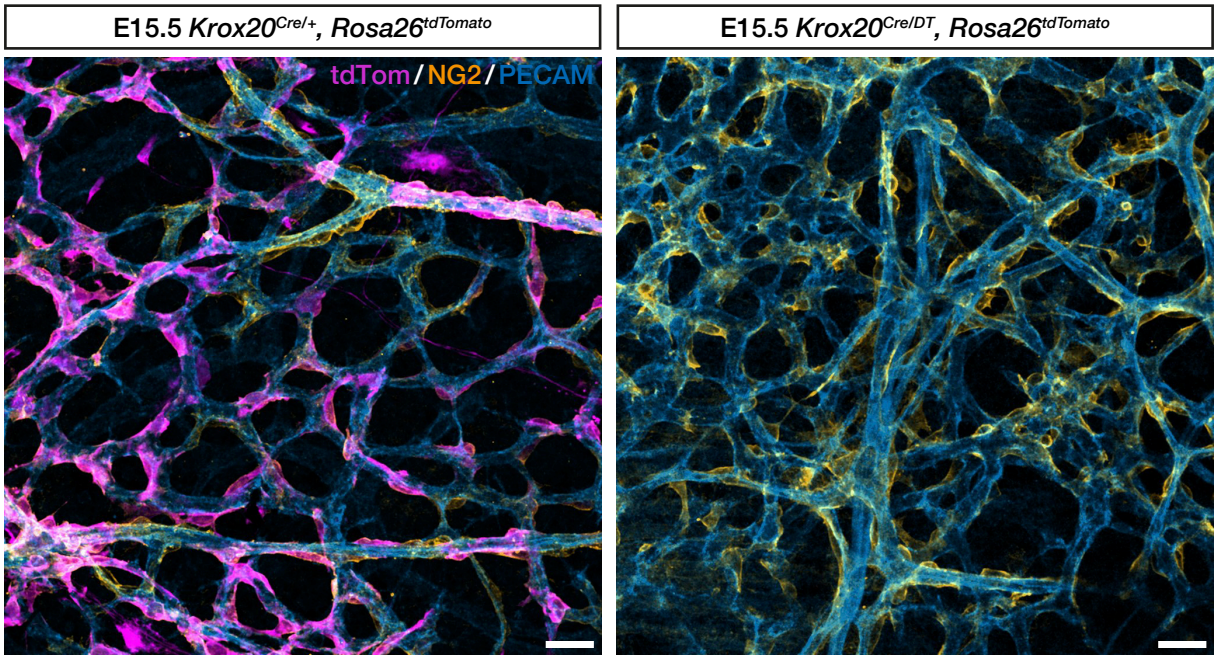

Figure 38. Genetic ablation of *Krox20*-traced boundary cap cells. Wholemount immunostainings of E15.5 dorsal skin of either control *Krox20*^{Cre},*Rosa26*^{tdTomato} or mutant *Krox20*$^{Cre/DT}$,*Rosa26*^{tdTomato} embryos labelled for tomato (magenta), PECAM (blue) and mural cell marker Ng2 (orange). In the absence of *Krox20*-traced BC cells there is no obvious vascular defect as Ng2-positive mural cells are attached to the vascular plexus. Scale bars: 50 µm.

1.2.2. Mural cells heterogeneity

Recent studies indicate that mural cells, in addition to include pericytes and vSMC, consist of a continuum between these two cell types rather than belonging to two distinct populations. Moreover, their molecular characterization was hampered by the lack of specific markers of mural cell subtypes (Armulik et al., 2011; Holm et al., 2018). Strikingly, the scRNA-seq analysis of Krox20-traced BC derivatives in E12.5 dorsal skin, revealed that despite their

attachment to nerves, the majority of traced cells possessed the transcriptomic signature of mural cell progenitors. Interestingly, they formed several sub-clusters, underlining their early heterogeneity. Defining a precise identity to each of these clusters appeared difficult for two reasons. First, it was not possible from a single time point to differentiate transient progenitors from terminal cell types. Second, although recently published large scale scRNA-seq analysis of adult brain vasculature offer insight into mural cell diversity, comparison remains limited due to the differences specific to organs and developmental stages (Vanlandewijck et al., 2018). For instance, we have identified clusters of cells expressing PDGFRα+ and Col1a1+ that also express several markers attributed to PVF in the CNS. This last population has been implicated in fibrosis and more recently, in the inflammatory response (Soderblom et al., 2013; Duan et al., 2018). However, preliminary reconstruction of lineage differentiation trajectories using STREAM (http://stream.pinellolab.org; Chen et al., 2018) suggests that in our case that Col1a1+ cells are rather transient progenitors (Figure 39). Hence, with further time points and more advanced bioinformatic analysis, scRNA-seq of Krox20-traced mural cells could allow us to better characterize mural cell diversity in the skin, which in turn would make possible functional studies in normal and pathological situations such as wound repair.

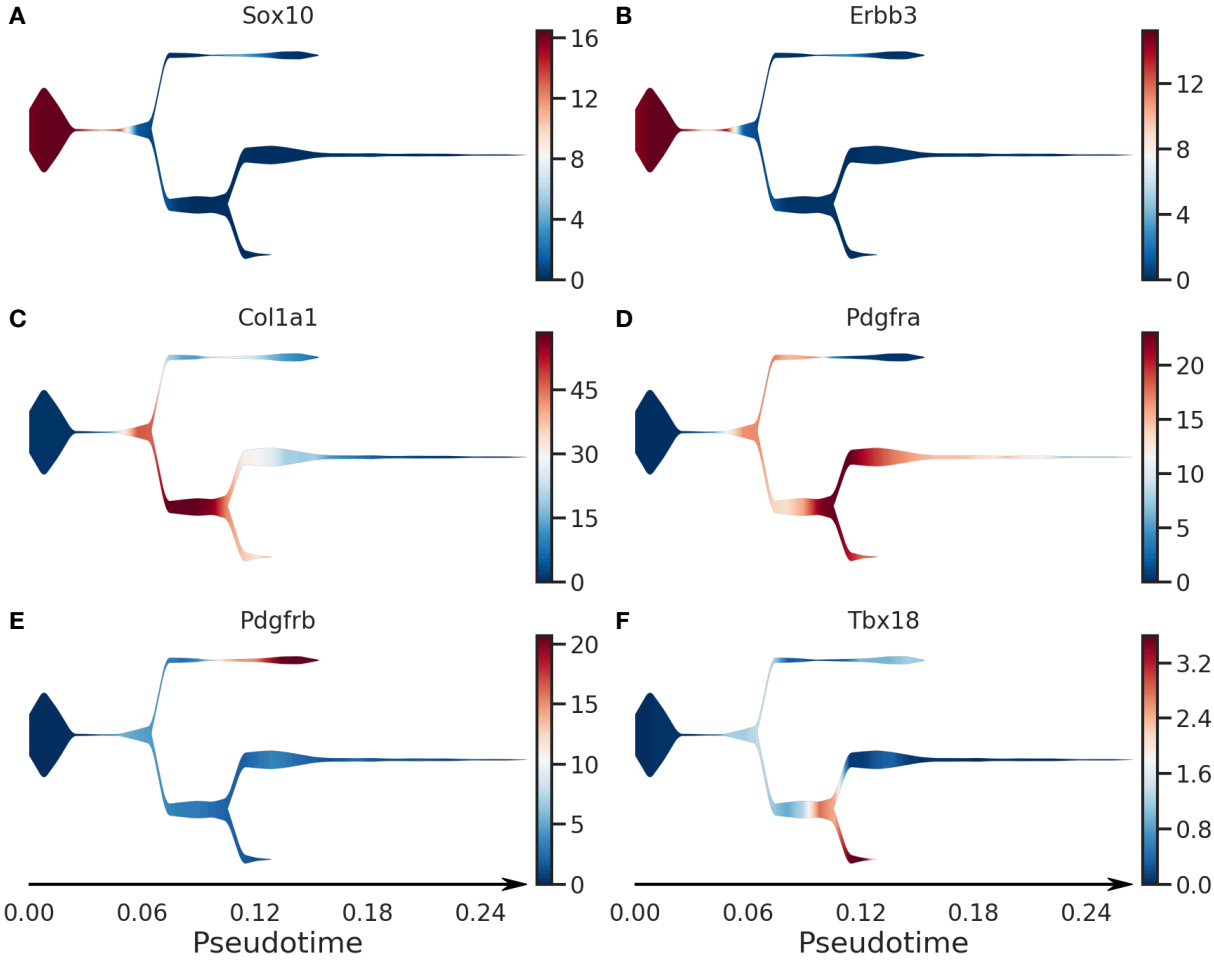

Figure 39. Trajectories reconstruction of *Krox20*-traced BC cell derivatives in E12.5 dorsal skin. Using the STREAM pipeline to reconstruct trajectories and organize them along a pseudotime we can observe that SCP (**A**,**B**) give rise to an intermediate and transient population of Col1a1-positive cells (**C**) that will either give rise to PDGFRα- (**D**), PDGFRβ- (**E**) or Tbx18-positive (**F**) mural cell subtypes.

1.3.On the glial to vascular switch

Between E12.5 and E13.5, Krox20-traced BC derivatives detach from nerves and undergo a profound change in identity. One of the aims of the bulk RNA-seq comparison between E12.5 and E13.5 Krox20-traced BC derivatives in the skin was to find among the genes dysregulated at E12.5 those involved in the glial to vascular switch. Surprisingly, one of the most upregulated gene at E12.5 in this comparison was the Robo3 receptor (log2 fold change 9.6, adjusted *P*-value < 0.001). Robo3 is a membrane bound receptor with multiple splice variants which has been described in the CNS to play a complex role in commissural axon guidance, and more specifically midline crossing (Friocourt and Chédotal, 2017). This complex process requires first to attract axons to the NT midline at the floor plate, before repelling them once they have crossed it to avoid their return. Robo3 is thought to promote attraction to the midline in two ways: by inhibiting the repulsion induced by Slit/Robo1-2 signaling; and by attracting directly through its interaction with the DCC receptor to Netrin-1. More recently, it has also been reported that Robo3 could exert a repulsive action upon binding its ligand, Nell2 (Jaworski et al., 2015). Interestingly, in our bulk RNA-seq comparison, Nell2 was also upregulated (log2 fold change 2.2, adjusted *P*-value < 0.001). Hence, Robo3 seemed to be an interesting candidate. We performed Robo3 immunolabelling on wholemount skin from E12.5 *Krox20*^{Cre}, *Rosa26*^{tdTom} embryos, and identified that numerous nerve-attached Krox20-traced derivatives express Robo3 (Figure 40). Moreover, Robo3 RT-PCR on labelled cells purified by fluorescence activated cell sorting (FACS) confirmed its expression in the skin. Surprisingly, scRNA-seq analysis of traced cells from E12.5 skin failed to detect Robo3 expression, but detected Nell2 expression in SCP. A possible explanation could be that Robo3 level of expression is too low to be detected, as the 10X Chromium technology is known to read at most 40% of mRNAs. Although, the implication of Robo3 in the glial to vascular switch remains speculative, we are currently generating *Krox20*^{Cre}, *Robo3*$^{fl/fl}$, *Rosa26*^{tdTomato} embryos to investigate this exciting possibility.

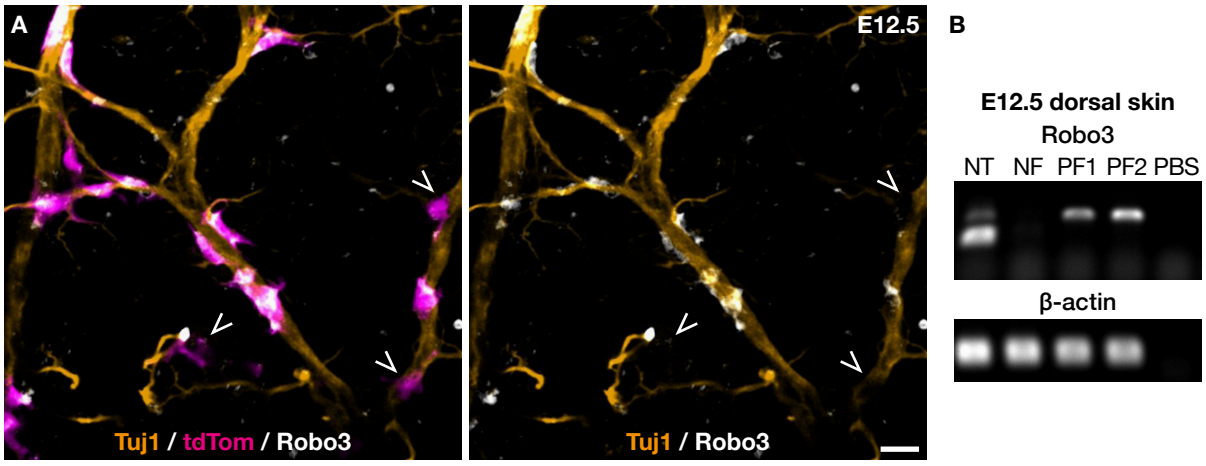

Figure 40. *Krox20*-traced BC derivatives express Robo3 before detaching. (**A**) Dorsal skin wholemount immunostaining of E12.5 *Krox20*^{Cre}, *Rosa26*^{tdTomato} embryos labelled for Tomato (magenta), Tuj1 (orange) and Robo3 (gray). Both Robo3-positive and negative (arrowheads) cells are visible on nerves. (B) Robo3 RT-PCR on purified Tomato+ cells from E12.5 dorsal skin (PF1-2) and the negative fraction (NF), compared with the neural tube (NT) as a positive control.

2. Origins of boundary cap cells

2.1. About Schwann cell precursors

Three multipotent stem-like cell types have been identified during the PNS development: NC cells, BC cells and more recently SCP. Hence, before discussing the diversity and heterogeneity of BC cells and their derivatives, I would like to briefly recapitulate our current knowledge regarding the plasticity of SCP. Over the last decade, our appreciation of SCP has profoundly changed from considering them as unipotent glial population committed to the SC lineage to a new multipotent stem cell niche (Figure 41). Indeed, several studies have revealed that nerve-associated SCP migrate along nerves, then detach and provide plethora of ectodermal and mesodermal derivatives including endoneurial fibroblasts, skin melanocytes, adrenal medulla chromaffin cells, tooth mesenchymal stem cells, enteric and parasympathetic neurons (Furlan and Adameyko, 2018). This broad range of cell types, all of them also in part NC-derived, have led to consider them as a "NC in disguise" that uses nerves as pathways to migrate further and fuel the rapidly growing embryos with a second source of multipotent cells (Figure 41). Indeed, it remains difficult to properly define the transition between the two cell types given that late emigrating NC cells and early SCP share several markers, and that we still do not know the mechanisms involved in the transition (Woodhoo and Sommer, 2008). In addition to their redundancy, their evolutionary relationship is also intriguing. This question

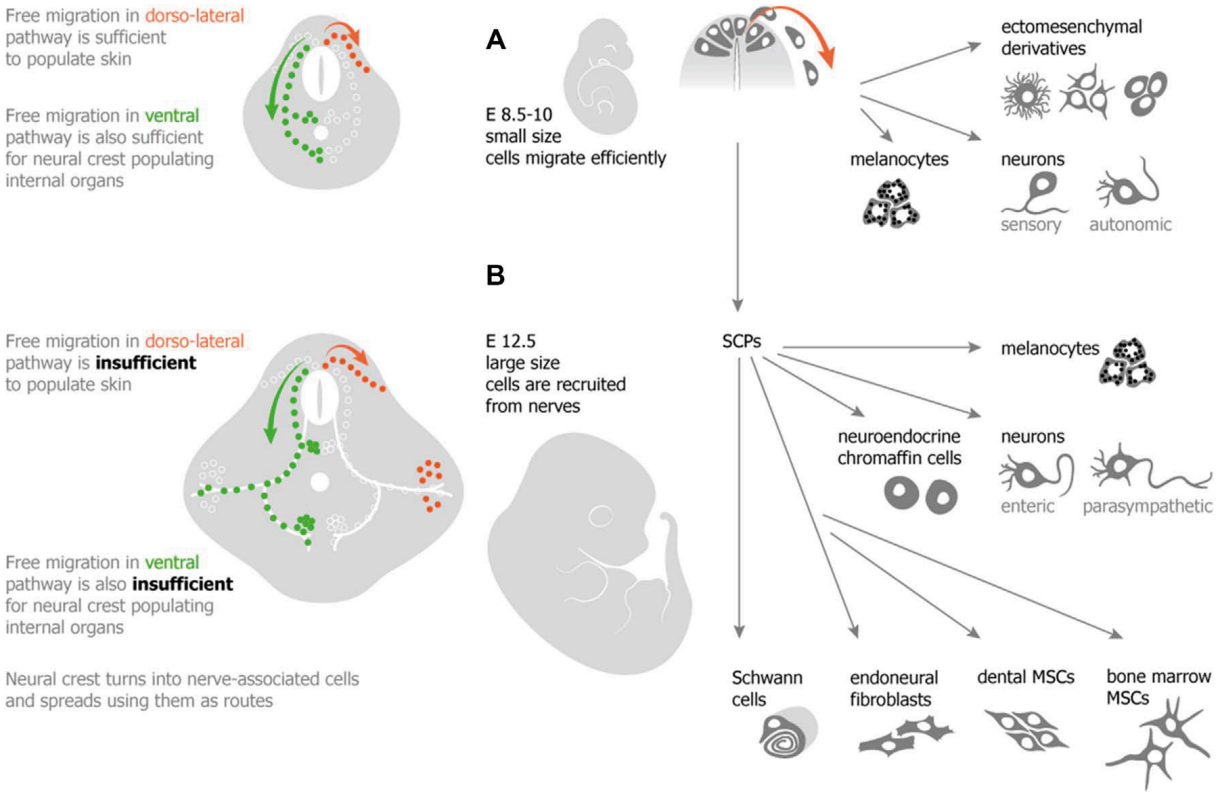

Figure 41. Schwann cell precursors, a « neural crest in disguise ». Neural crest cells (NCC) and nerve-attached Schwann cell precursors (SCP) constitute two sources of multipotent progenitors that migrate through the embryo to provide neural and non-neural cell types. SCP may represent an alternative dissemination strategy as the embryo grows, using peripheral nerves as pathway to migrate. MSC: mesenchymal stem cells. From Furlan and Adameyko (2018).

has been addressed recently in the sea lamprey (*Petromyzon marinus*), a jawless vertebrate (cyclostome) representing the most primitive currently living vertebrate with a well-defined NC (Green et al., 2017). In the sea lamprey, SCP migrate along nerves and give rise to enteric neurons, similarly to what has been described in mice (Green et al., 2017; Uesaka et al., 2015). However, in stark contrast with jawed vertebrates, the NC does not provide enteric neurons in the sea lamprey. These results suggest that in this case, the NC gained during evolution the ability to generate a new cell type previously provided by SCP. Thus, whether SCP evolved from the NC or the opposite remains an open and fascinating question. As for BC cells, they have been described in the chick and mouse embryo, but do not exist in the zebrafish (*Danio rerio*), suggesting that they are a more recent evolutionary acquisition.

2.2.Boundary cap cells and the neural crest

Boundary cap cells are characterized by their expression of *Krox20* and/or *Prss56* at the DREZ and MEP of all cranial and spinal nerves at E10.5 in mice (Coulpier et al., 2009). Krox20- and Prss56-traced dorsal BC cells give rise to dorsal root SC, GSC and either only TrkA+ nociceptors (Krox20) or all types of SN (Prss56). All these derivatives are also traced with $HtPA^{Cre}$ and $Wnt1^{Cre}$ NC lineage tracing mouse lines (Figure 42). Hence, dorsal BC cells are NC-derived and their fate appears to be restricted to the PNS. However, the situation is more complex for ventral BC cells which display a wider differentiation spectrum. Both Krox20- and Prss56-traced ventral BC cells give rise to ventral root SC that are also traced with *HtPA* and *Wnt1*, suggesting at least in part their NC origin. However, our studies identified two additional migratory streams of ventral BC cells. The first population corresponds to Prss56-traced derivatives that migrate to the skin and provide various types of glial cells and melanocytes, which can all be considered as typical NC derivatives. Here, the subepidermal glia might constitute an exception since this discrete population was never identified when lineage tracing was performed with NC or SCP-Cre driver lines. The second population consists of Krox20-traced derivatives that migrate along nerves, then detach and differentiate into mural progenitors in the skin. Several arguments suggest that their embryonic origin might be different: (i) while NC fate-mapping with *HtPA* and *Wnt1* traces pericytes in the head, this was never described in the trunk vasculature (Figure 42), (ii) dye labelling and quail/chick graft of the NC never generate labelled pericytes in the trunk skin. Thus, we attempted to identify their embryonic origin. Following the description in the zebrafish of a CNS-derived $Olig2^{+}$ MEP glia migrating along spinal nerves we performed fate mapping with two CNS-Cre drivers: $Olig2^{Cre}$ and $Brn4^{Cre}$. None of them allowed us to label mural cells in the trunk (Figure 42). Similar results were obtained when the fate mapping was performed with the mesodermal Cre driver $Myf5^{Cre}$ (Figure 42). While it cannot be excluded that both NC lineage tracing mouse lines used in this study might be incomplete and that these derivatives are in fact NC-derived, given our current knowledge, it appears that ventral BC cells have a more complex origin which remains to be elucidated.

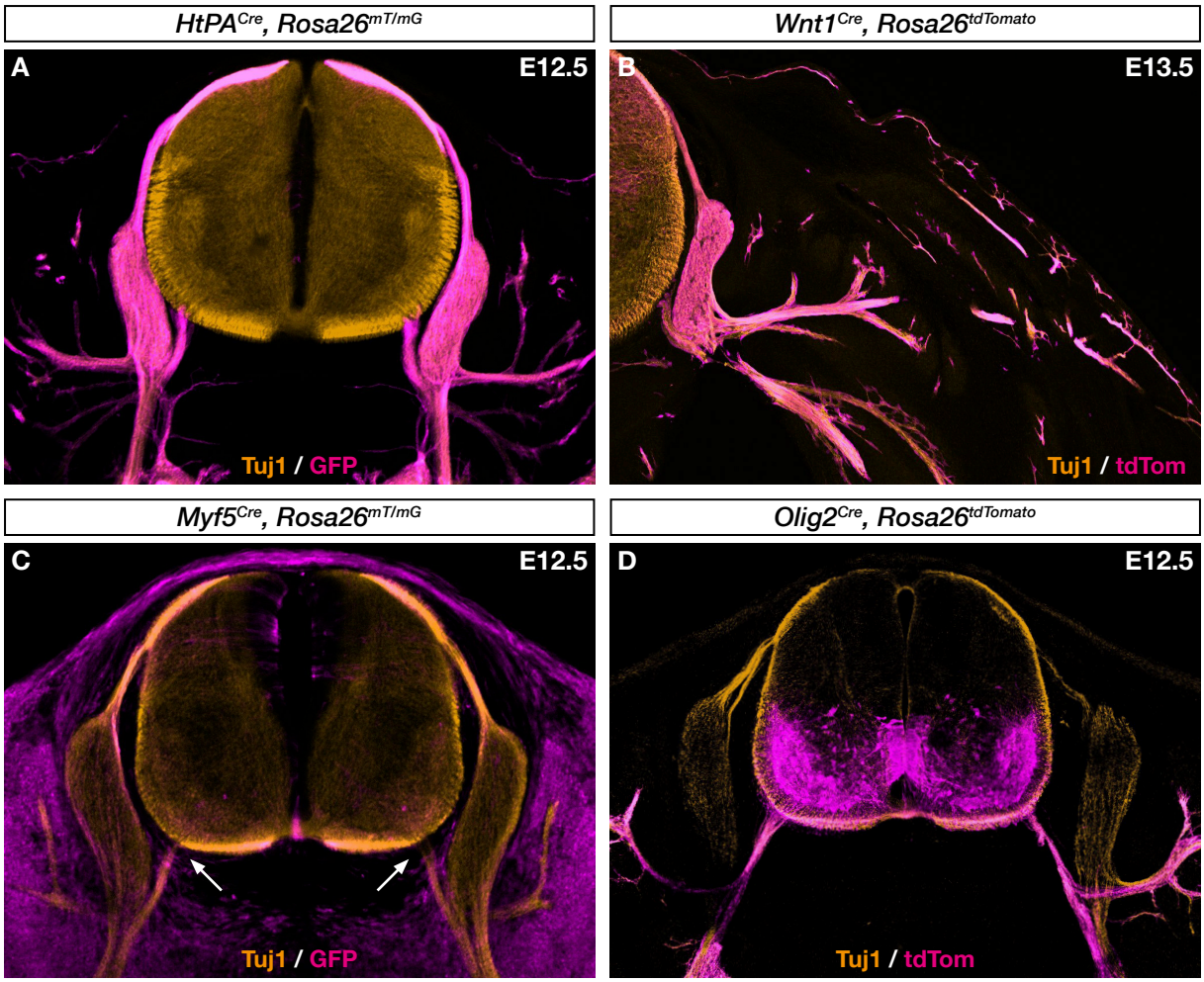

Figure 42. On the origin of boundary cap cells. Transverse sections from E12.5 embryos labelled against GFP (**A**,**C**) or Tomato (**B**,**D**) in magenta and Tuj1 (orange). (**A**,**B**) Dorsal and ventral boundary caps (BC) are traced with the *HtPA*^{Cre} and *Wnt1*^{Cre} neural crest driver lines. (**C**) Ventral BC are not traced with the *Myf5*^{Cre} mesodermal reporter line, with a clear lack of tracing (arrows). (**D**) Ventral BC are also not traced with the *Olig2*^{Cre} reporter line.

2.3.Boundary cap cells and Schwann cell precursors

Since BC cells and SCP are two multipotent cell populations that arise after the NC during PNS development, it has been questioned whether BC cells could be a SCP subtype (Furlan and Adameyko, 2018). Indeed, their fate was believed to be restricted to PNS cell types unlike SCP. However, the reality is more complex as we have shown that Prss56-traced BC cells also give rise to skin melanocytes (Radomska et al., 2019). Moreover, we have found in this study that Prss56- and Krox20-traced BC cells are respectively at the origin of subepidermal glia and mural cells in the peripheral vasculature. As mentioned before, these two populations arise from ventral BC cells, and might not be from a NC-origin. Hence, an alternative scenario could be that NC-derived BC cells give rise to a subset of typical SCP while ventral BC cells give rise to a subset of multipotent SCP-like cells (Figure 43). Finally, the fact that BC cells do not give rise *in vivo* to other cell types provided by SCP such as autonomic neurons or chromaffin cells does not necessarily exclude the possibility that BC cells have a broader differentiation potential that is never expressed due to their targets and

the timing of their migration. An interesting approach to test this hypothesis would be to transplant BC cells in those structures to assess their potential.

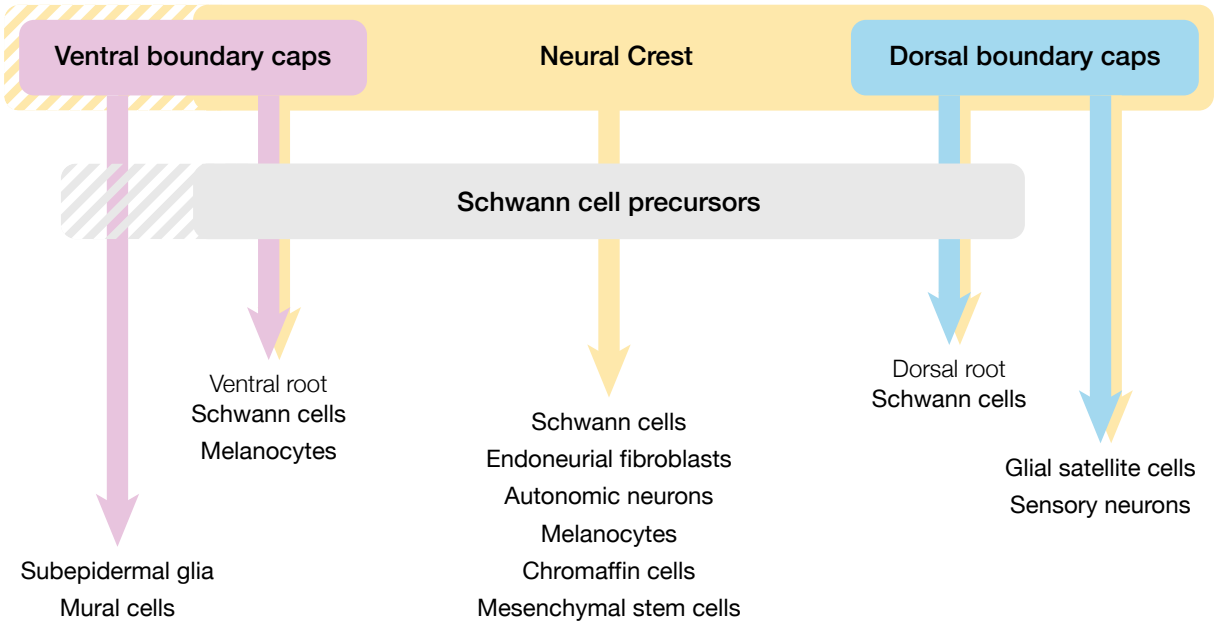

Figure 43. Boundary cap cells, the neural crest and Schwann cell precursors. While dorsal boundary caps (BC) are neural crest (NC)-derived, ventral BC may be in part non NC-derived (dashed yellow). Dorsal and ventral boundary cap cells (BC) give rise to subsets of Schwann cell precursors (SCP). The ventral BC subsets that give rise to subepidermal glia and mural cells have a SCP-like identity (dashed gray) during their migration.

3. Boundary cap cells heterogeneity

Our results have shown that while Krox20- and Prss56-expressing BC cells share common derivatives, they display several differences. Indeed, among dorsal BC cells, Prss56-traced derivatives give birth to all subtypes of SN, while Krox20-traced cells only provide nociceptors. But the most striking difference is between ventral BC cells, as the Prss56-traced and Krox20-traced BC derivatives give rise respectively to glial cells, including subepidermal glia, or mural cells. Altogether, this heterogeneity between, as well as within, ventral and dorsal BC cells raises the question whether pre-migratory BC cells are a unique population of multipotent stem cells whose initial potential is similar, or a group of cells already committed to specific lineages. Ideally, scRNA-seq analysis of E10.5 Krox20- and Prss56-expressing BC cells would enable us to address this fascinating question. However, this is not trivial since there are very few traced cells at this stage and a performing a proper dissection is challenging. Hence, we attempted to address this question by performing scRNA-seq on E11.5 *Krox20*^{Cre}*, Rosa26*^{tdTomato} meninges that contains BC cells as well as their nerve root and DRG derivatives (Figure 44). This preliminary experiment presented several limitations: we only had a small number of cells (704) and it was performed with the previous version of the 10X chromium technology which captured up to 20% of mRNAs. In spite of these limitations, we were still able to make several interesting observations, presented as overlays on a uniform manifold approximation and projection (UMAP) plot. First, we identified BC

cells expressing *Krox20* and/or *Prss56* in the main (dark purple) cluster. From this cluster we observed two differentiation trajectories. On the left there is a neurogenic stream with a cluster of proliferating neural progenitors (green), followed by Ngn1-positive neural progenitors (light blue) and finally TrkA-positive nociceptors (dark blue). The disconnect between the proliferating neural progenitors and the other clusters is likely due to the lack of cell cycle correction, which was not possible in this dataset because of the limited reading depth. On the right, there is a gliogenic pathway with a cluster of SCP (light purple) that express Sox10 and Dhh. Surprisingly, we also identified a cluster of mural cells (yellow) expressing PDGFRβ and Abcc9, that might originate from cells detached from the ventral roots. These results suggest an early commitment of BC cells to a neurogenic or gliogenic fate, and the comparison of both traced populations could help us decipher how these decisions are made.

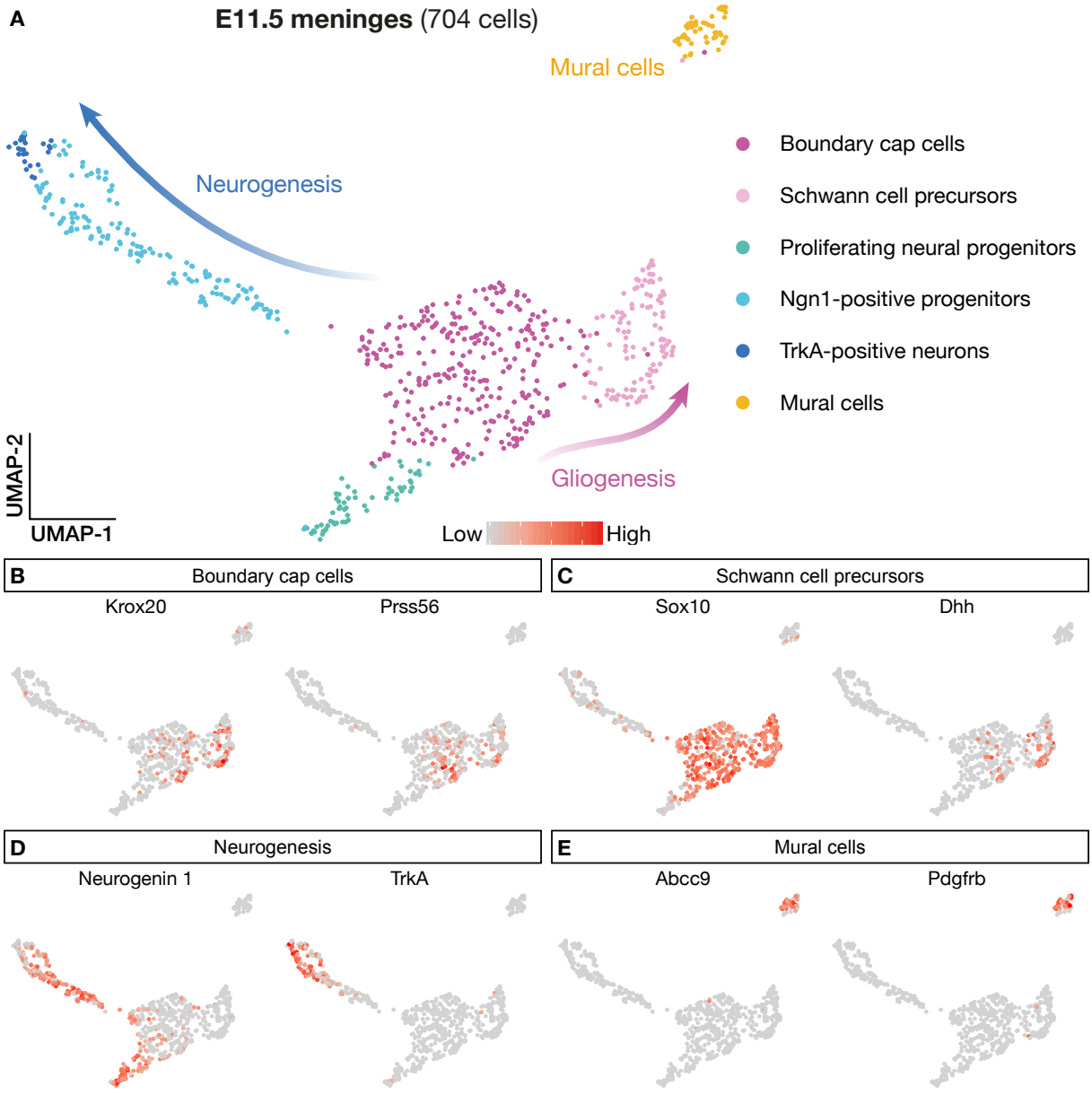

Figure 44. Single-cell transcriptomic analysis of purified traced cells from E11.5 *Krox20*^{Cre}, *Rosa26*^{tdTomato} meninges. Cluster analysis reveals that boundary cap cells (B; purple) choose between a neurogenic (D; light and deep blue) or a gliogenic (C; light purple) trajectory. (E) There also is a mural cell cluster that may correspond to cells detaching from the ventral roots.

General conclusions

The development of the peripheral nervous system in mice involves the successive engagement of three populations of multipotent stem-like cells: neural crest (NC) cells, boundary cap (BC) cells and Schwann cell precursors (SCP). BC cells are defined by their location at the dorsal root entry and motor root exit points, and their expression of *Krox20* and/or *Prss56*. They provide a major SC component to the nerve roots and a subset of sensory neurons and glial satellite cells to the dorsal root ganglia. In addition, ventral BC cells act as gatekeepers by preventing the emigration of motor neuron cell bodies to the periphery. In this study, we have discovered that Prss56-traced BC cells crawl along peripheral nerves to the skin where they provide Schwann cells, lanceolate and subepidermal glia and melanocytes. This nerve root-skin duality of BC-derivatives has led our lab to develop a Prss56-based mouse model of type 1 Neurofibromatosis, that faithfully recapitulates the different aspects of this severe disease, including plexiform and cutaneous neurofibromas. Our group is currently investigating the implication of subepidermal glia, which we suspect to be the population at the origin of cutaneous neurofibromas. Very unexpectedly, we discovered that Krox20-traced BC derivatives behave differently. They migrate along the same pathways and during the same period, then detach from nerves and differentiate into mural progenitors which in turn mature into pericytes and vascular smooth muscle cells. These results highlight the molecular and functional heterogeneity within the population of BC cells, as skin glial cells only derive from Prss56-expressing BC cells while mural cells only from Krox20-expressing BC cells. Exploring the molecular cues driving such heterogeneity in this transient cell population at the single-cell level will be the next and exciting step of our research.

Appendix

Unpublished results

Skin progenitor cells do not have the potential to generate functional cortical-like neurons

Following the discovery of the broad neuronal potential of BC-derived SKP grafted into the adult DRG, we decided to explore their regenerative capacity in the CNS in a model of ischemic stroke. Indeed, we believed that such an easily accessible cell type that could be used for autografts represented a promising approach. Moreover, this project was of particular interest for me as a neurology resident planning to specialize in stroke care. Disappointingly, I came to the conclusion that SKP do not have the potential to generate functional neurons *in vitro* after testing several differentiation protocols and *in vivo* when grafted in the injured brain parenchyma. I will detail these results, which will not be published, in the form of an article.

NOT FOR PUBLICATION

Skin progenitor cells do not have the potential to generate functional cortical-like neurons

Gaspard Gerschenfeld[a,b], Renata Santos[a,c], Pernelle Pulh[a], Stéphane Supplisson[a], Fanny Coulpier[a], Patrick Charnay[a] and Piotr Topilko[a]

[a] Ecole Normale Supérieure, PSL Research University, CNRS, Inserm, Institut de Biologie de l'Ecole Normale Supérieure (IBENS), Paris, France.

[b] Sorbonne Université, Collège Doctoral, F-75005 Paris, France

[c] Laboratory of Dynamic of Neuronal Structure in Health and Disease, Institute of Psychiatry and Neuroscience of Paris, INSERM UMRS 1266, University Paris Descartes, Paris, France.

Abstract

Ischemic stroke (IS) afflicts 13 million people each year and is the second leading cause of disability worldwide. There is an unmet need for new therapies beyond rehabilitation, and neuro-restorative strategies. The use of naïve or modified stem cells to reduce the scale of lesion or to promote regeneration appears to be a promising solution. We have recently discovered that the neural crest-derived boundary cap cells, which play an important role in the peripheral nervous system development, give rise in the skin to stem-like progenitor cells (SKP) with neurogenic potential. The purpose of this study was to: (i) explore the *in vitro* potential of SKP to generate mature and functional neurons and (ii) investigate the regeneration potential of these easily accessible cell population in the IS model in mice. For this, we have tested several protocols to differentiate SKP into cortical-like neurons in culture. In parallel, we have set up a robust right middle cerebral artery coagulation IS model, one week after which we grafted a cellular suspension of naïve SKP, SKP differentiated *in vitro* or embryonic cortical neurons. We have shown that while SKP express immature neuronal marker βIII-tubulin, they do not have the potential to generate functional cortical-like neurons *in vitro* defined either by the expression of molecular markers or electrophysiological properties. Moreover, when grafted in the brain one week after a stroke, they exhibit poor survival, do not integrate with the host brain and do not express neuronal markers in stark contrast to embryonic neurons.

1. Introduction

Ischemic stroke (IS) afflicts 13 million people each year and is the second leading cause of disability worldwide [1]. Reperfusion therapy is the current paradigm for IS acute phase treatment, and consists in preventing necrotic extension by removing the arterial clot, either with intravenous thrombolysis and/or mechanical thrombectomy (Figure 1). However, this treatment is only available for about 15% of IS patients, and despite recent advances more than a third of IS patients undergoing reperfusion therapy remain severely disabled [2]. Besides secondary prevention, their only available treatment is rehabilitation, possibly in association with serotonin reuptake inhibitors for motor deficits [3].

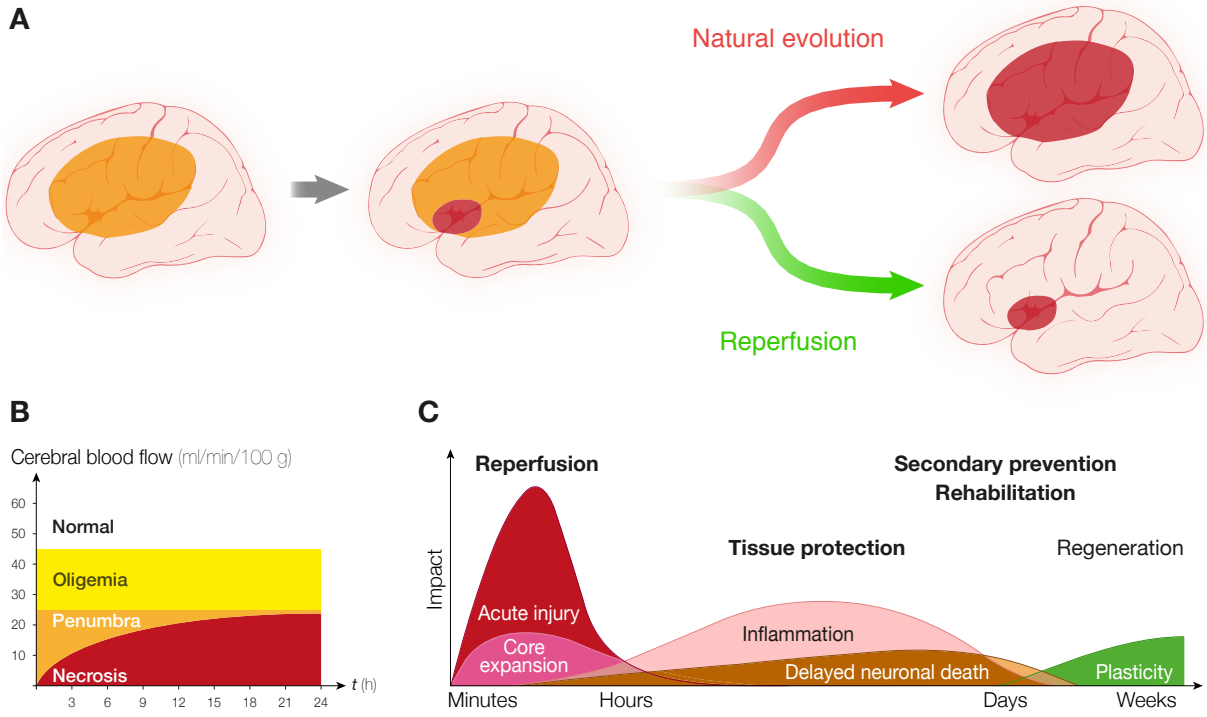

Figure 1. Current ischemic stroke (IS) treatments. (**A-B**) During an ischemic stroke, blood perfusion is no longer compatible with neuronal functioning and survival. Two areas can be distinguished: the already infarcted necrotic core (red) and the still salvable penumbra (orange). Without treatment, the penumbra will progressively become necrotic. Reperfusion strategy consists in removing the obstacle in emergency to save as much as possible of the penumbra, therefore limiting the extension of the constituted infarct. However most patients will always have a remaining infarct. (**C**) Current acute phase stroke treatment strategies consist in reperfusion and tissue protection, for instance by controlling parameters such as arterial blood pressure, blood glucose levels or body temperature. Later, secondary prevention protects from another stroke while rehabilitation can improve functional recovery. Neuroregenerative therapies would be a welcome addition to the therapeutic arsenal to improve functional recovery after a stroke. Adapted from Sinden et al. (2012).

New therapies to improve patient recovery are needed, and recently developed cell-based neuro-restorative strategies appear to be promising. A wide variety of cell types have been tested so far, either in pre-clinical rodent models of stroke or directly in clinical trials in patients [4,5]. The goal was to provide either paracrine trophic support with an indirect beneficial effect on the injured brain, or to directly reconstruct the missing cerebral parenchyma by providing neurons or neural stem cells (NSC) with neurogenic potential. In the paracrine trophic support paradigm, either adipose tissue or bone marrow-derived mesenchymal stem cells (MSC) and mononuclear cells (from the peripheral blood or bone marrow) have been administered in humans either intravenously or intracranially (in the parenchyma). These cells are only transiently present in the brain where they secrete various molecules which have been shown to reduce the inflammatory response, stimulate glial remodelling, angiogenesis and neural plasticity. There have been fewer direct neural repair paradigm studies in man, mainly consisting in intracranial injections of an immortalized NSC [6]. Pre-clinical studies with these cells have shown that while they can generate neurons and promote angiogenesis they have a poor survival rate [7,8]. In rodent models, various types of NSCs and embryonic cortical neurons have been used, included embryonic stem cells (ESC) or induced pluripotent stem cells (iPSC) [9]. Recently, it has been shown that embryonic neurons grafted in adult mouse brains integrated with the host and form stereotypic functional projections [10-13]. It has also been demonstrated that embedding the grafted cells within a biomaterial could improve their survival, promote their differentiation, lower the inflammation and promote reconstruction of destroyed parenchyma even in large strokes [14-16]. In contrast to MSCs which have immunomodulative and pro-angiogenic properties and are only present transiently, these allografts could require long-term immunosuppressive therapy. So far, the only way to perform autografts in IS patients would consist in injecting iPSC derived-NSCs. However, these genetically modified cells present a higher risk of developing tumours, as it has been shown in a mice model [9].

Therefore, there is a need to identify an easily accessible source of non-genetically modified stem cells with neurogenic potential for autografts in IS. Several groups have reported the existence a population of stem-like skin progenitor cells (SKP) with self-renewal and neurogenic properties [17-21]. More recently, we have shown that the neural crest-derived

boundary cap (BC) cells, transiently present at the interface between peripheral and central nervous system (CNS) migrate along nerves to the skin where they give rise to various types of Schwann cells and SKP [22]. The aim of this study was to investigate the regeneration potential of this easily accessible cell population in the IS paradigm in mice. For this, we have tested several *in vitro* differentiation protocols to differentiate SKP into cortical neurons. In parallel, we have set up a right middle cerebral artery coagulation IS model, one week after which we transplanted a cellular suspension of naïve or differentiated *in vitro* SKP or embryonic cortical neurons. We have shown that while SKP adopt multipolar morphology and express immature neuronal marker βIII-tubulin, they do not have the potential to generate functional cortical-like neurons *in vitro* defined either by the expression of molecular markers or electrophysiological properties. Moreover, when grafted in the brain one week after a stroke, oppositely to embryonic neurons they do not express neuronal markers, do not integrate with the host brain and do not survive after a month.

2. Materials and Methods

2.1. Ethical approval and animal management

All mouse lines were maintained in a mixed C57BL6/DBA2 background. We used the following alleles or transgenes as indicated in the original publications: PGK^{Cre} [23], $Rosa26^{tdTom}$ [24]. Day of the plug was considered E0.5. Nude mice from Janvier Labs were used for transplantation experiments. All animal manipulations were approved by a French Ethical Committee (Project Ce5/2016/3996) and were performed according to French and European Union regulations.

2.2. Skin progenitor cell isolation and culture

Sphere cultures were performed from neonatal $PGK^{Cre/+}$, $R26^{tdTom}$ mice as previously described [25]. Briefly, the back skin was carefully dissected free of other tissue and then digested with collagenase/dispase type I (Sigma/Roche) for 2 h at 37°C. Skin samples were then mechanically dissociated and the cell suspension was filtered. Dissociated cells were resuspended at 4.10^4 or 4.10^5 cells/ml, with or without orbital shaking, in DMEM-F12, 3:1 medium containing B-27 without vitamin A supplement (Invitrogen), 20 ng/ml EGF and 40 ng/ml bFGF (both from Sigma), referred to as proliferation medium. Cultures were fed every 4 days, by addition of 1/10 of fresh medium containing growth factors and supplements, and spheres were passaged every 7 days.

2.3. Neuronal differentiation protocols

Two protocols were tested for the induced differentiation into neurons: Noggin patterning and a combined small-molecule inhibition (CSMI, Figure 3). In the first, one week after the second passage spheres were not dissociated but resuspended in DMEM-F12, 3:1 medium containing B-27 without vitamin A supplement (Invitrogen) and 500 ng/ml Noggin (Sigma). Four days later 1/10 of fresh medium was added to feed the cultures. After one week of Noggin treatment, spheres were dissociated and cells either grafted or plated either on Matrigel- or laminin-poly-L-ornithine coated coverslips ($1.5.10^5$ cells per well in a Nunc 4-well plate). Cells were then cultured for up to two weeks in DMEM-F12 + GlutaMax medium supplemented

with N2/B27 (all from Life Technologies), 20 ng/ml BDNF, 20 ng/ml GDNF, 250 µg/ml cAMP, 200 µM Ascorbic acid and 1 µg/ml Laminin (all from Sigma) and Penicillin-Streptomycin (Life Technologies). Medium was replaced twice a week. In the second protocol, adapted from a published protocol [26], spheres were dissociated at the second passage and plated on Matrigel- or laminin-poly-L-ornithine coated coverslips ($1.5.10^5$ cells per well in a Nunc 4-well plate). Differentiation was started in knockout DMEM supplemented with 15% knockout serum replacement, 1 mM L-glutamine, 100 µM MEM nonessential amino acids and 0.1 mM β-mercaptoethanol. The following inhibitors were used: LDN193189 (250 nM; Stemgent), SB431542 (10 µM; Tocris) and XAV939 (5 µM; Tocris) from Day 0 to 3; PD0325901 (8 µM; Tocris), SU5402 (10 µM; Biovision) and DAPT (10 µM; Tocris) from day 1 to 6 (Figure 3). Neurobasal medium supplemented with B27 (NB/B27) and N2 supplements was added in increasing 50% increment every day from day 3, until reaching 100% on day 4. When used for grafts, cells were dissociated at day 4 with TrypLE (Life Technologies) for 10 minutes and resuspended at 5.10^4 cells per µl. Otherwise, cells were cultured for up to 10 days in NB/B27 supplemented with 200 mM L-glutamine, 20 ng/ml BDNF, 250 µg/ml cAMP, 200 µM Ascorbic acid and 1 µg/ml Laminin. Electrophysiological analysis was performed between day 12 and 14 in BrainPhys (StemCell) medium. Cells were fixed after 7 and 14 days of differentiation with 4% PFA for 15 minutes, then washed twice in PBS and stored at 4°C before analysis.

2.4. Electrophysiological analysis

Whole-cell currents were acquired with a Multiclamp 700B amplifier (Molecular Devices) controlled by the Clampex 10 software (Molecular Devices). Currents were filtered at 4 kHz and sampled at 10 kHz using a 1420 Digidata (Molecular Devices). Pipettes had a 3-5 MOhms resistance and were filled with an internal solution (in mM): 155 K-gluconate, 4 KCl, 0.1 EGTA, 5 Mg-ATP, 0.2 pyridoxal 5'-phosphate and 10 HEPES at pH 7.4. Cells were continuously bathed at ~32°C in a solution containing (in mM): 140 NaCl, 2.4 KCl; 2 $CaCl_2$, 1 $MgCl_2$ and 10 HEPES at pH 7.4.

2.5. Culture of mouse embryonic neurons

Neocortex was carefully dissected from E15.5/E17.5 PGK^{Cre}, $Rosa26^{tdTomato}$ embryos and digested in EBSS with 20 $U.ml^{-1}$ Papain, 0.005% DNase (Papain dissociation kit, Worthington) for 25 minutes at 37 °C. Samples were then mechanically dissociated in EBSS with 0.005% DNase and cells were resuspended at 5.10^4 cells per µl in Neurobasal medium (Life Technologies), supplemented with 1X SM1 supplement (Stem Cell), 200 mM GlutaMax (Life Technologies) and 2 mg/ml L-glutamic acid (Sigma). Cells were either used for transplantations, or seeded on poly-L-ornithine coated coverslips (75 µg/ml; Sigma) at 10^5 cells/ml. Culture medium was replaced after five days by BrainPhys supplemented with 1X SM1 supplement (both from Stem Cell). Cells were fixed after 7 and 14 days of culture with 4% PFA for 15 minutes, then washed twice in PBS and stored at 4°C before analysis.

2.6. Ischemic stroke induction and cellular graft

Ischemic stroke was induced by middle cerebral artery (MCA) electrocoagulation as previously described [27]. Briefly, animals were deeply anesthetized with isoflurane 5% and maintained with 2.5% isoflurane in a 70%/30% mixture of NO_2/O_2. Mice were placed in a stereotaxic device, the skin between the right eye and the right ear was incised, and the temporal muscle was retracted. A small craniotomy was performed, the dura was excised, and the middle cerebral artery (MCA) was exposed. The MCA was electro-coagulated before its bifurcation with bipolar forceps, under irrigation, then the craniotomy, muscle and skin were closed. One week later, mice were transplanted in the adjacent cortex with a suspension of 10^5 cells in 2 µl of either naïve SKP dissociated at passage 2, pre-differentiated SKP or embryonic neurons. Two weeks later, mice were injected with a lethal dose of ketamine and xylazine and perfused with saline, followed by a fixative solution containing 4% paraformaldehyde (PFA) in PBS. The brains were carefully dissected and post-fixed in 4% PFA overnight, and cryoprotected overnight in PBS containing 15% sucrose. Serial 50 µm cryosections were prepared and stored at -20°C until analysis.

2.7. Immunohistochemistry and imaging

The following immunostaining protocol was used for cryosections. Sections were incubated for 2h at room temperature with 10 % donkey serum, 0.25 % Triton X-100 in PBS. Primary antibodies were incubated in the same solution overnight at 4 °C and secondary antibodies were incubated for 2 h at room temperature in 1 % donkey serum, 0.25 % Triton X-100 in PBS solution. Sections were counterstained with Hoechst (H3570, Life Technologies) for nuclei detection. Primary antibodies were used at the following dilutions: rabbit anti-RFP (Rockland, 1:1000), -Tbr1 (Abcam, 1:500) and -Tuj1 (BioLegend, 1:1000); goat anti-mCherry (Sicgen, 1:500); and mouse anti-NeuN (Millipore, 1:500). Secondary antibodies were from Jackson Immuno Research. Scaffolds were mounted in 1X PBS under a coverslip for analysis, and optical sections were obtained on a confocal microscope (SP5, Leica). The ImageJ software was used to generate Z-stacks and assemble pictures.

3. Results

3.1. Higher cell plating density and orbital shaking increase SKP amplification

In order to have enough cells to perform the grafting experiments, I modified the protocol used in our lab to produce and amplify SKP [28] based on what had been published to optimize neurosphere cultures from induced pluripotent stem cells [29]. Increasing the cell plating density (from 4.10^4 to 4.10^5 cells/ml) combined with the addition of 40 rpm orbital shaking (Figure 2) resulted in 3.9 times more cells at passage two (P2) when compared with the original protocol. Hence, this modified protocol was used afterwards to produce SKP, which were collected at P2.

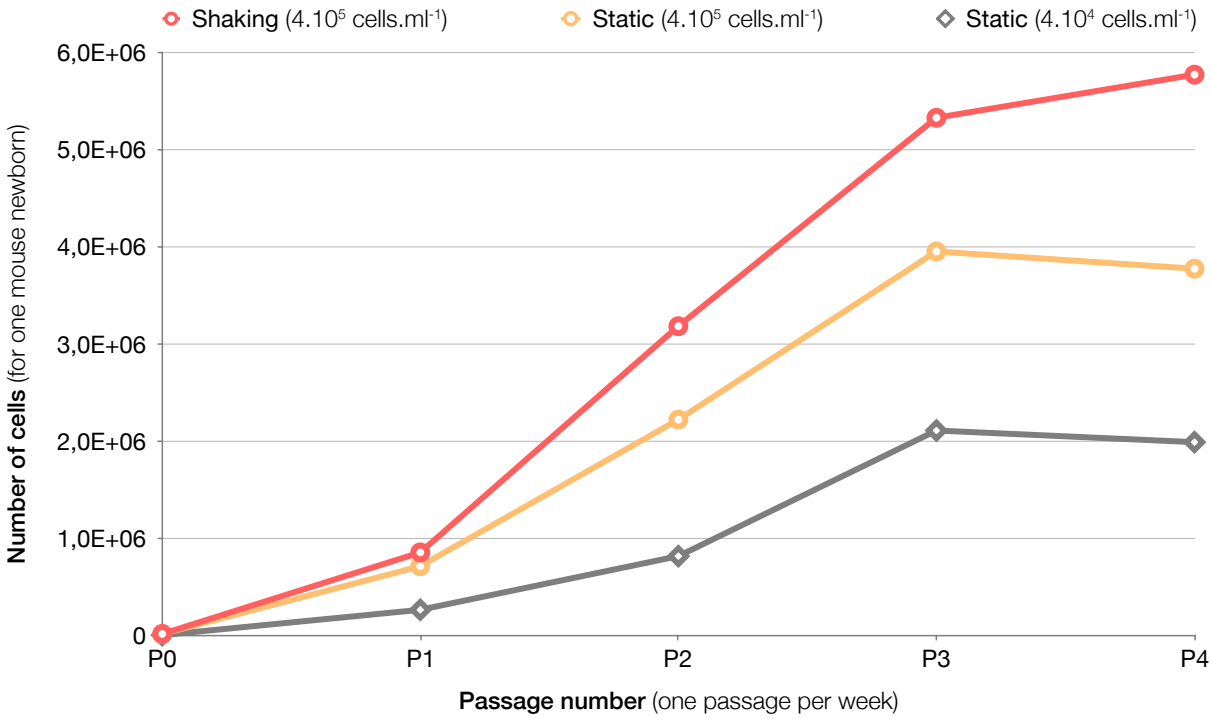

Figure 2. Numbers of SKP at successive passages (P) in floating sphere cultures from newborn skin. Cells were cultured in floating spheres and passaged every week. Increasing the plating concentration to 4.10^5 cells/ml led to a twofold increase in tdTom-positive cells at passage 2. When combined with slow orbital shaking (40 rpm), it led to a threefold increase at passage 2. This condition was further used to prepare the cells.

3.2. SKP do not generate cortical-like neurons in vitro

We tested two in vitro cortical neuronal differentiation protocols on P2 SKP: Noggin patterning on floating spheres and combined small-molecule inhibition (CSMI) on plated cells (Figure 3). Both protocols promote neurogenesis through SMAD inhibition, but the second also includes Wnt inhibition to promote CNS fate and Notch and FGF inhibition to accelerate differentiation. As both protocols yielded similar results in vitro, I will only show results for

CSMI. CSMI inhibition achieved an efficient generation rate of 66% βIII-tubulin (Tuj1, an early pan neuronal marker)-positive cells after 8 days (Figure 3).

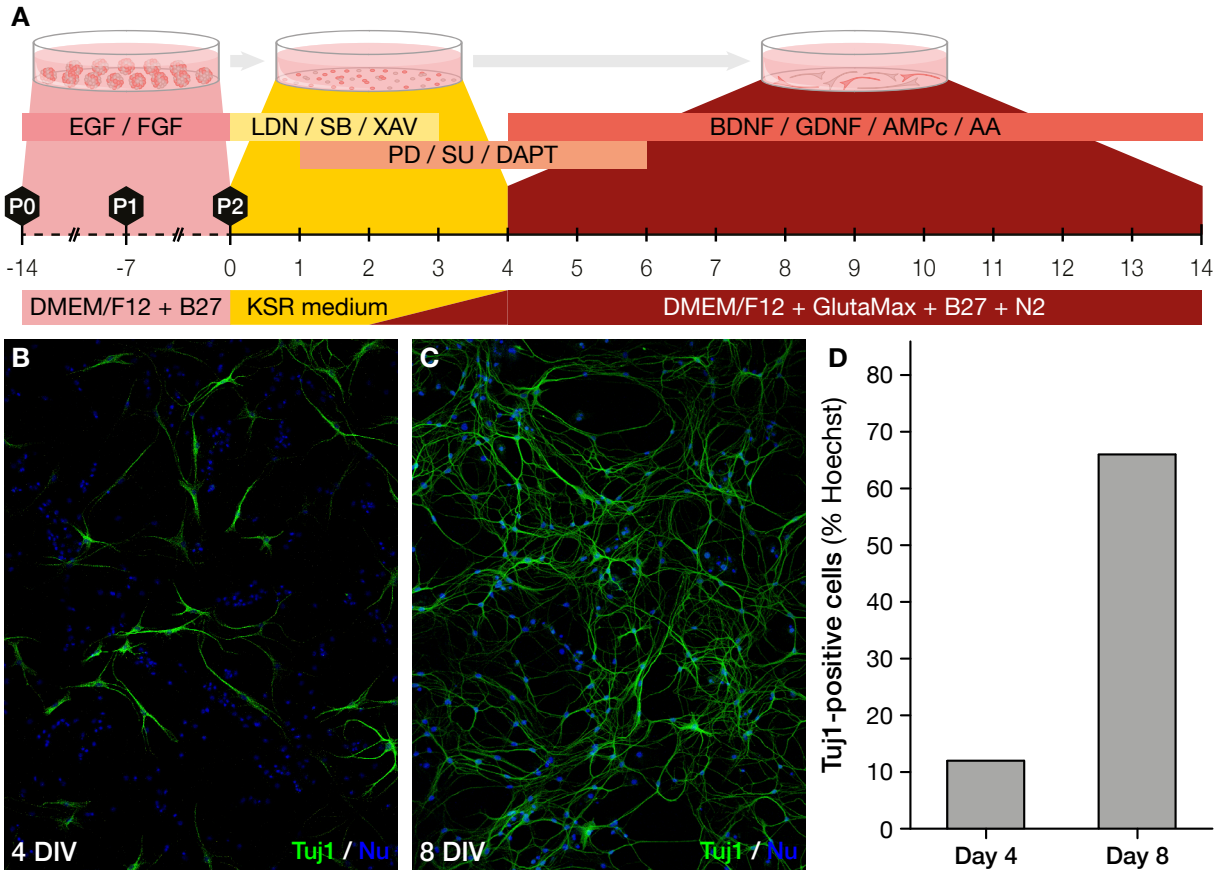

Figure 3. Skin progenitor cells (SKP) express immature neuronal marker Tuj1 *in vitro*. (**A**) After two passages to amplify them, spheres are dissociated, plated on a matrigel coated surface and then cultured for 2 weeks with a specific CNS differentiation medium (detailed in methods). (**B-D**) Confocal imaging after 4 and 8 days of differentiation revealed that the proportion of cells expressing immature neuron marker Tuj1 increased dramatically from 12% to 66%.

However, further analysis confirmed that they did not express neuron-specific transcription factors such as Tbr1 (Figure 4), Ctip2, Reelin or Satb2 (data not shown) contrary to cortical neurons culture. Finally, in collaboration with Stéphane Supplisson (IBENS, Paris), we set up patch clamp experiments to examine whether these cells expressed active conductances and could generate all-or-none action potentials. Most attempts to form a gigaseal between the pipette and the cell membrane failed as these cells displayed an unusually important membrane stiffness. Nevertheless, whole-cell recordings obtained in few trials revealed that: (i) these cells differed from usual neuronal values with a high membrane resistance (3-4 GOhms) and a low membrane capacitance (~10 pF); (ii) in current-clamp mode, applying brief (3-5 ms) depolarizing current steps did not evoke all-or-none action potentials ; (iii) in voltage-clamp

mode, in response to depolarizing voltage steps of 200 ms conductance was linear and activated at voltages superior to -40mV (Figure 4). In the absence of sodium channels and action potential, we concluded that these cells were not functional neurons, and we did not further characterize the active conductance, presumably carried by non-specific voltage-gated potassium channels.

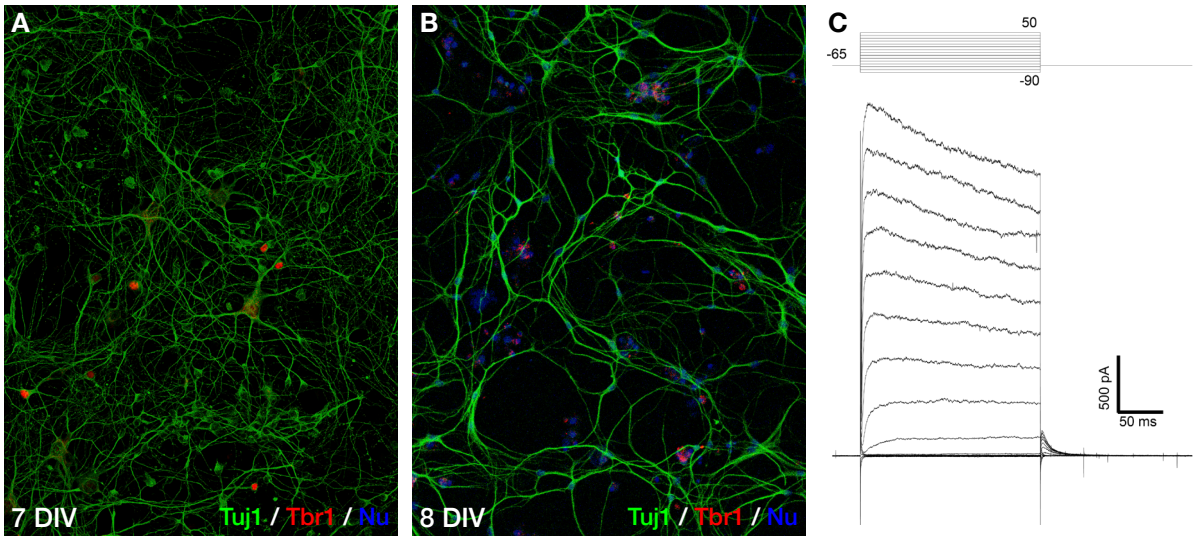

Figure 4. Skin progenitor cells (SKP) do not generate mature neurons *in vitro*. (**A**) After 7 days, embryonic neurons express specific transcription factors such as Tbr1. (**B**) After 8 days of differentiation *in vitro* SKP do not express Tbr1 and display significantly less branching than neurons. (**C**) Current traces recorded under the whole-cell configuration in voltage-clamp mode. Cells were hold at -65 mV and the membrane potential was stepped for 200 ms at potential ranging from -90 mV to +50mV by 10 mV increment. Outward currents with large amplitude were recorded at potentials superior to -40 mV, presumably due to non specific voltage-gated K^+ channels.

3.3. SKP do not generate neurons in vivo

To test their potential to generate neurons *in vivo*, we grafted naïve or pre-differentiated SKP one week after a MCA electrocoagulation IS, in the dorsally adjacent cortex. Experiments with naïve SKP had shown that they did not differentiate into neurons when grafted (data not shown), which led us to graft pre-differentiated SKP. As a positive control, we grafted dissociated tdTomato-positive neurons isolated from somatosensory embryonic cortex at E16.5 (Figure 5). After 11 days, we observed tdTomato-positive cells in the lower cortical layer, and multiple tdTomato-positive projections in the corpus callosum, the ipsi and contra-lateral cortexes and the striatum. We then grafted pre-differentiated SKP treated with Noggin or CSMI, which we analyzed after 10 days and one month (Figure 5). In both types of graft, after 10 days we also observed few tdTomato-positive fluorescent cells in the lower cortical layer. However, there wasn't any visible projections outside of the graft. Moreover, grafted cells did not express

post-mitotic neuronal marker NeuN, and after one month there was no remaining grafted cell in most mice.

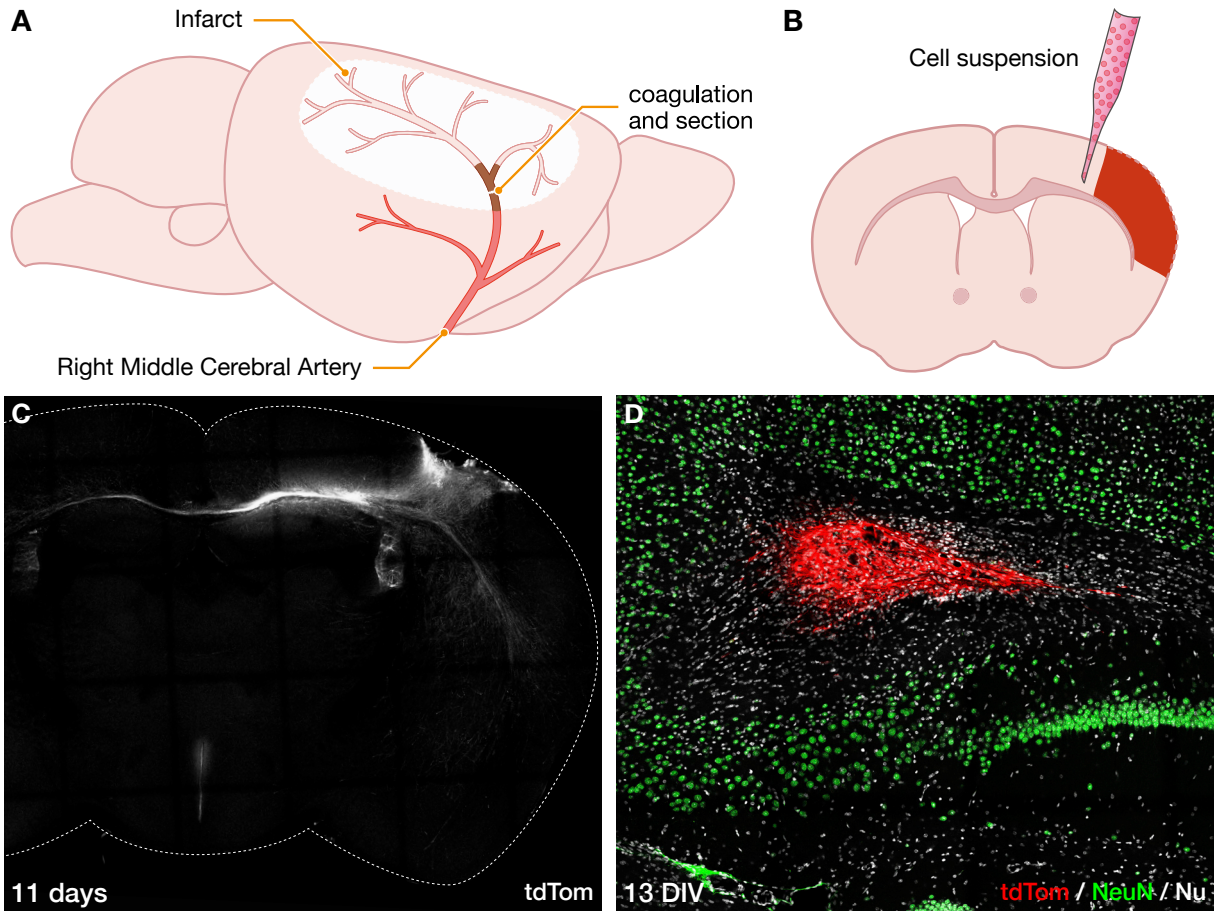

Figure 5. Skin progenitor cells do not differentiate into neurons *in vivo*. (**A-B**) A Stroke regeneration protocol. A superficial cortical stroke is induced by electrocoagulation and section of the right MCA. Graft is performed one week adter by injecting a suspension of either embryonic neurons (E16.5) or pre-dififerentiated SKP. (**C**) Embryonic neurons integrate well with the host brain after 11 days, with numerous projections throughout the brain. (**D**) After 13 days, grafted SKP did not express neuronal markers and there were no visible projections within the host brain.

4. From SKP to biomaterials

In this study, we have found that SKP do not have the potential to generate functional neurons both *in vitro*, with two differentiation protocols, and *in vivo* when transplanted in the brain one week after an IS. These disappoiting results led us to halt this project. However, this also led us to explore the use of biomaterials as a way to encapsulate and graft cell in the IS paradigm, as various biomaterials have been described to enhance cell survival and promote tissue regeneration after a lesion. We set up a surgical procedure in which one week after the stroke the necrotic tissue was removed by suction. Then, we developed a three-step approach to assess the usefulness of biomaterial to culture and manipulate embryonic neurons (Figure 6). First, we transplanted 2-3 mm^3 explant of embryonic cortex (E14.5) in the stroke cavity, as it had been shown that such explants efficiently integrates and form projections in the adult mouse brain in the case of a simple cortex suction [11]. Indeed, when grafted in the stroke cavity the explant efficiently integrates with the host brain, forming long distance projections in the corpus callosum and the striatum after 10 days. The second step consisted to graft the embryonic neurons cell suspension, that I described previously. The third step was to graft embryonic neurons encapsulated within a biomaterial.

We tested embryonic neurons encapsulation in three types of biomaterials: a commercial hyaluronic acid hydrogel (HyStem), a chitosan-based hydrogel and pullulan/dextran-based scaffolds. HyStem lacked functionalization with adhesion molecules and cross-linker cleavability by the cells, two key properties to promote cell attachment and differentiation. Therefore, we initiated a collaboration with Laurent Corté (ESPCI, Paris) to set up a customized, temperature-controlled gelification hydrogel based on chitosan polysaccharides. Unfortunately, this hydrogel appeared highly unreliable in practice with a variability between each batch, and was toxic for our cells. Finally, we established another collaboration with Didier Letourneur (LVTS, Bichat Hospital), to develop a neuron-compatible biomaterial based on pullulan/dextran that could be transplanted following an IS. The manuscript presented following this section will detail the development and use of this polysaccharide-based scaffold for the culture and manipulation of neurons.

Finally, we grafted pullulan/dextran scaffolds seeded with embryonic neurons one week after an IS following an experimental procedure described above (Figure 6). Twelve days after the graft, the biomaterial did not integrate well with the host brain, with a glial scar around it. Embryonic neurons seeded within it seemed to mostly die and the only cells remaining were GFAP-positive (astrocytes), surrounded by host Iba1-positive microglia. These results led us to focus only on the *in vitro* study presented in the attached manuscript.

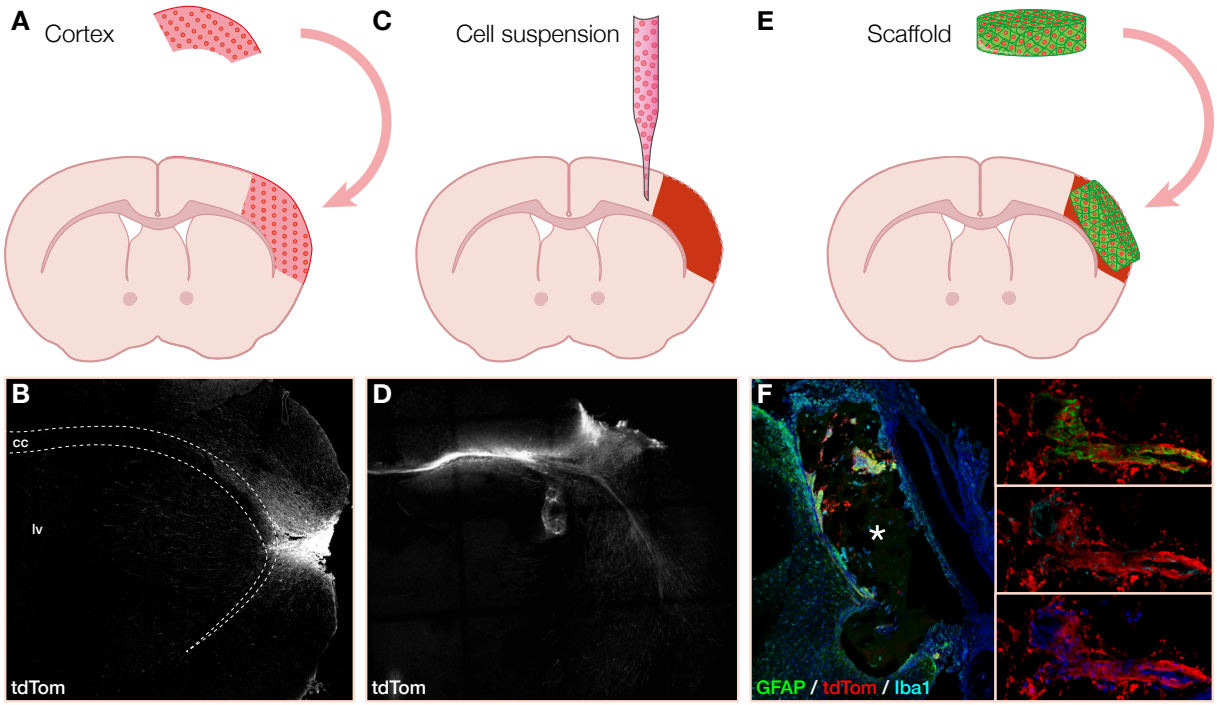

Figure 6. A three step approach to assess the usefulness of a biomaterial. A superficial cortical stroke is induced by electrocoagulation and section of the right MCA. Graft is performed after one week, after removing necrotic parenchyme for the cortex and biomaterial grafts. (**A**-**B**, **D**-**E**) Eleven days after graft, both embryonic cortex (E14.5) or injected embryonic neurons (E16.5) integrate well with the host brain. (**B**, **D**). Twelve days after graft, the PUDNC scaffold (*) does not integrate well with the host brain with a GFAP positive glial scarr around it. Embryonic neurons seeded within seem to mostly die and the only cells remaining are GFAP positive (astrocytes), surrounded by host Iba1 positive microglia.

5. References

[1] V.L. Feigin, M.H. Forouzanfar, R. Krishnamurthi, G.A. Mensah, M. Connor, D.A. Bennett, et al., Global and regional burden of stroke during 1990–2010: findings from the Global Burden of Disease Study 2010, 383 (2014) 245–255. doi:10.1016/s0140-6736(13)61953-4.

[2] M. Goyal, B.K. Menon, W.H. van Zwam, D.W.J. Dippel, P.J. Mitchell, A.M. Demchuk, et al., Endovascular thrombectomy after large-vessel ischaemic stroke: a meta-analysis of individual patient data from five randomised trials, 387 (2016) 1723–1731. doi:10.1016/S0140-6736(16)00163-X.

[3] F. Chollet, J. Tardy, J.-F. Albucher, C. Thalamas, E. Berard, C. Lamy, et al., Fluoxetine for motor recovery after acute ischaemic stroke (FLAME): a randomised placebo-controlled trial, 10 (2011) 123–130. doi:10.1016/S1474-4422(10)70314-8.

[4] O. Detante, A. Jaillard, A. Moisan, M. Barbieux, I.M. Favre, K. Garambois, et al., Biotherapies in stroke, Rev. Neurol. (Paris). 170 (2014) 779–798. doi:10.1016/j.neurol.2014.10.005.

[5] G. Mangin, N. Kubis, Cell Therapy for Ischemic Stroke: How to Turn a Promising Preclinical Research into a Successful Clinical Story, Stem Cell Rev. 17 (2018) 134–18. doi:10.1007/s12015-018-9864-3.

[6] D. Kalladka, J. Sinden, K. Pollock, C. Haig, J. McLean, W. Smith, et al., Human neural stem cells in patients with chronic ischaemic stroke (PISCES): a phase 1, first-in-man study, 388 (2016) 787–796. doi:10.1016/S0140-6736(16)30513-X.

[7] C. Hicks, L. Stevanato, R.P. Stroemer, E. Tang, S. Richardson, J.D. Sinden, In vivo and in vitro characterization of the angiogenic effect of CTX0E03 human neural stem cells, Cell Transplant. 22 (2013) 1541–1552. doi:10.3727/096368912X657936.

[8] J.D. Sinden, I. Vishnubhatla, K.W. Muir, Prospects for stem cell-derived therapy in stroke, Prog. Brain Res. 201 (2012) 119–167. doi:10.1016/B978-0-444-59544-7.00007-X.

[9] K. Oki, J. Tatarishvili, J. Wood, P. Koch, S. Wattananit, Y. Mine, et al., Human-induced pluripotent stem cells form functional neurons and improve recovery after grafting in stroke-damaged brain, Stem Cells. 30 (2012) 1120–1133. doi:10.1002/stem.1104.

[10] M. Terrigno, I. Busti, C. Alia, M. Pietrasanta, I. Arisi, M. D'Onofrio, et al., Neurons Generated by Mouse ESCs with Hippocampal or Cortical Identity Display Distinct Projection Patterns When Co-transplanted in the Adult Brain, Stem Cell Reports. 10 (2018) 1016–1029. doi:10.1016/j.stemcr.2018.01.010.

[11] K.A. Michelsen, S. Acosta-Verdugo, M. Benoit-Marand, I. Espuny-Camacho, N. Gaspard, B. Saha, et al., Area-specific reestablishment of damaged circuits in the adult cerebral cortex by cortical neurons derived from mouse embryonic stem cells, Neuron. 85 (2015) 982–997. doi:10.1016/j.neuron.2015.02.001.

[12] S. Falkner, S. Grade, L. Dimou, K.-K. Conzelmann, T. Bonhoeffer, M. Götz, et al., Transplanted embryonic neurons integrate into adult neocortical circuits, Nature. 539 (2016) 248–253. doi:10.1038/nature20113.

[13] D. Tornero, S. Wattananit, M. Grønning Madsen, P. Koch, J. Wood, J. Tatarishvili, et al., Human induced pluripotent stem cell-derived cortical neurons integrate in stroke-injured cortex and improve functional recovery, Brain. 136 (2013) 3561–3577. doi:10.1093/brain/awt278.

[14] J. Zhong, A. Chan, L. Morad, H.I. Kornblum, G. Fan, S.T. Carmichael, Hydrogel matrix to support stem cell survival after brain transplantation in stroke, Neurorehabil Neural Repair. 24 (2010) 636–644. doi:10.1177/1545968310361958.

[15] P. Moshayedi, L.R. Nih, I.L. Llorente, A.R. Berg, J. Cinkornpumin, W.E. Lowry, et al., Systematic optimization of an engineered hydrogel allows for selective control of human neural stem cell survival and differentiation after

transplantation in the stroke brain, Biomaterials. 105 (2016) 145–155. doi:10.1016/j.biomaterials.2016.07.028.

[16] K.I. Park, Y.D. Teng, E.Y. Snyder, The injured brain interacts reciprocally with neural stem cells supported by scaffolds to reconstitute lost tissue, Nat. Biotechnol. 20 (2002) 1111–1117. doi:10.1038/nbt751.

[17] T. Duncan, A. Lowe, K. Sidhu, P. Sachdev, T. Lewis, R.C.Y. Lin, et al., Replicable Expansion and Differentiation of Neural Precursors from Adult Canine Skin, Stem Cell Reports. 9 (2017) 557–570. doi:10.1016/j.stemcr.2017.07.008.

[18] U. Etxaniz, A. Pérez-San Vicente, N. Gago-López, M. García-Dominguez, H. Iribar, A. Aduriz, et al., Neural-competent cells of adult human dermis belong to the Schwann lineage, Stem Cell Reports. 3 (2014) 774–788. doi:10.1016/j.stemcr.2014.09.009.

[19] C.E. Wong, C. Paratore, M.T. Dours-Zimmermann, A. Rochat, T. Pietri, U. Suter, et al., Neural crest-derived cells with stem cell features can be traced back to multiple lineages in the adult skin, J. Cell Biol. 175 (2006) 1005–1015. doi:10.1083/jcb.200606062.

[20] K.J.L. Fernandes, I.A. McKenzie, P. Mill, K.M. Smith, M. Akhavan, F. Barnabé-Heider, et al., A dermal niche for multipotent adult skin-derived precursor cells, Nat Cell Biol. 6 (2004) 1082–1093. doi:10.1038/ncb1181.

[21] K.J.L. Fernandes, N.R. Kobayashi, C.J. Gallagher, F. Barnabé-Heider, A. Aumont, D.R. Kaplan, et al., Analysis of the neurogenic potential of multipotent skin-derived precursors, Exp. Neurol. 201 (2006) 32–48. doi:10.1016/j.expneurol.2006.03.018.

[22] A. Gresset, F. Coulpier, G. Gerschenfeld, A. Jourdon, G. Matesic, L. Richard, et al., Boundary Caps Give Rise to Neurogenic Stem Cells and Terminal Glia in the Skin, Stem Cell Reports. 0 (2015) 278–290. doi:10.1016/j.stemcr.2015.06.005.

[23] Y. Lallemand, V. Luria, R. Haffner-Krausz, P. Lonai, Maternally expressed PGK-Cre transgene as a tool for early and uniform activation of the Cre site-specific recombinase, Transgenic Res. 7 (1998) 105–112.

[24] L. Madisen, T.A. Zwingman, S.M. Sunkin, S.W. Oh, H.A. Zariwala, H. Gu, et al., A robust and high-throughput Cre reporting and characterization system for the whole mouse brain, Nat. Neurosci. 13 (2010) 133–140. doi:10.1038/nn.2467.

[25] A. Gresset, F. Coulpier, G. Gerschenfeld, A. Jourdon, G. Matesic, L. Richard, et al., Boundary Caps Give Rise to Neurogenic Stem Cells and Terminal Glia in the Skin, Stem Cell Reports. 5 (2015) 278–290. doi:10.1016/j.stemcr.2015.06.005.

[26] Y. Qi, X.-J. Zhang, N. Renier, Z. Wu, T. Atkin, Z. Sun, et al., Combined small-molecule inhibition accelerates the derivation of functional cortical neurons from human pluripotent stem cells, Nat. Biotechnol. 35 (2017) 154–163. doi:10.1038/nbt.3777.

[27] G. Llovera, S. Roth, N. Plesnila, R. Veltkamp, A. Liesz, Modeling stroke in mice: permanent coagulation of the distal middle cerebral artery, J Vis Exp. (2014) e51729. doi:10.3791/51729.

[28] J. Biernaskie, M. Paris, O. Morozova, B.M. Fagan, M. Marra, L. Pevny, et al., SKPs derive from hair follicle precursors and exhibit properties of adult dermal stem cells, Cell Stem Cell. 5 (2009) 610–623. doi:10.1016/j.stem.2009.10.019.

[29] O. Mohamad, S.P. Yu, D. Chen, M. Ogle, M. Song, L. Wei, Efficient neuronal differentiation of mouse ES and iPS cells using a rotary cell culture protocol, Differentiation. 86 (2013) 149–158. doi:10.1016/j.diff.2013.12.002.

Article three

Development and use of a 3D macroporous polysaccharide-based scaffold for neuronal culture

This study is the result of my work on the potential of skin progenitor cells to repair the brain parenchyma after a stroke. Indeed, during this project I started a collaboration with the group of Didier Letourneur (LVTS, Bichat Hospital, Paris) to set up a biomaterial compatible with neuronal culture to graft cells of interest. Initially, culture of embryonic neurons within non-functionalized scaffolds yielded a poor survival, neuronal attachment and neurite outgrowth. Based on these observations, we optimized the mechanical properties of the scaffold and functionalized it with freeze-dried laminin to enhance neuronal attachment to the scaffold and neurite outgrowth. We are currently submitting the article describing this *in vitro* study. As I mentioned in the previous section, grafts of embryonic neurons within this scaffold after stroke were unsuccessful both in terms of neuronal survival and biomaterial integration, which led us to focus on the *in vitro* work.

Development and use of a 3D macroporous polysaccharide-based scaffold for neuronal culture

Gaspard Gerschenfeld[a,b], Rachida Aid-Launais[c], Soraya Lanouar[c,d], Patrick Charnay[a], Didier Letourneur[c,d] and Piotr Topilko[a,*]

[a] Ecole Normale Supérieure, PSL Research University, CNRS, Inserm, Institut de Biologie de l'Ecole Normale Supérieure (IBENS), Paris, France.

[b] Sorbonne Université, Collège Doctoral, F-75005 Paris, France

[c] Laboratoire de recherche vasculaire translationnelle, INSERM UMR 1148 and Université Paris Diderot, Paris, France.

[d] Institut Galilée, Université Paris 13, Villetaneuse, France.

*Corresponding author. Piotr Topilko, Ecole Normale Supérieure, PSL Research University, CNRS, Inserm, Institut de Biologie de l'Ecole Normale Supérieure (IBENS), Paris,France. Email: topilko@biologie.ens.fr. Phone: +33 1 44 32 39 84. Fax: +33 1 44 32 39 88.

Key words: embryonic neurons
porous scaffold
polysaccharide
tissue regeneration
pullulan-dextran

Abstract

Central nervous system (CNS) lesions are a leading cause of death and disability worldwide. Given the often-associated tissue loss, biomaterials represent an interesting approach for CNS repair. Herein, we describe the development and use of pullulan/dextran polysaccharide-based scaffolds for neuronal culture. First, we modified scaffold properties by changing the concentration (1%, 1.5% and 3% (w/w)) of the cross-linking agent, sodium trimetaphosphate (STMP). The lower STMP concentration (1%) allowed us to generate scaffolds with higher porosity (59.9±4.6%), faster degradation rate (5.11±0.14 mg/min) and lower elastic modulus (384±26 Pa) compared to the 3% STMP scaffolds (47±2.1%, 1.39±0.03 mg/min, 916±44 Pa, respectively). In 3D culture, we observed that embryonic neurons within the scaffolds remained in aggregates and did not attach nor spread or differentiate. To enhance neuronal adhesion and neurite outgrowth, we then functionalized the 1% STMP scaffolds with laminin. Laminin in solution (100 μg/ml) was added with or without a subsequent freeze-drying step. The addition of freeze-drying created a laminin mesh network within the scaffold that significantly enhanced embryonic neurons adhesion, neurite outgrowth and survival when cultured within the scaffold for several days. Hence, these scaffolds represent a potentially interesting neuron-compatible and biodegradable biomaterial to be explored in CNS transplantation experiments.

Statement of significance

Central nervous system (CNS) injuries are often followed by a loss of tissue, which prevents proper functional recovery. Tissue engineering approaches could help in developing scaffolds to reconstruct the lost tissue and improve recovery. Many materials have been developed, but few are composed on natural biodegradable polymers already used in humans. In this study, we have developed a scaffold based on a combination of two polysaccharides, pullulan/dextran, to allow neuronal 3D culture. We have characterized them in terms of stiffness, porosity and embryonic neurons adhesion, neurite growth and survival. In the future, such a biomaterial could be transplanted in the CNS to promote its regeneration.

Graphical abstract

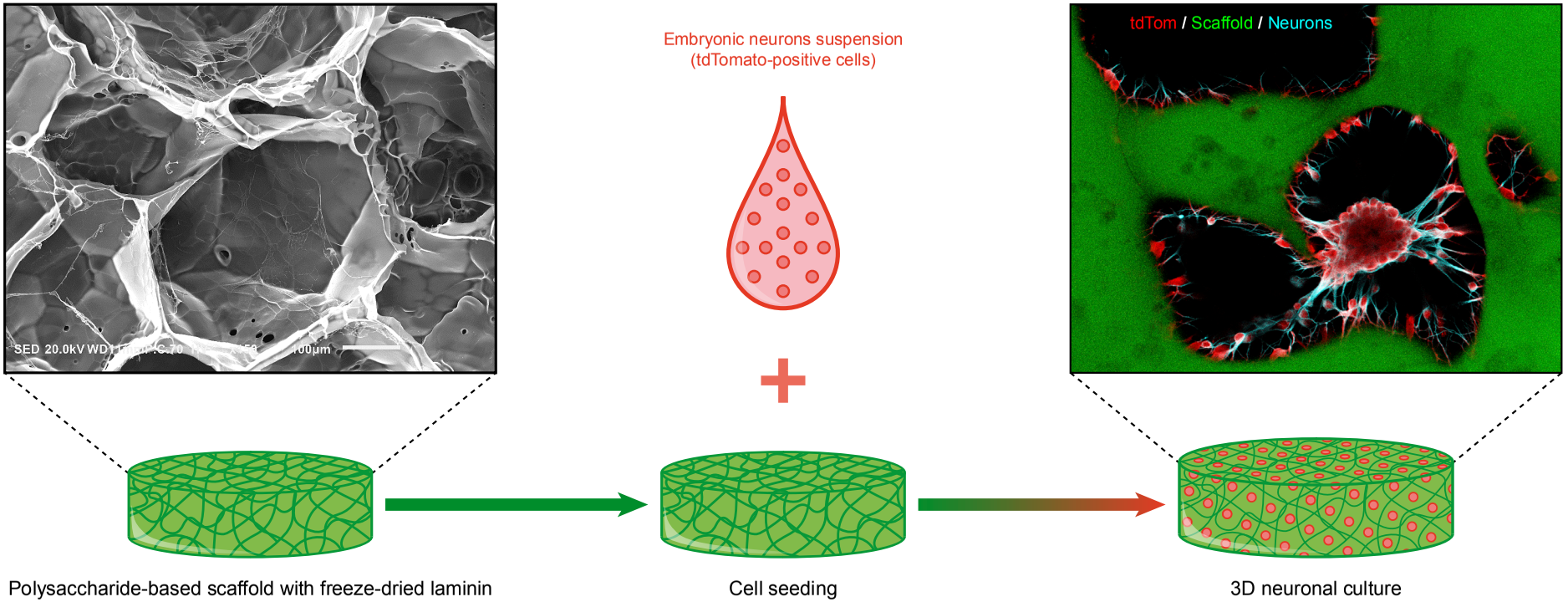

1. Introduction

Central nervous system (CNS) lesions such as stroke and traumatic brain injury (TBI) are leading causes of death and disability worldwide, afflicting millions of people each year [1,2]. Despite recent advances in acute phase treatments and management, there is an unmet need for new therapies beyond rehabilitation. In the CNS, tissue damage triggers diverse multi-cellular responses, associated with an acute inflammatory response glial scar, that evolve over time and lead to neuronal death and the formation of a cavity devoid of any extracellular matrix (ECM), which is associated with functional disability [3-5]. Filling this cavity with a biomaterial to modulate inflammation and promote vascularization may have a beneficial effect on the repair process. Neuro-restorative strategies are needed, and biomaterials represent an interesting approach to help rebuild the lost parenchyma and restore neurological function as a mechanical scaffold for cellular invasion [6]. Indeed, reconstructing the lost neuronal tissue allows, at least partially, to recreate lost neuronal connections, which in turn might improves the functional outcome [7]. Key requirements for any biomaterial are its biocompatibility, its non-immunogenicity, its biodegrability and its functionalization potential. Different types of liquid hydrogels based on hyaluronic acid [8], methylcellulose [9], polyacrylamide [10] or urinary bladder matrix [11] have been explored in CNS transplantation experimental paradigms *in vivo*. Their major advantage is their liquid form that allows to inject them in the CNS, where they solidify *in situ*. Another approach has focused on developing already preformed scaffolds that could be transplanted, such as dextran [12], gelatin [13], polyglycolic acid [14] or alginate and carboxymethyl-cellulose [15]. Compared to liquid hydrogels, they offer a better control of the gelification process and therefore of their mechanical properties, which is important for the biological responses, especially when scaling up for larger animals. Contrary to other applications, such as bone repair, biomaterials used in the CNS requires further functionalization to improve its biocompatibility and repairing potential [16]. Different types of functionalization have been explored, either by adding ECM molecules such as laminin or poly-L-lysin [12,15], the IKVAV [9] or RGD [8] adhesion peptides, the N-Cadherin [13] or integrins [17] attachment molecules. Their addition enhances cell adhesion, neurite outgrowth and improves revascularization both *in vitro* and *in vivo* transplantation assays.

In this work, we have developed a hydrogel based on two naturally-derived polymers: pullulan, a linear polysaccharide produced from starch fermentation by the fungus *Aureobasidium pullulan*, which consists of glucose units linked through α1,6- and α1,4-glucosidic bonds, and dextran, a polysaccharide synthesized from sucrose by bacteria, which is composed of glucose units joined mostly by α1,6-glycosidic bonds, with α1,2-, α1,3-, or α1,4- side chains [18-20]. Both are hydrophilic, neutral and nonimmunogenic polymers biochemically similar to the ECM, that can be degraded by enzymes present in most mammalian tissues [21]. Both can also be functionalized to adapt their physical and biological properties depending on specific needs [22]. Moreover, both are already used in humans, for instance as a plasma expander (dextran) or as capsules in pharmaceutical products (pullulan) [23]. To prepare porous polysaccharide-based hydrogels, we have developed a freeze-drying cross-linking process based on sodium trimetaphosphate (STMP), a non-toxic cyclic triphosphate already used to cross-link food grade starches [19,24]. We have already validated these polysaccharide-based scaffolds in several applications such as vascular grafts [21], endothelial cell [25] or vascular smooth muscle cell culture [20], mesenchymal stem cell delivery into myocardial infarction [26], and bone defect repair [16], but its use to repair the nervous system has never been explored.

The aim of this study was to explore the potential of new macroporous polysaccharide-based scaffolds for the culture and manipulation of embryonic neurons. For this, we have prepared and tested several formulations with different STMP concentrations (1%, 1.5% and 3%), with or without laminin functionalization. After assessing their mechanical properties and in vitro biodegradability, we have studied their capacity to promote the surviving and maturation of embryonic neurons. We have shown that softer scaffolds with 1% STMP (w/w), when functionalized with laminin, better support neuronal attachment, neurite outgrowth and survival, making them an interesting material as implantable scaffold for the CNS.

2. Materials and Methods

2.1. Porous scaffold synthesis

Polysaccharide-based scaffolds were prepared using a mixture of pullulan/dextran in water [20,27] (pullulan, MW 200,000, Hayashibara; dextran, MW 500,000, Pharmacosmos). 40% sodium carbonate (w/w) was added to the mixture as a porogen agent. Polysaccharides chemical cross-linking was carried out using three concentrations of 1%, 1.5% and 3% sodium trimetaphosphate (STMP) in 1M sodium hydroxide, referenced as Matrix 1%, 1.5% and 3%, respectively. Scaffolds were incubated at 50°C for 15 minutes, then cut into the desired shape (5 mm diameter, 350 µm thickness) before being immersed in 20% acetic acid for gas foaming and extensively washed in water. Finally, scaffolds were freeze-dried and stored at room temperature. One percent fluorescein isothiocyanate (FITC)-dextran was added to the solution as a fluorescent tracer for confocal microscopy. For functionalization studies, some of the freeze-dried Matrix 1% formulations were simply impregnated with laminin (Matrix 1% L) in solution at 100µg/ml, (Sigma-Aldrich), or with laminin plus another freeze-drying step (Matrix 1% L-FD).

2.2. Scaffolds characterization

2.2.1. Morphology and porosity

Structure of the dried polysaccharide-based scaffolds was analyzed by scanning electron microscopy (SEM) using a JOEL CarryScope after sputtering with gold. Samples were observed in secondary electron mode at an accelerating voltage of 20 kV. Scaffolds prepared with 1% FITC-dextran were analyzed by confocal microscopy (Carl Zeiss® LSM 780, 10X objective, 2x2 tile scan and Z-stack 70 µm image acquisitions) after hydration in PBS. Porosity was computed with the ImageJ® software.

2.2.2. Phosphorus content

Phosphorus content of polysaccharide-based scaffolds was quantified according to a colorimetric method [28]. About 2 mg of each scaffold were degraded in 1 mL of 10% nitric acid at 105 °C for 3 hours. Subsequently, 0.4 mL of 14.7 M nitric acid, 2 mL of 10 mM ammonium

metavanadate and 2 mL of 40 µM ammonium pentaphosphoric acid molybdate were added to scaffold lysates. The phosphorus content was finally determined according to a calibration curve based on phosphoric acid.

2.2.3. Swelling behavior

Hydrogels swelling behavior was assessed in water and in phosphate buffered saline (PBS). The freeze-dried scaffolds were weighted before and after hydration for at least 24 h. Samples soaked in water or PBS were weighted after removal of excess solvent. To determine the swelling ratio the following equation was used: Sw = (Ws – Wi) / Wi [29]. Where Sw is the swelling ratio, Ws and Wi are sample weights in swollen and dry states respectively.

2.2.4. In vitro degradation

Four samples of each formulation were investigated for *in vitro* enzymatic degradation. After complete hydration in PBS, samples were incubated in a pullulanase and dextranase mixture (10% and 5% v/v respectively) at 37°C. The immersed samples were weighted every 5 minutes until no relevant mass loss was observed. At each time point, the percentage of residual mass (Wt) was calculated according to the following equation: Wt = (Wa / Wb) x 100; Wb is the mass of the scaffolds before degradation and Wa is the residual mass at each time. Degradation rate was calculated using the slope of the degradation curves.

2.2.5. Rheological study

Hydrogel disks of 4 cm diameter and about 1 mm height where prepared and hydrated in PBS for mechanical testing. Shear oscillatory measurements were performed on a Discovery HR2 (TA Instrument) equipped with a stainless steel 40 mm diameter crosshatched geometry. Both base and geometry surfaces were rough in order to avoid sample slipping during acquisitions. Axial force was defined at 0.2N for all measurements. First, the linear viscoelasticity domain was determined along a deformation from 0.01 to 10% of (data not shown). Then storage (G') and viscous (G'') moduli were recorded according a frequency range of 0.05–5 Hz at a fixed deformation of 0.1%. The average value of the storage and loss moduli were measured at least three times and are given here at 1Hz frequency.

2.3. Culture of mouse embryonic neurons

2.3.1. Ethical approval and animal management

All mouse lines were maintained in a mixed C57BL6/DBA2 background. We used the following alleles or transgenes as indicated in the original publications: PGK^{Cre} [30], $Rosa26^{tdTom}$ [31]. Day of the plug was considered E0.5. All animal manipulations were approved by a French Ethical Committee (Project Ce5/ 2016/3996) and were performed according to French and European Union regulations.

2.3.2. Isolation and culture of mouse embryo cortical neurons

Neocortex was carefully dissected from E15.5/E17.5 PGK^{Cre}, $Rosa26^{tdTomato}$ embryos and digested in EBSS with 20 $U.ml^{-1}$ papain, 0.005% DNase (Papain dissociation kit, Worthington) for 25 minutes at 37 °C. Samples were then mechanically dissociated in EBSS with 0.005% DNase and cells were resuspended at 5.10^4 cells per µl in Neurobasal medium (Life Technologies), supplemented with 1X SM1 supplement (Stem Cell), 200 mM L-Glutamine and 1X penicillin-streptomycin (both from Life Technologies). Finally, cells were seeded on macroporous scaffolds at 3.10^5 cells per disk. Culture medium was replaced after five days by BrainPhys supplemented with 1X SM1 supplement (both from Stem Cell).

2.3.3. Immunohistochemistry and imaging

Scaffolds were fixed in 4 % paraformaldehyde (PFA) in phosphate buffered saline solution (PBS) at room temperature (RT) for 15 minutes and then washed and stored in PBS at 4°C. The following immunostaining protocol was used. Scaffolds were incubated for 1 h at room temperature with 10 % donkey serum, 0.25 % Triton X-100 in PBS. Primary antibodies were incubated in the same solution overnight at 4 °C and secondary antibodies were incubated for 2 h at room temperature in 1 % donkey serum, 0.25 % Triton X-100 in PBS solution. Scaffolds were counterstained with Hoechst (H3570, Life technologies) for nuclei detection. Primary antibodies were used at the following dilutions: rabbit anti-DCX (Abcam, 1:200), -Ki67 (Abcam, 1:200) and -Tbr1 (Abcam, 1:500), -Tuj1 (BioLegend, 1:1,000); goat anti-mCherry (Sicgen, 1:500); and mouse anti-NeuN (Millipore, 1:500). Secondary antibodies were from

Jackson Immuno Research. Scaffolds were mounted in 1X PBS under a coverslip for analysis, and optical sections were obtained on a confocal microscope (SP5, Leica). The ImageJ software was used to generate Z-stacks and assemble pictures.

2.3.4. Cell quantification

Four to height scaffolds (4 mm diameter) of each formulation were used to count cells after one, four and seven days of culture. Scaffolds were digested in a pullulanase and dextranase mixture (10% and 5% v/v respectively) at 37°C for 25 minutes, and then mechanically dissociated. Cell count was performed using a Countess II automated cell counter (Invitrogen).

2.4. Statistical analysis

All results are presented as mean ± standard deviation (SD). All experiments were performed at least in triplicate. GraphPad Prism® 5.0 software was used to perform statistical analysis using one-way ANOVA test with Tukey post-test for phosphorus content and degradation rate, 2-way ANOVA test with Bonferroni post-test for swelling ratio, degradation kinetics and MannWitney post-test for rheology measurement. Statistical significance is denoted as * $p < 0.05$; ** $p < 0.01$; *** $p < 0.001$.

3. Results

3.1. Hydrogel morphology and porosity are correlated to the STMP concentration

3D porous polysaccharide-based scaffolds were prepared by a chemical cross-linking process with STMP, and sodium carbonate as a porogen agent and then freeze-dried. Three formulations were prepared with 1%, 1.5% and 3% (w/w) STMP concentrations, and referenced as 1%, 1.5% and 3% matrices, respectively. Analysis by scanning electron microscopy (SEM) of scaffold surfaces and sections confirmed the presence of pores with a smooth and homogeneous wall surface in the three formulations (Fig. 1A-F). Gross scaffold morphology varied depending on STMP concentration, with the surface of 3% matrices that appeared denser and smoother. Porosity analysis based on the pore area and the total scaffold area ratio was obtained from confocal acquisitions using FITC-Dextran in the formulations. While there was no significant difference in porosity between 1% and 1.5% matrices (59.9 ± 4.6% and 58.8 ± 4% respectively), 3% matrices (47 ± 2.1%) displayed the lowest porosity. Since cross-linking is obtained through phosphate bridge formation between polysaccharide chains, the cross-linking ratio can be assessed by the phosphate content. Scaffold phosphorus content quantified by a colorimetric assay was positively correlated with the introduced STMP concentrations (Table 1). Indeed, Matrix 3% had significantly more phosphorus content (236 ± 7 µmol/g of dried scaffold) than Matrix 1.5% (108 ± 5 µmol/g) and Matrix 1% (84 ± 1 µmol/g).

Formulations	Phosphorus content (µmol/g)		Degradation rates (mg/min)	
Matrix 1%	84 ± 1	***	5.11 ± 0.14	***
Matrix 1.5%	108 ± 5	***	3.83 ± 0.12	***
Matrix 3%	236 ± 7	***	1.39 ± 0.03	***

Table 2. Physicochemical characterization of 1%, 1.5% and 3% matrices. Phosphorus content of pullulan/dextran scaffolds prepared with 1%, 1.5% and 3% (w/w) of STMP is presented as mean values ± standard deviation (SD) from dried state. Four samples were analyzed for each formulation. Degradation rates were calculated using the slope from the degradation curves of scaffolds prepared with 1%, 1.5% and 3% (w/w) of STMP, the cross-linking agent. Once incubated in the pullulanase/dextranase solution, samples were weighted every 5 minutes to measure the residual mass. Four samples were analyzed for each experiment. *** $p < 0.001$.

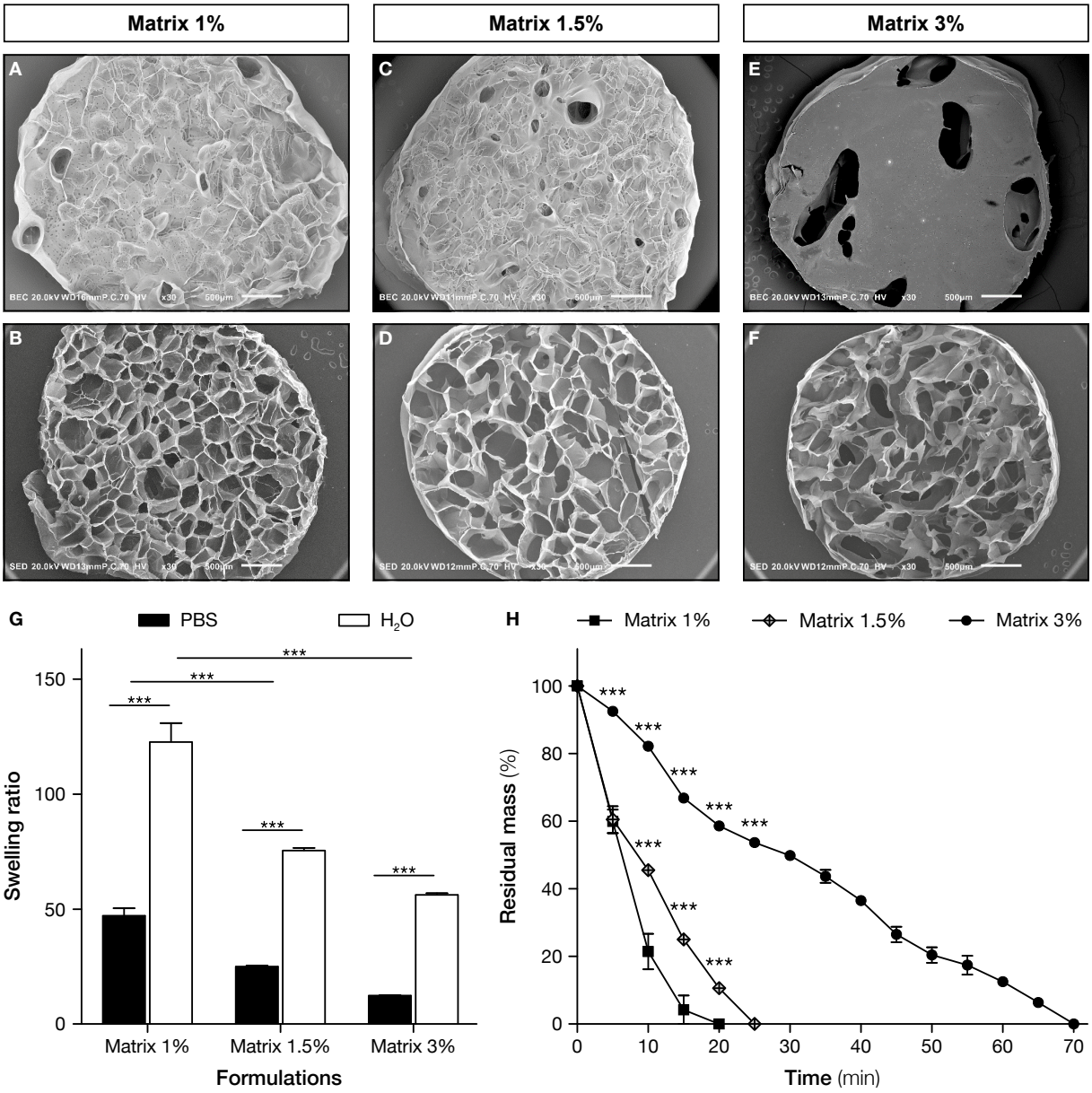

Figure 1. Scaffolds morphology and structure. (**A**-**F**) Scanning electron micrographs of pullulan/dextran scaffolds prepared with 1%, 1.5% and 3% (w/w) of STMP, the cross-linking agent. Top view of either scaffolds surface (A, C and E) or section (B, D and F). Scale bars: 500 µm. (**G**) Swelling behavior of pullulan/dextran scaffolds prepared with 1%, 1.5% and 3% (w/w) of STMP. Samples were hydrated in PBS or water until maximum hydration was reached. Results are presented as mean values ± SD from dried state. Four samples were analyzed for each formulation. (**H**) *In vitro* enzymatic degradation kinetics of scaffolds prepared with 1%, 1.5% and 3% (w/w) of STMP, the cross-linking agent. Once incubated in the pullulanase/dextranase solution, samples were weighted every 5 minutes to measure the residual mass. Four samples were analyzed for each time point. *** $p < 0.001$, ** $p < 0.005$.

3.2. Swelling behavior and rheological analysis

Next, to assess the physical hydrogel properties, their swelling ratio was measured before and after complete hydration in PBS and in water (Fig. 1G). A significant difference was noted between the swelling in PBS and in water for the three formulations, the swelling being higher

in water. In PBS the swelling ratio was significantly higher for 1% and 1.5% matrices than for 3% matrices (47 ± 6, 25 ± 1 and 12 ± 0.4 respectively). A similar significant difference was observed in water for 1%, 1.5% and 3% matrices (123 ± 16, 77 ± 2 and 56 ± 2 respectively). Therefore, the swelling ratio of these scaffolds is inversely correlated to the concentration of the crosslinking agent.

Mechanical properties of 1%, 1.5% and 3% matrices were also investigated by rheological measurements (Table 2). Storage G' and loss G'' moduli average of all conditions are given at a 1Hz frequency. For each formulation, G' was more than one order of magnitude higher than G''. Both moduli G' and G'' increased with the increase of STMP concentration. The elastic modulus measured in Matrix 3% was 1.4 times higher than in Matrix 1.5% (916 ± 44 Pa and 639 ± 10 respectively) and 2.4 times higher than Matrix 1% (384 ± 26 Pa). Hence, hydrogel stiffness was positively correlated to the crosslinking ratio.

Formulations	G' (Pa)		G'' (Pa)	
Matrix 1%	384 ± 26	**	27 ± 9	**
Matrix 1.5%	639 ± 10	***	36 ± 1	***
Matrix 3%	916 ± 44	**	44 ± 1	**

Table 2. Rheological characterization. Elastic (G') and viscosity (G'') moduli of hydrated pullulan/dextran scaffolds prepared with 1%, 1.5% and 3% (w/w) of STMP, the cross-linking agent. Three samples were analyzed for each formulation. *** $p < 0.001$, ** $p < 0.005$.

3.3. Degradation kinetics

To measure the degradation kinetics, polysaccharide-based scaffolds were degraded *in vitro* using a mixture of pullulanase and dextranase, which digest pullulan and dextran respectively. Measurements were made with the three formulations (matrices 1%, 1.5% and 3%) every ten minutes and degradation was determined by wet weight loss (Figure 1H). STMP concentration was positively correlated to the degradation time. Indeed, the Matrix 3% was degraded in 70 min while complete degradation of the lower cross-linked scaffolds, Matrix 1.5% and 1%, was reached after only 25 and 20 min, respectively. Degradation rates expressed in mg/min (Table 1) calculated from the degradation curves, were thus higher in Matrix 1% and 1.5% compared to Matrix 3% (5.11 ± 0.14 and 3.83 ± 0.12 versus 1.39 ± 0.03 respectively).

3.4. Embryonic neurons form cellular aggregates within the macroporous scaffolds

To assess the polysaccharide-based scaffolds biocompatibility with neuronal culture, we seeded embryonic neurons on matrices 1%, 1.5% and 3% and cultured them for up to four days. After two days of culture, embryonic neurons formed similar aggregates within the pores of each type of scaffold, despite of scaffold morphological differences (Fig. 2). Higher magnification analysis confirmed that while cells regrouped in aggregates, they did not attach directly to the scaffold whatever the STMP content, and there was no significant neurite extension.

3.5. Functionalized scaffolds preparation and characterization

In order to improve neuronal adhesion, Matrix 1% scaffolds that exhibited the optimal stiffness range for neuronal culture [32-34] and higher degradability, were then simply hydrated with a laminin solution (100 µg/ml) during cell seeding (Matrix 1% L), or hydrated with laminin and Freeze-Dried before cell seeding (Matrix 1% L-FD). SEM analysis (Fig. 3) confirmed that

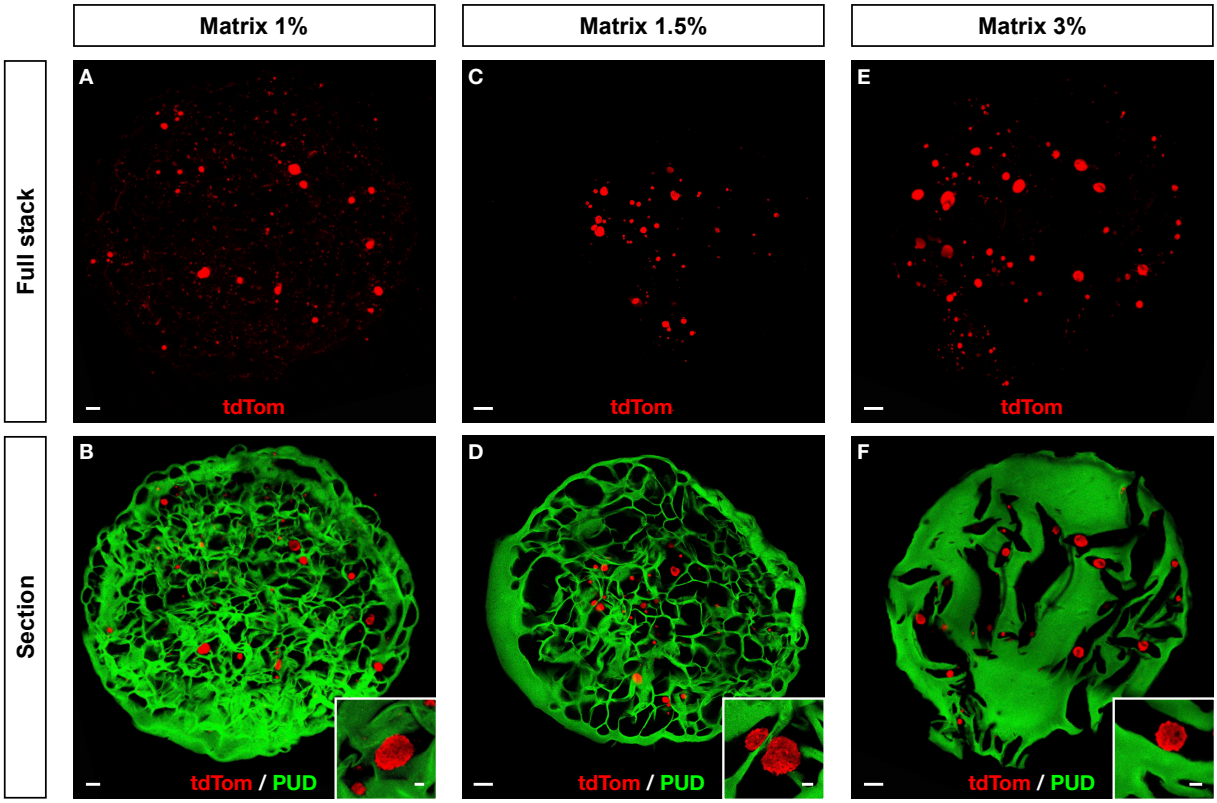

Figure 2. Embryonic neurons seeded in polysaccharide-based scaffolds form aggregates. Mouse embryonic neurons (red) were seeded and cultured for two days on FITC-traced scaffolds (green) prepared with 1% (**A**, **B**), 1.5% (**C**, **D**) and 3% (**E**, **F**) (w/w) of STMP. Maximum Z-stack projections (A, C and E) give an estimation of cell density and morphology. Simple Z-sections (B, D and F) include FITC scaffold tracing for morphology. Scale bars: (A-F), 200 µm; inserts, 30 µm.

Matrix 1% L-FD scaffolds displayed a similar morphology to the Matrix 1% formulation, but also revealed a mesh network of laminin around and within the scaffold. Compared to Matrix 1%, Matrix 1% L-FD scaffolds did not differ in terms of phosphorus content (84 ± 1 vs 86 ± 2 µmol/g) or swelling ratio (47.1 ± 6 vs 46.6 ± 6 in PBS and 123 ± 16 vs 118 ± 12 in water).

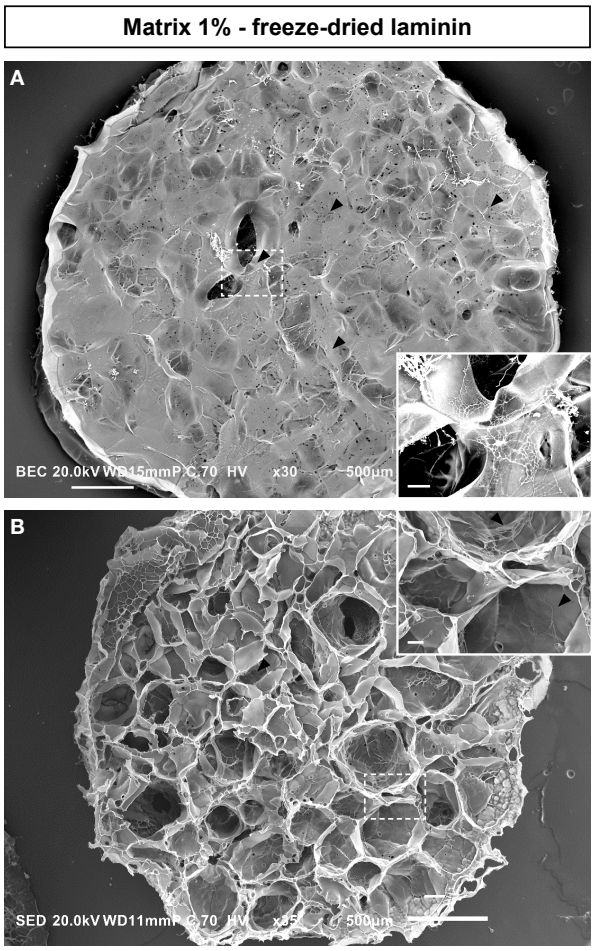

Figure 3. Freeze-dried laminin creates a mesh network within the scaffold. Scanning electron micrographs of a pullulan/dextran scaffold prepared with 1% (w/w) of STMP, hydrated with a laminin solution (100 µg/ml) and lyophilized again. Top view either of the scaffold surface (**A**) or section (**B**). Arrowheads point to the laminin filaments (in white). Scale bars: (A, B), 500 µm; insert, 50 µm.

3.6. Laminin functionalization promotes cellular attachment within the scaffold

To assess the impact of laminin functionalization of Matrix 1%, embryonic neurons were seeded on Matrix 1% without laminin, Matrix 1% with laminin only added (100 µg/ml) in the cell suspension during cell seeding (Matrix 1% L), and Matrix 1% L-FD (Fig. 4). After two days of culture, embryonic neurons seeded on Matrix 1% L-FD scaffolds formed large cell structures, extended neurites on and within the scaffold and expressed immature neuron marker βIII-tubulin (Tuj1, Fig. 4F). Seeded embryonic neurons also extended neurites in the Matrix 1% L condition, although less markedly.

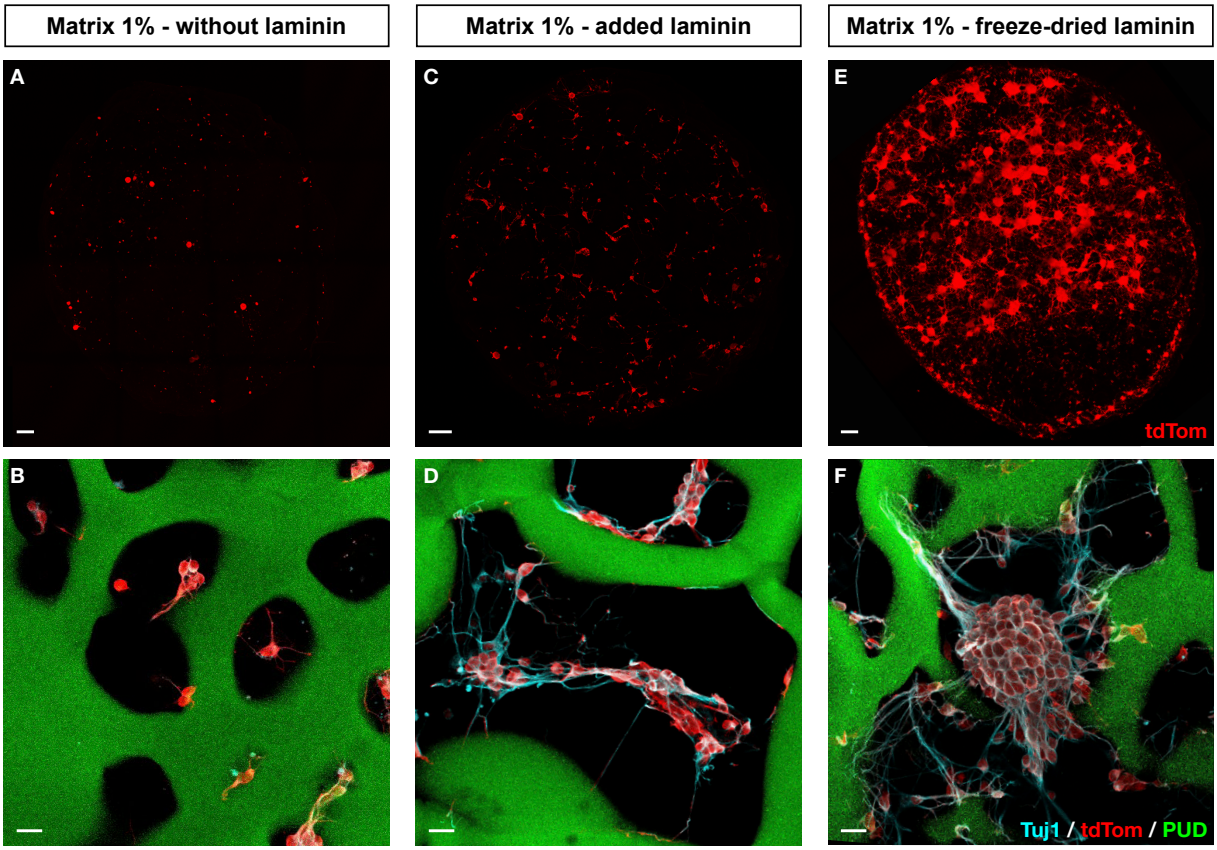

Figure 4. Freeze-dried laminin improves cell adhesion to the scaffold. Mouse embryonic neurons (red) were seeded and cultured for two days on FITC-traced scaffolds (green) prepared with 1% (w/w) of STMP, either without laminin (**A**, **B**), with added laminin (100 µg/ml) during cell seeding (**C**, **D**) or with freeze-dried laminin before cell seeding (**E**, **F**). Maximum Z-stack projections (A, C and E) give an estimation of cell density and morphology. Higher magnification pictures (B, D and F) include immature neuron marker βIII-tubulin (Tuj1, cyan) and FITC scaffold tracing (green). Scale bars: (A-F), 200 µm; inserts, 30 µm.

To further characterize the effect of laminin functionalization on cell adhesion, we measured the mean cell number within the three types of scaffolds after one, four and seven days of culture. While the mean cell number per scaffold was similar at day 1 around 10^4 cells per scaffold in Matrix 1% (10693), Matrix 1% L (10782) and Matrix L-FD (8645), after one week it decreased in the Matrix 1% (4114) and Matrix 1% L (4400), whereas in Matrix 1% L-FD it remained stable (8600).

We further characterized the embryonic neurons in 3D cell culture with Matrix 1% L-FD. At day two, embryonic neurons display an immature profile, with some cells proliferating (Ki67, Fig 5A). We also observed that most cells within the Matrix 1% L-FD expressed the neural progenitor marker doublecortin (DCX, Fig. 5B). After four days of culture, we also detected post-mitotic neuronal markers such as NeuN and transcription factor Tbr1 (Fig 5 C, D).

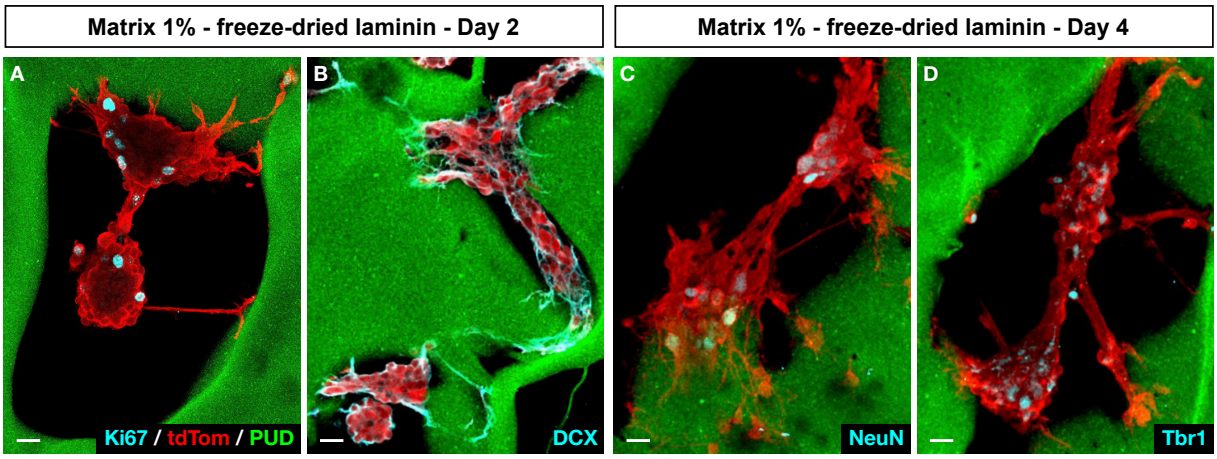

Figure 5. Cultured embryonic neurons characterization. (**A-B**) After two days of culture in scaffolds prepared with 1% (w/w) of STMP with freeze-dried laminin, some Ki67-positive traced cells are proliferating (A), and most cells express doublecortin (DCX), a neural progenitor marker (B). (**C-D**) After four days of culture, cells start expressing post-mitotic neuronal markers such as NeuN (C) and Tbr1 (D). Scale bars: 20 μm.

4. Discussion

In this study, we described the development of a new polysaccharide-based biomaterial optimized for neuronal culture. First, we optimized the STMP concentration which allowed to generate soft scaffolds with a high porosity. The resulting hydrogels were able to swell in water and physiological solutions. From all three formulations, we were able to generate 3D porous scaffolds that allow cell infiltration within few minutes. Interestingly, Matrix 1% scaffolds had an elastic modulus of 384±26 Pa, which is within the reported optimal stiffness range for neuronal culture, between 100 and 500 Pa [32-34]. The obtained matrices at 1% STMP also exhibited the faster degradation rates that could be more suitable for *in vivo* applications.

The fact that embryonic neurons neither significantly attached nor extended neurites in non-functionalized scaffolds was not surprising as the need for additional adhesion molecules has been largely reported [6]. We thus decided to add laminin in our scaffolds for two main reasons: (i) it is one of the main ECM components in the brain; (ii) it is known to promote neuronal adhesion in 2D and 3D cultures [6,35-37]. We have also tested several approaches to add laminin to the scaffold. When we added the laminin in the pullulan/dextran mixture before the cross-linking, laminin was denatured. When laminin was simply added during cell seeding (Matrix 1% L), it yielded poor cell adhesion and neurite outgrowth. In contrast, laminin was added and then freeze-dried, it created a mesh network of laminin within and on the scaffold. This technique has several advantages as it does not require additional cross-linking steps, it is a non-toxic process and it allows to store scaffolds at room temperature for several months. The remarkable enhanced cell adhesion and neurite outgrowth seen with the addition of freeze-dried laminin confirmed that this formulation optimized for 3D neuronal culture. Interestingly, this formulation could be used in clinical applications as we have the capacity to synthesize these scaffolds in compliance with the good manufacturing practice (GMP) guidelines, and with already available clinical grade laminin.

This new biomaterial could be used in two ways for CNS repair. First, it could be seeded with cells, such as embryonic neurons, before being transplanted in the lesion site. However, such an approach has other limitations. Indeed, it has been shown that for proper neuronal integration,

grafted neurons need to be very precisely differentiated into the neurons they are replacing [38,39]. Moreover, depending on the scaffold thickness, the initial lack of vascularization could lead to the death of most transplanted cells. However, one way to overcome this limitation could be for instance to add another polysaccharide in the formulation, fucoidan, which we have reported to have the ability to sequester and release vascular endothelial growth factor (VEGF) and to promote neovascularization *in vivo* [40]. Second, it could be used as an acellular scaffold to regrow the lost tissue. Our polysaccharide-based scaffold presents several advantages for this type of applications: it can be prepared at the desired shape prior to the grafting; it is easy to handle and can be stored for long periods at room temperature in its dried state; its initial swelling once in contact with fluids can help maintain it in the grafting site; and the presence of freeze-dried laminin will be crucial for neurite growth during regeneration. Indeed, it has been shown that enhancing neuronal networks is correlated with a better functional recovery in mice after stroke [7]. Here, enhancing *in situ* neovascularization and promoting neuronal survival could be of interest.

5. Conclusion

The objective of this study was to develop a macroporous polysaccharide-based scaffold compatible with neuronal 3D culture. By reducing cross-linker concentration, we have set up a pullulan/dextran biomaterial with a high porosity ratio and low stiffness. We have functionalized this scaffold with freeze-dried laminin and shown that embryonic neurons seeded within this scaffold displayed a better survival as well as an enhanced attachment and neurite outgrowth. Our capacity to produce these scaffolds with clinical grade components in compliance with the GMP guidelines offers a promising lead for further 3D *in vitro* and *in vivo* studies after CNS injury.

6. References

[1] S.L. James, A. Theadom, R.G. Ellenbogen, M.S. Bannick, W. Montjoy-Venning, L.R. Lucchesi, et al., Global, regional, and national burden of traumatic brain injury and spinal cord injury, 1990–2016: a systematic analysis for the Global Burden of Disease Study 2016, The Lancet Neurology. 18 (2019) 56–87. doi:10.1016/S1474-4422(18)30415-0.

[2] V.L. Feigin, M.H. Forouzanfar, R. Krishnamurthi, G.A. Mensah, M. Connor, D.A. Bennett, et al., Global and regional burden of stroke during 1990–2010: findings from the Global Burden of Disease Study 2010, 383 (2014) 245–255. doi:10.1016/s0140-6736(13)61953-4.

[3] U. Dirnagl, C. Iadecola, M.A. Moskowitz, Pathobiology of ischaemic stroke: an integrated view, Trends Neurosci. 22 (1999) 391–397.

[4] J. Silver, M.E. Schwab, P.G. Popovich, Central nervous system regenerative failure: role of oligodendrocytes, astrocytes, and microglia, 7 (2014) a020602. doi:10.1101/cshperspect.a020602.

[5] M.T. Fitch, C. Doller, C.K. Combs, G.E. Landreth, J. Silver, Cellular and molecular mechanisms of glial scarring and progressive cavitation: in vivo and in vitro analysis of inflammation-induced secondary injury after CNS trauma, J. Neurosci. 19 (1999) 8182–8198.

[6] G. Orive, E. Anitua, J.L. Pedraz, D.F. Emerich, Biomaterials for promoting brain protection, repair and regeneration, Nat. Rev. Neurosci. 10 (2009) 682–692. doi:10.1038/nrn2685.

[7] L.R. Nih, S. Gojgini, S.T. Carmichael, T. Segura, Dual-function injectable angiogenic biomaterial for the repair of brain tissue following stroke, Nat Mater. 129 (2018) e28–651. doi:10.1038/s41563-018-0083-8.

[8] P. Moshayedi, L.R. Nih, I.L. Llorente, A.R. Berg, J. Cinkornpumin, W.E. Lowry, et al., Systematic optimization of an engineered hydrogel allows for selective control of human neural stem cell survival and differentiation after transplantation in the stroke brain, Biomaterials. 105 (2016) 145–155. doi:10.1016/j.biomaterials.2016.07.028.

[9] B.G. Ballios, M.J. Cooke, L. Donaldson, B.L.K. Coles, C.M. Morshead, D. van der Kooy, et al., A Hyaluronan-Based Injectable Hydrogel Improves the Survival and Integration of Stem Cell Progeny following Transplantation, Stem Cell Reports. 4 (2015) 1031–1045. doi:10.1016/j.stemcr.2015.04.008.

[10] A. Farrukh, F. Ortega, W. Fan, N. Marichal, J.I. Paez, B. Berninger, et al., Bifunctional Hydrogels Containing the Laminin Motif IKVAV Promote Neurogenesis, Stem Cell Reports. 9 (2017) 1432–1440. doi:10.1016/j.stemcr.2017.09.002.

[11] A.R. Massensini, H. Ghuman, L.T. Saldin, C.J. Medberry, T.J. Keane, F.J. Nicholls, et al., Concentration-dependent rheological properties of ECM hydrogel for intracerebral delivery to a stroke cavity, Acta Biomater. 27 (2015) 116–130. doi:10.1016/j.actbio.2015.08.040.

[12] M. Jurga, M.B. Dainiak, A. Sarnowska, A. Jablonska, A. Tripathi, F.M. Plieva, et al., The performance of laminin-containing cryogel scaffolds in neural tissue regeneration, Biomaterials. 32 (2011) 3423–3434. doi:10.1016/j.biomaterials.2011.01.049.

[13] H. Jinnou, M. Sawada, K. Kawase, N. Kaneko, V. Herranz-Pérez, T. Miyamoto, et al., Radial Glial Fibers Promote Neuronal Migration and Functional Recovery after Neonatal Brain Injury, Cell Stem Cell. 22 (2017) 128–137.e9. doi:10.1016/j.stem.2017.11.005.

[14] K.I. Park, Y.D. Teng, E.Y. Snyder, The injured brain interacts reciprocally with neural stem cells supported by scaffolds to reconstitute lost tissue, Nat. Biotechnol. 20 (2002) 1111–1117. doi:10.1038/nbt751.

[15] A. Béduer, T. Braschler, O. Peric, G.E. Fantner, S. Mosser, P.C. Fraering, et al., A compressible scaffold for minimally invasive delivery of large intact neuronal networks, Adv Healthc Mater. 4 (2015) 301–312. doi:10.1002/

adhm.201400250.

[16] S. Frasca, F. Norol, C. Le Visage, J.-M. Collombet, D. Letourneur, X. Holy, et al., Calcium-phosphate ceramics and polysaccharide-based hydrogel scaffolds combined with mesenchymal stem cell differently support bone repair in rats, J Mater Sci Mater Med. 28 (2017) 35. doi:10.1007/s10856-016-5839-6.

[17] S. Li, L.R. Nih, H. Bachman, P. Fei, Y. Li, E. Nam, et al., Hydrogels with precisely controlled integrin activation dictate vascular patterning and permeability, Nat Mater. 16 (2017) 953–961. doi:10.1038/nmat4954.

[18] D. Letourneur, D. Machy, A. Pellé, E. Marcon-Bachari, G. D'Angelo, M. Vogel, et al., Heparin and non-heparin-like dextrans differentially modulate endothelial cell proliferation: in vitro evaluation with soluble and crosslinked polysaccharide matrices, J. Biomed. Mater. Res. 60 (2002) 94–100. doi:10.1002/jbm.10072.

[19] A. Autissier, C. Le Visage, C. Pouzet, F. Chaubet, D. Letourneur, Fabrication of porous polysaccharide-based scaffolds using a combined freeze-drying/cross-linking process, Acta Biomater. 6 (2010) 3640–3648. doi:10.1016/j.actbio.2010.03.004.

[20] A. Autissier, D. Letourneur, C. Le Visage, Pullulan-based hydrogel for smooth muscle cell culture, J Biomed Mater Res A. 82 (2007) 336–342. doi:10.1002/jbm.a.30998.

[21] M. Chaouat, C. Le Visage, A. Autissier, F. Chaubet, D. Letourneur, The evaluation of a small-diameter polysaccharide-based arterial graft in rats, Biomaterials. 27 (2006) 5546–5553. doi:10.1016/j.biomaterials.2006.06.032.

[22] G. Sun, Y.-I. Shen, C.C. Ho, S. Kusuma, S. Gerecht, Functional groups affect physical and biological properties of dextran-based hydrogels, J Biomed Mater Res A. 93 (2010) 1080–1090. doi:10.1002/jbm.a.32604.

[23] T.D. Leathers, Biotechnological production and applications of pullulan, Appl. Microbiol. Biotechnol. 62 (2003) 468–473. doi:10.1007/s00253-003-1386-4.

[24] I. Gliko-Kabir, B. Yagen, A. Penhasi, A. Rubinstein, Phosphated crosslinked guar for colon-specific drug delivery. I. Preparation and physicochemical characterization, J Control Release. 63 (2000) 121–127.

[25] N.-B. Thébaud, D. Pierron, R. Bareille, C. Le Visage, D. Letourneur, L. Bordenave, Human endothelial progenitor cell attachment to polysaccharide-based hydrogels: a pre-requisite for vascular tissue engineering, J Mater Sci Mater Med. 18 (2007) 339–345. doi:10.1007/s10856-006-0698-1.

[26] C. Le Visage, O. Gournay, N. Benguirat, S. Hamidi, L. Chaussumier, N. Mougenot, et al., Mesenchymal stem cell delivery into rat infarcted myocardium using a porous polysaccharide-based scaffold: a quantitative comparison with endocardial injection, Tissue Engineering Part A. 18 (2012) 35–44. doi:10.1089/ten.TEA.2011.0053.

[27] M. Lavergne, M. Derkaoui, C. Delmau, D. Letourneur, G. Uzan, C. Le Visage, Porous polysaccharide-based scaffolds for human endothelial progenitor cells, Macromol Biosci. 12 (2012) 901–910. doi:10.1002/mabi.201100431.

[28] S. Lanouar, R. Aid-Launais, A. Oliveira, L. Bidault, B. Closs, M.-N. Labour, et al., Effect of cross-linking on the physicochemical and in vitro properties of pullulan/dextran microbeads, J Mater Sci Mater Med. 29 (2018) 77. doi:10.1007/s10856-018-6085-x.

[29] B. Joddar, E. Garcia, A. Casas, C.M. Stewart, Development of functionalized multi-walled carbon-nanotube-based alginate hydrogels for enabling biomimetic technologies, Sci Rep. 6 (2016) 32456. doi:10.1038/srep32456.

[30] Y. Lallemand, V. Luria, R. Haffner-Krausz, P. Lonai, Maternally expressed PGK-Cre transgene as a tool for early and uniform activation of the Cre site-specific recombinase, Transgenic Res. 7 (1998) 105–112.

[31] L. Madisen, T.A. Zwingman, S.M. Sunkin, S.W. Oh, H.A. Zariwala, H. Gu, et al., A robust and high-throughput Cre reporting and characterization system for the whole mouse brain, Nat. Neurosci. 13 (2010) 133–140. doi:10.1038/nn.2467.

[32] E.R. Aurand, K.J. Lampe, K.B. Bjugstad, Defining and designing polymers and hydrogels for neural tissue engineering, Neuroscience Research. 72 (2012) 199–213. doi:10.1016/j.neures.2011.12.005.

[33] A.J. Engler, S. Sen, H.L. Sweeney, D.E. Discher, Matrix elasticity directs stem cell lineage specification, Cell. 126 (2006) 677–689. doi:10.1016/j.cell.2006.06.044.

[34] L.A. Flanagan, Y.-E. Ju, B. Marg, M. Osterfield, P.A. Janmey, Neurite branching on deformable substrates, Neuroreport. 13 (2002) 2411–2415. doi:10.1097/01.wnr.0000048003.96487.97.

[35] S.E. Stabenfeldt, M.C. LaPlaca, Variations in rigidity and ligand density influence neuronal response in methylcellulose–laminin hydrogels, Acta Biomater. 7 (2011) 4102–4108. doi:10.1016/j.actbio.2011.07.026.

[36] S. Hou, Q. Xu, W. Tian, F. Cui, Q. Cai, J. Ma, et al., The repair of brain lesion by implantation of hyaluronic acid hydrogels modified with laminin, J. Neurosci. Methods. 148 (2005) 60–70. doi:10.1016/j.jneumeth.2005.04.016.

[37] T.C. Lim, M. Spector, Biomaterials for Enhancing CNS Repair, Transl. Stroke Res. 8 (2017) 57–64. doi:10.1007/s12975-016-0470-x.

[38] M. Terrigno, I. Busti, C. Alia, M. Pietrasanta, I. Arisi, M. D'Onofrio, et al., Neurons Generated by Mouse ESCs with Hippocampal or Cortical Identity Display Distinct Projection Patterns When Co-transplanted in the Adult Brain, Stem Cell Reports. 10 (2018) 1016–1029. doi:10.1016/j.stemcr.2018.01.010.

[39] K.A. Michelsen, S. Acosta-Verdugo, M. Benoit-Marand, I. Espuny-Camacho, N. Gaspard, B. Saha, et al., Area-specific reestablishment of damaged circuits in the adult cerebral cortex by cortical neurons derived from mouse embryonic stem cells, Neuron. 85 (2015) 982–997. doi:10.1016/j.neuron.2015.02.001.

[40] A. Purnama, R. Aid-Launais, O. Haddad, M. Maire, D. Mantovani, D. Letourneur, et al., Fucoidan in a 3D scaffold interacts with vascular endothelial growth factor and promotes neovascularization in mice, Drug Deliv Transl Res. 5 (2015) 187–197. doi:10.1007/s13346-013-0177-4.

Bibliography

Abraira, V.E., and Ginty, D.D. (2013). The sensory neurons of touch. Neuron *79*, 618–639.

Abramsson, A., Kurup, S., Busse, M., Yamada, S., Lindblom, P., Schallmeiner, E., Stenzel, D., Sauvaget, D., Ledin, J., Ringvall, M., et al. (2007). Defective N-sulfation of heparan sulfate proteoglycans limits PDGF-BB binding and pericyte recruitment in vascular development. Genes Dev. *21*, 316–331.

Abzhanov, A., and Tabin, C.J. (2004). Shh and Fgf8 act synergistically to drive cartilage outgrowth during cranial development. Dev. Biol. *273*, 134–148.

Adams, R.H., and Alitalo, K. (2007). Molecular regulation of angiogenesis and lymphangiogenesis. Nat. Rev. Mol. Cell Biol. *8*, 464–478.

Adams, R.H., and Eichmann, A. (2010). Axon guidance molecules in vascular patterning. Cold Spring Harb Perspect Biol *2*, a001875.

Aguayo, A.J., Charron, L., and Bray, G.M. (1976a). Potential of Schwann cells from unmyelinated nerves to produce myelin: a quantitative ultrastructural and radiographic study. J. Neurocytol. *5*, 565–573.

Aguayo, A.J., Epps, J., Charron, L., and Bray, G.M. (1976b). Multipotentiality of Schwann cells in cross-anastomosed and grafted myelinated and unmyelinated nerves: quantitative microscopy and radioautography. Brain Res. *104*, 1–20.

Ahlgren, S.C., and Bronner-Fraser, M. (1999). Inhibition of sonic hedgehog signaling in vivo results in craniofacial neural crest cell death. Curr. Biol. *9*, 1304–1314.

Aird, W.C. (2007a). Phenotypic Heterogeneity of the Endothelium: I. Structure, Function, and Mechanisms. Circ. Res. *100*, 158–173.

Aird, W.C. (2007b). Phenotypic heterogeneity of the endothelium: II. Representative vascular beds. Circ. Res. *100*, 174–190.

Aird, W.C. (2012). Endothelial cell heterogeneity. Cold Spring Harb Perspect Med *2*, a006429.

Akert, K., Sandri, C., Weibel, E.R., Peper, K., and Moor, H. (1976). The fine structure of the perineural endothelium. Cell Tissue Res. *165*, 281–295.

Alexander, M.R., and Owens, G.K. (2012). Epigenetic control of smooth muscle cell differentiation and phenotypic switching in vascular development and disease. Annu. Rev. Physiol. *74*, 13–40.

Allende, M.L., and Proia, R.L. (2002). Sphingosine-1-phosphate receptors and the development of the vascular system. Biochim. Biophys. Acta *1582*, 222–227.

Altman, J., and Bayer, S.A. (1984). The development of the rat spinal cord. Adv Anat Embryol Cell Biol *85*, 1–164.

Ando, K., Fukuhara, S., Izumi, N., Nakajima, H., Fukui, H., Kelsh, R.N., and Mochizuki, N. (2016). Clarification of mural cell coverage of vascular endothelial cells by live imaging of zebrafish. Development *143*, 1328–1339.

Andreeva, E.R., Pugach, I.M., Gordon, D., and Orekhov, A.N. (1998). Continuous subendothelial network formed by pericyte-like cells in human vascular bed. Tissue Cell *30*, 127–135.

Aoki, Y., Saint-Germain, N., Gyda, M., Magner-Fink, E., Lee, Y.-H., Credidio, C., and Saint-Jeannet, J.-P. (2003). Sox10 regulates the development of neural crest-derived melanocytes in Xenopus. Dev. Biol. *259*, 19–33.

Apte, R.S., Chen, D.S., and Ferrara, N. (2019). VEGF in Signaling and Disease: Beyond Discovery and Development. Cell *176*, 1248–1264.

Aquino, J.B., Hjerling-Leffler, J., Edlund, T., Villar, M.J., and Ernfors, P. (2006). In vitro and in vivo differentiation of boundary cap neural crest stem cells into mature Schwann cells. Exp. Neurol. *198*, 438–449.

Armulik, A., Genové, G., and Betsholtz, C. (2011). Pericytes: developmental, physiological, and pathological perspectives, problems, and promises. Dev. Cell *21*, 193–215.

Armulik, A., Genové, G., Mäe, M., Nisancioglu, M.H., Wallgard, E., Niaudet, C., He, L., Norlin, J., Lindblom, P., Strittmatter, K., et al. (2010). Pericytes regulate the blood-brain barrier. Nature *468*, 557–561.

Arroyo, E.J., and Scherer, S.S. (2000). On the molecular architecture of myelinated fibers. Histochem. Cell Biol. *113*, 1–18.

Arthur-Farraj, P., Wanek, K., Hantke, J., Davis, C.M., Jayakar, A., Parkinson, D.B., Mirsky, R., and Jessen, K.R. (2011). Mouse schwann cells need both NRG1 and cyclic AMP to myelinate. Glia *59*, 720–733.

Asahina, K., Zhou, B., Pu, W.T., and Tsukamoto, H. (2011). Septum transversum-derived mesothelium gives rise to hepatic stellate cells and perivascular mesenchymal cells in developing mouse liver. Hepatology *53*, 983–995.

Aspalter, I.M., Gordon, E., Dubrac, A., Ragab, A., Narloch, J., Vizán, P., Geudens, I., Collins, R.T., Franco, C.A., Abrahams, C.L., et al. (2015). Alk1 and Alk5 inhibition by Nrp1 controls vascular sprouting downstream of Notch. Nat Commun *6*, 7264.

Auld, D.S., and Robitaille, R. (2003). Perisynaptic Schwann cells at the neuromuscular junction: nerve- and activity-dependent contributions to synaptic efficacy, plasticity, and reinnervation. Neuroscientist *9*, 144–157.

Averill, S., McMahon, S.B., Clary, D.O., Reichardt, L.F., and Priestley, J.V. (1995). Immunocytochemical localization of trkA receptors in chemically identified subgroups of adult rat sensory neurons. Eur. J. Neurosci. *7*, 1484–1494.

Ayres-Sander, C.E., Lauridsen, H., Maier, C.L., Sava, P., Pober, J.S., and Gonzalez, A.L. (2013). Transendothelial migration enables subsequent transmigration of neutrophils through underlying pericytes. PLoS ONE *8*, e60025.

Baggiolini, A., Varum, S., Mateos, J.M., Bettosini, D., John, N., Bonalli, M., Ziegler, U., Dimou, L., Clevers, H., Furrer, R., et al. (2015). Premigratory and migratory neural crest cells are multipotent in vivo. Cell Stem Cell *16*, 314–322.

Baker, C.L., and Pera, M.F. (2018). Capturing Totipotent Stem Cells. Cell Stem Cell *22*, 25–34.

Balice-Gordon, R.J. (1996). Schwann cells: Dynamic roles at the neuromuscular junction. Curr. Biol. *6*, 1054–1056.

Baroffio, A., Dupin, E., and Le Douarin, N.M. (1988). Clone-forming ability and differentiation potential of migratory neural crest cells. Proc. Natl. Acad. Sci. U.S.a. *85*, 5325–5329.

Baroffio, A., Dupin, E., and Le Douarin, N.M. (1991). Common precursors for neural and mesectodermal derivatives in the cephalic neural crest. Development *112*, 301–305.

Bear, M.F., Connors, B.W., and Paradiso, M.A. (2016). Neuroscience (Lippincott Williams & Wilkins).

Becker, A.J., McCulloch, E.A., and Till, J.E. (1963). Cytological demonstration of the clonal nature of spleen colonies derived from transplanted mouse marrow cells. Nature *197*, 452–454.

Bedell, V.M., Yeo, S.-Y., Park, K.W., Chung, J., Seth, P., Shivalingappa, V., Zhao, J., Obara, T., Sukhatme, V.P., Drummond, I.A., et al. (2005). roundabout4 is essential for angiogenesis in vivo. Proc. Natl. Acad. Sci. U.S.a. *102*, 6373–6378.

Bendayan, M. (2002). Morphological and cytochemical aspects of capillary permeability. Microsc. Res. Tech. *57*, 327–349.

Bergwerff, M., Verberne, M.E., DeRuiter, M.C., Poelmann, R.E., and Gittenberger-de Groot, A.C. (1998). Neural crest cell contribution to the developing circulatory system: implications for vascular morphology? Circ. Res. *82*, 221–231.

Bermingham, J.R., Scherer, S.S., O'Connell, S., Arroyo, E., Kalla, K.A., Powell, F.L., and Rosenfeld, M.G. (1996). Tst-1/Oct-6/SCIP regulates a unique step in peripheral myelination and is required for normal respiration. Genes Dev. *10*, 1751–1762.

Berthiaume, A.-A., Grant, R.I., McDowell, K.P., Underly, R.G., Hartmann, D.A., Levy, M., Bhat, N.R., and Shih, A.Y. (2018). Dynamic Remodeling of Pericytes In Vivo Maintains Capillary Coverage in the Adult Mouse Brain. Cell Rep *22*, 8–16.

Berti, C., Bartesaghi, L., Ghidinelli, M., Zambroni, D., Figlia, G., Chen, Z.-L., Quattrini, A., Wrabetz, L., and Feltri, M.L. (2011). Non-redundant function of dystroglycan and β1 integrins in radial sorting of axons. Development *138*, 4025–4037.

Bertrand, N., Castro, D.S., and Guillemot, F. (2002). Proneural genes and the specification of neural cell types. Nat. Rev. Neurosci. *3*, 517–530.

Betsholtz, C. (2018). Cell-cell signaling in blood vessel development and function. EMBO Mol Med *10*.

Bhatt, S., Diaz, R., and Trainor, P.A. (2013). Signals and switches in Mammalian neural crest cell differentiation. Cold Spring Harb Perspect Biol *5*.

Bianconi, R., and van der Meulen, J. (1963). The response to vibration of the end organs of mammalian muscle spindles. J. Neurophysiol. *26*, 177–190.

Bibel, M., and Barde, Y.A. (2000). Neurotrophins: key regulators of cell fate and cell shape in the vertebrate nervous system. Genes Dev. *14*, 2919–2937.

Bilbao, J.M., and Schmidt, R.E. (2014). Normal Anatomy of the Peripheral (Sural) Nerve. In Biopsy Diagnosis of Peripheral Neuropathy, (Cham: Springer International Publishing), pp. 21–41.

Birchmeier, C., and Nave, K.-A. (2008). Neuregulin-1, a key axonal signal that drives Schwann cell growth and differentiation. Glia *56*, 1491–1497.

Blanco, R., and Gerhardt, H. (2013). VEGF and Notch in tip and stalk cell selection. Cold Spring Harb Perspect Med *3*, a006569.

Blockus, H., and Chédotal, A. (2016). Slit-Robo signaling. Development *143*, 3037–3044.

Blomhoff, R., and Blomhoff, H.K. (2006). Overview of retinoid metabolism and function. J. Neurobiol. *66*, 606–630.

Bourane, S., Garces, A., Venteo, S., Pattyn, A., Hubert, T., Fichard, A., Puech, S., Boukhaddaoui, H., Baudet, C., Takahashi, S., et al. (2009). Low-threshold mechanoreceptor subtypes selectively express MafA and are specified by Ret signaling. Neuron *64*, 857–870.

Brennan, A., Dean, C.H., Zhang, A.L., Cass, D.T., Mirsky, R., and Jessen, K.R. (2000). Endothelins control the timing of Schwann cell generation in vitro and in vivo. Dev. Biol. *227*, 545–557.

Britsch, S., Goerich, D.E., Riethmacher, D., Peirano, R.I., Rossner, M., Nave, K.A., Birchmeier, C., and Wegner, M. (2001). The transcription factor Sox10 is a key regulator of peripheral glial development. Genes Dev. *15*, 66–78.

Bron, R., Vermeren, M., Kokot, N., Andrews, W., Little, G.E., Mitchell, K.J., and Cohen, J. (2007). Boundary cap cells constrain spinal motor neuron somal migration at motor exit points by a semaphorin-plexin mechanism. Neural Dev *2*, 21.

Bronner-Fraser, M., and Fraser, S. (1988). Cell lineage analysis reveals multipotency of some avian neural crest cells. Nature *335*, 161–164.

Bronner-Fraser, M., and Fraser, S. (1989). Developmental potential of avian trunk neural crest cells in situ. Neuron *3*, 755–766.

Brose, K., Bland, K.S., Wang, K.H., Arnott, D., Henzel, W., Goodman, C.S., Tessier-Lavigne, M., and Kidd, T. (1999). Slit proteins bind Robo receptors and have an evolutionarily conserved role in repulsive axon guidance. Cell *96*, 795–806.

Brown, M.C., Engberg, I., and Matthews, P.B. (1967). The relative sensitivity to vibration of muscle receptors of the cat. J. Physiol. (Lond.) *192*, 773–800.

Bunge, R.P., Bunge, M.B., and Eldridge, C.F. (1986). Linkage between axonal ensheathment and basal lamina production by Schwann cells. Annu. Rev. Neurosci. *9*, 305–328.

Burke, R.E., Strick, P.L., Kanda, K., Kim, C.C., and Walmsley, B. (1977). Anatomy of medial gastrocnemius and soleus motor nuclei in cat spinal cord. J. Neurophysiol. *40*, 667–680.

Cappellari, O., Benedetti, S., Innocenzi, A., Tedesco, F.S., Moreno-Fortuny, A., Ugarte, G., Lampugnani, M.G., Messina, G., and Cossu, G. (2013). Dll4 and PDGF-BB convert committed skeletal myoblasts to pericytes without erasing their myogenic memory. Dev. Cell *24*, 586–599.

Carmeliet, P., Ferreira, V., Breier, G., Pollefeyt, S., Kieckens, L., Gertsenstein, M., Fahrig, M., Vandenhoeck, A., Harpal, K., Eberhardt, C., et al. (1996). Abnormal blood vessel development and lethality in embryos lacking a single VEGF allele. Nature *380*, 435–439.

Carmeliet, P., and Tessier-Lavigne, M. (2005). Common mechanisms of nerve and blood vessel wiring. Nature *436*, 193–200.

Carney, T.J., Dutton, K.A., Greenhill, E., Delfino-Machín, M., Dufourcq, P., Blader, P., and Kelsh, R.N. (2006). A direct role for Sox10 in specification of neural crest-derived sensory neurons. Development *133*, 4619–4630.

Carr, M.J., Toma, J.S., Johnston, A.P.W., Steadman, P.E., Yuzwa, S.A., Mahmud, N., Frankland, P.W., Kaplan, D.R., and Miller, F.D. (2019). Mesenchymal Precursor Cells in Adult Nerves Contribute to Mammalian Tissue Repair and Regeneration. Cell Stem Cell *24*, 240–256.e249.

Carroll, R.G. (2007). Elsevier's Integrated Physiology (Mosby Incorporated).

Castets, M., Coissieux, M.-M., Delloye-Bourgeois, C., Bernard, L., Delcros, J.-G., Bernet, A., Laudet, V., and Mehlen, P. (2009). Inhibition of endothelial cell apoptosis by netrin-1 during angiogenesis. Dev. Cell *16*, 614–620.

Cattin, A.-L., Burden, J.J., Van Emmenis, L., Mackenzie, F.E., Hoving, J.J.A., Garcia Calavia, N., Guo, Y., McLaughlin, M., Rosenberg, L.H., Quereda, V., et al. (2015). Macrophage-Induced Blood Vessels Guide Schwann Cell-Mediated Regeneration of Peripheral Nerves. Cell *162*, 1127–1139.

Cauna, N. (1973). The free penicillate nerve endings of the human hairy skin. J. Anat. *115*, 277–288.

Ceradini, D.J., Kulkarni, A.R., Callaghan, M.J., Tepper, O.M., Bastidas, N., Kleinman, M.E., Capla, J.M., Galiano, R.D., Levine, J.P., and Gurtner, G.C. (2004). Progenitor cell trafficking is regulated by hypoxic gradients through HIF-1 induction of SDF-1. Nat. Med. *10*, 858–864.

Chen, H., Albergante, L., Hsu, J.Y., Lareau, C.A., Bosco, Lo, G., Guan, J., Zhou, S., Gorban, A.N., Bauer, D.E., Aryee, M.J., et al. (2018). STREAM: Single-cell Trajectories Reconstruction, Exploration And Mapping of omics data. bioRxiv 302554.

Chen, C.-L., Broom, D.C., Liu, Y., de Nooij, J.C., Li, Z., Cen, C., Samad, O.A., Jessell, T.M., Woolf, C.J., and Ma, Q. (2006). Runx1 determines nociceptive sensory neuron phenotype and is required for thermal and neuropathic pain. Neuron *49*, 365–377.

Chen, Q., Zhang, H., Liu, Y., Adams, S., Eilken, H., Stehling, M., Corada, M., Dejana, E., Zhou, B., and Adams, R.H. (2016). Endothelial cells are progenitors of cardiac pericytes and vascular smooth muscle cells. Nat Commun *7*, 12422.

Chen, S., Kulik, M., and Lechleider, R.J. (2003). Smad proteins regulate transcriptional induction of the SM22alpha gene by TGF-beta. Nucleic Acids Res. *31*, 1302–1310.

Chernousov, M.A., Yu, W.-M., Chen, Z.-L., Carey, D.J., and Strickland, S. (2008). Regulation of Schwann cell function by the extracellular matrix. Glia *56*, 1498–1507.

Chédotal, A. (2007). Slits and their receptors. Adv. Exp. Med. Biol. *621*, 65–80.

Chi, J.-T., Chang, H.Y., Haraldsen, G., Jahnsen, F.L., Troyanskaya, O.G., Chang, D.S., Wang, Z., Rockson, S.G., van de Rijn, M., Botstein, D., et al. (2003). Endothelial cell diversity revealed by global expression profiling. Proc. Natl. Acad. Sci. U.S.a. *100*, 10623–10628.

Chong, D.C., Koo, Y., Xu, K., Fu, S., and Cleaver, O. (2011). Stepwise arteriovenous fate acquisition during mammalian vasculogenesis. Dev. Dyn. *240*, 2153–2165.

Christ, B., Huang, R., and Scaal, M. (2004). Formation and differentiation of the avian sclerotome. Anat. Embryol. *208*, 333–350.

Chung, A.S., and Ferrara, N. (2011). Developmental and pathological angiogenesis. Annu. Rev. Cell Dev. Biol. *27*, 563–584.

Clark, E.R., and Clark, E.L. (1925). A. The development of adventitial (Rouget) cells on the blood capillaries of amphibian larvae. Am. J. Anat. *35*, 239–264.

Cleaver, O., and Melton, D.A. (2003). Endothelial signaling during development. Nat. Med. *9*, 661–668.

Clevers, H., and Watt, F.M. (2018). Defining Adult Stem Cells by Function, not by Phenotype. Annu. Rev. Biochem. *87*, 1015–1027.

Collins, T., Read, M.A., Neish, A.S., Whitley, M.Z., Thanos, D., and Maniatis, T. (1995). Transcriptional regulation of endothelial cell adhesion molecules: NF-kappa B and cytokine-inducible enhancers. Faseb J. *9*, 899–909.

Cotter, L., Özçelik, M., Jacob, C., Pereira, J.A., Locher, V., Baumann, R., Relvas, J.B., Suter, U., and Tricaud, N. (2010). Dlg1-PTEN interaction regulates myelin thickness to prevent damaging peripheral nerve overmyelination. Science *328*, 1415–1418.

Coulpier, F., Le Crom, S., Maro, G.S., Manent, J., Giovannini, M., Maciorowski, Z., Fischer, A., Gessler, M., Charnay, P., and Topilko, P. (2009). Novel features of boundary cap cells revealed by the analysis of newly identified molecular markers. Glia *57*, 1450–1457.

Crisan, M., Yap, S., Casteilla, L., Chen, C.-W., Corselli, M., Park, T.S., Andriolo, G., Sun, B., Zheng, B., Zhang, L., et al. (2008). A perivascular origin for mesenchymal stem cells in multiple human organs. Cell Stem Cell *3*, 301–313.

D'Antonio, M., Droggiti, A., Feltri, M.L., Roes, J., Wrabetz, L., Mirsky, R., and Jessen, K.R. (2006). TGFbeta type II receptor signaling controls Schwann cell death and proliferation in developing nerves. J. Neurosci. *26*, 8417–8427.

Daneman, R., and Keller, A. (2015). **Pericytes in Vascular Development and Function**. In Endothelial Signaling in Development and Disease, M.H. Schmidt, and S. Liebner, eds. (New York, NY: Springer New York), pp. 65–92.

Daneman, R., Zhou, L., Kebede, A.A., and Barres, B.A. (2010). Pericytes are required for blood–brain barrier integrity during embryogenesis. Nature *468*, 562–566.

Dasen, J.S. (2009). Hox networks and the origins of motor neuron diversity. Curr. Top. Dev. Biol. *88*, 169–200.

Davis, S., Aldrich, T.H., Jones, P.F., Acheson, A., Compton, D.L., Jain, V., Ryan, T.E., Bruno, J., Radziejewski, C., Maisonpierre, P.C., et al. (1996). Isolation of angiopoietin-1, a ligand for the TIE2 receptor, by secretion-trap expression cloning. Cell *87*, 1161–1169.

De Smet, F., Segura, I., De Bock, K., Hohensinner, P.J., and Carmeliet, P. (2009). Mechanisms of vessel branching: filopodia on endothelial tip cells lead the way. Arterioscler. Thromb. Vasc. Biol. *29*, 639–649.

Decker, L., Desmarquet-Trin-Dinh, C., Taillebourg, E., Ghislain, J., Vallat, J.-M., and Charnay, P. (2006). Peripheral myelin maintenance is a dynamic process requiring constant Krox20 expression. J. Neurosci. *26*, 9771–9779.

Dejana, E., and Orsenigo, F. (2013). Endothelial adherens junctions at a glance. Journal of Cell Science *126*, 2545–2549.

Delfino-Machín, M., Madelaine, R., Busolin, G., Nikaido, M., Colanesi, S., Camargo-Sosa, K., Law, E.W.P., Toppo, S., Blader, P., Tiso, N., et al. (2017). Sox10 contributes to the balance of fate choice in dorsal root ganglion progenitors. PLoS ONE *12*, e0172947–29.

Dellavalle, A., Maroli, G., Covarello, D., Azzoni, E., Innocenzi, A., Perani, L., Antonini, S., Sambasivan, R., Brunelli, S., Tajbakhsh, S., et al. (2011). Pericytes resident in postnatal skeletal muscle differentiate into muscle fibres and generate satellite cells. Nat Commun *2*, 499.

Dellavalle, A., Sampaolesi, M., Tonlorenzi, R., Tagliafico, E., Sacchetti, B., Perani, L., Innocenzi, A., Galvez, B.G., Messina, G., Morosetti, R., et al. (2007). Pericytes of human skeletal muscle are myogenic precursors distinct from satellite cells. Nat Cell Biol *9*, 255–267.

Dias Moura Prazeres, P.H., Sena, I.F.G., Borges, I.D.T., de Azevedo, P.O., Andreotti, J.P., de Paiva, A.E., de Almeida, V.M., de Paula Guerra, D.A., Pinheiro Dos Santos, G.S., Mintz, A., et al. (2017). Pericytes are heterogeneous in their origin within the same tissue. Dev. Biol. *427*, 6–11.

Dias, D.O., Kim, H., Holl, D., Werne Solnestam, B., Lundeberg, J., Carlén, M., Göritz, C., and Frisén, J. (2018). Reducing Pericyte-Derived Scarring Promotes Recovery after Spinal Cord Injury. Cell.

Dickinson, D.P., Machnicki, M., Ali, M.M., Zhang, Z., and Sohal, G.S. (2004). Ventrally emigrating neural tube (VENT) cells: a second neural tube-derived cell population. J. Anat. *205*, 79–98.

Dijke, ten, P., and Arthur, H.M. (2007). Extracellular control of TGFbeta signalling in vascular development and disease. Nat. Rev. Mol. Cell Biol. *8*, 857–869.

Ditadi, A., Sturgeon, C.M., Tober, J., Awong, G., Kennedy, M., Yzaguirre, A.D., Azzola, L., Ng, E.S., Stanley, E.G., French, D.L., et al. (2015). Human definitive haemogenic endothelium and arterial vascular endothelium represent distinct lineages. Nat Cell Biol *17*, 580–591.

Díaz-Flores, L., Gutiérrez, R., Madrid, J.F., Varela, H., Valladares, F., Acosta, E., and Martín-Vasallo, P. (2009). Pericytes. Morphofunction, interactions and pathology in a quiescent and activated mesenchymal cell niche. Histol. Histopathol. *24*, 909–969.

Djonov, V., Schmid, M., Tschanz, S.A., and Burri, P.H. (2000). Intussusceptive angiogenesis: its role in embryonic vascular network formation. Circ. Res. *86*, 286–292.

Domenga, V., Fardoux, P., Lacombe, P., Monet, M., Maciazek, J., Krebs, L.T., Klonjkowski, B., Berrou, E., Mericskay, M., Li, Z., et al. (2004). Notch3 is required for arterial identity and maturation of vascular smooth muscle cells. Genes Dev. *18*, 2730–2735.

Dong, Z., Brennan, A., Liu, N., Yarden, Y., Lefkowitz, G., Mirsky, R., and Jessen, K.R. (1995). Neu differentiation factor is a neuron-glia signal and regulates survival, proliferation, and maturation of rat Schwann cell precursors. Neuron *15*, 585–596.

Dore-Duffy, P., Katychev, A., Wang, X., and Van Buren, E. (2006). CNS microvascular pericytes exhibit multipotential stem cell activity. J Cereb Blood Flow Metab *26*, 613–624.

Dowsing, B.J., Morrison, W.A., Nicola, N.A., Starkey, G.P., Bucci, T., and Kilpatrick, T.J. (1999). Leukemia inhibitory factor is an autocrine survival factor for Schwann cells. J. Neurochem. *73*, 96–104.

Drake, C.J., and Fleming, P.A. (2000). Vasculogenesis in the day 6.5 to 9.5 mouse embryo. Blood *95*, 1671–1679.

Drake, C.J., Hungerford, J.E., and Little, C.D. (1998). Morphogenesis of the first blood vessels. Ann. N. Y. Acad. Sci. *857*, 155–179.

Duan, L., Zhang, X.-D., Miao, W.-Y., Sun, Y.-J., Xiong, G., Wu, Q., Li, G., Yang, P., Yu, H., Li, H., et al. (2018). PDGFRβ Cells Rapidly Relay Inflammatory Signal from the Circulatory System to Neurons via Chemokine CCL2. Neuron *100*, 183–200.e188.

Dubrac, A., Genet, G., Ola, R., Zhang, F., Pibouin-Fragner, L., Han, J., Zhang, J., Thomas, J.-L., Chédotal, A., Schwartz, M.A., et al. (2016). Targeting NCK-Mediated Endothelial Cell Front-Rear Polarity Inhibits Neovascularization. Circulation *133*, 409–421.

Dulauroy, S., Di Carlo, S.E., Langa, F., Eberl, G., and Peduto, L. (2012). Lineage tracing and genetic ablation of ADAM12(+) perivascular cells identify a major source of profibrotic cells during acute tissue injury. Nat. Med. *18*, 1262–1270.

Dumont, D.J., Gradwohl, G.J., Fong, G.H., Auerbach, R., and Breitman, M.L. (1993). The endothelial-specific receptor tyrosine kinase, tek, is a member of a new subfamily of receptors. Oncogene *8*, 1293–1301.

Dupin, E., Glavieux, C., Vaigot, P., and Le Douarin, N.M. (2000). Endothelin 3 induces the reversion of melanocytes to glia through a neural crest-derived glial-melanocytic progenitor. Proc. Natl. Acad. Sci. U.S.a. *97*, 7882–7887.

Dupin, E., and Sommer, L. (2012). Neural crest progenitors and stem cells: from early development to adulthood. Dev. Biol. *366*, 83–95.

Dupin, E., Calloni, G.W., Coelho-Aguiar, J.M., and Le Douarin, N.M. (2018). The issue of the multipotency of the neural crest cells. Dev. Biol.

Dziewulska, D., and Lewandowska, E. (2012). Pericytes as a new target for pathological processes in CADASIL. Neuropathology *32*, 515–521.

Eberth, K.J. (1871). Handbuch der Lehre von den Geweben des Menschen und der Thiere (Leipzig).

Eichmann, A., Marcelle, C., Bréant, C., and Le Douarin, N.M. (1993). Two molecules related to the VEGF receptor are expressed in early endothelial cells during avian embryonic development. Mech. Dev. *42*, 33–48.

Eichmann, A., Yuan, L., Moyon, D., Lenoble, F., Pardanaud, L., and Breant, C. (2005). Vascular development: from precursor cells to branched arterial and venous networks. Int. J. Dev. Biol. *49*, 259–267.

Einheber, S., Hannocks, M.J., Metz, C.N., Rifkin, D.B., and Salzer, J.L. (1995). Transforming growth factor-beta 1 regulates axon/Schwann cell interactions. J. Cell Biol. *129*, 443–458.

Eliades, A., Wareing, S., Marinopoulou, E., Fadlullah, M.Z.H., Patel, R., Grabarek, J.B., Plusa, B., Lacaud, G., and Kouskoff, V. (2016). The Hemogenic Competence of Endothelial Progenitors Is Restricted by Runx1 Silencing during Embryonic Development. Cell Rep *15*, 2185–2199.

Enomoto, S., Mitsui, K., Kawamura, T., Iwanari, H., Daigo, K., Horiuchi, K., Minami, T., Kodama, T., and Hamakubo, T. (2016). Suppression of Slit2/Robo1 mediated HUVEC migration by Robo4. Biochem. Biophys. Res. Commun. *469*, 797–802.

Erickson, C.A., and Weston, J.A. (1999). VENT cells: a fresh breeze in a stuffy field? Trends Neurosci. *22*, 486–488.

Etchevers, H.C., Vincent, C., Le Douarin, N.M., and Couly, G.F. (2001). The cephalic neural crest provides pericytes and smooth muscle cells to all blood vessels of the face and forebrain. Development *128*, 1059–1068.

Fantin, A., Vieira, J.M., Gestri, G., Denti, L., Schwarz, Q., Prykhozhij, S., Peri, F., Wilson, S.W., and Ruhrberg, C. (2010). Tissue macrophages act as cellular chaperones for vascular anastomosis downstream of VEGF-mediated endothelial tip cell induction. Blood *116*, 829–840.

Fariñas, I., Jones, K.R., Backus, C., Wang, X.Y., and Reichardt, L.F. (1994). Severe sensory and sympathetic deficits in mice lacking neurotrophin-3. Nature *369*, 658–661.

Fazal, S.V., Gomez-Sanchez, J.A., Wagstaff, L.J., Musner, N., Otto, G., Janz, M., Mirsky, R., and Jessen, K.R. (2017). Graded Elevation of c-Jun in Schwann Cells In Vivo: Gene Dosage Determines Effects on Development, Remyelination, Tumorigenesis, and Hypomyelination. Journal of Neuroscience *37*, 12297–12313.

Feltri, M.L., Graus Porta, D., Previtali, S.C., Nodari, A., Migliavacca, B., Cassetti, A., Littlewood-Evans, A., Reichardt, L.F., Messing, A., Quattrini, A., et al. (2002). Conditional disruption of beta 1 integrin in Schwann cells impedes interactions with axons. J. Cell Biol. *156*, 199–209.

Ferrara, N., Carver-Moore, K., Chen, H., Dowd, M., Lu, L., O'Shea, K.S., Powell-Braxton, L., Hillan, K.J., and Moore, M.W. (1996). Heterozygous embryonic lethality induced by targeted inactivation of the VEGF gene. Nature *380*, 439–442.

Fex Svenningsen, A., COLMAN, D.R., and PEDRAZA, L. (2004). Satellite cells of dorsal root ganglia are multipotential glial precursors. Neuron Glia Biol. *1*, 85–93.

Fleming, I., Bauersachs, J., and Busse, R. (1996). Paracrine functions of the coronary vascular endothelium. Mol. Cell. Biochem. *157*, 137–145.

Fleming, T.P. (1987). A quantitative analysis of cell allocation to trophectoderm and inner cell mass in the mouse blastocyst. Dev. Biol. *119*, 520–531.

Fontenas, L., and Kucenas, S. (2017). Livin' On The Edge: glia shape nervous system transition zones. Curr. Opin. Neurobiol. *47*, 44–51.

Fontenas, L., and Kucenas, S. (2018). Motor Exit Point (MEP) Glia: Novel Myelinating Glia That Bridge CNS and PNS Myelin. Front Cell Neurosci *12*, 333.

Foo, S.S., Turner, C.J., Adams, S., Compagni, A., Aubyn, D., Kogata, N., Lindblom, P., Shani, M., Zicha, D., and Adams, R.H. (2006). Ephrin-B2 controls cell motility and adhesion during blood-vessel-wall assembly. Cell *124*, 161–173.

Forsythe, J.A., Jiang, B.H., Iyer, N.V., Agani, F., Leung, S.W., Koos, R.D., and Semenza, G.L. (1996). Activation of vascular endothelial growth factor gene transcription by hypoxia-inducible factor 1. Mol. Cell. Biol. *16*, 4604–4613.

Frank, E., and Sanes, J.R. (1991). Lineage of neurons and glia in chick dorsal root ganglia: analysis in vivo with a recombinant retrovirus. Development *111*, 895–908.

Fricker, F.R., Zhu, N., Tsantoulas, C., Abrahamsen, B., Nassar, M.A., Thakur, M., Garratt, A.N., Birchmeier, C., McMahon, S.B., Wood, J.N., et al. (2009). Sensory axon-derived neuregulin-1 is required for axoglial signaling and normal sensory function but not for long-term axon maintenance. J. Neurosci. *29*, 7667–7678.

Friocourt, F., and Chédotal, A. (2017). The Robo3 receptor, a key player in the development, evolution, and function of commissural systems. Dev Neurobiol *77*, 876–890.

Fritz, R.D., Menshykau, D., Martin, K., Reimann, A., Pontelli, V., and Pertz, O. (2015). SrGAP2-Dependent Integration of Membrane Geometry and Slit-Robo-Repulsive Cues Regulates Fibroblast Contact Inhibition of Locomotion. Dev. Cell *35*, 78–92.

Fu, S.Y., Sharma, K., Luo, Y., and Raper, J.A. (2000). SEMA3A regulates developing sensory projections in the chicken spinal cord. *45*, 227–236.

Furchgott, R.F., and Zawadzki, J.V. (1980). The obligatory role of endothelial cells in the relaxation of arterial smooth muscle by acetylcholine. Nature *288*, 373–376.

Furlan, A., and Adameyko, I. (2018). Schwann cell precursor: a neural crest cell in disguise? Dev. Biol. *444* Suppl 1, S25–S35.

Furlan, A., Dyachuk, V., Kastriti, M.E., Calvo-Enrique, L., Abdo, H., Hadjab, S., Chontorotzea, T., Akkuratova, N., Usoskin, D., Kamenev, D., et al. (2017). Multipotent peripheral glial cells generate neuroendocrine cells of the adrenal medulla. Science *357*.

Gaengel, K., Genové, G., Armulik, A., and Betsholtz, C. (2009). Endothelial-mural cell signaling in vascular development and angiogenesis. Arterioscler. Thromb. Vasc. Biol. *29*, 630–638.

Gambardella, L., Schneider-Maunoury, S., Voiculescu, O., Charnay, P., and Barrandon, Y. (2000). Pattern of expression of the transcription factor Krox-20 in mouse hair follicle. Mech. Dev. *96*, 215–218.

Gans, C., and Glenn Northcutt, R.G. (1983). Neural crest and the origin of vertebrates: a new head. Science *220*, 268–273.

García-Castro, M.I., Marcelle, C., and Bronner-Fraser, M. (2002). Ectodermal Wnt function as a neural crest inducer. Science *297*, 848–851.

Garratt, A.N., Britsch, S., and Birchmeier, C. (2000). Neuregulin, a factor with many functions in the life of a schwann cell. Bioessays *22*, 987–996.

Garrett, A.M., Jucius, T.J., Sigaud, L.P.R., Tang, F.-L., Xiong, W.-C., Ackerman, S.L., and Burgess, R.W. (2016). Analysis of Expression Pattern and Genetic Deletion of Netrin5 in the Developing Mouse. Front. Mol. Neurosci. *9*, 3.

Gascon, E., Gaillard, S., Malapert, P., Liu, Y., Rodat-Despoix, L., Samokhvalov, I.M., Delmas, P., Helmbacher, F., Maina, F., and Moqrich, A. (2010). Hepatocyte growth factor-Met signaling is required for Runx1 extinction and peptidergic differentiation in primary nociceptive neurons. J. Neurosci. *30*, 12414–12423.

Gerhardt, H., and Betsholtz, C. (2003). Endothelial-pericyte interactions in angiogenesis. *314*, 15–23.

Gerhardt, H., Golding, M., Fruttiger, M., Ruhrberg, C., Lundkvist, A., Abramsson, A., Jeltsch, M., Mitchell, C., Alitalo, K., Shima, D., et al. (2003). VEGF guides angiogenic sprouting utilizing endothelial tip cell filopodia. J. Cell Biol. *161*, 1163–1177.

Gerhardt, H., Ruhrberg, C., Abramsson, A., Fujisawa, H., Shima, D., and Betsholtz, C. (2004). Neuropilin-1 is required for endothelial tip cell guidance in the developing central nervous system. Dev. Dyn. *231*, 503–509.

Ghislain, J., Desmarquet-Trin-Dinh, C., Jaegle, M., Meijer, D., Charnay, P., and Frain, M. (2002). Characterisation of cis-acting sequences reveals a biphasic, axon-dependent regulation of Krox20 during Schwann cell development. Development *129*, 155–166.

Gilbert, S.F. (2016). Developmental Biology (Sinauer Associates Incorporated U.S.).

Girard, J.-P., Moussion, C., and Förster, R. (2012). HEVs, lymphatics and homeostatic immune cell trafficking in lymph nodes. Nat. Rev. Immunol. *12*, 762–773.

Glenn Northcutt, R. (2005). The new head hypothesis revisited. J. Exp. Zool. B Mol. Dev. Evol. *304*, 274–297.

Glenn, T.D., and Talbot, W.S. (2013a). Signals regulating myelination in peripheral nerves and the Schwann cell response to injury. Curr. Opin. Neurobiol. *23*, 1041–1048.

Glenn, T.D., and Talbot, W.S. (2013b). Analysis of Gpr126 function defines distinct mechanisms controlling the initiation and maturation of myelin. Development *140*, 3167–3175.

Goebbels, S., Oltrogge, J.H., Kemper, R., Heilmann, I., Bormuth, I., Wolfer, S., Wichert, S.P., Möbius, W., Liu, X., Lappe-Siefke, C., et al. (2010). Elevated phosphatidylinositol 3,4,5-trisphosphate in glia triggers cell-autonomous membrane wrapping and myelination. J. Neurosci. *30*, 8953–8964.

Gonçalves, N.P., Vægter, C.B., and Pallesen, L.T. (2018). Peripheral Glial Cells in the Development of Diabetic Neuropathy. Front. Neurol. *9*, 268.

Goodell, M.A., Nguyen, H., and Shroyer, N. (2015). Somatic stem cell heterogeneity: diversity in the blood, skin and intestinal stem cell compartments. Nat. Rev. Mol. Cell Biol. *16*, 299–309.

Goossens, S., Janzen, V., Bartunkova, S., Yokomizo, T., Drogat, B., Crisan, M., Haigh, K., Seuntjens, E., Umans, L., Riedt, T., et al. (2011). The EMT regulator Zeb2/Sip1 is essential for murine embryonic hematopoietic stem/progenitor cell differentiation and mobilization. Blood *117*, 5620–5630.

Goumans, M.-J., Valdimarsdottir, G., Itoh, S., Rosendahl, A., Sideras, P., and Dijke, ten, P. (2002). Balancing the activation state of the endothelium via two distinct TGF-beta type I receptors. Embo J. *21*, 1743–1753.

Göritz, C., Dias, D.O., Tomilin, N., Barbacid, M., Shupliakov, O., and Frisén, J. (2011). A pericyte origin of spinal cord scar tissue. Science *333*, 238–242.

Green, S.A., Uy, B.R., and Bronner, M.E. (2017). Ancient evolutionary origin of vertebrate enteric neurons from trunk-derived neural crest. Nature *544*, 88–91.

Greenhalgh, S.N., Iredale, J.P., and Henderson, N.C. (2013). Origins of fibrosis: pericytes take centre stage. F1000Prime Rep *5*, 37.

Gresset, A., Coulpier, F., Gerschenfeld, G., Jourdon, A., Matesic, G., Richard, L., Vallat, J.-M., Charnay, P., and Topilko, P. (2015). Boundary Caps Give Rise to Neurogenic Stem Cells and Terminal Glia in the Skin. Stem Cell Reports *0*, 278–290.

Grim, M., Halata, Z., and Franz, T. (1992). Schwann cells are not required for guidance of motor nerves in the hindlimb in Splotch mutant mouse embryos. Anat. Embryol. *186*, 311–318.

Grocott, T., Tambalo, M., and Streit, A. (2012). The peripheral sensory nervous system in the vertebrate head: a gene regulatory perspective. Dev. Biol. *370*, 3–23.

Groves, A.K., and LaBonne, C. (2014). Setting appropriate boundaries: fate, patterning and competence at the neural plate border. Dev. Biol. *389*, 2–12.

Gu, C., Rodriguez, E.R., Reimert, D.V., Shu, T., Fritzsch, B., Richards, L.J., Kolodkin, A.L., and Ginty, D.D. (2003). Neuropilin-1 conveys semaphorin and VEGF signaling during neural and cardiovascular development. Dev. Cell *5*, 45–57.

Gu, C., Yoshida, Y., Livet, J., Reimert, D.V., Mann, F., Merte, J., Henderson, C.E., Kolodkin, A.L., and Ginty, D.D. (2005). Semaphorin 3E and plexin-D1 control vascular pattern independently of neuropilins. Science *307*, 265–268.

Guillemot, F., Lo, L.C., Johnson, J.E., Auerbach, A., Anderson, D.J., and Joyner, A.L. (1993). Mammalian achaete-scute homolog 1 is required for the early development of olfactory and autonomic neurons. Cell *75*, 463–476.

Guimarães-Camboa, N., Cattaneo, P., Sun, Y., Moore-Morris, T., Gu, Y., Dalton, N.D., Rockenstein, E., Masliah, E., Peterson, K.L., Stallcup, W.B., et al. (2017). Pericytes of Multiple Organs Do Not Behave as Mesenchymal Stem Cells In Vivo. Cell Stem Cell *20*, 345–359.e345.

Hall, C.N., Reynell, C., Gesslein, B., Hamilton, N.B., Mishra, A., Sutherland, B.A., O'Farrell, F.M., Buchan, A.M., Lauritzen, M., and Attwell, D. (2014). Capillary pericytes regulate cerebral blood flow in health and disease. Nature *508*, 55–60.

Hall, J.E. (2016). Guyton and Hall Textbook of Medical Physiology (Elsevier Health Sciences).

Hanani, M. (2005). Satellite glial cells in sensory ganglia: from form to function. Brain Res. Brain Res. Rev. *48*, 457–476.

Hanani, M. (2012). Intercellular communication in sensory ganglia by purinergic receptors and gap junctions: implications for chronic pain. Brain Res. *1487*, 183–191.

Hari, L., Brault, V., Kléber, M., Lee, H.-Y., Ille, F., Leimeroth, R., Paratore, C., Suter, U., Kemler, R., and Sommer, L. (2002). Lineage-specific requirements of beta-catenin in neural crest development. J. Cell Biol. *159*, 867–880.

Harris, M.L., and Erickson, C.A. (2007). Lineage specification in neural crest cell pathfinding. Dev. Dyn. *236*, 1–19.

Hartmann, D.A., Underly, R.G., Grant, R.I., Watson, A.N., Lindner, V., and Shih, A.Y. (2015). Pericyte structure and distribution in the cerebral cortex revealed by high-resolution imaging of transgenic mice. Neurophotonics *2*, 041402.

Harty, B.L., and Monk, K.R. (2017). Unwrapping the unappreciated: recent progress in Remak Schwann cell biology. Curr. Opin. Neurobiol. *47*, 131–137.

Hayashi, H., and Kume, T. (2008). Foxc transcription factors directly regulate Dll4 and Hey2 expression by interacting with the VEGF-Notch signaling pathways in endothelial cells. PLoS ONE *3*, e2401.

Hellström, M., Gerhardt, H., Kalén, M., Li, X., Eriksson, U., Wolburg, H., and Betsholtz, C. (2001). Lack of pericytes leads to endothelial hyperplasia and abnormal vascular morphogenesis. J. Cell Biol. *153*, 543–553.

Hellström, M., Kalén, M., Lindahl, P., Abramsson, A., and Betsholtz, C. (1999). Role of PDGF-B and PDGFR-beta in recruitment of vascular smooth muscle cells and pericytes during embryonic blood vessel formation in the mouse. Development *126*, 3047–3055.

Hellström, M., Phng, L.-K., Hofmann, J.J., Wallgard, E., Coultas, L., Lindblom, P., Alva, J., Nilsson, A.-K., Karlsson, L., Gaiano, N., et al. (2007). Dll4 signalling through Notch1 regulates formation of tip cells during angiogenesis. Nature *445*, 776–780.

Henion, P.D., and Weston, J.A. (1997). Timing and pattern of cell fate restrictions in the neural crest lineage. Development *124*, 4351–4359.

Herbert, S.P., and Stainier, D.Y.R. (2011). Molecular control of endothelial cell behaviour during blood vessel morphogenesis. Nat. Rev. Mol. Cell Biol. *12*, 551–564.

Herbert, S.P., Huisken, J., Kim, T.N., Feldman, M.E., Houseman, B.T., Wang, R.A., Shokat, K.M., and Stainier, D.Y.R. (2009). Arterial-venous segregation by selective cell sprouting: an alternative mode of blood vessel formation. Science *326*, 294–298.

Herring, B.P., Hoggatt, A.M., Burlak, C., and Offermanns, S. (2014). Previously differentiated medial vascular smooth muscle cells contribute to neointima formation following vascular injury. Vasc Cell *6*, 21.

Herzog, Y., Guttmann-Raviv, N., and Neufeld, G. (2005). Segregation of arterial and venous markers in subpopulations of blood islands before vessel formation. Dev. Dyn. *232*, 1047–1055.

High, F.A., Lu, M.M., Pear, W.S., Loomes, K.M., Kaestner, K.H., and Epstein, J.A. (2008). Endothelial expression of the Notch ligand Jagged1 is required for vascular smooth muscle development. Proc. Natl. Acad. Sci. U.S.a. *105*, 1955–1959.

Hill, R.A., Tong, L., Yuan, P., Murikinati, S., Gupta, S., and Grutzendler, J. (2015). Regional Blood Flow in the Normal and Ischemic Brain Is Controlled by Arteriolar Smooth Muscle Cell Contractility and Not by Capillary Pericytes. Neuron *87*, 95–110.

His, W. (1868). Untersuchungen über die erste Anlage des Wirbelthierleibes : die erste Entwickelung des Hühnchens im Ei. (Leipzig: F.C.W. Vogel).

Hjerling-Leffler, J., Marmigère, F., Heglind, M., Cederberg, A., and Ernfors, P. (2005). The boundary cap: a source of neural crest stem cells that generate multiple sensory neuron subtypes. Development *132*, 2623–2632.

Hlushchuk, R., Styp-Rekowska, B., Dzambazi, J., Wnuk, M., Huynh-Do, U., Makanya, A., and Djonov, V. (2017). Endoglin inhibition leads to intussusceptive angiogenesis via activation of factors related to COUP-TFII signaling pathway. PLoS ONE *12*, e0182813–e0182817.

Holm, A., Heumann, T., and Augustin, H.G. (2018). Microvascular Mural Cell Organotypic Heterogeneity and Functional Plasticity. Trends Cell Biol. *28*, 302–316.

Huang, L.-Y.M., Gu, Y., and Chen, Y. (2013). Communication between neuronal somata and satellite glial cells in sensory ganglia. Glia *61*, 1571–1581.

Huminiecki, L., Gorn, M., Suchting, S., Poulsom, R., and Bicknell, R. (2002). Magic roundabout is a new member of the roundabout receptor family that is endothelial specific and expressed at sites of active angiogenesis. Genomics *79*, 547–552.

Hung, C., Linn, G., Chow, Y.-H., Kobayashi, A., Mittelsteadt, K., Altemeier, W.A., Gharib, S.A., Schnapp, L.M., and Duffield, J.S. (2013). Role of lung pericytes and resident fibroblasts in the pathogenesis of pulmonary fibrosis. Am. J. Respir. Crit. Care Med. *188*, 820–830.

Hungerford, J.E., and Little, C.D. (1999). Developmental biology of the vascular smooth muscle cell: building a multilayered vessel wall. J. Vasc. Res. *36*, 2–27.

Hunt, C.C., and Kuffler, S.W. (1951). Further study of efferent small-nerve fibers to mammalian muscle spindles; multiple spindle innervation and activity during contraction. J. Physiol. (Lond.) *113*, 283–297.

Iivanainen, E., Nelimarkka, L., Elenius, V., Heikkinen, S.-M., Junttila, T.T., Sihombing, L., Sundvall, M., Määttä, J.A., Laine, V.J.O., Ylä-Herttuala, S., et al. (2003). Angiopoietin-regulated recruitment of vascular smooth muscle cells by endothelial-derived heparin binding EGF-like growth factor. Faseb J. *17*, 1609–1621.

Iruela-Arispe, M.L. (2018). A dual origin for blood vessels. Nature *562*, 195–197.

Iruela-Arispe, M.L., and Davis, G.E. (2009). Cellular and molecular mechanisms of vascular lumen formation. Dev. Cell *16*, 222–231.

Ishii, A., Furusho, M., and Bansal, R. (2013). Sustained activation of ERK1/2 MAPK in oligodendrocytes and schwann cells enhances myelin growth and stimulates oligodendrocyte progenitor expansion. J. Neurosci. *33*, 175–186.

Ivanova, E., Kovacs-Oller, T., and Sagdullaev, B.T. (2017). Vascular Pericyte Impairment and Connexin43 Gap Junction Deficit Contribute to Vasomotor Decline in Diabetic Retinopathy. J. Neurosci. *37*, 7580–7594.

Jaegle, M., Mandemakers, W., Broos, L., Zwart, R., Karis, A., Visser, P., Grosveld, F., and Meijer, D. (1996). The POU factor Oct-6 and Schwann cell differentiation. Science *273*, 507–510.

Jaegle, M., Ghazvini, M., Mandemakers, W., Piirsoo, M., Driegen, S., Levavasseur, F., Raghoenath, S., Grosveld, F., and Meijer, D. (2003). The POU proteins Brn-2 and Oct-6 share important functions in Schwann cell development. Genes Dev. *17*, 1380–1391.

Jain, R.K. (2003). Molecular regulation of vessel maturation. Nat. Med. *9*, 685–693.

Jakobsson, L., and van Meeteren, L.A. (2013). Transforming growth factor β family members in regulation of vascular function: in the light of vascular conditional knockouts. Exp. Cell Res. *319*, 1264–1270.

Jakobsson, L., Franco, C.A., Bentley, K., Collins, R.T., Ponsioen, B., Aspalter, I.M., Rosewell, I., Busse, M., Thurston, G., Medvinsky, A., et al. (2010). Endothelial cells dynamically compete for the tip cell position during angiogenic sprouting. Nat Cell Biol *12*, 943–953.

James, J.M., and Mukouyama, Y.-S. (2011). Neuronal action on the developing blood vessel pattern. Seminars in Cell & Developmental Biology *22*, 1019–1027.

Jaworski, A., Tom, I., Tong, R.K., Gildea, H.K., Koch, A.W., Gonzalez, L.C., and Tessier-Lavigne, M. (2015). Operational redundancy in axon guidance through the multifunctional receptor Robo3 and its ligand NELL2. Science *350*, 961–965.

Jeansson, M., Gawlik, A., Anderson, G., Li, C., Kerjaschki, D., Henkelman, M., and Quaggin, S.E. (2011). Angiopoietin-1 is essential in mouse vasculature during development and in response to injury. J. Clin. Invest. *121*, 2278–2289.

Jessen, K.R., and Mirsky, R. (2005). The origin and development of glial cells in peripheral nerves. Nat. Rev. Neurosci. *6*, 671–682.

Jessen, K.R., and Mirsky, R. (2008). Negative regulation of myelination: Relevance for development, injury, and demyelinating disease. Glia *56*, 1552–1565.

Jessen, K.R., Mirsky, R., and Lloyd, A.C. (2015). Schwann Cells: Development and Role in Nerve Repair. Cold Spring Harb Perspect Biol *7*, a020487.

Jin, S., Hansson, E.M., Tikka, S., Lanner, F., Sahlgren, C., Farnebo, F., Baumann, M., Kalimo, H., and Lendahl, U. (2008). Notch signaling regulates platelet-derived growth factor receptor-beta expression in vascular smooth muscle cells. Circ. Res. *102*, 1483–1491.

Jones, C.A., Nishiya, N., London, N.R., Zhu, W., Sorensen, L.K., Chan, A.C., Lim, C.J., Chen, H., Zhang, Q., Schultz, P.G., et al. (2009). Slit2-Robo4 signalling promotes vascular stability by blocking Arf6 activity. Nat Cell Biol *11*, 1325–1331.

Jones, E.A.V., Yuan, L., Breant, C., Watts, R.J., and Eichmann, A. (2008). Separating genetic and hemodynamic defects in neuropilin 1 knockout embryos. Development *135*, 2479–2488.

Jones, N., Voskas, D., Master, Z., Sarao, R., Jones, J., and Dumont, D.J. (2001). Rescue of the early vascular defects in Tek/Tie2 null mice reveals an essential survival function. EMBO Rep. *2*, 438–445.

Joseph, N.M., Mukouyama, Y.-S., Mosher, J.T., Jaegle, M., Crone, S.A., Dormand, E.-L., Lee, K.-F., Meijer, D., Anderson, D.J., and Morrison, S.J. (2004). Neural crest stem cells undergo multilineage differentiation in developing peripheral nerves to generate endoneurial fibroblasts in addition to Schwann cells. Development *131*, 5599–5612.

Joutel, A., Corpechot, C., Ducros, A., Vahedi, K., Chabriat, H., Mouton, P., Alamowitch, S., Domenga, V., Cécillion, M., Marechal, E., et al. (1996). Notch3 mutations in CADASIL, a hereditary adult-onset condition causing stroke and dementia. Nature *383*, 707–710.

Kalcheim, C., and Teillet, M.A. (1989). Consequences of somite manipulation on the pattern of dorsal root ganglion development. Development *106*, 85–93.

Kanning, K.C., Kaplan, A., and Henderson, C.E. (2010). Motor neuron diversity in development and disease. Annu. Rev. Neurosci. *33*, 409–440.

Karkkainen, M.J., Mäkinen, T., and Alitalo, K. (2002). Lymphatic endothelium: a new frontier of metastasis research. Nat Cell Biol *4*, E2–E5.

Kedzierski, R.M., and Yanagisawa, M. (2001). Endothelin system: the double-edged sword in health and disease. Annu. Rev. Pharmacol. Toxicol. *41*, 851–876.

Keller, G. (2005). Embryonic stem cell differentiation: emergence of a new era in biology and medicine. Genes Dev. *19*, 1129–1155.

Kelly, M.A., and Hirschi, K.K. (2009). Signaling hierarchy regulating human endothelial cell development. Arterioscler. Thromb. Vasc. Biol. *29*, 718–724.

Kennedy-Lydon, T.M., Crawford, C., Wildman, S.S.P., and Peppiatt-Wildman, C.M. (2013). Renal pericytes: regulators of medullary blood flow. Acta Physiol (Oxf) *207*, 212–225.

Keynes, R.J., and Stern, C.D. (1984). Segmentation in the vertebrate nervous system. Nature *310*, 786–789.

Khudyakov, J., and Bronner-Fraser, M. (2009). Comprehensive spatiotemporal analysis of early chick neural crest network genes. Dev. Dyn. *238*, 716–723.

Kidd, G.J., Ohno, N., and Trapp, B.D. (2013). Biology of Schwann cells. Handb Clin Neurol *115*, 55–79.

Kidd, T., Bland, K.S., and Goodman, C.S. (1999). Slit is the midline repellent for the robo receptor in Drosophila. Cell *96*, 785–794.

Kim, J., Dormand, E., and Anderson, D.J. (2003). SOX10 maintains multipotency and inhibits neuronal differentiation of neural crest stem cells. Neuron *38*, 17–31.

Klabunde, R. (2011). Cardiovascular Physiology Concepts (Baltimore: Lippincott Williams & Wilkins).

Klein, R., Silos-Santiago, I., Smeyne, R.J., Lira, S.A., Brambilla, R., Bryant, S., Zhang, L., Snider, W.D., and Barbacid, M. (1994). Disruption of the neurotrophin-3 receptor gene trkC eliminates la muscle afferents and results in abnormal movements. Nature *368*, 249–251.

Klein, R., Smeyne, R.J., Wurst, W., Long, L.K., Auerbach, B.A., Joyner, A.L., and Barbacid, M. (1993). Targeted disruption of the trkB neurotrophin receptor gene results in nervous system lesions and neonatal death. Cell *75*, 113–122.

Ko, C.-P., and Robitaille, R. (2015). Perisynaptic Schwann Cells at the Neuromuscular Synapse: Adaptable, Multitasking Glial Cells. Cold Spring Harb Perspect Biol *7*, a020503.

Koch, A.W., Mathivet, T., Larrivée, B., Tong, R.K., Kowalski, J., Pibouin-Fragner, L., Bouvrée, K., Stawicki, S., Nicholes, K., Rathore, N., et al. (2011). Robo4 maintains vessel integrity and inhibits angiogenesis by interacting with UNC5B. Dev. Cell *20*, 33–46.

Kohli, V., Schumacher, J.A., Desai, S.P., Rehn, K., and Sumanas, S. (2013). Arterial and venous progenitors of the major axial vessels originate at distinct locations. Dev. Cell *25*, 196–206.

Komarova, Y., and Malik, A.B. (2010). Regulation of endothelial permeability via paracellular and transcellular transport pathways. Annu. Rev. Physiol. *72*, 463–493.

Korn, J., Christ, B., and Kurz, H. (2002). Neuroectodermal origin of brain pericytes and vascular smooth muscle cells. J. Comp. Neurol. *442*, 78–88.

Kos, R., Reedy, M.V., Johnson, R.L., and Erickson, C.A. (2001). The winged-helix transcription factor FoxD3 is important for establishing the neural crest lineage and repressing melanogenesis in avian embryos. Development *128*, 1467–1479.

Kramer, I., Sigrist, M., Taniuchi, I., and Arber, S. (2006). A role for Runx transcription factor signaling in dorsal root ganglion sensory neuron diversification. Neuron *49*, 379–393.

Krautler, N.J., Kana, V., Kranich, J., Tian, Y., Perera, D., Lemm, D., Schwarz, P., Armulik, A., Browning, J.L., Tallquist, M., et al. (2012). Follicular dendritic cells emerge from ubiquitous perivascular precursors. Cell *150*, 194–206.

Krebs, L.T., Xue, Y., Norton, C.R., Sundberg, J.P., Beatus, P., Lendahl, U., Joutel, A., and Gridley, T. (2003). Characterization of Notch3-deficient mice: normal embryonic development and absence of genetic interactions with a Notch1 mutation. Genesis *37*, 139–143.

Krispin, S., Nitzan, E., Kassem, Y., and Kalcheim, C. (2010). Evidence for a dynamic spatiotemporal fate map and early fate restrictions of premigratory avian neural crest. Development *137*, 585–595.

Krueger, M., and Bechmann, I. (2010). CNS pericytes: concepts, misconceptions, and a way out. Glia *58*, 1–10.

Krull, C.E. (2001). Segmental organization of neural crest migration. Mech. Dev. *105*, 37–45.

Kubu, C.J., Orimoto, K., Morrison, S.J., Weinmaster, G., Anderson, D.J., and Verdi, J.M. (2002). Developmental changes in Notch1 and numb expression mediated by local cell-cell interactions underlie progressively increasing delta sensitivity in neural crest stem cells. Dev. Biol. *244*, 199–214.

Kucenas, S. (2015). Perineurial glia. Cold Spring Harb Perspect Biol *7*.

Kucenas, S., Takada, N., Park, H.-C., Woodruff, E., Broadie, K., and Appel, B. (2008). CNS-derived glia ensheath peripheral nerves and mediate motor root development. Nat. Neurosci. *11*, 143–151.

Kucera, J., Fan, G., Jaenisch, R., and Linnarsson, S. (1995). Dependence of developing group Ia afferents on neurotrophin-3. J. Comp. Neurol. *363*, 307–320.

Kuffler, S.W., Hunt, C.C., and Quilliam, J.P. (1951). Function of medullated small-nerve fibers in mammalian ventral roots; efferent muscle spindle innervation. J. Neurophysiol. *14*, 29–54.

Kuhlbrodt, K., Herbarth, B., Sock, E., Enderich, J., Hermans-Borgmeyer, I., and Wegner, M. (1998). Cooperative function of POU proteins and SOX proteins in glial cells. J. Biol. Chem. *273*, 16050–16057.

Kumar, A., D'Souza, S.S., Moskvin, O.V., Toh, H., Wang, B., Zhang, J., Swanson, S., Guo, L.-W., Thomson, J.A., and Slukvin, I.I. (2017). Specification and Diversification of Pericytes and Smooth Muscle Cells from Mesenchymoangioblasts. Cell Rep *19*, 1902–1916.

La Marca, R., Cerri, F., Horiuchi, K., Bachi, A., Feltri, M.L., Wrabetz, L., Blobel, C.P., Quattrini, A., Salzer, J.L., and Taveggia, C. (2011). TACE (ADAM17) inhibits Schwann cell myelination. Nat. Neurosci. *14*, 857–865.

Lallemend, F., and Ernfors, P. (2012). Molecular interactions underlying the specification of sensory neurons. Trends Neurosci. *35*, 373–381.

Lanahan, A.A., Hermans, K., Claes, F., Kerley-Hamilton, J.S., Zhuang, Z.W., Giordano, F.J., Carmeliet, P., and Simons, M. (2010). VEGF receptor 2 endocytic trafficking regulates arterial morphogenesis. Dev. Cell *18*, 713–724.

Lanahan, A., Zhang, X., Fantin, A., Zhuang, Z., Rivera-Molina, F., Speichinger, K., Prahst, C., Zhang, J., Wang, Y., Davis, G., et al. (2013). The neuropilin 1 cytoplasmic domain is required for VEGF-A-dependent arteriogenesis. Dev. Cell *25*, 156–168.

Langenhan, T., Aust, G., and Hamann, J. (2013). Sticky signaling--adhesion class G protein-coupled receptors take the stage. Sci Signal *6*, re3–re3.

Larrivée, B., Freitas, C., Suchting, S., Brunet, I., and Eichmann, A. (2009). Guidance of vascular development: lessons from the nervous system. Circ. Res. *104*, 428–441.

Larrivée, B., Freitas, C., Trombe, M., Lv, X., Delafarge, B., Yuan, L., Bouvrée, K., Breant, C., del Toro, R., Bréchot, N., et al. (2007). Activation of the UNC5B receptor by Netrin-1 inhibits sprouting angiogenesis. Genes Dev. *21*, 2433–2447.

Lawson, N.D., Scheer, N., Pham, V.N., Kim, C.H., Chitnis, A.B., Campos-Ortega, J.A., and Weinstein, B.M. (2001). Notch signaling is required for arterial-venous differentiation during embryonic vascular development. Development *128*, 3675–3683.

Lawson, N.D., Vogel, A.M., and Weinstein, B.M. (2002). sonic hedgehog and vascular endothelial growth factor act upstream of the Notch pathway during arterial endothelial differentiation. Dev. Cell *3*, 127–136.

Lawson, S.N., and Biscoe, T.J. (1979). Development of mouse dorsal root ganglia: an autoradiographic and quantitative study. J. Neurocytol. *8*, 265–274.

Le Douarin, N., and Kalcheim, C. (1999). The Neural Crest (Cambridge University Press).

Le, L.Q., Shipman, T., Burns, D.K., and Parada, L.F. (2009). Cell of origin and microenvironment contribution for NF1-associated dermal neurofibromas. Cell Stem Cell *4*, 453–463.

LeBleu, V.S., Taduri, G., O'Connell, J., Teng, Y., Cooke, V.G., Woda, C., Sugimoto, H., and Kalluri, R. (2013). Origin and function of myofibroblasts in kidney fibrosis. Nat. Med. *19*, 1047–1053.

Ledda, M., De Palo, S., and Pannese, E. (2004). Ratios between number of neuroglial cells and number and volume of nerve cells in the spinal ganglia of two species of reptiles and three species of mammals. Tissue Cell *36*, 55–62.

Lee, D., Park, C., Lee, H., Lugus, J.J., Kim, S.H., Arentson, E., Chung, Y.S., Gomez, G., Kyba, M., Lin, S., et al. (2008). ER71 acts downstream of BMP, Notch, and Wnt signaling in blood and vessel progenitor specification. Cell Stem Cell *2*, 497–507.

Lee, H.-Y., Kléber, M., Hari, L., Brault, V., Suter, U., Taketo, M.M., Kemler, R., and Sommer, L. (2004). Instructive role of Wnt/beta-catenin in sensory fate specification in neural crest stem cells. Science *303*, 1020–1023.

Lee, K.F., Kucera, J., and Jaenisch, R. (1994). Lack of neurotrophin-3 leads to deficiencies in the peripheral nervous system and loss of limb proprioceptive afferents. Cell *77*, 503–512.

Lee, M.J., Thangada, S., Claffey, K.P., Ancellin, N., Liu, C.H., Kluk, M., Volpi, M., Sha'afi, R.I., and Hla, T. (1999). Vascular endothelial cell adherens junction assembly and morphogenesis induced by sphingosine-1-phosphate. Cell *99*, 301–312.

Leimeroth, R., Lobsiger, C., Lüssi, A., Taylor, V., Suter, U., and Sommer, L. (2002). Membrane-bound neuregulin1 type III actively promotes Schwann cell differentiation of multipotent Progenitor cells. Dev. Biol. *246*, 245–258.

Levanon, D., and Groner, Y. (2004). Structure and regulated expression of mammalian RUNX genes. Oncogene *23*, 4211–4219.

Levanon, D., Bettoun, D., Harris-Cerruti, C., Woolf, E., Negreanu, V., Eilam, R., Bernstein, Y., Goldenberg, D., Xiao, C., Fliegauf, M., et al. (2002). The Runx3 transcription factor regulates development and survival of TrkC dorsal root ganglia neurons. Embo J. *21*, 3454–3463.

Levéen, P., Pekny, M., Gebre-Medhin, S., Swolin, B., Larsson, E., and Betsholtz, C. (1994). Mice deficient for PDGF B show renal, cardiovascular, and hematological abnormalities. Genes Dev. *8*, 1875–1887.

Li, F., Lan, Y., Wang, Y., Wang, J., Yang, G., Meng, F., Han, H., Meng, A., Wang, Y., and Yang, X. (2011). Endothelial Smad4 maintains cerebrovascular integrity by activating N-cadherin through cooperation with Notch. Dev. Cell *20*, 291–302.

Li, L., and Ginty, D.D. (2014). The structure and organization of lanceolate mechanosensory complexes at mouse hair follicles. Elife *3*, e01901.

Li, S., Quarto, N., and Longaker, M.T. (2010). Activation of FGF signaling mediates proliferative and osteogenic differences between neural crest derived frontal and mesoderm parietal derived bone. PLoS ONE *5*, e14033.

Li, W., Kohara, H., Uchida, Y., James, J.M., Soneji, K., Cronshaw, D.G., Zou, Y.-R., Nagasawa, T., and Mukouyama, Y.-S. (2013). Peripheral nerve-derived CXCL12 and VEGF-A regulate the patterning of arterial vessel branching in developing limb skin. Dev. Cell *24*, 359–371.

Liebscher, I., Schön, J., Petersen, S.C., Fischer, L., Auerbach, N., Demberg, L.M., Mogha, A., Cöster, M., Simon, K.-U., Rothemund, S., et al. (2014). A tethered agonist within the ectodomain activates the adhesion G protein-coupled receptors GPR126 and GPR133. Cell Rep *9*, 2018–2026.

Lindahl, P., Johansson, B.R., Levéen, P., and Betsholtz, C. (1997). Pericyte loss and microaneurysm formation in PDGF-B-deficient mice. Science *277*, 242–245.

Lindblom, P., Gerhardt, H., Liebner, S., Abramsson, A., Enge, M., Hellström, M., Backstrom, G., Fredriksson, S., Landegren, U., Nystrom, H.C., et al. (2003). Endothelial PDGF-B retention is required for proper investment of pericytes in the microvessel wall. Genes Dev. *17*, 1835–1840.

Liu, H., Kennard, S., and Lilly, B. (2009). NOTCH3 expression is induced in mural cells through an autoregulatory loop that requires endothelial-expressed JAGGED1. Circ. Res. *104*, 466–475.

Lu, X., Le Noble, F., Yuan, L., Jiang, Q., De Lafarge, B., Sugiyama, D., Breant, C., Claes, F., De Smet, F., Thomas, J.-L., et al. (2004). The netrin receptor UNC5B mediates guidance events controlling morphogenesis of the vascular system. Nature *432*, 179–186.

Luo, R., Gao, J., Wehrle-Haller, B., and Henion, P.D. (2003). Molecular identification of distinct neurogenic and melanogenic neural crest sublineages. Development *130*, 321–330.

Luo, W., Enomoto, H., Rice, F.L., Milbrandt, J., and Ginty, D.D. (2009). Molecular identification of rapidly adapting mechanoreceptors and their developmental dependence on ret signaling. Neuron *64*, 841–856.

Lyons, D.A., Pogoda, H.-M., Voas, M.G., Woods, I.G., Diamond, B., Nix, R., Arana, N., Jacobs, J., and Talbot, W.S. (2005). erbb3 and erbb2 are essential for schwann cell migration and myelination in zebrafish. Curr. Biol. *15*, 513–524.

Ma, Q., Fode, C., Guillemot, F., and Anderson, D.J. (1999). Neurogenin1 and neurogenin2 control two distinct waves of neurogenesis in developing dorsal root ganglia. Genes Dev. *13*, 1717–1728.

Madisen, L., Zwingman, T.A., Sunkin, S.M., Oh, S.W., Zariwala, H.A., Gu, H., Ng, L.L., Palmiter, R.D., Hawrylycz, M.J., Jones, A.R., et al. (2010). A robust and high-throughput Cre reporting and characterization system for the whole mouse brain. Nat. Neurosci. *13*, 133–140.

Majesky, M.W. (2007). Developmental basis of vascular smooth muscle diversity. Arterioscler. Thromb. Vasc. Biol. *27*, 1248–1258.

Marcelo, K.L., Goldie, L.C., and Hirschi, K.K. (2013). Regulation of endothelial cell differentiation and specification. Circ. Res. *112*, 1272–1287.

Marmigère, F., and Ernfors, P. (2007). Specification and connectivity of neuronal subtypes in the sensory lineage. Nat. Rev. Neurosci. *8*, 114–127.

Marmigère, F., Wegner, M., Groner, Y., Reichardt, L.F., and Ernfors, P. (2006). The Runx1/AML1 transcription factor selectively regulates development and survival of TrkA nociceptive sensory neurons. Nat. Neurosci. *9*, 180–187.

Maro, G.S., Vermeren, M., Voiculescu, O., Melton, L., Cohen, J., Charnay, P., and Topilko, P. (2004). Neural crest boundary cap cells constitute a source of neuronal and glial cells of the PNS. Nat. Neurosci. *7*, 930–938.

Martik, M.L., and Bronner, M.E. (2017). Regulatory Logic Underlying Diversification of the Neural Crest. Trends Genet. *33*, 715–727.

Martinez-Morales, J.-R., Henrich, T., Ramialison, M., and Wittbrodt, J. (2007). New genes in the evolution of the neural crest differentiation program. Genome Biol. *8*, R36.

Masuda, T., Tsuji, H., Taniguchi, M., Yagi, T., Tessier-Lavigne, M., Fujisawa, H., Okado, N., and Shiga, T. (2003). Differential non-target-derived repulsive signals play a critical role in shaping initial axonal growth of dorsal root ganglion neurons. Dev. Biol. *254*, 289–302.

Mauti, O., Domanitskaya, E., Andermatt, I., Sadhu, R., and Stoeckli, E.T. (2007). Semaphorin6A acts as a gate keeper between the central and the peripheral nervous system. Neural Dev *2*, 28.

Mayes, D.A., Rizvi, T.A., Cancelas, J.A., Kolasinski, N.T., Ciraolo, G.M., Stemmer-Rachamimov, A.O., and Ratner, N. (2011). Perinatal or adult Nf1 inactivation using tamoxifen-inducible PlpCre each cause neurofibroma formation. Cancer Res. *71*, 4675–4685.

Mayor, R., and Theveneau, E. (2013). The neural crest. Development *140*, 2247–2251.

McFerrin, J., Patton, B.L., Sunderhaus, E.R., and Kretzschmar, D. (2017). NTE/PNPLA6 is expressed in mature Schwann cells and is required for glial ensheathment of Remak fibers. Glia *65*, 804–816.

McKee, K.K., Yang, D.-H., Patel, R., Chen, Z.-L., Strickland, S., Takagi, J., Sekiguchi, K., and Yurchenco, P.D. (2012). Schwann cell myelination requires integration of laminin activities. Journal of Cell Science *125*, 4609–4619.

McKinney, M.C., Fukatsu, K., Morrison, J., McLennan, R., Bronner, M.E., and Kulesa, P.M. (2013). Evidence for dynamic rearrangements but lack of fate or position restrictions in premigratory avian trunk neural crest. Development *140*, 820–830.

Meier, C., Parmantier, E., Brennan, A., Mirsky, R., and Jessen, K.R. (1999). Developing Schwann cells acquire the ability to survive without axons by establishing an autocrine circuit involving insulin-like growth factor, neurotrophin-3, and platelet-derived growth factor-BB. J. Neurosci. *19*, 3847–3859.

Mentzer, S.J., and Konerding, M.A. (2014). Intussusceptive angiogenesis: expansion and remodeling of microvascular networks. Angiogenesis *17*, 499–509.

Michailov, G.V., Sereda, M.W., Brinkmann, B.G., Fischer, T.M., Haug, B., Birchmeier, C., Role, L., Lai, C., Schwab, M.H., and Nave, K.-A. (2004). Axonal neuregulin-1 regulates myelin sheath thickness. Science *304*, 700–703.

Michiels, C. (2003). Endothelial cell functions. J. Cell. Physiol. *196*, 430–443.

Milet, C., and Monsoro-Burq, A.H. (2012). Neural crest induction at the neural plate border in vertebrates. Dev. Biol. *366*, 22–33.

Mogha, A., Benesh, A.E., Patra, C., Engel, F.B., Schöneberg, T., Liebscher, I., and Monk, K.R. (2013). Gpr126 functions in Schwann cells to control differentiation and myelination via G-protein activation. J. Neurosci. *33*, 17976–17985.

Moncada, S., Gryglewski, R., Bunting, S., and Vane, J.R. (1976). An enzyme isolated from arteries transforms prostaglandin endoperoxides to an unstable substance that inhibits platelet aggregation. Nature *263*, 663–665.

Monje, P.V., Bartlett Bunge, M., and Wood, P.M. (2006). Cyclic AMP synergistically enhances neuregulin-dependent ERK and Akt activation and cell cycle progression in Schwann cells. Glia *53*, 649–659.

Monk, K.R., Naylor, S.G., Glenn, T.D., Mercurio, S., Perlin, J.R., Dominguez, C., Moens, C.B., and Talbot, W.S. (2009). A G protein-coupled receptor is essential for Schwann cells to initiate myelination. Science *325*, 1402–1405.

Monk, K.R., Oshima, K., Jörs, S., Heller, S., and Talbot, W.S. (2011). Gpr126 is essential for peripheral nerve development and myelination in mammals. Development *138*, 2673–2680.

Monsoro-Burq, A.-H., Wang, E., and Harland, R. (2005). Msx1 and Pax3 cooperate to mediate FGF8 and WNT signals during Xenopus neural crest induction. Dev. Cell *8*, 167–178.

Montelius, A., Marmigère, F., Baudet, C., Aquino, J.B., Enerbäck, S., and Ernfors, P. (2007). Emergence of the sensory nervous system as defined by Foxs1 expression. Differentiation *75*, 404–417.

Moqrich, A., Earley, T.J., Watson, J., Andahazy, M., Backus, C., Martin-Zanca, D., Wright, D.E., Reichardt, L.F., and Patapoutian, A. (2004). Expressing TrkC from the TrkA locus causes a subset of dorsal root ganglia neurons to switch fate. Nat. Neurosci. *7*, 812–818.

Morrison, S.J., Perez, S.E., Qiao, Z., Verdi, J.M., Hicks, C., Weinmaster, G., and Anderson, D.J. (2000). Transient Notch activation initiates an irreversible switch from neurogenesis to gliogenesis by neural crest stem cells. Cell *101*, 499–510.

Moya, I.M., Umans, L., Maas, E., Pereira, P.N.G., Beets, K., Francis, A., Sents, W., Robertson, E.J., Mummery, C.L., Huylebroeck, D., et al. (2012). Stalk cell phenotype depends on integration of Notch and Smad1/5 signaling cascades. Dev. Cell *22*, 501–514.

Mu, X., Silos-Santiago, I., Carroll, S.L., and Snider, W.D. (1993). Neurotrophin receptor genes are expressed in distinct patterns in developing dorsal root ganglia. Journal of Neuroscience *13*, 4029–4041.

Mukouyama, Y.-S., Gerber, H.-P., Ferrara, N., Gu, C., and Anderson, D.J. (2005). Peripheral nerve-derived VEGF promotes arterial differentiation via neuropilin 1-mediated positive feedback. Development *132*, 941–952.

Mukouyama, Y.-S., Shin, D., Britsch, S., Taniguchi, M., and Anderson, D.J. (2002). Sensory nerves determine the pattern of arterial differentiation and blood vessel branching in the skin. Cell *109*, 693–705.

Muller, W.A. (2011). Mechanisms of leukocyte transendothelial migration. Annu Rev Pathol *6*, 323–344.

Murry, C.E., and Keller, G. (2008). Differentiation of embryonic stem cells to clinically relevant populations: lessons from embryonic development. Cell *132*, 661–680.

Müller, S.M., Stolt, C.C., Terszowski, G., Blum, C., Amagai, T., Kessaris, N., Iannarelli, P., Richardson, W.D., Wegner, M., and Rodewald, H.-R. (2008). Neural crest origin of perivascular mesenchyme in the adult thymus. J. Immunol. *180*, 5344–5351.

Nagasawa, T., Hirota, S., Tachibana, K., Takakura, N., Nishikawa, S., Kitamura, Y., Yoshida, N., Kikutani, H., and Kishimoto, T. (1996). Defects of B-cell lymphopoiesis and bone-marrow myelopoiesis in mice lacking the CXC chemokine PBSF/SDF-1. Nature *382*, 635–638.

Nakayama, M., Nakayama, A., van Lessen, M., Yamamoto, H., Hoffmann, S., Drexler, H.C.A., Itoh, N., Hirose, T., Breier, G., Vestweber, D., et al. (2013). Spatial regulation of VEGF receptor endocytosis in angiogenesis. Nat Cell Biol *15*, 249–260.

Nascimento, R.S., Santiago, M.F., Marques, S.A., Allodi, S., and Martinez, A.M.B. (2008). Diversity among satellite glial cells in dorsal root ganglia of the rat. Braz. J. Med. Biol. Res. *41*, 1011–1017.

Nathan, C. (2002). Points of control in inflammation. Nature *420*, 846–852.

Nave, K.-A., and Salzer, J.L. (2006). Axonal regulation of myelination by neuregulin 1. Curr. Opin. Neurobiol. *16*, 492–500.

Nave, K.-A., and Schwab, M.H. (2005). Glial cells under remote control. Nat. Neurosci. *8*, 1420–1422.

Neal, A., Nornes, S., Payne, S., Wallace, M.D., Fritzsche, M., Louphrasitthiphol, P., Wilkinson, R.N., Chouliaras, K.M., Liu, K., Plant, K., et al. (2019). Venous identity requires BMP signalling through ALK3. Nat Commun *10*, 453.

Nemenoff, R.A., Horita, H., Ostriker, A.C., Furgeson, S.B., Simpson, P.A., VanPutten, V., Crossno, J., Offermanns, S., and Weiser-Evans, M.C.M. (2011). SDF-1α induction in mature smooth muscle cells by inactivation of PTEN is a critical mediator of exacerbated injury-induced neointima formation. Arterioscler. Thromb. Vasc. Biol. *31*, 1300–1308.

Newbern, J.M., Li, X., Shoemaker, S.E., Zhou, J., Zhong, J., Wu, Y., Bonder, D., Hollenback, S., Coppola, G., Geschwind, D.H., et al. (2011). Specific functions for ERK/MAPK signaling during PNS development. Neuron *69*, 91–105.

Nicoli, S., Standley, C., Walker, P., Hurlstone, A., Fogarty, K.E., and Lawson, N.D. (2010). MicroRNA-mediated integration of haemodynamics and Vegf signalling during angiogenesis. Nature *464*, 1196–1200.

Niederländer, C., and Lumsden, A. (1996). Late emigrating neural crest cells migrate specifically to the exit points of cranial branchiomotor nerves. Development *122*, 2367–2374.

Nielsen, C.M., and Dymecki, S.M. (2010). Sonic hedgehog is required for vascular outgrowth in the hindbrain choroid plexus. Dev. Biol. *340*, 430–437.

Nitta, T., Hata, M., Gotoh, S., Seo, Y., Sasaki, H., Hashimoto, N., Furuse, M., and Tsukita, S. (2003). Size-selective loosening of the blood-brain barrier in claudin-5-deficient mice. J. Cell Biol. *161*, 653–660.

Nitzan, E., Krispin, S., Pfaltzgraff, E.R., Klar, A., Labosky, P.A., and Kalcheim, C. (2013a). A dynamic code of dorsal neural tube genes regulates the segregation between neurogenic and melanogenic neural crest cells. Development *140*, 2269–2279.

Nitzan, E., Pfaltzgraff, E.R., Labosky, P.A., and Kalcheim, C. (2013b). Neural crest and Schwann cell progenitor-derived melanocytes are two spatially segregated populations similarly regulated by Foxd3. Proc. Natl. Acad. Sci. U.S.a. *110*, 12709–12714.

Noguera-Troise, I., Daly, C., Papadopoulos, N.J., Coetzee, S., Boland, P., Gale, N.W., Lin, H.C., Yancopoulos, G.D., and Thurston, G. (2006). Blockade of Dll4 inhibits tumour growth by promoting non-productive angiogenesis. Nature *444*, 1032–1037.

Olsson, A.-K., Dimberg, A., Kreuger, J., and Claesson-Welsh, L. (2006). VEGF receptor signalling - in control of vascular function. Nat. Rev. Mol. Cell Biol. *7*, 359–371.

Ota, T., Fujii, M., Sugizaki, T., Ishii, M., Miyazawa, K., Aburatani, H., and Miyazono, K. (2002). Targets of transcriptional regulation by two distinct type I receptors for transforming growth factor-beta in human umbilical vein endothelial cells. J. Cell. Physiol. *193*, 299–318.

Owens, G.K. (1995). Regulation of differentiation of vascular smooth muscle cells. Physiol. Rev. *75*, 487–517.

Owens, G.K., Kumar, M.S., and Wamhoff, B.R. (2004). Molecular regulation of vascular smooth muscle cell differentiation in development and disease. Physiol. Rev. *84*, 767–801.

Ozcelik, M., Cotter, L., Jacob, C., Pereira, J.A., Relvas, J.B., Suter, U., and Tricaud, N. (2010). Pals1 Is a Major Regulator of the Epithelial-Like Polarization and the Extension of the Myelin Sheath in Peripheral Nerves. Journal of Neuroscience *30*, 4120–4131.

Paik, J.-H., Skoura, A., Chae, S.-S., Cowan, A.E., Han, D.K., Proia, R.L., and Hla, T. (2004). Sphingosine 1-phosphate receptor regulation of N-cadherin mediates vascular stabilization. Genes Dev. *18*, 2392–2403.

Palmer, R.M., Ferrige, A.G., and Moncada, S. (1987). Nitric oxide release accounts for the biological activity of endothelium-derived relaxing factor. Nature *327*, 524–526.

Pannese, E. (2010). The structure of the perineuronal sheath of satellite glial cells (SGCs) in sensory ganglia. Neuron Glia Biol. *6*, 3–10.

Paratore, C., Goerich, D.E., Suter, U., Wegner, M., and Sommer, L. (2001). Survival and glial fate acquisition of neural crest cells are regulated by an interplay between the transcription factor Sox10 and extrinsic combinatorial signaling. Development *128*, 3949–3961.

Pardanaud, L., and Dieterlen-Lièvre, F. (1993). Emergence of endothelial and hemopoietic cells in the avian embryo. Anat. Embryol. *187*, 107–114.

Parkinson, D.B., Dong, Z., Bunting, H., Whitfield, J., Meier, C., Marie, H., Mirsky, R., and Jessen, K.R. (2001). Transforming growth factor beta (TGFbeta) mediates Schwann cell death in vitro and in vivo: examination of c-Jun activation, interactions with survival signals, and the relationship of TGFbeta-mediated death to Schwann cell differentiation. J. Neurosci. *21*, 8572–8585.

Parkinson, D.B., Bhaskaran, A., Arthur-Farraj, P., Noon, L.A., Woodhoo, A., Lloyd, A.C., Feltri, M.L., Wrabetz, L., Behrens, A., Mirsky, R., et al. (2008). c-Jun is a negative regulator of myelination. J. Cell Biol. *181*, 625–637.

Parmantier, E., Lynn, B., Lawson, D., Turmaine, M., Namini, S.S., Chakrabarti, L., Jessen, K.R., and Mirsky, R. (1999). Schwann cell-derived Desert hedgehog controls the development of peripheral nerve sheaths. Neuron *23*, 713–724.

Parrinello, S., and Lloyd, A.C. (2009). Neurofibroma development in NF1--insights into tumour initiation. Trends Cell Biol. *19*, 395–403.

Parrinello, S., Napoli, I., Ribeiro, S., Wingfield Digby, P., Fedorova, M., Parkinson, D.B., Doddrell, R.D.S., Nakayama, M., Adams, R.H., and Lloyd, A.C. (2010). EphB signaling directs peripheral nerve regeneration through Sox2-dependent Schwann cell sorting. Cell *143*, 145–155.

Patan, S. (1998). TIE1 and TIE2 receptor tyrosine kinases inversely regulate embryonic angiogenesis by the mechanism of intussusceptive microvascular growth. Microvascular Research *56*, 1–21.

Patel-Hett, S., and DAmore, P.A. (2011). Signal transduction in vasculogenesis and developmental angiogenesis. Int. J. Dev. Biol. *55*, 353–363.

Patthey, C., Edlund, T., and Gunhaga, L. (2009). Wnt-regulated temporal control of BMP exposure directs the choice between neural plate border and epidermal fate. Development *136*, 73–83.

Peles, E., and Salzer, J.L. (2000). Molecular domains of myelinated axons. Curr. Opin. Neurobiol. *10*, 558–565.

Pellegatta, M., De Arcangelis, A., D'Urso, A., Nodari, A., Zambroni, D., Ghidinelli, M., Matafora, V., Williamson, C., Georges-Labouesse, E., Kreidberg, J., et al. (2013). α6β1 and α7β1 integrins are required in Schwann cells to sort axons. J. Neurosci. *33*, 17995–18007.

Pereira, J.A., Lebrun-Julien, F., and Suter, U. (2012). Molecular mechanisms regulating myelination in the peripheral nervous system. Trends Neurosci. *35*, 123–134.

Pereira, M., Birtele, M., Shrigley, S., Benitez, J.A., Hedlund, E., Parmar, M., and Ottosson, D.R. (2017). Direct Reprogramming of Resident NG2 Glia into Neurons with Properties of Fast-Spiking Parvalbumin-Containing Interneurons. Stem Cell Reports *9*, 742–751.

Petersen, S.C., Luo, R., Liebscher, I., Giera, S., Jeong, S.-J., Mogha, A., Ghidinelli, M., Feltri, M.L., Schöneberg, T., Piao, X., et al. (2015). The adhesion GPCR GPR126 has distinct, domain-dependent functions in Schwann cell development mediated by interaction with laminin-211. Neuron *85*, 755–769.

Plein, A., Fantin, A., Denti, L., Pollard, J.W., and Ruhrberg, C. (2018). Erythro-myeloid progenitors contribute endothelial cells to blood vessels. Nature *146*, 1–21.

Poliak, S., and Peles, E. (2003). The local differentiation of myelinated axons at nodes of Ranvier. Nat. Rev. Neurosci. *4*, 968–980.

Pond, A., Roche, F.K., and Letourneau, P.C. (2002). Temporal regulation of neuropilin-1 expression and sensitivity to semaphorin 3A in NGF- and NT3-responsive chick sensory neurons. *51*, 43–53.

Potente, M., and Mäkinen, T. (2017). Vascular heterogeneity and specialization in development and disease. Nat. Rev. Mol. Cell Biol. *18*, 477–494.

Potente, M., Gerhardt, H., and Carmeliet, P. (2011). Basic and therapeutic aspects of angiogenesis. Cell *146*, 873–887.

Proebstl, D., Voisin, M.-B., Woodfin, A., Whiteford, J., D'Acquisto, F., Jones, G.E., Rowe, D., and Nourshargh, S. (2012). Pericytes support neutrophil subendothelial cell crawling and breaching of venular walls in vivo. J Exp Med *209*, 1219–1234.

Proske, U., and Gandevia, S.C. (2012). The proprioceptive senses: their roles in signaling body shape, body position and movement, and muscle force. Physiol. Rev. *92*, 1651–1697.

Prömel, S., Frickenhaus, M., Hughes, S., Mestek, L., Staunton, D., Woollard, A., Vakonakis, I., Schöneberg, T., Schnabel, R., Russ, A.P., et al. (2012). The GPS motif is a molecular switch for bimodal activities of adhesion class G protein-coupled receptors. Cell Rep *2*, 321–331.

Que, J., Wilm, B., Hasegawa, H., Wang, F., Bader, D., and Hogan, B.L.M. (2008). Mesothelium contributes to vascular smooth muscle and mesenchyme during lung development. Proc. Natl. Acad. Sci. U.S.a. *105*, 16626–16630.

Radomska, K.J., and Topilko, P. (2017). Boundary cap cells in development and disease. Curr. Opin. Neurobiol. *47*, 209–215.

Radomska, K.J., Coulpier, F., Gresset, A., Schmitt, A., Debbiche, A., Lemoine, S., Wolkenstein, P., Vallat, J.-M., Charnay, P., and Topilko, P. (2019). Cellular Origin, Tumor Progression, and Pathogenic Mechanisms of Cutaneous Neurofibromas Revealed by Mice with Nf1 Knockout in Boundary Cap Cells. Cancer Discov *9*, 130–147.

Rama, N., Dubrac, A., Mathivet, T., Ní Chárthaigh, R.-A., Genet, G., Cristofaro, B., Pibouin-Fragner, L., Ma, L., Eichmann, A., and Chédotal, A. (2015). Slit2 signaling through Robo1 and Robo2 is required for retinal neovascularization. Nat. Med. *21*, 483–491.

Reinisch, C.M., and Tschachler, E. (2012). The dimensions and characteristics of the subepidermal nerve plexus in human skin--terminal Schwann cells constitute a substantial cell population within the superficial dermis. J. Dermatol. Sci. *65*, 162–169.

Ren, S., and Duffield, J.S. (2013). Pericytes in kidney fibrosis. Curr. Opin. Nephrol. Hypertens. *22*, 471–480.

Rensen, S.S.M., Doevendans, P.A.F.M., and van Eys, G.J.J.M. (2007). Regulation and characteristics of vascular smooth muscle cell phenotypic diversity. Neth Heart J *15*, 100–108.

Ricard, N., Ciais, D., Levet, S., Subileau, M., Mallet, C., Zimmers, T.A., Lee, S.-J., Bidart, M., Feige, J.-J., and Bailly, S. (2012). BMP9 and BMP10 are critical for postnatal retinal vascular remodeling. Blood *119*, 6162–6171.

Rice, F.L., and Albrecht, P.J. (2008). Cutaneous Mechanisms of Tactile Perception: Morphological and Chemical Organization of the Innervation to the Skin. In The Senses: a Comprehensive Reference, (Elsevier), pp. 1–31.

Richard, L., Topilko, P., Magy, L., Decouvelaere, A.-V., Charnay, P., Funalot, B., and Vallat, J.-M. (2012). Endoneurial fibroblast-like cells. J. Neuropathol. Exp. Neurol. *71*, 938–947.

Richard, L., Védrenne, N., Vallat, J.-M., and Funalot, B. (2014). Characterization of Endoneurial Fibroblast-like Cells from Human and Rat Peripheral Nerves. J. Histochem. Cytochem. *62*, 424–435.

Ridgway, J., Zhang, G., Wu, Y., Stawicki, S., Liang, W.-C., Chanthery, Y., Kowalski, J., Watts, R.J., Callahan, C., Kasman, I., et al. (2006). Inhibition of Dll4 signalling inhibits tumour growth by deregulating angiogenesis. Nature *444*, 1083–1087.

Ridley, A.J., Davis, J.B., Stroobant, P., and Land, H. (1989). Transforming growth factors-beta 1 and beta 2 are mitogens for rat Schwann cells. J. Cell Biol. *109*, 3419–3424.

Riethmacher, D., Sonnenberg-Riethmacher, E., Brinkmann, V., Yamaai, T., Lewin, G.R., and Birchmeier, C. (1997). Severe neuropathies in mice with targeted mutations in the ErbB3 receptor. Nature *389*, 725–730.

Risau, W. (1997). Mechanisms of angiogenesis. Nature *386*, 671–674.

Risau, W., and Flamme, I. (1995). Vasculogenesis. Annu. Rev. Cell Dev. Biol. *11*, 73–91.

Romanes, G.J. (1951). The motor cell columns of the lumbo-sacral spinal cord of the cat. J. Comp. Neurol. *94*, 313–363.

Rouget, C.M.B. (1873). Mémoire sur le développement, la structure et les propriétés des capillaires sanguins and lymphatiques. Arch Physiol Norm Pathol *5*, 603–633.

Ruchoux, M.M., Guerouaou, D., Vandenhaute, B., Pruvo, J.P., Vermersch, P., and Leys, D. (1995). Systemic vascular smooth muscle cell impairment in cerebral autosomal dominant arteriopathy with subcortical infarcts and leukoencephalopathy. Acta Neuropathol. *89*, 500–512.

Rucker, H.K., Wynder, H.J., and Thomas, W.E. (2000). Cellular mechanisms of CNS pericytes. Brain Res. Bull. *51*, 363–369.

Saher, G., Quintes, S., Mobius, W., Wehr, M.C., Kramer-Albers, E.M., Brugger, B., and Nave, K.A. (2009). Cholesterol Regulates the Endoplasmic Reticulum Exit of the Major Membrane Protein P0 Required for Peripheral Myelin Compaction. Journal of Neuroscience *29*, 6094–6104.

Sainz, J., Haj Zen, Al, A., Caligiuri, G., Demerens, C., Urbain, D., Lemitre, M., and Lafont, A. (2006). Isolation of “side population” progenitor cells from healthy arteries of adult mice. Arterioscler. Thromb. Vasc. Biol. *26*, 281–286.

Sakurai, Y., Ohgimoto, K., Kataoka, Y., Yoshida, N., and Shibuya, M. (2005). Essential role of Flk-1 (VEGF receptor 2) tyrosine residue 1173 in vasculogenesis in mice. Proc. Natl. Acad. Sci. U.S.a. *102*, 1076–1081.

Salzer, J.L. (2003). Polarized domains of myelinated axons. Neuron *40*, 297–318.

Salzer, J.L. (2015). Schwann cell myelination. Cold Spring Harb Perspect Biol *7*, a020529.

Santiago, A., and Erickson, C.A. (2002). Ephrin-B ligands play a dual role in the control of neural crest cell migration. Development *129*, 3621–3632.

Sauka-Spengler, T., Meulemans, D., Jones, M., and Bronner-Fraser, M. (2007). Ancient evolutionary origin of the neural crest gene regulatory network. Dev. Cell *13*, 405–420.

Sawamiphak, S., Seidel, S., Essmann, C.L., Wilkinson, G.A., Pitulescu, M.E., Acker, T., and Acker-Palmer, A. (2010). Ephrin-B2 regulates VEGFR2 function in developmental and tumour angiogenesis. Nature *465*, 487–491.

Schneider-Maunoury, S., Topilko, P., Seitandou, T., Levi, G., Cohen-Tannoudji, M., Pournin, S., Babinet, C., and Charnay, P. (1993). Disruption of Krox-20 results in alteration of rhombomeres 3 and 5 in the developing hindbrain. Cell *75*, 1199–1214.

Schwann, T. (1839). Mikroskopische Untersuchungen über die Uebereinstimmung in der Struktur und dem Wachsthum der Thiere und Pflanzen (Berlin: Sander).

Serafini, T., Colamarino, S.A., Leonardo, E.D., Wang, H., Beddington, R., Skarnes, W.C., and Tessier-Lavigne, M. (1996). Netrin-1 is required for commissural axon guidance in the developing vertebrate nervous system. Cell *87*, 1001–1014.

Shah, N.M., Groves, A.K., and Anderson, D.J. (1996). Alternative neural crest cell fates are instructively promoted by TGFbeta superfamily members. Cell *85*, 331–343.

Shah, N.M., Marchionni, M.A., Isaacs, I., Stroobant, P., and Anderson, D.J. (1994). Glial growth factor restricts mammalian neural crest stem cells to a glial fate. Cell *77*, 349–360.

Shalaby, F., Ho, J., Stanford, W.L., Fischer, K.D., Schuh, A.C., Schwartz, L., Bernstein, A., and Rossant, J. (1997). A requirement for Flk1 in primitive and definitive hematopoiesis and vasculogenesis. Cell *89*, 981–990.

Shalaby, F., Rossant, J., Yamaguchi, T.P., Gertsenstein, M., Wu, X.F., Breitman, M.L., and Schuh, A.C. (1995). Failure of blood-island formation and vasculogenesis in Flk-1-deficient mice. Nature *376*, 62–66.

Shanthaveerappa, T.R., and Bourne, G.H. (1963). The Perineural Epithelium: Nature and Significance. Nature *199*, 577–579.

Sherman, D.L., Krols, M., Wu, L.-M.N., Grove, M., Nave, K.-A., Gangloff, Y.-G., and Brophy, P.J. (2012). Arrest of myelination and reduced axon growth when Schwann cells lack mTOR. J. Neurosci. *32*, 1817–1825.

Shevde, N. (2012). Stem Cells: Flexible friends. Nature *483*, S22–S26.

Shi, G., and Jin, Y. (2010). Role of Oct4 in maintaining and regaining stem cell pluripotency. Stem Cell Res Ther *1*, 39.

Siminovitch, L., McCulloch, E.A., and Till, J.E. (1963). The Distribution of Colony-forming Cells Among Spleen Colonies. J Cell Comp Physiol *62*, 327–336.

Simionescu, M., Gafencu, A., and Antohe, F. (2002). Transcytosis of plasma macromolecules in endothelial cells: a cell biological survey. Microsc. Res. Tech. *57*, 269–288.

Simoes-Costa, M., and Bronner, M.E. (2015). Establishing neural crest identity: a gene regulatory recipe. Development *142*, 242–257.

Simons, B.D., and Clevers, H. (2011). Strategies for homeostatic stem cell self-renewal in adult tissues. Cell *145*, 851–862.

Simons, M., and Eichmann, A. (2015). Molecular controls of arterial morphogenesis. Circ. Res. *116*, 1712–1724.

Simons, M., Gordon, E., and Claesson-Welsh, L. (2016). Mechanisms and regulation of endothelial VEGF receptor signalling. Nat. Rev. Mol. Cell Biol. *17*, 611–625.

Sims, D.E. (1986). The pericyte--a review. Tissue Cell *18*, 153–174.

Smeyne, R.J., Klein, R., Schnapp, A., Long, L.K., Bryant, S., Lewin, A., Lira, S.A., and Barbacid, M. (1994). Severe sensory and sympathetic neuropathies in mice carrying a disrupted Trk/NGF receptor gene. Nature *368*, 246–249.

Smith, C.J., Morris, A.D., Welsh, T.G., and Kucenas, S. (2014). Contact-mediated inhibition between oligodendrocyte progenitor cells and motor exit point glia establishes the spinal cord transition zone. PLoS Biol *12*, e1001961.

Snippert, H.J., van der Flier, L.G., Sato, T., van Es, J.H., van den Born, M., Kroon-Veenboer, C., Barker, N., Klein, A.M., van Rheenen, J., Simons, B.D., et al. (2010). Intestinal crypt homeostasis results from neutral competition between symmetrically dividing Lgr5 stem cells. Cell *143*, 134–144.

Soderblom, C., Luo, X., Blumenthal, E., Bray, E., Lyapichev, K., Ramos, J., Krishnan, V., Lai-Hsu, C., Park, K.K., Tsoulfas, P., et al. (2013). Perivascular fibroblasts form the fibrotic scar after contusive spinal cord injury. J. Neurosci. *33*, 13882–13887.

Sohal, G.S., Ali, M.M., Ali, A.A., and Bockman, D.E. (1999). Ventral neural tube cells differentiate into hepatocytes in the chick embryo. Cell. Mol. Life Sci. *55*, 128–130.

Sommer, L. (2013). Specification of Neural Crest- and Placode-Derived Neurons (Elsevier Inc.).

Soriano, P. (1994). Abnormal kidney development and hematological disorders in PDGF beta-receptor mutant mice. Genes Dev. *8*, 1888–1896.

Sörensen, I., Adams, R.H., and Gossler, A. (2009). DLL1-mediated Notch activation regulates endothelial identity in mouse fetal arteries. Blood *113*, 5680–5688.

Stark, K., Eckart, A., Haidari, S., Tirniceriu, A., Lorenz, M., Brühl, von, M.-L., Gärtner, F., Khandoga, A.G., Legate, K.R., Pless, R., et al. (2013). Capillary and arteriolar pericytes attract innate leukocytes exiting through venules and «instruct» them with pattern-recognition and motility programs. Nat. Immunol. *14*, 41–51.

Stemple, D.L., and Anderson, D.J. (1992). Isolation of a stem cell for neurons and glia from the mammalian neural crest. Cell *71*, 973–985.

Stephenson, R.O., Rossant, J., and Tam, P.P.L. (2012). Intercellular interactions, position, and polarity in establishing blastocyst cell lineages and embryonic axes. Cold Spring Harb Perspect Biol *4*.

Stewart, H.J., Brennan, A., Rahman, M., Zoidl, G., Mitchell, P.J., Jessen, K.R., and Mirsky, R. (2001). Developmental regulation and overexpression of the transcription factor AP-2, a potential regulator of the timing of Schwann cell generation. Eur. J. Neurosci. *14*, 363–372.

Stifani, N. (2014). Motor neurons and the generation of spinal motor neuron diversity. 1–22.

Stratman, A.N., Malotte, K.M., Mahan, R.D., Davis, M.J., and Davis, G.E. (2009). Pericyte recruitment during vasculogenic tube assembly stimulates endothelial basement membrane matrix formation. Blood *114*, 5091–5101.

Stratman, A.N., Pezoa, S.A., Farrelly, O.M., Castranova, D., Dye, L.E., Butler, M.G., Sidik, H., Talbot, W.S., and Weinstein, B.M. (2017). Interactions between mural cells and endothelial cells stabilize the developing zebrafish dorsal aorta. Development *144*, 115–127.

Stratman, A.N., Schwindt, A.E., Malotte, K.M., and Davis, G.E. (2010). Endothelial-derived PDGF-BB and HB-EGF coordinately regulate pericyte recruitment during vasculogenic tube assembly and stabilization. Blood *116*, 4720–4730.

Strilic, B., KuCera, T., Eglinger, J., Hughes, M.R., McNagny, K.M., Tsukita, S., Dejana, E., Ferrara, N., and Lammert, E. (2009). The molecular basis of vascular lumen formation in the developing mouse aorta. Dev. Cell *17*, 505–515.

Suadicani, S.O., Cherkas, P.S., Zuckerman, J., Smith, D.N., Spray, D.C., and Hanani, M. (2010). Bidirectional calcium signaling between satellite glial cells and neurons in cultured mouse trigeminal ganglia. Neuron Glia Biol. *6*, 43–51.

Suchting, S., Freitas, C., Le Noble, F., Benedito, R., Breant, C., Duarte, A., and Eichmann, A. (2007). The Notch ligand Delta-like 4 negatively regulates endothelial tip cell formation and vessel branching. Proc. Natl. Acad. Sci. U.S.a. *104*, 3225–3230.

Sundberg, C., Kowanetz, M., Brown, L.F., Detmar, M., and Dvorak, H.F. (2002). Stable expression of angiopoietin-1 and other markers by cultured pericytes: phenotypic similarities to a subpopulation of cells in maturing vessels during later stages of angiogenesis in vivo. Lab. Invest. *82*, 387–401.

Suri, C., Jones, P.F., Patan, S., Bartunkova, S., Maisonpierre, P.C., Davis, S., Sato, T.N., and Yancopoulos, G.D. (1996). Requisite role of angiopoietin-1, a ligand for the TIE2 receptor, during embryonic angiogenesis. Cell *87*, 1171–1180.

Svaren, J., and Meijer, D. (2008). The molecular machinery of myelin gene transcription in Schwann cells. Glia *56*, 1541–1551.

Swiers, G., Baumann, C., O'Rourke, J., Giannoulatou, E., Taylor, S., Joshi, A., Moignard, V., Pina, C., Bee, T., Kokkaliaris, K.D., et al. (2013). Early dynamic fate changes in haemogenic endothelium characterized at the single-cell level. Nat Commun *4*, 2924.

Swift, M.R., and Weinstein, B.M. (2009). Arterial–Venous Specification During Development. Circ. Res. *104*, 576–588.

Szabó, A., and Mayor, R. (2018). Mechanisms of Neural Crest Migration. Annu. Rev. Genet. *52*, 43–63.

Tachibana, K., Hirota, S., Iizasa, H., Yoshida, H., Kawabata, K., Kataoka, Y., Kitamura, Y., Matsushima, K., Yoshida, N., Nishikawa, S., et al. (1998). The chemokine receptor CXCR4 is essential for vascularization of the gastrointestinal tract. Nature *393*, 591–594.

Tachibana, K., Jones, N., Dumont, D.J., Puri, M.C., and Bernstein, A. (2005). Selective role of a distinct tyrosine residue on Tie2 in heart development and early hematopoiesis. Mol. Cell. Biol. *25*, 4693–4702.

Takahashi, K., and Yamanaka, S. (2006). Induction of pluripotent stem cells from mouse embryonic and adult fibroblast cultures by defined factors. Cell *126*, 663–676.

Takahashi, K., Tanabe, K., Ohnuki, M., Narita, M., Ichisaka, T., Tomoda, K., and Yamanaka, S. (2007). Induction of pluripotent stem cells from adult human fibroblasts by defined factors. Cell *131*, 861–872.

Takahashi-Iwanaga, H. (2005). Calcium signaling in terminal Schwann cells associated with lanceolate sensory endings in rat vibrissae. Ital J Anat Embryol *110*, 19–24.

Takakura, N., Watanabe, T., Suenobu, S., Yamada, Y., Noda, T., Ito, Y., Satake, M., and Suda, T. (2000). A role for hematopoietic stem cells in promoting angiogenesis. Cell *102*, 199–209.

Taneyhill, L.A. (2008). To adhere or not to adhere: the role of Cadherins in neural crest development. Cell Adh Migr *2*, 223–230.

Tang, W., Zeve, D., Suh, J.M., Bosnakovski, D., Kyba, M., Hammer, R.E., Tallquist, M.D., and Graff, J.M. (2008). White fat progenitor cells reside in the adipose vasculature. Science *322*, 583–586.

Tang, Z., Wang, A., Yuan, F., Yan, Z., Liu, B., Chu, J.S., Helms, J.A., and Li, S. (2012). Differentiation of multipotent vascular stem cells contributes to vascular diseases. Nat Commun *3*, 875.

Taniguchi, M., Yuasa, S., Fujisawa, H., Naruse, I., Saga, S., Mishina, M., and Yagi, T. (1997). Disruption of semaphorin III/D gene causes severe abnormality in peripheral nerve projection. Neuron *19*, 519–530.

Tarkowski, A.K., Suwińska, A., Czołowska, R., and Ożdżeński, W. (2010). Individual blastomeres of 16- and 32-cell mouse embryos are able to develop into foetuses and mice. Dev. Biol. *348*, 190–198.

Taveggia, C., Zanazzi, G., Petrylak, A., Yano, H., Rosenbluth, J., Einheber, S., Xu, X., Esper, R.M., Loeb, J.A., Shrager, P., et al. (2005). Neuregulin-1 type III determines the ensheathment fate of axons. Neuron *47*, 681–694.

Taylor, M.K., Yeager, K., and Morrison, S.J. (2007). Physiological Notch signaling promotes gliogenesis in the developing peripheral and central nervous systems. Development *134*, 2435–2447.

Tessier-Lavigne, M., and Goodman, C.S. (1996). The molecular biology of axon guidance. Science *274*, 1123–1133.

Theveneau, E., and Mayor, R. (2012). Neural crest delamination and migration: from epithelium-to-mesenchyme transition to collective cell migration. Dev. Biol. *366*, 34–54.

Thurston, G., Suri, C., Smith, K., McClain, J., Sato, T.N., Yancopoulos, G.D., and McDonald, D.M. (1999). Leakage-resistant blood vessels in mice transgenically overexpressing angiopoietin-1. Science *286*, 2511–2514.

Topilko, P., Schneider-Maunoury, S., Levi, G., Baron-Van Evercooren, A., Chennoufi, A.B., Seitanidou, T., Babinet, C., and Charnay, P. (1994). Krox-20 controls myelination in the peripheral nervous system. Nature *371*, 796–799.

Trost, A., Schroedl, F., Lange, S., Rivera, F.J., Tempfer, H., Korntner, S., Stolt, C.C., Wegner, M., Bogner, B., Kaser-Eichberger, A., et al. (2013). Neural crest origin of retinal and choroidal pericytes. Invest. Ophthalmol. Vis. Sci. *54*, 7910–7921.

Uemura, A., Ogawa, M., Hirashima, M., Fujiwara, T., Koyama, S., Takagi, H., Honda, Y., Wiegand, S.J., Yancopoulos, G.D., and Nishikawa, S.-I. (2002). Recombinant angiopoietin-1 restores higher-order architecture of growing blood vessels in mice in the absence of mural cells. J. Clin. Invest. *110*, 1619–1628.

Ueno, H., and Weissman, I.L. (2006). Clonal analysis of mouse development reveals a polyclonal origin for yolk sac blood islands. Dev. Cell *11*, 519–533.

Vanlandewijck, M., He, L., Mäe, M.A., Andrae, J., Ando, K., Del Gaudio, F., Nahar, K., Lebouvier, T., Laviña, B., Gouveia, L., et al. (2018). A molecular atlas of cell types and zonation in the brain vasculature. Nature *554*, 1–35.

Vermeren, M., Maro, G.S., Bron, R., McGonnell, I.M., Charnay, P., Topilko, P., and Cohen, J. (2003). Integrity of developing spinal motor columns is regulated by neural crest derivatives at motor exit points. Neuron *37*, 403–415.

Vesalius, A. (1543). De Humani Corporis Fabrica (Basel: Johannes Oporinus).

Voisin, M.-B., Pröbstl, D., and Nourshargh, S. (2010). Venular basement membranes ubiquitously express matrix protein low-expression regions: characterization in multiple tissues and remodeling during inflammation. Am. J. Pathol. *176*, 482–495.

Vokes, S.A., and Krieg, P.A. (2015). Vascular Molecular Embryology. In PanVascular Medicine, P. Lanzer, ed. (Berlin, Heidelberg: Springer Berlin Heidelberg), pp. 27–51.

Volz, K.S., Jacobs, A.H., Chen, H.I., Poduri, A., McKay, A.S., Riordan, D.P., Kofler, N., Kitajewski, J., Weissman, I., and Red-Horse, K. (2015). Pericytes are progenitors for coronary artery smooth muscle. Elife *4*, 2139.

Wakamatsu, Y., Maynard, T.M., and Weston, J.A. (2000). Fate determination of neural crest cells by NOTCH-mediated lateral inhibition and asymmetrical cell division during gangliogenesis. Development *127*, 2811–2821.

Wang, G., Jacquet, L., Karamariti, E., and Xu, Q. (2015). Origin and differentiation of vascular smooth muscle cells. J. Physiol. (Lond.) *593*, 3013–3030.

Wang, H.U., Chen, Z.F., and Anderson, D.J. (1998). Molecular distinction and angiogenic interaction between embryonic arteries and veins revealed by ephrin-B2 and its receptor Eph-B4. Cell *93*, 741–753.

Wang, S., Cao, C., Chen, Z., Bankaitis, V., Tzima, E., Sheibani, N., and Burridge, K. (2012). Pericytes regulate vascular basement membrane remodeling and govern neutrophil extravasation during inflammation. PLoS ONE *7*, e45499.

Wang, S., Voisin, M.-B., Larbi, K.Y., Dangerfield, J., Scheiermann, C., Tran, M., Maxwell, P.H., Sorokin, L., and Nourshargh, S. (2006). Venular basement membranes contain specific matrix protein low expression regions that act as exit points for emigrating neutrophils. J Exp Med *203*, 1519–1532.

Wang, Y., Nakayama, M., Pitulescu, M.E., Schmidt, T.S., Bochenek, M.L., Sakakibara, A., Adams, S., Davy, A., Deutsch, U., Lüthi, U., et al. (2010). Ephrin-B2 controls VEGF-induced angiogenesis and lymphangiogenesis. Nature *465*, 483–486.

Wanner, I.B., Mahoney, J., Jessen, K.R., Wood, P.M., Bates, M., and Bunge, M.B. (2006). Invariant mantling of growth cones by Schwann cell precursors characterize growing peripheral nerve fronts. Glia *54*, 424–438.

Watson, C. (2012). The Mouse Nervous System (Academic Press).

Webster, H.D., Martin, R., and O'Connell, M.F. (1973). The relationships between interphase Schwann cells and axons before myelination: a quantitative electron microscopic study. Dev. Biol. *32*, 401–416.

Weiner, J.A., and Chun, J. (1999). Schwann cell survival mediated by the signaling phospholipid lysophosphatidic acid. Proc. Natl. Acad. Sci. U.S.a. *96*, 5233–5238.

Westbury, D.R. (1982). A comparison of the structures of alpha and gamma-spinal motoneurones of the cat. J. Physiol. (Lond.) *325*, 79–91.

White, P.M., Morrison, S.J., Orimoto, K., Kubu, C.J., Verdi, J.M., and Anderson, D.J. (2001). Neural crest stem cells undergo cell-intrinsic developmental changes in sensitivity to instructive differentiation signals. Neuron *29*, 57–71.

Wilkinson, D.G., Bhatt, S., Chavrier, P., Bravo, R., and Charnay, P. (1989). Segment-specific expression of a zinc-finger gene in the developing nervous system of the mouse. Nature *337*, 461–464.

Willem, M., Garratt, A.N., Novak, B., Citron, M., Kaufmann, S., Rittger, A., DeStrooper, B., Saftig, P., Birchmeier, C., and Haass, C. (2006). Control of peripheral nerve myelination by the beta-secretase BACE1. Science *314*, 664–666.

Wilm, B., Ipenberg, A., Hastie, N.D., Burch, J.B.E., and Bader, D.M. (2005). The serosal mesothelium is a major source of smooth muscle cells of the gut vasculature. Development *132*, 5317–5328.

Woldeyesus, M.T., Britsch, S., Riethmacher, D., Xu, L., Sonnenberg-Riethmacher, E., Abou-Rebyeh, F., Harvey, R., Caroni, P., and Birchmeier, C. (1999). Peripheral nervous system defects in erbB2 mutants following genetic rescue of heart development. Genes Dev. *13*, 2538–2548.

Woo, S.-H., Ranade, S., Weyer, A.D., Dubin, A.E., Baba, Y., Qiu, Z., Petrus, M., Miyamoto, T., Reddy, K., Lumpkin, E.A., et al. (2014). Piezo2 is required for Merkel-cell mechanotransduction. Nature *509*, 622–626.

Woodhoo, A., and Sommer, L. (2008). Development of the Schwann cell lineage: From the neural crest to the myelinated nerve. Glia *56*, 1481–1490.

Woodhoo, A., Alonso, M.B.D., Droggiti, A., Turmaine, M., D'Antonio, M., Parkinson, D.B., Wilton, D.K., Al-Shawi, R., Simons, P., Shen, J., et al. (2009). Notch controls embryonic Schwann cell differentiation, postnatal myelination and adult plasticity. Nat. Neurosci. *12*, 839–847.

Woodhoo, A., Dean, C.H., Droggiti, A., Mirsky, R., and Jessen, K.R. (2004). The trunk neural crest and its early glial derivatives: a study of survival responses, developmental schedules and autocrine mechanisms. Mol. Cell. Neurosci. *25*, 30–41.

Wu, J., Williams, J.P., Rizvi, T.A., Kordich, J.J., Witte, D., Meijer, D., Stemmer-Rachamimov, A.O., Cancelas, J.A., and Ratner, N. (2008). Plexiform and dermal neurofibromas and pigmentation are caused by Nf1 loss in desert hedgehog-expressing cells. Cancer Cell *13*, 105–116.

Wu, J., and Izpisua Belmonte, J.C. (2016). Stem Cells: A Renaissance in Human Biology Research. Cell *165*, 1572–1585.

Yamamoto, S., Muramatsu, M., Azuma, E., Ikutani, M., Nagai, Y., Sagara, H., Koo, B.-N., Kita, S., O'Donnell, E., Osawa, T., et al. (2017). A subset of cerebrovascular pericytes originates from mature macrophages in the very early phase of vascular development in CNS. Sci Rep *7*, 3855.

Yamashita, J., Itoh, H., Hirashima, M., Ogawa, M., Yurugi, T., Naito, M., Nakao, K., and Nishikawa, S. (2000). Flk1-positive cells derived from embryonic stem cells serve as vascular progenitors. Nature *408*, 92–96.

Yamazaki, T., and Mukouyama, Y.-S. (2018). Tissue Specific Origin, Development, and Pathological Perspectives of Pericytes. Front Cardiovasc Med *5*, 78.

Yamazaki, T., Nalbandian, A., Uchida, Y., Li, W., Arnold, T.D., Kubota, Y., Yamamoto, S., Ema, M., and Mukouyama, Y.-S. (2017). Tissue Myeloid Progenitors Differentiate into Pericytes through TGF-β Signaling in Developing Skin Vasculature. Cell Rep *18*, 2991–3004.

Yanagisawa, M., Kurihara, H., Kimura, S., Tomobe, Y., Kobayashi, M., Mitsui, Y., Yazaki, Y., Goto, K., and Masaki, T. (1988). A novel potent vasoconstrictor peptide produced by vascular endothelial cells. Nature *332*, 411–415.

Yaneza, M., Gilthorpe, J.D., Lumsden, A., and Tucker, A.S. (2002). No evidence for ventrally migrating neural tube cells from the mid- and hindbrain. Dev. Dyn. *223*, 163–167.

Yaron, A., Huang, P.-H., Cheng, H.-J., and Tessier-Lavigne, M. (2005). Differential Requirement for Plexin-A3 and -A4 in Mediating Responses of Sensory and Sympathetic Neurons to Distinct Class 3 Semaphorins. Neuron *45*, 513–523.

You, L.-R., Lin, F.-J., Lee, C.T., DeMayo, F.J., Tsai, M.-J., and Tsai, S.Y. (2005). Suppression of Notch signalling by the COUP-TFII transcription factor regulates vein identity. Nature *435*, 98–104.

Yu, J., Zhang, X., Kuzontkoski, P.M., Jiang, S., Zhu, W., Li, D.Y., and Groopman, J.E. (2014). Slit2N and Robo4 regulate lymphangiogenesis through the VEGF-C/VEGFR-3 pathway. Cell Commun. Signal *12*, 25.

Yu, J., Vodyanik, M.A., Smuga-Otto, K., Antosiewicz-Bourget, J., Frane, J.L., Tian, S., Nie, J., Jonsdottir, G.A., Ruotti, V., Stewart, R., et al. (2007). Induced pluripotent stem cell lines derived from human somatic cells. Science *318*, 1917–1920.

Yu, W.-M., Feltri, M.L., Wrabetz, L., Strickland, S., and Chen, Z.-L. (2005). Schwann cell-specific ablation of laminin gamma1 causes apoptosis and prevents proliferation. J. Neurosci. *25*, 4463–4472.

Zachariah, M.A., and Cyster, J.G. (2010). Neural crest-derived pericytes promote egress of mature thymocytes at the corticomedullary junction. Science *328*, 1129–1135.

Zeeb, M., Strilic, B., and Lammert, E. (2010). Resolving cell-cell junctions: lumen formation in blood vessels. Curr. Opin. Cell Biol. *22*, 626–632.

Zhang, F., Prahst, C., Mathivet, T., Pibouin-Fragner, L., Zhang, J., Genet, G., Tong, R., Dubrac, A., and Eichmann, A. (2016). The Robo4 cytoplasmic domain is dispensable for vascular permeability and neovascularization. Nat Commun *7*, 13517.

Zhou, B., Ma, Q., Rajagopal, S., Wu, S.M., Domian, I., Rivera-Feliciano, J., Jiang, D., Gise, von, A., Ikeda, S., Chien, K.R., et al. (2008). Epicardial progenitors contribute to the cardiomyocyte lineage in the developing heart. Nature *454*, 109–113.

Zhu, Y., Matsumoto, T., Nagasawa, T., Mackay, F., and Murakami, F. (2015). Chemokine Signaling Controls Integrity of Radial Glial Scaffold in Developing Spinal Cord and Consequential Proper Position of Boundary Cap Cells. J. Neurosci. *35*, 9211–9224.

Zhu, Y., Ghosh, P., Charnay, P., Burns, D.K., and Parada, L.F. (2002). Neurofibromas in NF1: Schwann cell origin and role of tumor environment. Science *296*, 920–922.

Zimmerman, A., Bai, L., and Ginty, D.D. (2014). The gentle touch receptors of mammalian skin. Science *346*, 950–954.

Zimmermann, K.W. (1923). Der feinere Bau der Blutcapillaren. Anat. Embryol. *68*, 29–109.

Zirlinger, M., Lo, L., McMahon, J., McMahon, A.P., and Anderson, D.J. (2002). Transient expression of the bHLH factor neurogenin-2 marks a subpopulation of neural crest cells biased for a sensory but not a neuronal fate. Proc. Natl. Acad. Sci. U.S.a. *99*, 8084–8089.

Zujovic, V., Thibaud, J., Bachelin, C., Vidal, M., Coulpier, F., Charnay, P., Topilko, P., and Baron-Van Evercooren, A. (2010). Boundary cap cells are highly competitive for CNS remyelination: fast migration and efficient differentiation in PNS and CNS myelin-forming cells. Stem Cells *28*, 470–479.

Zujovic, V., Thibaud, J., Bachelin, C., Vidal, M., Deboux, C., Coulpier, F., Stadler, N., Charnay, P., Topilko, P., and Baron-Van Evercooren, A. (2011). Boundary cap cells are peripheral nervous system stem cells that can be redirected into central nervous system lineages. Proc. Natl. Acad. Sci. U.S.a. *108*, 10714–10719.